QUANTITATIVE MEASUREMENTS ON TLC PLATES USING CCD DETECTION

MICHAEL LANCASTER

A thesis submitted in partial fulfilment of the requirements for the degree of Doctor of Philosophy at the University of York

Department of Chemistry

University of York

October 2006

Abstract

This thesis is concerned with (i) quantitative measurements on wetted thin layer chromatography (TLC) plates, (ii) the real time imaging of TLC separations, and (iii) imaging of TLC separations in the ultraviolet (UV) part of the electromagnetic spectrum using a charge coupled device (CCD) camera.

Quantitative measurements were carried out on wetted TLC plates for the first time, as a preliminary to real time study. After signal referencing was carried out in order to compensate for fixed pattern effects, it was possible to obtain good linearity and precision in both reflectance and transmission modes. Direct comparisons were made of ε values with those from spectrophotometry and inferences drawn on the amount of scatter present in dry and wetted layers.

Real time imaging was studied in the visible spectrum initially. A series of images were taken during development, then a novel signal referencing method was applied to these images in order to compensate for fixed pattern effects and also for the effect of the moving solvent on absorbance measurements. The results obtained from these compensated images were found to be greatly improved when signal averaging was carried out. Microsoft Excel was used to average the absorbance results from up to 80 images taken during a chromatographic development, and the improvement in S/N ratio and LOD was shown to scale with the square root of the number of images averaged.

TLC plates were imaged in UV, both offline and in real time using a CCD camera. Using a mercury lamp at 254 nm, quantitative UV results were obtained for the first time by this method. Once again, signal referencing was used as in the visible work A loading of 0.5 ng benzophenone was detectable after averaging 80 images using the real-time technique. 2 ng was not detectable by scanning densitometry using the same plates, mobile phase and analyte. This represents a 5 times improvement in LOD.

Contents

List of tables

List of figures

Abbreviations

AU	absorbance units
CCD	charge-coupled device
DCM	dichloromethane
EPC	Electro-planar chromatography
HETP	height equivalent to a theoretical plate
HPLC	high performance liquid chromatography
HPTLC	high performance thin-layer chromatography
IUPAC	international union of pure and applied chemistry
LC	liquid chromatography
LOD	limit of detection
OPLC	overpressured-layer chromatography
RPC	rotational planar chromatography
RSD	relative standard deviation
SN	separation number
S/N	signal to noise
TLC	thin-layer chromatography
UTLC	ultra thin-layer chromatography
UV	ultraviolet

Symbols

A	absorbance
$A_{B\text{-}L}$	Beer-Lambert absorbance
A_c	column cross sectional area available to the mobile phase
A_{corr}	corrected absorbance
A_0	apparent absorbance of the chromatographic adsorbent
A_p	peak area
a	molar absorption coefficient of the sample
a_i	area imaged by pixel i

B	longitudinal molecular diffusion in the mobile phase
C	resistance to mass transfer
c	concentration
d	path length
d_p	average particle diameter
d_z	distance between zone centres
F_c	volumetric flow rate
h	peak height
H	height equivalent to a theoretical plate
H_{obs}	observed plate height
H_{real}	real plate height
I	light intensity
I_o	reference light intensity
k	retention factor
K_o	permeability constant of the layer
k_v	velocity constant
L	column length
N	number of theoretical plates
N_{obs}	observed number of theoretical plates
N_{real}	real plate number
n_i	number of images averaged
q_i	quantity of analyte imaged by one pixel
R	resolution
R_f	retardation factor
R_i	reflectance for an infinitely thick opaque layer
S	scatter coefficient of the layer
S_a	signal
t	time
t_l	layer thickness
t_r	retention time
u	mobile phase velocity
u_f	solvent front velocity
u_{ff}	linear mobile phase velocity under forced flow conditions

u_o	mobile phase velocity at the outlet
w_b	peak width at base
w_h	peak width at half height
w_i	peak width at the inflection point
z	grey values
z_f	distance travelled by the mobile phase
z_o	distance from the sample origin to the origin for the mobile phase
z_x	distance travelled by the sample from its origin
α	selectivity
ε	absorption coefficient
ε_{app}	apparent absorption coefficient
ε^0	solvent strength
ε_r	dielectric constant
λ	wavelength
γ	surface tension of the mobile phase
η	mobile phase viscosity
θ	contact angle.

ACKNOWLEDGEMENTS

I would like to thank my supervisors at York, Professor David Goodall and Dr Ed Bergström, for their help, advice and support throughout my PhD study time spent in York.

I would also like to thank my industrial supervisors and sponsors, Dr Sean McCrossen (GlaxoSmithKline) and Professor Peter Myers (Waters) for help, advice and financial support of this project.

Many thanks to Rachel Crawford for her hard work on the offline UV experiments, to Andy Penrose for help in the early days and to Bo Zhang for many useful ideas. Also thanks to everyone in the ASEC group for making York a pleasant working environment – shame we didn't win that football tournament!

Finally, thank you to my family and friends for their support during my study and a special thank you to Harriet for putting up with me when things weren't going well.

Declaration

I hereby declare that the work presented in this thesis is my own, except where otherwise acknowledged, and has not been submitted previously for a degree at this or any other university.

Michael Lancaster

CHAPTER ONE

Introduction

1.1 Fundamentals of chromatography

1.1.1 Definition of chromatography

The International Union of Pure and Applied Chemistry (IUPAC) define chromatography as follows: "chromatography is a physical method of separation in which the components to be separated are distributed between two phases, one of which is stationary (stationary phase) while the other (the mobile phase) moves in a definite direction".

The chromatographic process occurs as a result of repeated sorption and desorption during the movement of the analyte along the stationary phase. The separation occurs due to differences in the distribution constants of the individual analyte components.

1.1.2 Principal methods of chromatography

The main chromatographic methods can be distinguished by the type of mobile phase used. In gas chromatography, the mobile phase is an inert gas (usually nitrogen or helium); in liquid chromatography the mobile phase is a liquid of low viscosity.

In liquid chromatography the stationary phase particles are generally densely packed into a tube (column) able to withstand the operating pressures employed. The sorbent particles are usually porous solids of high surface area, which may be chemically modified on the surface to tune the retention characteristics. In capillary gas chromatography the stationary phase is normally a viscous liquid distributed as a thin film or layer on the wall of a capillary leaving the centre of the column open. For thin layer chromatography the sorbent is spread as a thin, homogeneous layer on flat glass or similar inert support plate. In this case the mobile phase moves through the layer by the

action of capillary forces, or sometimes by forced flow if special equipment is employed.

1.1.3 The chromatogram

The information obtained from a chromatographic experiment is contained in the chromatogram, a record of the concentration or mass profile of the sample components as a function of the movement of the mobile phase. Information readily extracted from the chromatogram includes an indication of sample complexity based on the number of observed peaks, qualitative identification of sample components based on the accurate determination of peak position, quantitative assessment of the concentration or amount in each peak and an indication of chromatographic performance (Karger *et al.*, 1973).

1.1.4 Adsorption chromatography

Adsorption is a process in which material (contained in a contacting fluid) interacts by physical forces (dispersive, polar or ionic) with a surface, thereby causing a layer (or layers) of the material to adhere to that surface. The surface in most cases will be a solid (e.g. silica gel, alumina, or charcoal) or sometimes a liquid (e.g. surfactants on a water surface). The contacting fluid may be a liquid or a gas. The surface layer(s) may be single, double or multiple. The relationship between the concentration of the adsorbed material on the surface and the concentration of the material in the contacting fluid is called the adsorption isotherm: the term isotherm implies that the relationship holds at constant temperature. The simplest form is the Langmuir isotherm, and this holds when the binding to any one site is not affected by binding to other sites. This isotherm has the form of a rectangular hyperbola, with the limit value of concentration of bound species equal to the concentration of binding sites. Because the amount of material adsorbed depends upon the number of binding sites and thus the area of the interfacial surface, the separation achieved in adsorption chromatography is strongly dependent upon the surface area of the adsorbent. In the region at low pressures or solute concentrations, the adsorption coefficient ($C_{adsorbed}/C_{free}$) is constant and the isotherm is approximately linear. The relationships are generally less simple for adsorption from solutions than for the adsorption of gases, since solvent and solute compete for the adsorption sites on the surface (Snyder, 1968).

Figure 1.1 shows three isotherms of CO_2 on charcoal at 200, 300 and 400 K. The steepest isotherm being at the lowest temperature (200 K). The relationship between amount absorbed and pressure is parabolic but approximately linear at low pressures (or solute concentrations).

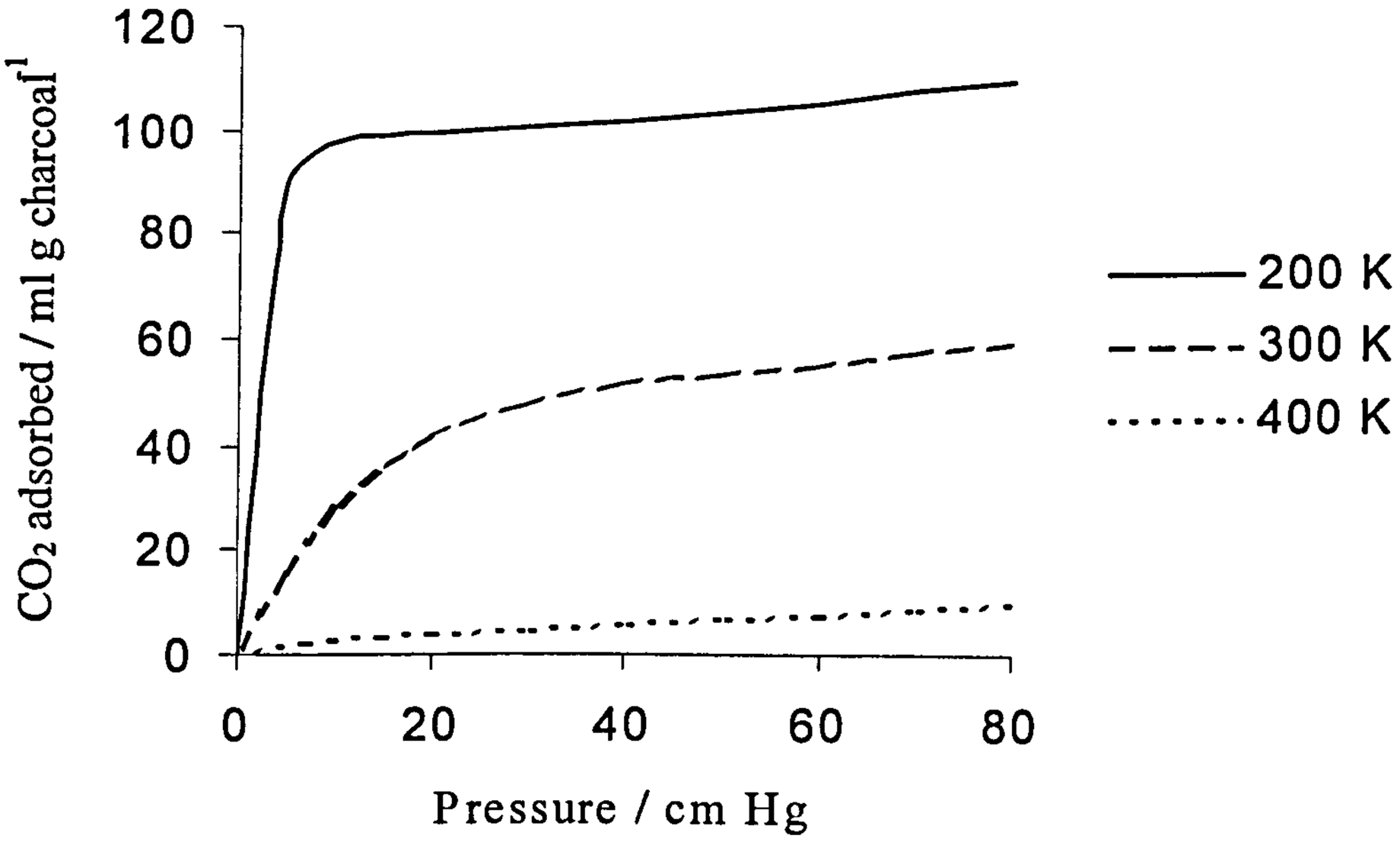

Figure 1.1 Adsorption isotherms of CO_2 on charcoal (Adapted from Randerath, 1968)

The consequences for TLC of two extreme cases of the adsorption isotherm may be considered.

a) The adsorption isotherm coincides with the abscissa. That is to say the substance is not adsorbed at all.
b) The adsorption isotherm coincides with the ordinate. That is to say it is completely (irreversibly) adsorbed.

Case a) occurs when the substance is completely dissolved in the solvent and is carried along by it, travelling with the solvent front. The substance has $R_f = 1$.

Case b) occurs when the substance is not dissolved off the adsorbent when the solvent flows over it. The substance remains at the origin and has $R_f = 0$. If the adsorption isotherm lies between these two extremes, the slope of the isotherm determines the extent to which the substance is transported since the overall process involves a

continual sequence of adsorption and desorption processes. The steeper the slope of the isotherm, the lower the value of R_f and the slower the substance travels.

1.1.5 Retention

In all chromatographic processes, sample molecules spend part of the time in the mobile phase and part in the stationary phase. The retention factor, *k*, of a sample zone is defined as the ratio of the time spent by the substance in the stationary phase compared to the time it spends in the mobile phase, and it is related to the retardation factor by equation 1.1 (Snyder, 1967).

$$k = \frac{(1 - R_f)}{R_f} \qquad (1.1)$$

1.1.6 Band broadening

1.1.6.1 Flow in porous media

In order to understand band broadening in chromatographic systems, linear velocity is more important than volumetric flow rate. The mobile phase velocity and flow rate in an open tubular column are related by equation 1.2

$$u_o = \frac{F_c}{A_c} \qquad (1.2)$$

where u_o is the mobile phase velocity at the outlet, F_c the volumetric flow rate and A_c the column cross sectional area available to the mobile phase. In a packed bed only part of the column cross sectional area is available to the mobile phase; the rest is occupied by the stationary phase. The flow of mobile phase in a packed bed occurs predominantly through the interstitial spaces; the mobile phase trapped within the porous particles is largely stagnant (Guiochon, 1979).

1.1.6.2 Band broadening mechanisms

As an analyte travels down a sorbent bed its distribution about the zone centre increases in proportion to its migration distance or time in the bed. The extent of zone broadening determines the chromatographic efficiency, *N*, alternatively termed the number of theoretical plates. If the bed is assumed to function as a Gaussian operator then the efficiency is readily expressed in terms of the peak retention time and variance according to equation 1.3.

$$N = \left(\frac{t_r}{\sigma_t}\right)^2 \tag{1.3}$$

where σ_t is the standard deviation in time units. In practice, various peak width parameters are used based on the properties of a Gaussian peak profile, as shown in equation 1.4

$$N = a\left(\frac{t_r}{w}\right)^2 \tag{1.4}$$

where the proportionality constant a depends on the form of peak width w used: $a = 4$ with w_i the peak width at the inflection point of the Gaussian peak; $a = 5.54$ with w_h the peak width at half height; $a = 16$ with w_b the peak width at base. Alternatively the ratio of the peak height to the area of a Gaussian peak can be used to define N

$$N = 2\pi\left(\frac{t_r h}{A_p}\right)^2 \tag{1.5}$$

where h is the peak height and A_p the peak area.

The height equivalent to a theoretical plate (HETP), H, is given by the ratio of the column length, L, to the number of theoretical plates

$$H = \frac{L}{N} \tag{1.6}$$

As equation 1.6 shows, the inverse proportionality between H and N means that the higher the value of N, the lower the value of H. An advantage of using H as a measure of the quality of a column is that H is independent of column length, whereas N increases in proportion to column length.

The terms plate number and plate height have their origin in the plate model of the chromatographic process (Katz *et al.*, 1983). The plate model assumes that the column can be visualised as being divided into a number of imaginary volume elements called plates. The plate model is useful for characterising the efficiency of distillation columns but its applicability to chromatography is at best questionable as several of the assumptions made do not hold under chromatographic conditions. Nevertheless, the quantity N is a useful parameter for characterising chromatographic efficiency and is not limited by the deficiencies of the plate model.

The various rate models of the chromatographic process enable similar expressions for the theoretical plate to be derived (Grushka *et al.*, 1975). The rate theory makes three main assumptions in its explanation of band broadening during chromatography. Firstly, resistance to mass transfer in both the stationary and mobile phase prevents the existence of an instantaneous equilibrium; this is the most important cause of band broadening under most practical conditions. Secondly, the flow velocity through a packed column varies with radial position in the column, some analyte molecules will travel more quickly by following open pathways; others will diffuse into restricted areas and lag behind the zone centre (eddy diffusion). These differing flow velocities will cause zone dispersion about the average velocity. This does not apply to open tubular columns. Thirdly, longitudinal diffusion (diffusion in the axial direction) leads to band broadening that is independent of the mobile phase velocity. Its contribution to band broadening is proportional to the amount of time the analyte spends in the chromatographic system.

A number of equations have been developed that relate the efficiency of chromatography to the extent to which the three processes outlined above (eddy diffusion, longitudinal diffusion and non-equilibrium mass transfer) occur (Miller, 1975). The earliest and simplest of these, the van Deemter equation, was derived for

gas-liquid chromatography. It provides an approximate relationship between the mobile phase flow velocity, u, and plate height, H

$$H = A + \frac{B}{u} + Cu \tag{1.8}$$

where, H is the height equivalent to a theoretical plate (column length divided by N). A low value of H indicates high efficiency. A is the term describing eddy diffusion, which results from unequal flow velocities or path lengths experienced by different molecules of sample as they travel along the column. The B term involves longitudinal molecular diffusion in the mobile phase. The C term expresses non-equilibrium resulting from resistance to mass transfer between the mobile and stationary phases. In other words, time is required for sorption and desorption of the sample. It can be seen that the B and C terms are not totally independent of one another as they are respectively inversely and directly proportional to the mobile phase velocity u.

The A term may be lowered if the layer is made up of small, regular particles as in commercial HPTLC plates. Small particle size also lowers C by increasing the possibility of equilibration. In HPTLC, resistance to mass transfer can usually be ignored at normal mobile phase velocities. In conventional TLC with larger particle sorbent layers, mass transfer kinetics cannot be ignored (Guiochon *et al.*, 1978). Molecular diffusion (B) is of less importance in liquid chromatography (both column and planar) than in gas chromatography. It is longitudinal molecular diffusion that controls zone broadening in HPTLC (Guiochon *et al.*, 1978).

An exact model of TLC is almost impossible to determine because of the complexities of the system (Poole, 1988; Guiochon and Siouff; 1978). The mobile, stationary and vapour phases in the chamber are not well defined and are changing during development. The degree of activation of the plates is impossible to control exactly. Evaporation of solvent within the tank (Stewart and Wendel, 1975) and the temperature gradient between the front and bulk solvent as the mobile phase moves along the dry bed (Miller, 1975) are also major variables. The speed of mobile phase migration is dependent on the distance of development, the type and size of sorbent particles, the

type of chamber and other variables (Geiss 1987, 1988; Guiochon and Siouffi, 1978; Poole 1989). Greater control of these parameters may be achieved by use of a low-volume horizontal development chamber or by use of OPLC, however even in these cases the system is much too complicated to for an exact theoretical description.

1.1.6.3 Overall effect of band broadening processes

The figure below shows the contribution of each term in the van Deemter equation as a function of mobile phase velocity as well as their net effect on plate height. Optimum efficiency is realised at a flow rate corresponding to the minimum on the thick solid curve. The van Deemter equation provides only an approximation of plate height, and several modifications have been developed that give a more precise description of the variables affecting column efficiency (Giddings, 1965)

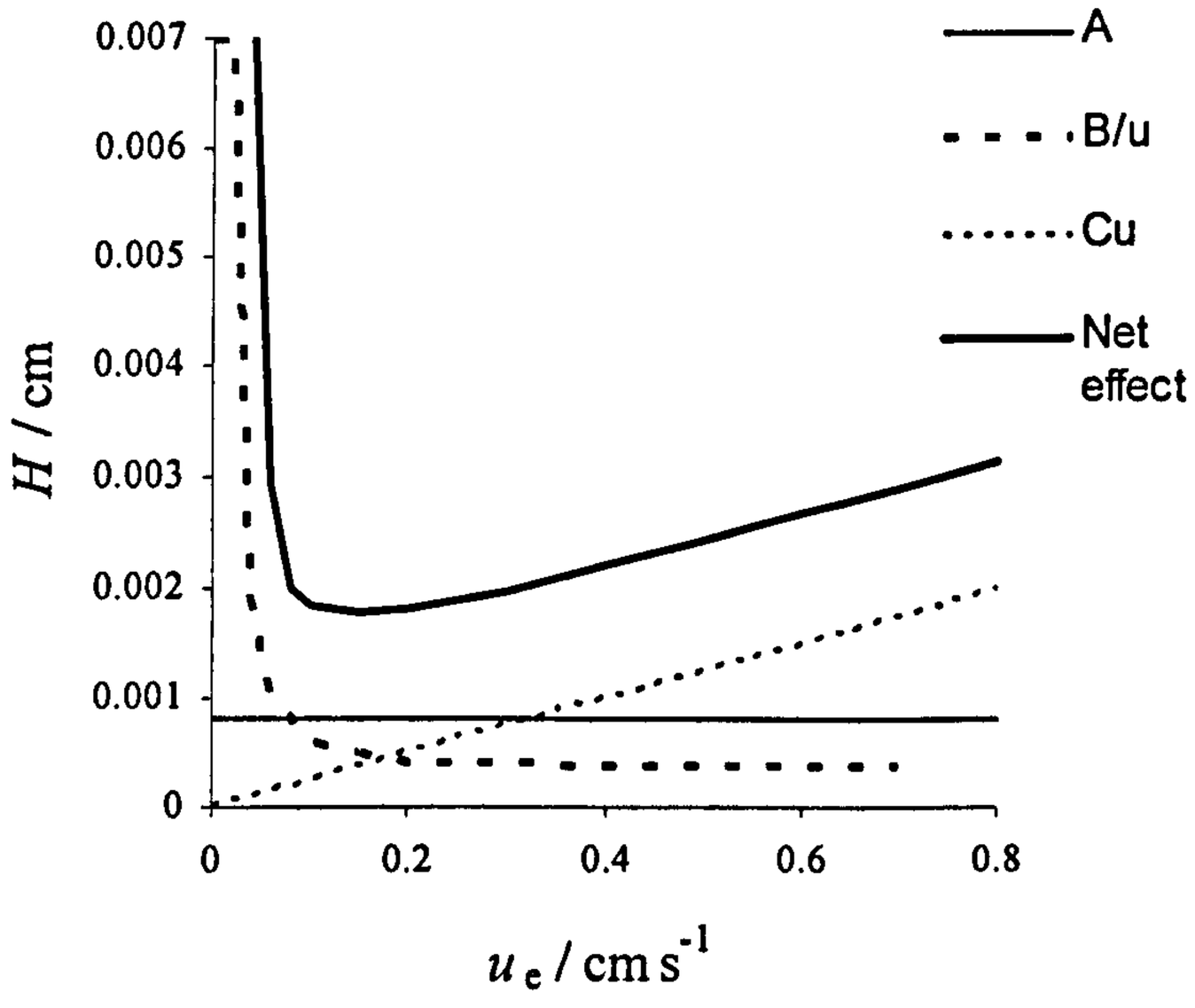

Figure 1.2 Relationship between band broadening and mobile phase velocity (van Deemter equation) and effect of variables on plate height.

1.1.7 Comparison of TLC and HPLC

HPLC and TLC are both non-destructive unless the compounds are unstable on the chromatographic medium or in the mobile phase used, and derivatisation is not necessary prior to separation by these techniques. A comparison of HPLC and TLC was made by Sherma (1991). The techniques have similar chromatographic capabilities, both can be operated under normal- or reversed-phase conditions, isocratically or with a solvent gradient, and similar stationary phases are available for each technique. The ultraviolet and fluorescence modes of detection are common to both techniques, but each also has alternatives (e.g. refractive index in HPLC and fluorescence quenching in TLC). The detection limits are lower with HPLC, ranging from picogram to nanogram amounts depending upon the mode of detection employed (Geiss, 1987).

There are some properties of TLC which make it a more flexible technique to be considered for the detection of drugs and their intermediates and precursors. An important difference in the techniques is that HPLC is dynamic (Snyder and Kirkland, 1979) whereas TLC is static (although we will see that it can be used as a dynamic technique too). With HPLC, after the eluent has passed through the detector, it is lost. In the case of TLC, after development, the plate can be scanned again and again if necessary as the analyte is immobilised on the plate after drying. Post chromatographic derivatisation on TLC is more flexible than with HPLC because reaction times are less important and heating can be used for slow reactions. TLC is an archiveable technique in terms of detection and for retrieval of separated components for identification. The open planar chromatographic bed provides a degree of flexibility that the closed tubular columns of HPLC do not have.

A further advantage of TLC, particularly when an unknown number of compounds is present, is that at all times the whole of the sample that has been applied to the plate must be between the origin and the solvent front, two limits which are defined clearly. When a complex mixture of components with a wide range of polarities has been injected into an HPLC column, it is difficult to be certain if the entire sample has been eluted and measured at any time. Thus in HPLC there can be loss of peaks, or the unexpected appearance of peaks from previous samples.

Another point of comparison is that HPLC columns are re-useable whereas TLC plates are disposable. A TLC plate is only used one therefore it can be damaged in use, but the conditions under which HPLC can be operated are limited by the need for the column to be used repeatedly. This might be of importance because it could be necessary to apply crude samples to ensure that all analytes are present. Similarly, the choice of solvent is not limited in TLC, whereas in HPLC the solvent must be compatible with the column packing material. Furthermore, because the solvent is evaporated from the stationary phase in TLC before detection, the use of solvents with UV absorbing properties is feasible, whereas in a fully dynamic system (HPLC or online TLC) their use would hamper detection of analytes of interest.

In terms of available theoretical plates, HPLC is more efficient than HPTLC. A typical HPLC column of 10-20 cm in length packed with 5 μm particles will provide 10-20,000 theoretical plates. The number of theoretical plates normally available in HPTLC is <5,000 for a 5 cm development (Geiss, 1987).

It may be concluded that TLC has a number of unique advantages, which make it an attractive technique that complements other methods of analysis. However, there are some disadvantages compared to other techniques, the main ones being the limited resolving power of capillary driven separations and poorer detection limits as mentioned above (Geiss, 1987). Also, TLC may be affected by environmental factors such as humidity as it is an open system so control is often necessary.

As discussed previously, high-performance thin-layer chromatography (HPTLC) has a number of attributes, which make it potentially useful for detecting analytes. HPTLC itself provides two main chromatographic mechanisms and various modes of operation, each of which has advantages in certain applications.

The mode most widely used is linear development on either square or rectangular chromatographic plates. Other modes are circular, in which development is performed from the centre of a circle out towards the circumference, and anti-circular in which development occurs towards the centre (Kaiser, 1988). Their use can improve resolution of strongly retained compounds in the case of circular development and less strongly retained components in the case of anti-circular development. Both of these techniques

require specialist equipment, and are not generally applicable. Linear development is considered to be the most suitable technique for most analytes.

Chromatographic mechanisms in TLC (and other liquid chromatographic techniques) can be divided broadly between normal-phase (adsorbtion) and reversed phase (partition) chromatography.

The separation of analytes in a mixture often requires that the chromatography used must be selective to small structural changes as well as being operable over a wide polarity range.

Reversed-phase chromatography can be carried out on a wide variety of stationary phases, the most popular being alkyl bonded silicas. Those commonly available for TLC are C_{18}, C_8, C_2, CN and NH_2 (the CN and NH_2 phases can be used in either the normal- or reversed-phase mode).

Adsorption chromatography can also be carried out on a wide variety of stationary phases, but silica and alumina are used most commonly. Silica is used more widely than alumina partly because silica HPTLC plates are commercially available and also because alumina has the capacity to alter some analytes chemically (Neher, 1958). These factors make silica the most reasonable choice between the two phases for the present studies. The interactions that occur between silica and molecules on its surface are polar, including hydrogen bonding, dipole-dipole, induced dipole-dipole, and pi-pi interactions (Unger, 1979). Functional groups that exhibit this type of behaviour include hydroxyls, amines, carbonyls, aromatic rings and double bonds.

1.1.8 Fundamentals of thin layer chromatography

1.1.8.1 The sorbent layer

Silica gel is the most common TLC sorbent. It is an amorphous, porous adsorbent. Silica gels used in column and planar chromatography are similar; the particle sizes used in HPLC and HPTLC are comparable at approximately 4-10 μm (Sherma, 1994).

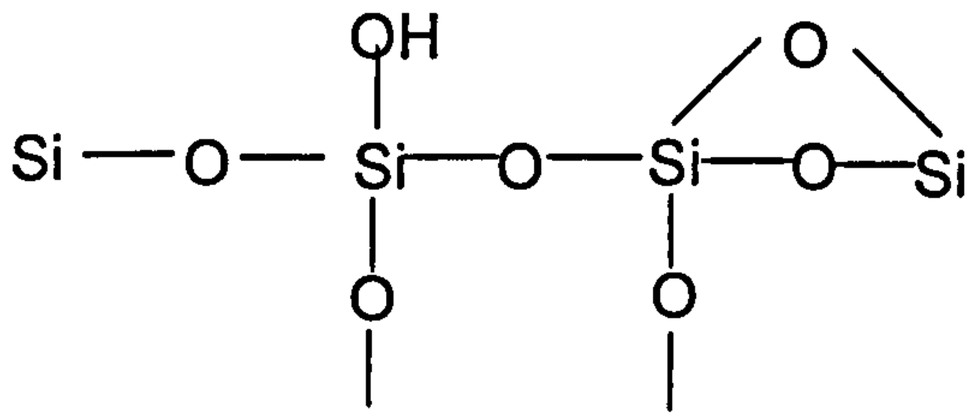

Figure 1.3 Surface groups in silica gel framework

Normal phase chromatography is used most commonly in TLC: in this mode of chromatography, the stationary phase is polar. The -OH groups in the surface layer of the silica gel (Figure 1.3) are mainly responsible for the adsorptive properties but there are many different types of active sites. The surface hydroxyls form hydrogen bonds with polar groups in the substances being adsorbed (Snyder, 1975).

The ideal condition for general TLC separations is considered to be 11-12% water by weight in the silica gel (Felton, 1979). This amount leaves the most plentiful mid-activity adsorption sites, the most active sites being attached to the water. This level of water is achieved when silica gel is at equilibrium with air having a relative humidity of 50% at 20 °C, conditions that are approximated in most laboratories. Heat activation is, therefore, often not required prior to TLC.

Many other types of sorbent layer are available for TLC. These include reversed-phase layers (where a long chain hydrocarbon or other organic compound is bound to the silica gel); these non-polar layers strongly attract non-polar compounds whilst polar compounds move readily – the opposite of what happens with a normal-phase polar layer. Other layer types available include alumina (crystalline Al_2O_3), cellulose, and Kieselguhr (mainly SiO_2).

1.1.8.2 The mobile phase

The mobile phase (also called the solvent system) is usually chosen based on experience and the literature, and optimised if necessary. It is normally possible to find a layer – solvent combination reported for compounds of interest or similar compounds. Several

handbooks and review articles are available detailing these (Kirchner, 1978; Meyers, 2000; Sherma, 2000). As the mobile phase competes with the chromatographed substances for sorbent sites, polar substances will require a polar solvent to effect migration on a normal phase silica gel layer. A stronger solvent would increase the R_f value and in normal phase TLC would be more polar. In reversed phase TLC the converse is true; non-polar substances are attracted to the layer and non-polar mobile phases are needed to effect migration (stronger solvents are more non-polar). In adsorption chromatography solvents can be grouped into an elutropic series according to their elution strength (Table 1.1); solvent strength, ε^0, increases with the polarity of the solvent. The polarity is conveniently expressed by the dielectric constant (ε_r). Chromatography grade solvents should always be used.

Table 1.1 Solvent strength data for some common solvents (Adapted from Fried and Sherma, 1994)

Solvent	Dielectric constant (ε_r)	Solvent strength (ε^0)
Methanol	37.5	0.95
Acetonitrile	32.6	0.65
Toluene	2.4	0.29
Xylene	2.4	0.26
Carbon tetrachloride	2.2	0.18
Pentane	1.8	0.00

Several approaches have been used for mobile phase optimisation when complex mixtures are to be separated (Geiss, 1987; Nyiredy, 1988). All optimisation approaches involve the use of some statistical design to select a series of solvents for evaluation or to indicate the best system by comparing the results obtained from an arbitrarily selected group of solvents (Snyder, 1974; Poole and Poole, 1991).

1.1.8.3 Retardation and retention factor

In thin layer chromatography the stationary phase consists of a thin layer of sorbent coated on an inert backing material. The sample is applied to the layer as a spot or band near the bottom edge of the plate. Separation is carried out in an enclosed chamber by either movement of solvent through the layer by capillary forces or forcing the mobile phase at a controlled velocity by application of an external pressure gradient. A separation of the sample results from the different rates of migration of the sample components in the direction travelled by the mobile phase. The sample components are separated in space; their position and quantity are subsequently determined by visual evaluation, elution or *in situ* densitometry.

The fundamental parameter used to characterise the position of a spot or band in a TLC chromatogram is the retardation factor, or R_f value. The R_f value represents the ratio of the distance migrated by the sample compared with that travelled by the solvent front. The R_f for linear development is given by equation 1.9.

$$R_f = \frac{z_x}{(z_f - z_o)} \tag{1.9}$$

where z_x is the distance travelled by the sample from its origin, z_f the distance travelled by the mobile phase and z_o the distance from the sample origin to the position used as the origin for the mobile phase. The boundary conditions for R_f values are given in equation 1.10:

$$1 \geq R_f \geq 0 \tag{1.10}$$

When R_f is equal to zero, the spot does not migrate from the origin. When R_f is equal to one, the spot is unretained by the stationary phase and migrates with the solvent front. Although R_f values are widely quoted, they are difficult to determine accurately (Geiss, 1987). Systematic errors result from the difficulty in locating the exact position of the solvent front. If the adsorbent layer, mobile phase and vapour phase are not in equilibrium then condensation of the vapour phase or evaporation of the mobile phase

in the region of the solvent front will give an erroneous R_f value. This value may be either too high or low, depending on the prevailing conditions (Snyder and Poppe, 1980).

1.1.8.4 Solvent migration through porous layers

In the absence of any other external force, the mobile phase flows through the sorbent layer by capillary action. The flow of solvent at the developing front is generally unsaturated and the speed at which the developing front moves is dependent on the experimental conditions (Guiochon and Siouffi, 1978). Capillary forces are stronger in the narrower interparticle channels in the layer, leading to more rapid advancement of the mobile phase. Larger pores behind the solvent front are filled more slowly, resulting in an increased thickness of the layer. If the vapour phase and mobile phase are not in equilibrium, evaporation will cause a loss of mobile phase from the plate surface and a decrease in the solvent front velocity. Also, the dry layer ahead of the solvent front progressively adsorbs vapour, filling some of the pores and interparticle channels, increasing the apparent velocity with which the solvent front migrates. For mixed-solvent systems, a solvent composition gradient is produced during chromatography due to selective adsorption of one component by the stationary phase or selective permeation of the channels and pores (Poole and Poole, 1993). Even nominally single-component mobile phases can exhibit impurity gradients. Gaining satisfactory control of the above processes in large volume chambers is almost impossible. The employment of various kinds of sandwich chambers (which eliminate or minimise contact of the sorbent layer with the vapour phase) can provide reasonable control over the mobile phase velocity.

It is an empirical fact that when the solvated plate is in equilibrium with the vapour phase the position of the solvent front with respect to time is reasonably represented by

$$Z_f^{\,2} = k_v t \qquad (1.11)$$

where k_v is the velocity constant (units $m^2\ s^{-1}$) and t is the time from contacting the sorbent layer with the solvent (Poole and Poole, 1991). After differentiation of equation 1.11 the velocity of the solvent front is given by

$$u_f = \frac{k_v}{2Z_f} \tag{1.12}$$

where u_f is the solvent front velocity. If equilibrium does not exist then the situation becomes far more complex. Equation 1.12 indicates the well-known undesirable effect associated with capillary controlled flow chromatography. That is decreasing solvent velocity with increasing migration distance, resulting in longer separation times and a reduced separation potential.

The velocity constant, k_v, is related to properties of the solvent and stationary phase by equation 1.13 (Poole and Poole, 1991)

$$k_v = 2K_o d_p \left(\frac{\gamma}{\eta}\right) \cos\theta \tag{1.13}$$

where K_o is the permeability constant of the layer, d_p the average particle diameter, γ the surface tension of the mobile phase, η the mobile phase viscosity and θ the contact angle.

The permeability constant is a dimensionless constant which allows for the pore size distribution, the effect of porosity on the permeability of the layer, and the ratio of the bulk liquid velocity to the solvent front. Experimental values vary according to layer type but typical values fall in the range 0.001 - 0.002 and are not very different from typical values for slurry-packed HPLC columns.

Equation 1.13 indicates that the velocity constant should increase linearly with the average particle size. The solvent front velocity should be larger for layers with coarse particles than for layers with finer particles, and this is in good agreement with experimental results (Geiss, 1988).

Also from equation 1.13 it is clear than the velocity constant depends linearly on the ratio of the surface tension of the solvent to its viscosity and that solvents which

maximise this ratio (rather than having a high value of γ or a low value of η) are preferred for TLC (Poole 1989). The contact angle for most organic solvents on silica gel is generally close to zero and since cos $\theta = 1$ the term is normally unimportant when making a choice between solvents. This is not generally the case on reversed-phase layers.

The above discussion relates to layers unperturbed by the presence of a vapour phase, or with complete vapour equilibrium. In practice, most separations are carried out in large volume chambers in the presence of a vapour phase. It is almost impossible to fully saturate such chambers, so a temporal and spatial vapour equilibrium in unlikely to exist. Two opposing phenomena can be expected to influence the rate of solvent migration. Vaporisation of solvent from the wetted layer might reasonably be expected to depend on the wetted surface area of the plate and the vapour pressure of solvent in the tank. The loss of solvent from the layer will result in a reduction of the mobile phase velocity from that indicated by equation 1.12. When the dried plate is placed in the developing chamber it progressively adsorbs solvent vapour. The pores of the unwetted layer ahead of the solvent front fill slowly with adsorbed vapour and the apparent porosity of the layer diminishes. Since the porosity of the layer decreases, the velocity constant increases slowly with increasing time. The effect of vaporisation is generally small if the atmosphere of the tank is close to saturation whilst adsorption of solvent vapours by the dry sorbent will tend to dominate. Thus, the mobile phase velocity in a large volume chamber will tend to be greater than that given by equation 1.12 and should increase continually with time, if the layer is not conditioned in the chamber prior to development. This is illustrated in Figure 1.4 (Kalasz, 1984).

Forced flow development enables the mobile phase velocity to be optimised without regard to the deficiencies of a capillary controlled flow system (Kalasz, 1984; Tyihak and Mincsovics, 1988). Two types of forced flow development are rotational planar chromatography (RPC) and over-pressure liquid chromatography (OPLC). In RPC, centrifugal force is generated by spinning the sorbent layer about a central axis and is used to drive the solvent through the layer (Nyiredy *et al.,* 1989). The rate of solvent migration is a function of the speed of rotation and also the rate at which the mobile phase is delivered to the sorbent layer. Since the layer is not enclosed in RPC, the

velocity of the solvent front is limited by the amount of solvent that can be kept within the layer before it begins to float over the surface. At high rotation speeds the velocity of the solvent front becomes approximately constant in the linear development mode.

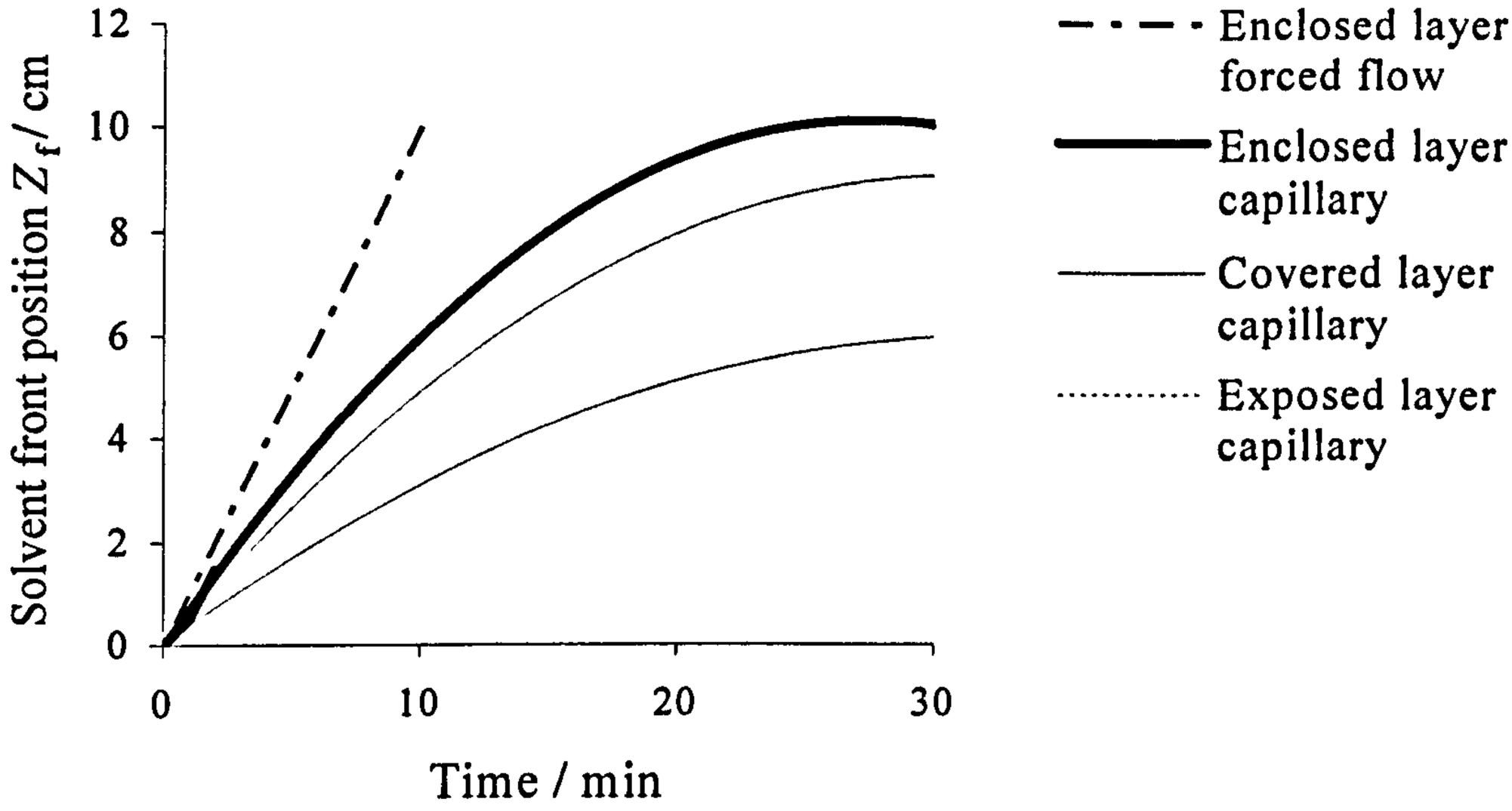

Figure 1.4 Relationship between solvent front position and time for an enclosed layer with forced flow development, an exposed layer in a saturated chamber with capillary controlled development, a covered layer (sandwich chamber) with capillary controlled flow, and an exposed layer in an unsaturated atmosphere with capillary controlled flow. Adapted from Poole (1989).

In OPLC the sorbent layer is sealed with a flexible membrane or an optically flat, rigid surface under hydraulic pressure and the mobile phase is delivered to the layer by a pump (Witkiewicz and Bladek, 1986). The mobile phase velocity can be controlled and optimised by adjusting the volume delivered by the pump. In the linear development mode the mobile phase velocity will be constant and the position of the solvent front position is described by

$$Z_f = u_{ff} t \qquad (1.14)$$

where u_{ff} is the linear velocity of the mobile phase under forced flow development conditions.

1.1.8.5 Band broadening and the plate height equation

The ultimate chromatographic performance and therefore resolution of a TLC plate is dependent on several parameters: the velocity constant of the mobile phase, the diffusion coefficient of the substance in the mobile phase, the mean particle diameter, and the particle size distribution of the stationary phase. Also, the presence of binder certainly has an effect but this is not easy to measure. Performance is improved by using particles of a narrow size distribution. Modern HPTLC plates are prepared from particles of small diameter and, more importantly, of a very narrow size distribution. Separations on these plates are characterised by compact symmetrical spots, with the exception of components eluting close to the solvent front. Zone broadening is dominated by molecular diffusion. The plate height contribution from resistance to mass transfer can be ignored at normal mobile phase velocities. For conventional TLC plates, elongated and irregular spots are not uncommon, and in this case the contribution of mass transfer kinetics to spot broadening cannot be ignored.

Layer efficiency can be evaluated in terms of the chromatographic parameters introduced in section 1.1.5.2; number of theoretical plates, *N*, and the height equivalent to a theoretical plate, *H*. There are however, some features of TLC that are different from column chromatographic systems, for which the parameters introduced above have been more widely adopted. In column chromatographic techniques, all substances travel the same migration distance (the length of the column). This contrasts with TLC, where all substances have the same diffusion time (the plate is developed for a fixed time) but migration distances vary. The chromatographic measures of performance in TLC (*N*, *H*) are all correlated to the migration distance of the substance. Their numerical values are evaluated for a specific R_f value and are thus dependent on their position in the chromatogram.

In modern TLC the distribution of sample within a spot is essentially Gaussian and the observed number of theoretical plates, N_{obs}, and plate height, H_{obs}, can be expressed by the equations

$$N_{obs} = a\left(\frac{Z_x}{W}\right)^2 \tag{1.15}$$

$$H_{obs} = \frac{W^2}{aZ_x} \tag{1.16}$$

where W is a parameter describing the peak width and a is a scaling factor. When W is the peak width at the base (determined from densitometric recordings), a has a value of 16, and when W is the peak width at half height, a is 5.54. It is clear from the equations above that there is a dependency between N_{obs} or H_{obs} and the sample migration distance. The plate height decreases linearly with the reciprocal of the R_f value.

An alternative method of determining the plate height can be developed based on the linear extrapolation of the peak width at half height (symbol b, equivalent to w_h (eqn 1.4)) as a function of R_f. This is done to determine the expected peak widths at half height corresponding to $R_f = 0$ (b_o) and $R_f = 1$ (b_1) as shown in Figure 1.5 (Poole, 1988).

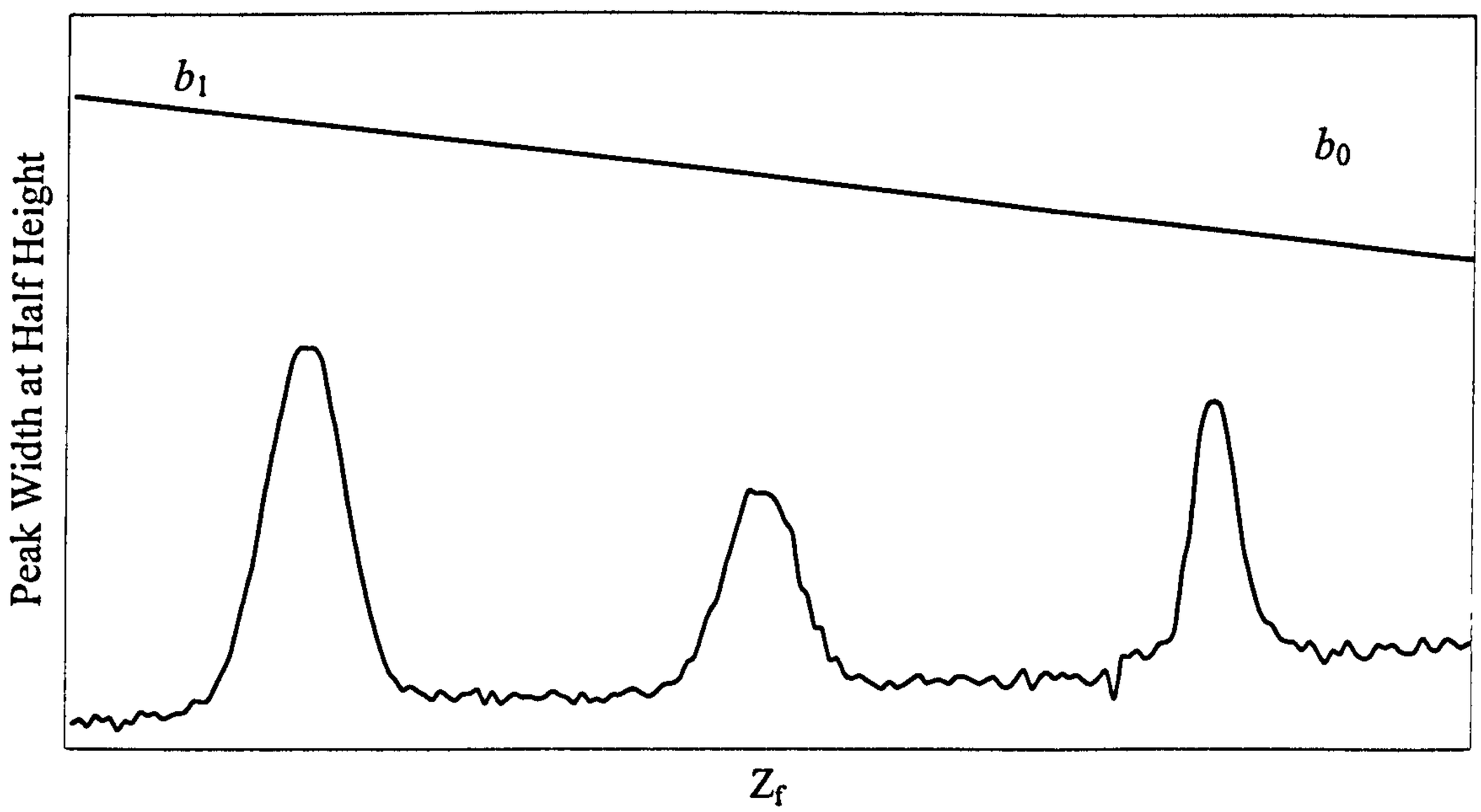

Figure 1.5 Typical change in peak width at half height as a function of migration distance on a HPTLC plate. The values for b_0 and b_1 are calculated by extrapolation using linear regression. (Adapted from Poole, 1998)

The real plate number, (N_{real}) and the real plate height (H_{real}) can then be defined according to the following equations

$$N_{real} = 5.54\left(\frac{z_x}{(b_x - b_0)}\right)^2 \qquad (1.17)$$

$$H_{real} = \frac{(b_x - b_0)^2}{5.54 z_x} \qquad (1.18)$$

This approach recognises the importance of the starting zone dimensions on the plate height value and provides a simple means to normalise plate height values using the b values calculated from linear regression. The value for N_{real} at $R_f = 1$ is not realisable in practice, since spots moving close to the solvent front are generally distorted and flattened in the direction of migration.

Ideally, to maximise N_{real}, b_0 should be small compared to b_1. In practice the extrapolated value for b_0 will generally exceed the value obtained densitometrically for the initial starting zone, due to the very rapid expansion and reshaping of the zone which occurs as the mobile phase first reaches the starting zone. In this region, the solvent velocity is high, uneven, and the sample requires a finite time to equilibrate with the mobile phase. The extrapolated value is then a more realistic value of the zone dimensions at the beginning of migration than the value recorded for the spot dimensions prior to contact with the solvent. The eventual spot width is independent of the initial spot size for spots about 1 mm in diameter (Fenimore, 1980). Thus, b_0 is determined by layer quality primarily and is always finite compared to the size of developed spots (generally < 5 mm).

The influence of the layer structure on the plate height can only be interpreted with the aid of a suitable model (Siouffi *et al.*, 1981). The treatment by Siouffi *et al.* assumes that the TLC plate has the properties of a normal column bed, the local plate height is described by the Knox equation (Knox, 1980), and that the velocity of the eluent is constant at all points in the layer at a given time with the velocity decreasing with time.

Equation 1.19 was then derived for the average plate height (Guiochon and Siouffi, 1978).

$$\bar{H} = \left(\frac{a}{Z_f - Z_o}\right)\left(Z_f^{2/3} - Z_o^{2/3}\right) + b(Z_f + Z_o) + \left(\frac{c}{Z_f - Z_o}\right)\log\left(\frac{Z_f}{Z_o}\right) \qquad (1.19)$$

The coefficients *a*, *b*, and *c* are functions of experimental parameters (Poole, 1988). The *c* term is rarely significant and can be neglected in most cases. The *a* term may be neglected for fine particle layers ($d_p < 10$ μm) but must be considered for coarse particle layers.

In a qualitative sense, equation 1.19 predicts that under capillary flow controlled conditions with fine particle layers, the plate height first passes through a minimum and then increases sharply for longer migration distances. For coarse particle layers the plate height is less dependent on the migration distance and eventually the two curves cross over, indicating that a greater number of theoretical plates can be obtained using coarse particle layers and long migration distances. This is illustrated in Figure 1.6.

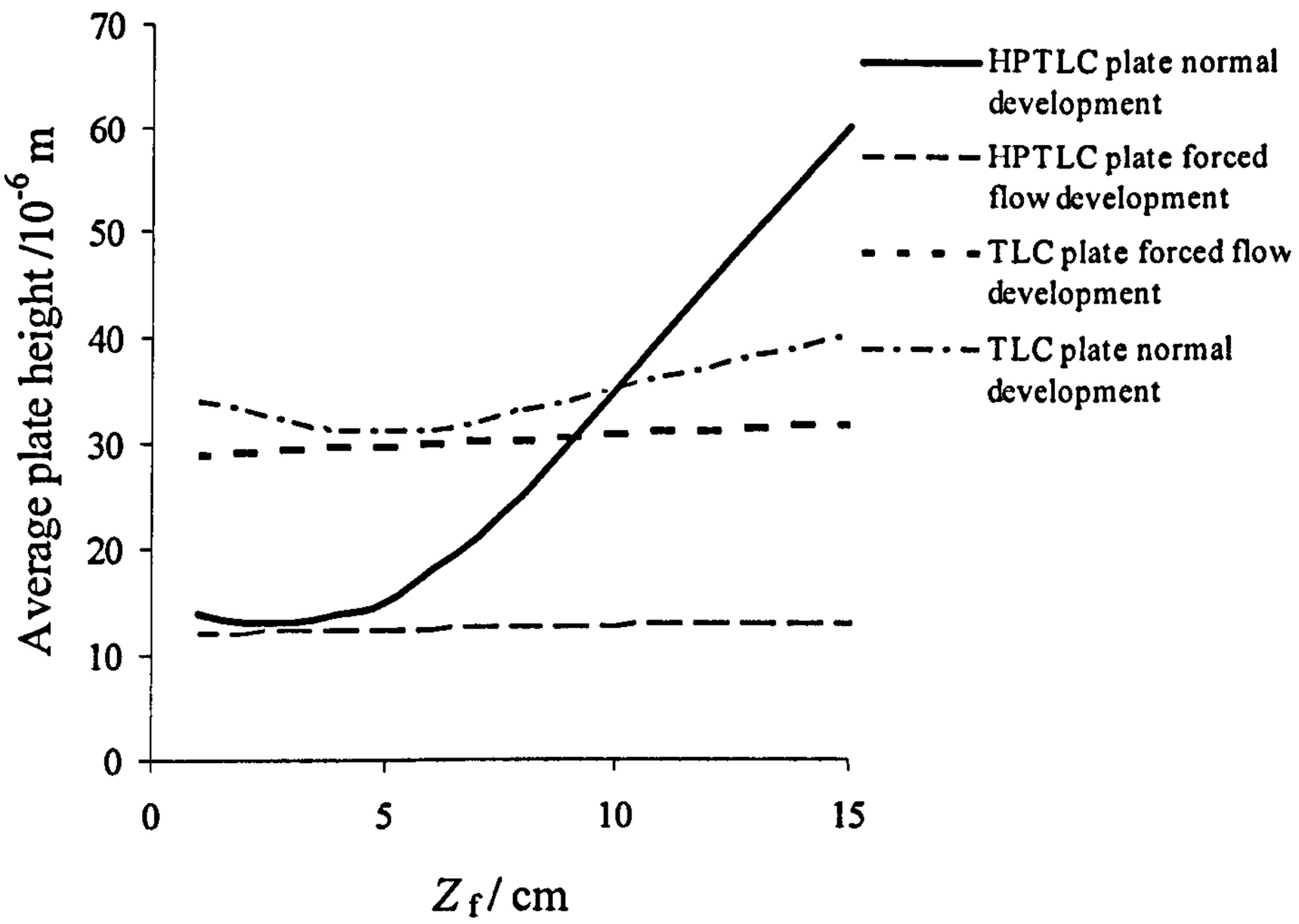

Figure 1.6 Variation of the average plate height as a function of the solvent migration distance. Adapted from Poole (1988).

This contrary finding is easily explained by the relative permeability of the layers. The mobile phase velocity for fine particle layers declines sharply with migration distance until eventually the zone broadening becomes diffusion controlled (the *b* term in equation 1.20). The coarse particle layer is more permeable (equation 1.13) and so the solvent velocity is higher for longer plate lengths and the efficiency is greater. For fine particle layers, 2,500 to 5,000 theoretical plates should be possible with a development length of about 5 cm. However, it will be difficult to exceed this number with capillary controlled development. For coarse particle layers a development length of about 15 cm will be required to obtain around 5,000 theoretical plates and although possible to exceed this number, in practice it is very difficult and leads to long separation times. TLC plates often have a wide particle size distribution and may provide only a fraction of the number of theoretical plates calculated theoretically.

In forced flow TLC the average plate height is largely independent of the migration distance and is smaller for fine than for coarse particle layers (see Figure 1.6 above). This arises from the control of mobile phase velocity by external force, overcoming the limitations of capillary flow where there is a quadratic decrease in mobile phase velocity with time. In forced flow development there is an optimum linear velocity for a fixed development length corresponding to a minimum plot of average plate height as a function of mobile phase velocity (Hauck and Jost, 1983).

This optimum value decreases with the migration distance and becomes approximately constant for migration distances exceeding about 25 cm. Compared with capillary flow controlled systems zone broadening by diffusion is now restricted to a minor role even for long migration distances, since the optimum mobile phase velocity is always higher than that observed for ascending development by capillary flow. The average plate height in forced flow TLC is approximately constant, so that the number of theoretical plates increases linearly with the solvent migration distance. Plate height values as low as 8 μm have been observed, corresponding to a limit of 31,000 theoretical plates for a substance migrating 25 cm (Poole and Poole, 1991). The ultimate efficiency of forced flow systems is limited only by the layer particle size, the available plate length and the pressure required to maintain the optimum mobile phase velocity.

1.1.8.6 Resolution and separation capacity

The resolution, R between two sample zones is defined as the ratio between the separation of the two zone centres and the average width of the zones. This is expressed in equation 1.20 (Snyder and Saunders, 1969; Poole and Poole, 1989)

$$R = \frac{d_z}{(W_1 + W_2)/2} \qquad (1.20)$$

where d_z is the distance between the zone centres, W_b the width of the zone at its base, and the subscripts 1 and 2 refer to the zones, numbered such that the larger number corresponds to the zone with the highest R_f value.

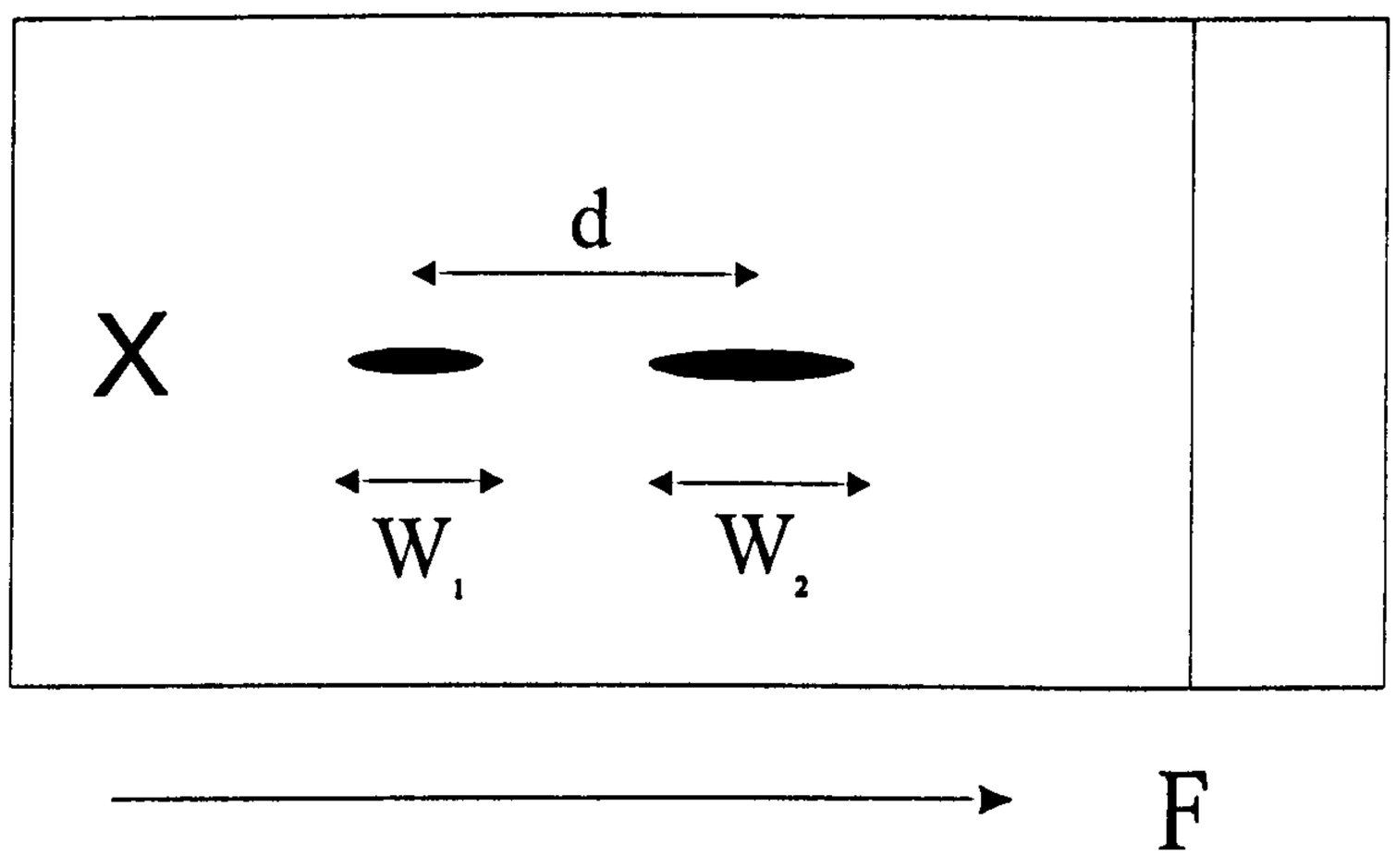

Figure 1.7 Chromatographic resolution determined from spots as the ratio of the separation of zone centres (d_z) to the average zone width (W_1 and W_2). Where X is the origin, F is the final solvent front position and the large arrow shows the direction of development.

It should be noted that retention parameters such as R_f are significant to only one component and are invariant in a given solvent system. Parameters such as resolution (R) are component pair specific.

.

The potential of a chromatographic system to provide a certain separation can be estimated from the separation number, SN, also referred to as the spot capacity. The separation number in TLC is defined as the number of spots that can be completely separated ($R = 1$) between $R_f = 0$ and $R_f = 1$ (Zlatkis and Kaiser, 1977). It may be calculated in an approximate form by equation 1.24 with b_0 and b_1 as defined in figure 1.5.

$$\mathrm{SN} = \left(\frac{(Z_f - Z_0)}{(b_0 + b_1)}\right) - 1 \qquad (1.24)$$

Models used to interpret separation number are not straightforward as the separation number is a complex function of various characteristics of solvent and layer as well as other parameters such as development length (Guiochon and Siouffi 1982). The results show that with capillary controlled flow it should be easy to achieve a separation number of 10 to 20, but it is extremely difficult to reach 25.

An analogy that describes the separation number envisages the chromatogram as being similar to a string of beads, each bead touching the next with no space on the string between them. The separation number is thus a high estimate of the real separation capacity, since real chromatograms do not normally consist of evenly spaced peaks. In general, unless the separation number exceeds the number of components in the sample by a significant amount the separation will be difficult to achieve. An alternative equation for resolution is

$$R = 0.25\left(\frac{\alpha - 1}{\alpha}\right)\mathrm{N}^{1/2}\left(\frac{k'}{1 + k'}\right) \qquad (1.25)$$

this equation shows that resolution is a function of three factors, selectivity (α), number of theoretical plates (N), and retention factor (k). Selectivity is related to the ability to separate zones (difference in R_f values), the number of theoretical plates measures zone spreading throughout the chromatographic system The retention factor describes retention of a component by the stationary phase (Snyder, 1971).

It can be seen clearly that for optimum resolution values of α and N should be large and that *k'* should be within its optimum range.

1.2 History of TLC development

1.2.1 Historical background

The term "chromatography" denotes a procedure in which a solution of substances to be separated is passed, in a direction determined by the arrangement of the apparatus, over a stationary phase, resulting in retention of the individual components to different extents. The underlying mechanisms are the partitioning of the moving compounds between the mobile and stationary phases and the reversibility of the process. If physical surface forces are mainly involved then the procedure is referred to as adsorption chromatography. In practice, a combination of adsorption and partition chromatography is usually involved, with one of the types predominating.

Adsorption chromatography was discovered by Michael Tswett (1903). Tswett found that plant pigments could be separated by filtering a solution of them in petroleum ether through a column of calcium carbonate. He noticed that different coloured zones were formed on the column.

The real development of adsorption chromatography began in 1931 when Kuhn and Lederer (Kuhn and Lederer 1931) introduced the method into preparative chemistry of pigments. The paper describes a separation of carotene and an isolation of α- and β-carotene.

Adsorption chromatography is primarily suitable for separating lipophilic substances. There was no chromatographic method suitable for separating hydrophilic substances until Martin and Synge (1941) introduced partition chromatography. They used silica gel columns containing definite amounts of water. The compounds were adsorbed on the column and then developed with suitable organic solvents. The mobile organic phase transported the compounds over the stationary aqueous phase and the transported

compounds were partitioned between the two phases. The Nobel Prize for Chemistry was awarded for this work in 1952.

The silica gel support was then replaced by strips of paper and so paper chromatography was invented (Consden *et al.,* 1944). A rapid development in paper chromatography followed after amino acids were successfully separated. It was possible to use milligrams of material for analysis instead of tens of grams required by classical procedures.

It was ten years or so before the limitations of paper chromatography were clearly recognised. Considerable difficulties are encountered when the method is applied to lipophilic substances, which are easily separated by the Tswett adsorption procedure. There was no generally applicable technique for analytical adsorption chromatography, although Izmailov and Schraiber (1938) had already described the principle of thin-layer chromatography (TLC). They dusted aluminium oxide onto glass plates and separated various substances on the loose layers. Meinhard and Hall (1949) were the first to use a binding agent (starch) to give the layers greater mechanical stability, in order to hold the stationary phase onto a microscope slide in this case. The procedure was developed further by Kirchner and Miller and its applicability to the separation and identification of terpenes was demonstrated (Kirchner *et al.,* 1951). Whereas these authors used narrow strips of glass (chromatostrips), Reitsema (1954) used wider glass plates (chromatoplates) on which several samples could be chromatographed side by side or two-dimensional chromatographs could be run.

Thin-layer chromatography was first introduced as a procedure for analytical adsorption chromatography by Stahl (1956, 1958, 1959 and 1961). He described a practicable device for preparing layers about 250 μm thick of a special adsorbent Kieselgel G (silica gel with a plaster of Paris binder).

The historical development of thin-layer chromatography (TLC) has been documented by Stahl (1969), and Jupille (1977) reviewed the principles, practice and potential of TLC with particular reference to high-performance (HP)TLC which was emerging as a technique with significant advantages over traditional TLC at about that time.

According to Kirchner (1973) the principle of TLC was first known in 1889 when the Dutch biologist Beyerinck allowed a drop of a mixture of hydrochloric and sulfuric acids to fall through a thin layer of gelatin. The hydrochloric acid travelled faster, forming a ring around the sulfuric acid.

Stahl first used the term 'thin-layer chromatography' in 1956, and in 1958 recommended standard conditions for the technique were published following production of special grade silica by Merck and the manufacture of basic equipment and accessories by Desaga (Stahl, 1983). TLC was used extensively as a quantitative technique up until and during the 1970s and continues to be widely used, principally for qualitative analysis by synthetic chemists. The instrumental development of gas chromatography occurred in parallel with further development of TLC, and the separating capacity of the fine particle size layers used in TLC stimulated attempts to pack tubular columns with these materials. Success with this led to the development of high-performance liquid chromatography (HPLC), a technique, which lends itself readily to automated instrumentation. The popularity of HPLC meant that in many areas it gradually replaced TLC during the 1980s. This is reflected by the large increase in publications referring to HPLC during this time (Lochmuller, 1987), and the tendency of some authors to ignore the current value and potential of TLC.

1.2.2 High performance thin layer chromatography (HPTLC)

Zlatkis and Kaiser edited a book on high–performance thin-layer chromatography, which helped to stimulate renewed interest in TLC (Zlatkis and Kaiser, 1977). In an article entitled "HPTLC: taking off", Borman (1982) described the differences between conventional and high-performance TLC. The main feature that resulted in the increased performance was the use of finer sized silica material with a much tighter particle size distribution (4-8 μm in HPTLC in contrast to 5-20 μm in TLC). The greater resolution obtained meant that shorter development distances were required to effect separation and hence the separation time was reduced along with solvent consumption. The thinner layer on HPTLC plates (typically 100 μm for HPTLC, 200 μm for TLC) has a smaller sample capacity than conventional TLC plates, thus to prevent overloading and to minimise spot spreading on sample application, smaller volumes are applied.

Various authors described the advances in instrumentation, mainly in sample application, plate development and quantification which occurred around 1980 (Fenimore and Davis, 1981). These increased the sample throughput of HPTLC and also the accuracy and precision of the technique. Many of these early reviews and a more recent review on modern TLC (Poole and Poole, 1989) emphasise the economy of HPTLC in terms of high sample throughput compared with HPLC.

1.3 Recent developments

1.3.1 Overpressured-layer chromatography (OPLC)

Recent advances in forced flow planar chromatography have been reviewed by Nurok (2000) and Nyiredy (2003). Both authors highlight the development of overpressured layer chromatography (OPLC) in which the mobile phase is forced along the chromatographic bed by an external pump as in HPLC. The technique may be operated in an online fashion (as in HPLC), in which the mobile phase is allowed to flow directly into a detector, or offline where the plate is dried after development and measured as in conventional TLC. The major advantages are the ability to operate at the optimum flow rate in order to improve efficiency and analyse complex mixtures (Botz *et al.,* 1990), the ability to develop several plates simultaneously in order to facilitate high throughput screening (Tyihak and Mincsovics, 1989), and the possibility of predicting column separations by using results from OPLC separations (Nyiredy *et al.,* 1990).

1.3.2 Electro-planar chromatography (EPC)

Nurok and Nyiredy also both described advances in electro-planar chromatography. Applying an electric field across a wet TLC layer containing ionised silanol groups and mobile ions results in an electroosmotic flow. In principle the electric field can be selected to yield an optimal flow velocity, which is independent of the distance travelled by the mobile phase and, under most conditions, the particle diameter. The expected plug flow profile should have a uniform cross sectional velocity and result in higher efficiencies than the laminar profile in a pressure driven system. These combined properties should yield a fast and efficient system when working with small particles

and a high electric field. The speed of the technique has been confirmed for normal phase chromatography, analysis time being twelve times faster than with conventional TLC (Howard, 1999). Separation in the reversed-phase mode was found to be two to three times faster (Nurok, 2000).

1.3.3 Enantiomeric separations

Separation of enantiomers has become a well-established technique in many fields over the last decade. The literature on enantiomeric TLC separations has recently been reviewed by Bereznitski *et al.* (2001). They commented that TLC has three major advantages. Firstly, the detection of analytes in TLC is more flexible than in HPLC, including techniques such as Raman spectroscopy (Koglin, 1994) and mass spectrometry (Busch, 1992). Secondly, sample throughput is higher in TLC than in HPLC and, thirdly, the possibility of using different types of interactions in 2-dimensional TLC can deliver excellent separations.

1.3.4 Ultra thin layer chromatography

The need for layers with smaller average particle sizes to improve performance and separation speed was identified by Poole in his review article "Planar chromatography at the turn of the century" (Poole 1999). Shortly after this monolithic HPLC column technology (Hjerten *et al.*, 1989) was applied to planar chromatography (Hauck *et al.*, 2001). In contrast to normal TLC or HPTLC plates, these layers are not based on granular adsorbents but have a monolithic structure based on a silica gel matrix, so there are no separate particles. Also, no binder is necessary to fix the layer onto the glass support. This new mode of planar chromatography was first described in 2001 (Hauck *et al.*, 2001); several qualitative separations were presented but no quantitative work. More separations were published in 2003 (Hauck and Schulz, 2003) along with some discussion of the advantages and drawbacks of the technique. A comparison of UTLC with other modes of planar chromatography is presented in Table 1.2.

The advantages of UTLC are high separation efficiency leading to short migration distances and short development times, along with low solvent consumption. Disadvantages are that the number of substances that can be separated in a short

distance is limited. This is largely because appropriate equipment has yet to be developed in order to get the best out of the plates; crucially, sample application of very small volumes, development chambers for very small plates and evaluation techniques with very high resolution.

Table 1.2 Comparison of different modes of planar chromatography (adapted from Geiss, 1987).

	TLC	HPTLC	UTLC
Typical layer thickness / μm	200	100-200	10
Sample application volume / nL	1000-5000	500-1000	5-20
Solvent migration distance / cm	10-15	3-7	1-3
Development time / min	15-200	5-30	1-6
Solvent consumption / mL	100	20	1-4
Average particle size / μm	10-12	5-6	-
Particle size distribution / μm	5-20	4-8	-

1.4 Development of CCD cameras

1.4.1 History of charge transfer devices

The term 'charge transfer device' is generally used to describe a family of solid–state devices which, when a sequence of pulses is applied to them, move quantities of electrical charge in a controlled manner across a semiconductor substrate. These devices, which include charge coupled devices (CCDs) and 'bucket brigade devices' perform a wide range of functions, which includes image sensing, data storage, signal processing and logic operations (Benyon, 1980).

In 1970, Boyle and Smith at the Bell Laboratories suggested that capacitors closely spaced on an isolated semiconductor surface could be used to store and transfer electrical charge (Boyle and Smith, 1970). When pulsed with voltages in a suitable

sequence, moving potential wells, each carrying packets of minority carriers, would be generated. The first CCD used as an optical device was announced in 1970 and consisted of just three aluminium electrodes, each 100 μm by 100 μm, separated by 3 μm gaps and deposited on an oxide film grown on an n-type silicon substrate (Amelio *et al.,* 1970). Soon after this, the first CCD with 8 bits readout was demonstrated (Tompsett, 1970 and 1972) as a simple linear image sensor and a few years later a 13,000 element CCD was produced for use as an image sensor for low-resolution television work (Sequin, 1974).

Throughout the 1970s there followed a rapid development of the CCD as a televisual sensor by the large semiconductor manufacturers, who recognised the potential of such a device. When mass-produced devices become available, scientists were quick to recognise this potential and developed systems using CCDs, particularly for astronomical applications where the low noise and high quantum efficiency could be exploited. This, together with the suitability of the sensor for computer acquisition of image data has meant that the use of these devices in the scientific world has grown considerably, with CCDs being used not only in ground-based equipment but also on space-borne ventures such as the Hubble telescope. Commercially, they are now widely used for TV and radio applications where they allow very compact camera systems to be built. Sweedler and Epperson reviewed the theory, design, operation, and analytical applications of CCD cameras in two related articles (Sweedler *et al.,* 1988; Epperson *et al.,* 1988). The earliest use of a CCD for spectroscopy was the evaluation of a linear detector for molecular absorption spectroscopy (Ratzlaff and Paul, 1979).

1.4.2 Operation of a charge coupled device

The CCD basically consists of a thin slice of silicon substrate covered by a two dimensional array of electrodes which are separated by oxide insulation layers. A cross section of a typical CCD is shown in Figure 1.8.

The electrodes are held at different potentials and, when the CCD is exposed, photons of light incident on the surface of the CCD pass through the electrodes and cause electrons to be generated in a doped depletion layer on the silicon substrate. These electrons are held in position by the applied voltages on the electrodes and are stored in potential wells. This active part is called the channel and is surrounded by inactive channel-stop regions

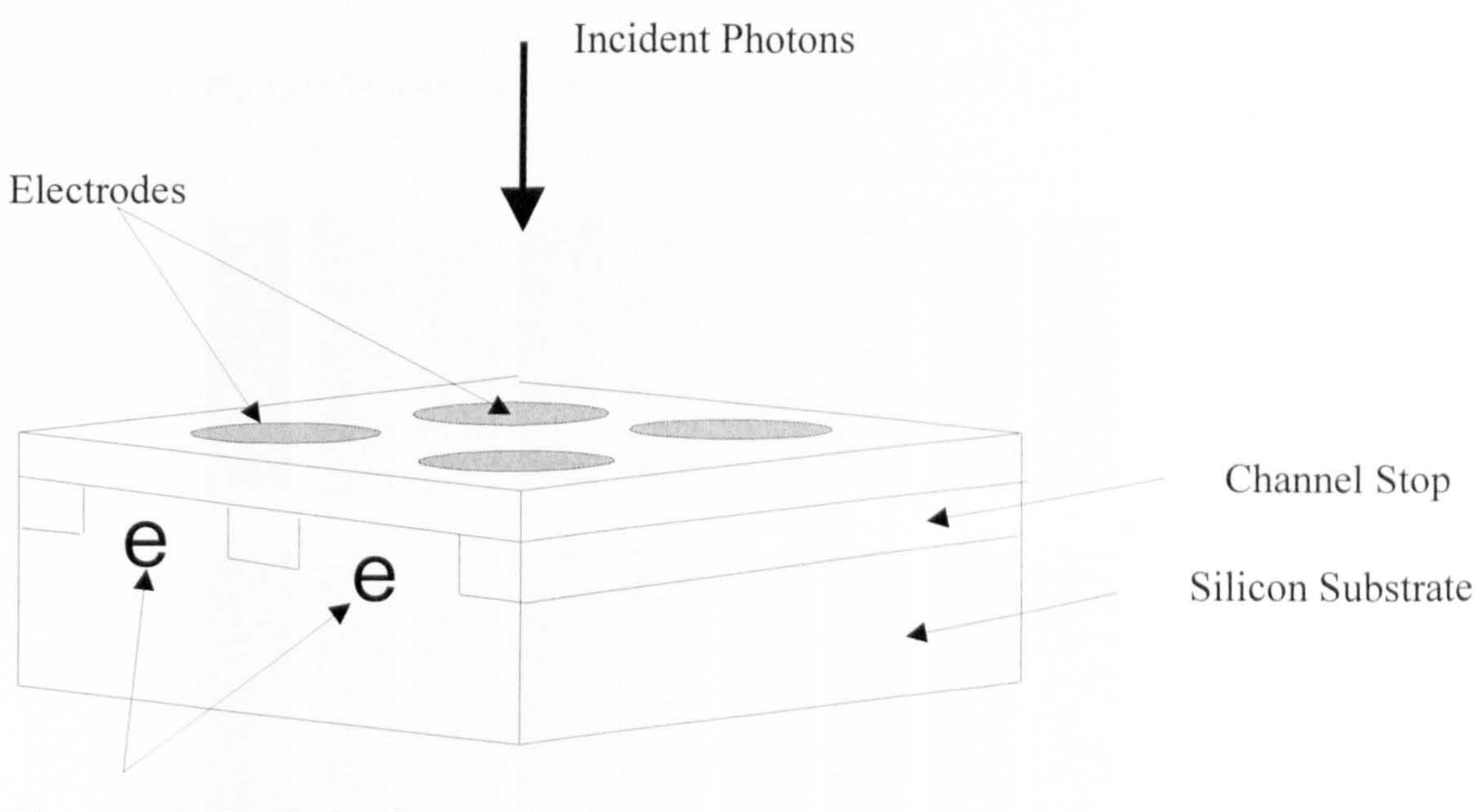

Figure 1.8 Cross section of CCD

After the CCD has been exposed to light, the accumulated charge in each potential well is then transferred (or coupled) to adjacent electrodes by altering their relative potentials. In this way the charge pattern, corresponding to the pattern of intensity of light, may be moved along the CCD array and into an output register and amplifier for digitisation.

A common type of CCD is known as a 'three phase CCD'. In this type of CCD the silicon is covered with three sets of electrode strips, each set of electrodes being isolated from the substrate and from one another. One of the three electrodes is biased more positively than the other two, and it is under this one that the generated electrons are accumulated.

The electrons are restrained from moving along the length of the electrode by channel stops, which are regions of heavily doped material. Their negative charge repels electrons and prevents movement across the stop. This defines the pixel extent in that direction as illustrated in Figure 1.9

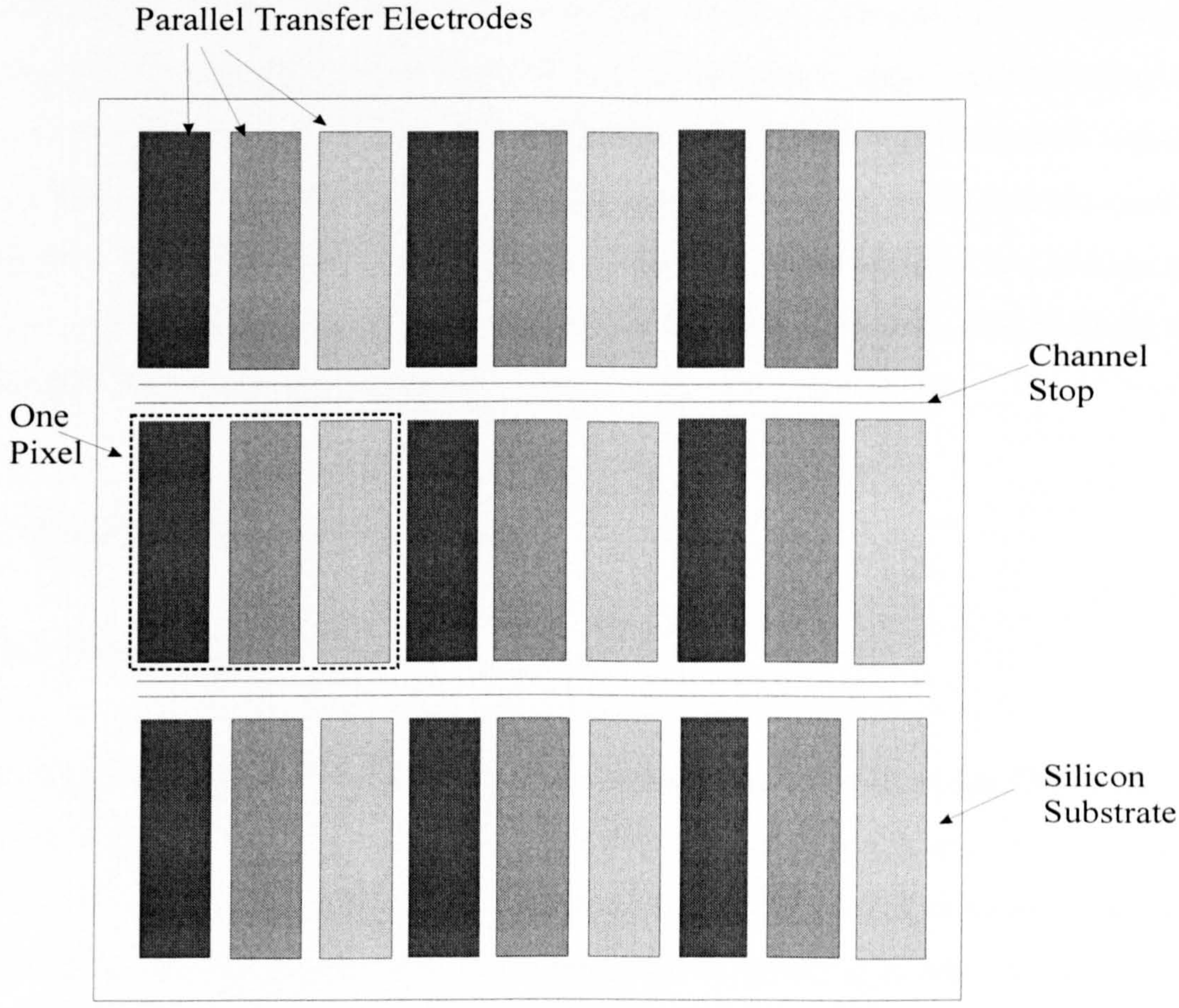

Figure 1.9 Layout of a three-phase CCD

1.4.3 CCD readout

The electrodes are grouped into two sections; the image and readout section used to transfer the charges in each line to a charge detection amplifier, which converts the charge into a voltage for output to external circuitry. The electrodes are constructed

from polycrystalline silicon, which is semi-transparent to light. An image is focussed onto the image section, and photons penetrate the electrodes, generating electron-hole pairs in the silicon substrate underneath. The electrons diffuse to the nearest biased electrode where they are collected as signal and the holes diffuse down into the substrate where they are effectively lost. Therefore, the quantity of charge collected is proportional to the local light intensity and the collection time.

Following this collection, or integration, period, all the separate charges that have been collected in the image section are transferred up one line by applying drive pulses to the electrodes in the image section. The top line gets transferred into the readout register. This line of charges is transferred sequentially by the read-out pulses into the on-chip charge detection amplifier where it is converted from a charge signal to a voltage signal for external output. The next line is read out in the same way, and so on, until the whole charge pattern has been transferred.

1.4.4 Characteristics and limitations

1.4.4.1 Resolution

The resolution of a CCD is determined horizontally by the element spacing of the charge transfer columns (as defined by the channel-stop regions), and vertically by the centre-to-centre spacing of the CCD elements. It should be noted that any image detail that has a spatial frequency close to the sampling frequency (e.g. lines that have similar distances to the horizontal or vertical element spacing) can give rise to intensity modulations on the displayed image in the form of 'beating' between the two frequencies, commonly called 'alias' or 'moire' patterns. These arise because the maximum and minimum intensities do not always coincide fully with a sensor element. This is a fundamental limitation of all solid-state image sensors that have discrete elements, and there is unfortunately no solution at present to this problem (Burt, 1980).

1.4.4.2 Optical response

The range of light levels over which a CCD sensor operates is dependent on the quantum efficiency, a measure of the light-to-charge conversion process, the signal handling capability and noise of the device once the charges have been generated. Quantum efficiency is defined as the mean number of free electrons created by one photon incident on the detector. A quantum efficiency of 100% means that an electron-hole pair is generated for every incident photon. For a CCD, only those photons that penetrate the electrode layer will contribute to the signal; losses will occur because of optical interference, reflection and absorption in the electrode layer. Loss of response occurs at both ends of the spectrum: at shorter wavelengths (towards the blue) because of absorption in the electrodes, and at longer wavelengths (near infra-red) because the electrons are generated too deeply for collection. Figure 1.10 shows the typical quantum efficiencies of types of CCD sensors

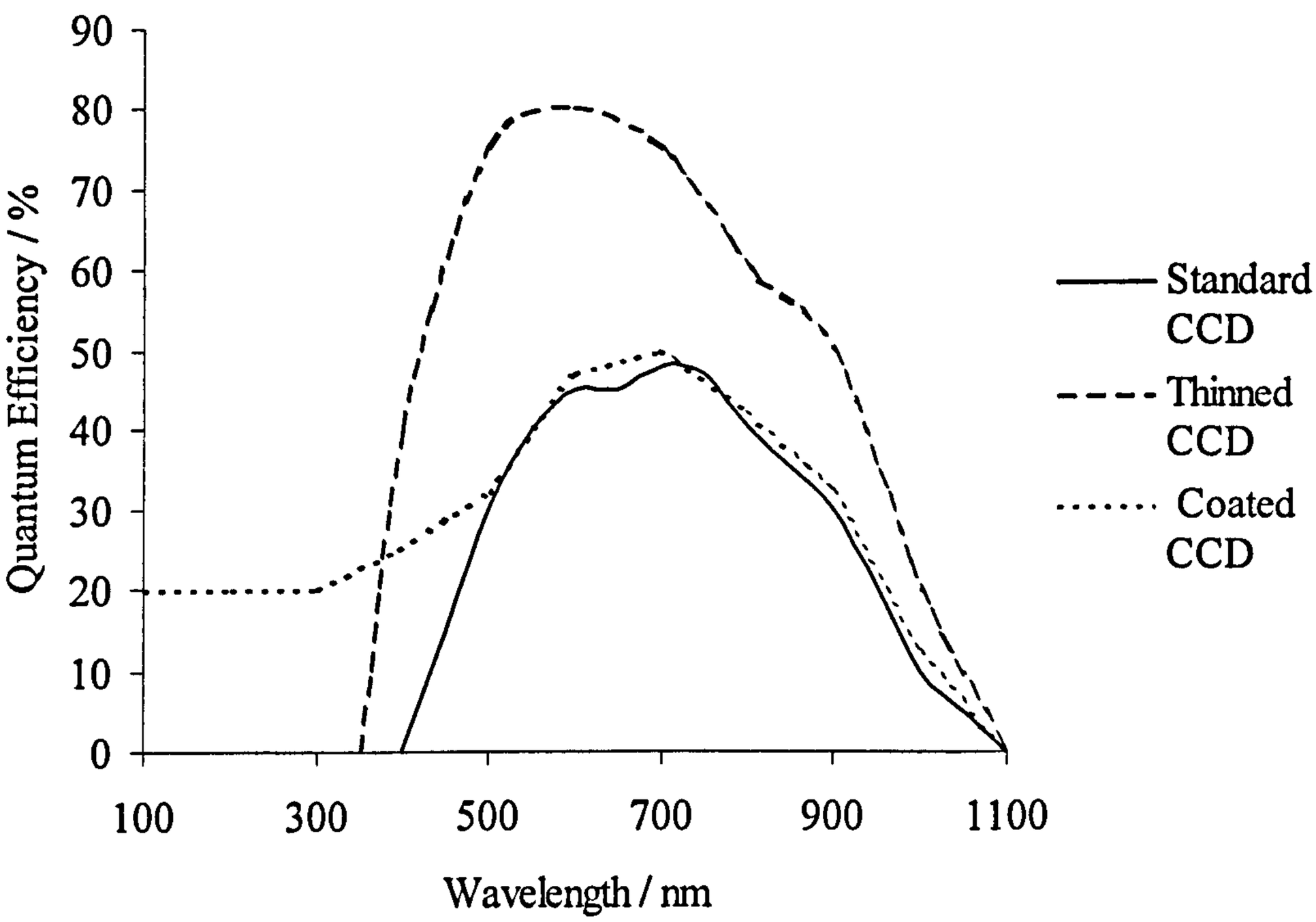

Figure 1.10 Typical quantum efficiencies of CCD sensor types as a function of wavelength. (AstroCam Ltd, 1995)

The optical response at lower wavelengths may be enhanced in two ways. Firstly, by use of a back-thinned CCD chip and back illumination, the photons do not have to pass through the covering electrodes so a much higher efficiency is achieved, especially in

the blue region. The second method is by use of a phosphor coating, which typically absorbs strongly between 90-480 nm and emits green light at around 560 nm, extending the sensitivity of the CCD at approximately 15% quantum efficiency over the region covered by the coating. These coatings (e.g. coronene) were first developed for use with space telescopes (Blouke *et al.*, 1980).

1.4.4.3 Dark current

This effect arises from the thermal generation of electrons that accumulate in the CCD and add directly to the image signal. A typical figure for this dark current is 1 % or less of the peak signal level. The resulting fixed pattern noise tends to set a minimum light intensity below which imaging is not practical at room temperature. If the device is operated at lower temperatures, however, the dark current noise can be reduced significantly, thereby facilitating better detection limits. Cooling to temperatures readily achieved with thermoelectric cooling (-20 to -40 °C) reduces the dark current by 100-1000 fold (Table 1.3) At this level other noise sources become significant and further cooling is not usually worthwhile unless both the lowest dark current and high full well capacity are necessary (Kim, 1980).

Table 1.3 Dark Current at different temperatures.

Operational mode	Temperature / °C	Dark Current / electrons $pixel^{-1}$ s^{-1}
No active cooling	20	10,000
Thermoelectric air cooled	-40	10
Thermoelectric water cooled	-60	1
Liquid N_2 cooled	-130	< 0.001

1.4.4.4 Charge transfer efficiency

The basic limitation on a CCD performance is how effectively it can transfer a charge from one potential well to the next. Ideally, the charge should remain until the clock

pulses are altered, and then transfer instantaneously and completely to the next potential well. Due to the dynamic structure of the device, incomplete transfer occurs, so that a small amount of charge is left behind each time. This effect is cumulative, and after many transfers the charges becomes significantly smeared together. This limits the number of transfers that can be executed. Typically 3000 transfers can take place without significant loss, a typical value for charge transfer efficiency being 0.99999 (Buss *et al.*, 1980).

1.4.4.5 Linearity

Photons are absorbed in the CCD and generate electrons that are held in place by the voltages applied. Once an electron has been generated there is nowhere for it to go or be lost to. The absorption of other photons is unaffected by the charge already present so the CCD is intrinsically a linear device. That is to say that as the exposure time is increased the output signal goes up in exactly the same proportion as the exposure. Two parts of an image with a certain brightness ratio will be detected with that same ratio over a wide range of exposure times (Buss *et al.*, 1980). Linearity will eventually break down once the CCD reaches saturation, typically 500,000 electrons per pixel for 25 μm pixels (Robson *et al.*, 1993).

1.4.4.6 Dynamic range

The dynamic range of a detector is defined as the ratio of the largest signal, which the detector can handle to the readout noise in a single exposure. Typical values are 500,000 and 5 electrons respectively. This gives a dynamic rage of 10^5. Cooling the CCD and reading it out slowly dramatically reduces the minimum noise level but has no effect on the maximum signal that the CCD can store (Buss *et al.*, 1980).

1.5 Detection in TLC

1.5.1 Basic requirements

Manual inspection of a TLC plate is capable of detecting approximately 1-10 μg of coloured material with a reproducibility of around 10-30 %. Removal of separated spots, eluting the substance and measurement by photometry are too time consuming and inaccurate to be used as a reliable analytical technique. Instrumentation for direct reading of TLC plates was first introduced in the 1960s, and *in situ* measurements are now considered essential for the accurate determination of both spot size and location, for a good measure of resolution and for rapid, accurate quantification. Modern densitometers have evolved into sophisticated, automated, computer controlled devices.

There are two categories of methods for the quantitative evaluation of thin-layer chromatograms. In the first category, analytes are measured directly on the layer. In the second approach, analytes are eluted from the sorbent layer before being examined further.

The requirements are more stringent for various aspects of TLC when quantitative measurements are to be made. Here it is critical that application of samples is carried out accurately and precisely (Brain and Turner, 1971). The development step should completely separate the compound of interest, and there should be no loss of substance by evaporation, decomposition or irreversible adsorption during application, chromatography or drying. Samples and standards are always chromatographed simultaneously, on the same plate.

In situ methods of quantification are always based on instrumental measurement of spots directly on the sorbent layer. The samples should be spotted within an optimum concentration range that provides maximum sensitivity consistent with the greatest linearity of response. It is best to apply the same volumes of differing concentrations, so that all initial zone areas are as compact as possible (Poole *et al.*, 1986). *In situ* determination requires that a separated zone should contrast with the background of the layer, and a detection reagent may be applied if this is not naturally the case.

1.5.2 Scraping and elution

Quantification can be carried out after scraping separated analyte zones from the sorbent bed. The scraped sorbent is collected and then eluted and measured. Collection and elution must be complete if reliable quantitative measurements are to be made: however, often the area to be scraped is not obvious.

The eluates from scraped zones can be analysed by any appropriate method, e.g. titration, gas chromatography or spectrophotometry. Ultraviolet, visible or fluorescence spectrophotometry is often used. However, for each of these modes densitometry can be carried out directly on the plate and the analyte will usually be more concentrated on the plate than in a cuvette. A further disadvantage of scraping and elution is that this approach is labour intensive and subject to error, by irreversible adsorption for example.

Automated elution systems have been developed in which analytes are eluted directly from the plate through plastic tubing and collected into cells. This technique is mostly used for preparative applications.

1.5.3 *In situ* densitometry

Densitometry is the instrumental measurement of UV or visible absorbance, fluorescence, or fluorescence quenching directly on the sorbent layer. Measurements can be made either through the plate (transmission), by reflection from the plate or by both simultaneously. All optical methods for the quantitative evaluation of TLC separations are based upon measuring the difference in optical response between a blank portion of the plate and regions where a separated substance is present.

Measurements in transmission mode provide greater peak heights (up to a factor of two) accompanied by higher baseline noise when compared to reflectance (Coddens *et al.*, 1983). In reflectance mode most of the scattered light arises from layers close to the surface and is influenced less by changes in the thickness of the TLC plate, which is responsible for much of the background noise in transmission measurements.

Transmission measurements are generally limited to wavelengths greater than 320 nm due to strong absorption by the glass support and also by the silica gel itself at even shorter wavelengths. Reflectance measurements can be made at any wavelength from `the UV to the near infrared (185-2500 nm).

UV-absorbing compounds can be measured by fluorescence quenching as well as by reflectance. The fluorescence quenching technique provides a means of visualising spots absorbing UV light on TLC plates incorporating a fluorescent indicator. When such a plate is exposed to UV light, the UV-absorbing compounds appear as dark spots against the brightly fluorescing background of the plate. These UV-absorbing spots behave similarly to an optical filter, absorbing a portion of the fluorescence excitation radiation, thus diminishing the fluorescent intensity. The fluorescence quenching method is only applicable to substances whose absorption spectra overlap the excitation spectrum of the fluorescent indicator. The indicators in common use have a maximum absorption around 280 nm and almost no absorption below 240 nm. Fluorescence quenching methods are thus less specific and less sensitive than absorption measurements. Fluorescence quenching is mainly utilised as a visualisation technique in qualitative analysis.

1.5.4 Theoretical considerations

When light falls on an opaque medium, some light is reflected from the surface, some absorbed by the medium and dissipated (e.g. as conversion to heat), and the remainder is diffusely reflected or transmitted by the medium. It is the diffusely reflected or transmitted component that is of interest when making quantitative measurements. It must be assumed that the specularly-reflected component (from the surface of the layer) is small. The specularly-reflected component contributes to the background signal (noise) but carries no information regarding the properties of the sample. The propagation of light within an opaque medium is a very complex process (Huf, 1988; Bush and Greeley, 1984). The theoretical treatment most generally applied is that of Kubelka and Munk (1931), which is often expressed in the following form

$$\frac{(1-R_i)^2}{2R_i} = 2.303a\frac{c}{S} \qquad (1.26)$$

where R_i is the reflectance for an infinitely thick opaque layer, a is the molar absorption coefficient of the sample, c the sample concentration, and S the scatter coefficient of the layer. Equation 1.26 is only an approximation for thin layer plates, since it is derived from a situation involving a layer of infinite thickness. However, it illustrates the general properties of a solid sorbent matrix on the observed sample response and explains why calibration curves on TLC plates do not obey the Beer-Lambert law. The work of Kubelka and Munk predicts a non-linear relationship between signal and sample concentration in the reflectance mode, an increase in response with increasing molar absorption coefficient, and an increase in response for sorbents having low scatter coefficients. Since equation 1.26 is only approximate it is not used directly for quantitation in TLC.

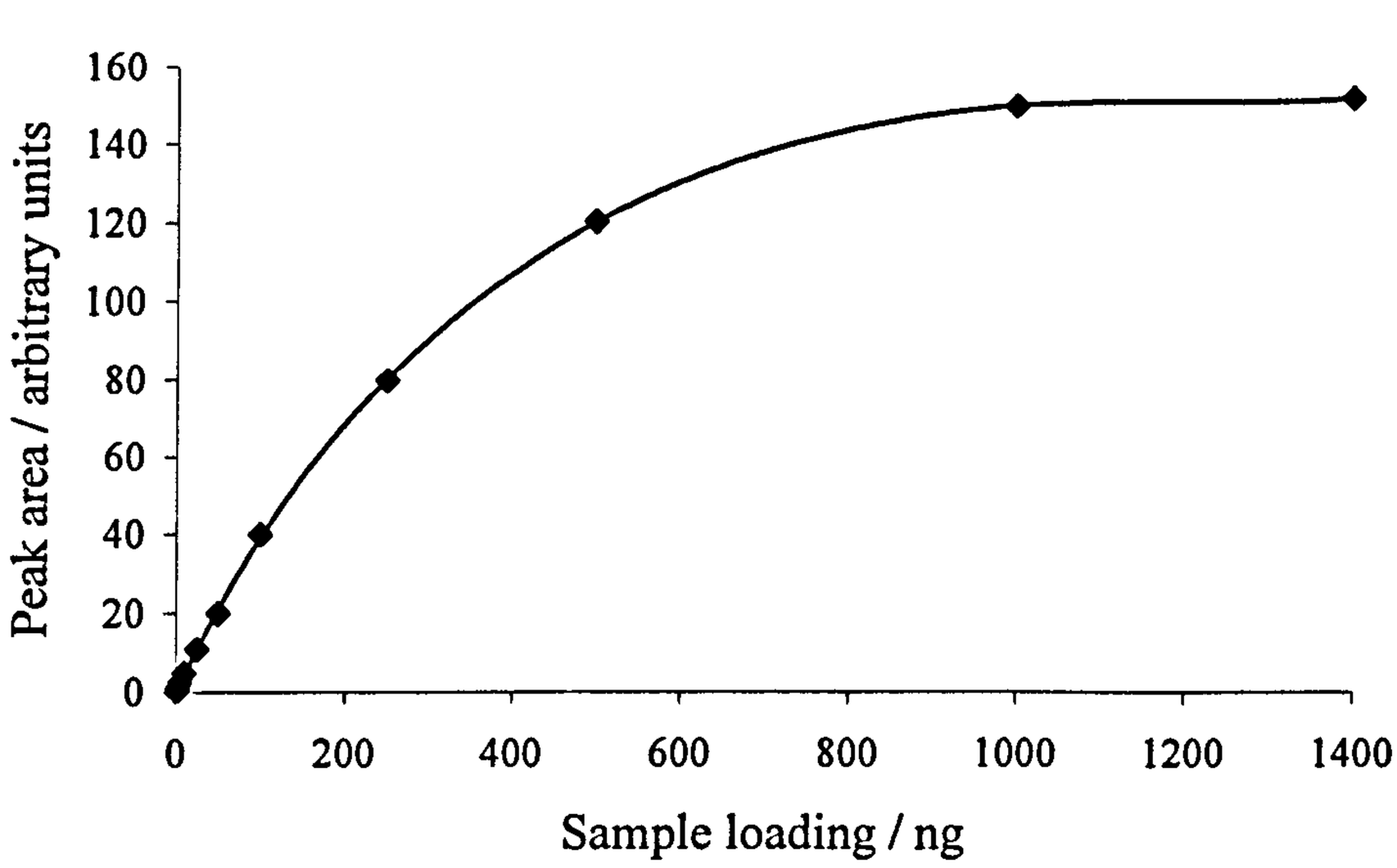

Figure 1.11 A typical calibration curve obtained from a thin-layer chromatogram

The principal method of quantitation is by calibration using a series of standards spanning the concentration range of the sample to be determined. Peak area measurements are usually used for calibration. Calibration curves generally comprise an

effectively linear region at low sample loading, curving towards the loading axis at higher sample loading, and eventually reaching an asymptotic value where signal and sample loading are no longer correlated. An example is given in Figure 1.11

The extent of the individual ranges or sections of the calibration curve are frequently very different for different substances and often the pseudo-linear portion of the curve is adequate for most analytical purposes. However, sometimes no suitable linear range might exist. This lack of linearity in calibration curves has given rise to the use of several mathematical transformation techniques in order to linearise the non-linear parts of the calibration curves (Treiber, 1974; De Speigeleer, 1985). Typical examples include the conversion of the correlation between signal and sample loading into relationships involving reciprocals, logarithms, squared terms (Betheke and Frei, 1974) or use of the Michaelis-Menten function (Ebel, 1984). None of these methods has a sound theoretical basis for the treatment of thin-layer chromatography calibration curves and all can lead to the propagation of significant errors in the transformed data. Alternatively a non-linear regression based on a second order polynomial could be used to describe the calibration curve without inappropriately weighting error distribution.

1.5.5 Scanning densitometry

Instruments for scanning densitometry using absorbance or fluorescence measurements in reflectance or transmission modes first appeared in the 1960s (Jork, 1962) and since then have undergone continuous evolution (Fenimore and Davis, 1981; Geiss, 1987). The most obvious technical change has been the greater use of computers, which have revolutionised data handling whilst also permitting a greater degree of automation of the scanning process.

Commercial instruments share many common features. Different lamps must be used as light sources in order to cover the entire UV-visible range from 200 to 800 nm. Tungsten halogen lamps are generally used for the visible region and deuterium lamps for the UV region. High intensity mercury or xenon arc sources are preferred for fluorescence measurements. For polychromatic light sources, the measuring wavelength is normally selected by using either a monochromator or a filter. Filter densitometers often employ a mercury line source and filters to pass only the light corresponding to

individual lines available from the source. Their main advantage is low cost. Broad spectral sources and grating monochromators offer greater versatility for optimising sample absorption wavelengths.

Two optical geometries are predominantly used in contemporary scanning densitometers. The single-beam mode is the simplest optical arrangement and is capable of producing excellent quantitative results, but problems can arise due to background noise resulting from fluctuations in the source output, inhomogeneity in adsorbed impurities on the plate, along with irregularities in the plate surface. Background disturbances can be compensated for, to some extent, by double-beam operation. The two beams are usually separated in time at the same point on the plate.

In the single-beam dual-wavelength mode, fluctuations caused by scattering at the light-absorbing wavelength are compensated for by subtracting the fluctuations at a different wavelength at which the spot exhibits no absorption but experiences similar scatter (Yamamoto *et al.*, 1976; Cheng and Poole, 1983). The two beams are alternated by a chopper and combined into a single beam to provide the difference signal at the detector. Since the scatter is normally wavelength dependent, the background correction is best when the measuring and reference wavelengths are as close together as possible. This requirement is often very difficult to fulfil, since absorption spectra are usually broad, and it may be impossible to find two similar wavelengths at which absorption occurs for one and not the other.

The sample beam is usually in a fixed position and the plate is scanned on a computer-controlled moving stage. The most common method of scanning is slit scanning in which the sample beam is shaped into a rectangular area on the plate surface through which the plate is transported, usually in the direction of development. Each scan thus represents a lane with length defined by the sample migration distance and width determined by the slit dimensions. As well as slit scanning, point scanning can also be used. The measuring beam is shaped into a spot or rectangle of dimensions much smaller than the chromatographic zones to be scanned. By moving the scanning stage in the x and y directions a zig-zag or meander scan is possible. Zig-zag and meander scanning allow zones of any shape to be accurately quantified using computer alogrithms to perform the integration. For very small spots errors may arise because the

scanning beam dimensions cannot be made sufficiently small to permit a large enough number of sampling points for the spot.

For linear slit scanning densitometers it is well established that chromatographic resolution and detectability can be affected by the choice of slit dimensions, the scan rate, and the electronic time constants of both the scanner and recording device (Coddens and Poole, 1983; Butler and Poole, 1983; Poole *et al.,* 1985; Butler *et al.*, 1983). The ratio of slit height to spot diameter has a large influence on sample detectability in the absorbance mode. Slit heights less than the diameter of the spot result in the highest sensitivity but may lead to unacceptable errors due to incorrect alignment of the sample beam and spot centres along the lane. Generally, a slit height equivalent to the diameter of the largest spot to be scanned is selected as a compromise. At high scan rates resolution can be impaired and the signal attenuated if the time constant of the processing device is too long. A standard protocol has been suggested for comparing the sensitivity of slit scanning densitometers based on the use of standard substances, chromatographic conditions, and instrument parameters (Coddens and Poole, 1983; Allwhon and Ebel, 1989).

Most modern densitometers are designed for automatic scanning of a complete plate. Normally, the values for the lanes to be scanned (lane length, distance between lanes, number of lanes, wavelength(s) to be scanned) are entered into a computer. The densitometer then scans the plate without further intervention. The disadvantage of this method is that if the samples have migrated irregularly then the spots may become misaligned with respect to the beam position and erroneous results may be generated. More sophisticated instruments have the ability to realign the measuring beam when necessary for the first spot in each lane prior to scanning in a linear manner, execute a meander or zig-zag scan or optimise the beam and spot co-ordinates for each spot in the chromatogram.

The principal sources of error in quantitative TLC have been identified as the reproducibility of sample application, the reproducibility of chromatographic conditions, the reproducibility of positioning the sample spots in the measuring beam, and in the detection step the reproducibility of the scanning densitometry measurements (Ebel and Glaser, 1979; Allwohn and Ebel, 1989). The measurement error can be

determined by repeatedly scanning a single lane of the TLC plate without changing any of the experimental conditions between scans. It is composed of errors due to the optical measurement, electronic amplification, and the recording device. The measurement error is dependent on the signal-to-noise ratio but for a properly adjusted instrument typical values fall into the range of 0.2-0.7% RSD (Ebel and Glaser, 1979). The error in positioning the spot in the measuring beam and the sample application error can be controlled to a large extent by good analytical practice. The chromatographic error is generally the most significant error and is only reduced by minimising the variability in the development process. The data pair technique can be used to minimise errors due to migration differences as a result of edge effects, deviations in layer thickness, nonlinear solvent fronts etc (Betheke *et al.,* 1974). In this technique an internal compensation approach is used, pairing up the measurements of two spots on the same plate. In modern scanning densitometry with HPTLC plates the relative standard deviation from all errors can be maintained below 2%, making it a very reliable quantitative tool.

Most scanning densitometers make provision for automatically recording the *in situ* spectra of any desired number of spots (Allwohn and Ebel, 1979). For automatic spectrum recording a motor-driven monochromator controlled by a microprocessor is often used. The band pass of most monochromators used in scanning densitometers is in the range 10-30 nm, so that the resultant low-resolution absorption spectra obtained are in themselves rarely sufficient for substance identification. Also, differences between the sorbent spectrum and the solution spectrum (which is more likely to be available for comparison) can be significant.

It is less time consuming to scan a separation sequentially at several different wavelengths than to record the full spectrum of each spot (Butler and Coddens, 1984). The ratios of the response values obtained at these pre-selected wavelengths can be used to confirm the similarity between samples and standards or to indicate contamination of sample spot with other components. If standards are run on the same plate with the samples then the reproducibility of absorbance ratios should be reasonable (1-6% RSD) (Lee *et al.,* 1980). Combining the information from similar retention characteristics of samples and standards on the same plate and acceptable agreement between the absorbance response ratios is the most widely used technique for *in situ* substance identification in TLC.

1.5.6. Diode array detection

A diode array consists of a number of photosensitive diodes place side by side and insulated from one another. The output from each diode can be scanned, stored and subsequently processed by a computer. The common use of a diode array is to monitor light that has passed through a liquid sensor cell as in a liquid chromatography detector. The light source is usually polychromatic (e.g. light from a deuterium lamp) and after passing through the cell, the light is dispersed by a quartz prism or a diffraction grating onto the surface of the diode array. Thus, each diode will receive light of a different wavelength to that received by its neighbour. The quality of the measured spectra is excellent (Spangenberg and Klein, 2000).

1.5.7. Development of image analysis or video densitometry

Slit scanning densitometry is the dominant method of recording thin layer separations for quantification (Poole and Poole, 1989). This is now a mature technology and evolution of slit scanning densitometry is progressive and major changes in operation and performance are unlikely with the possible exception of using fibre optics for illumination of zones and collection of light (Spangenberg and Klein, 2000; Spangenberg *et al*, 2002; Ahrens *et al*, 2002). This approach may improve the quality of available data, but does not overcome the principal limitations of scanning densitometry. A major difference between scanning and video densitometry is that whilst scanning densitometry is a stable technology, image analysis is rapidly evolving, driven by its broad applicability to many areas of science, of which thin layer chromatography is a minor component of the market. Thin layer chromatography will almost certainly benefit from developments in other areas of science and from reduced costs of CCDs.

Major improvements may be realised through image analysis, also known as video densitometry, which was first demonstrated in 1976 (Ebel and Hocke, 1976). In video densitometry optical scanning takes place electronically, using a computer with video digitiser, light source and appropriate optics to illuminate the plate and focus the image onto a charge-coupled device (CCD) video camera (Cosgrove and Bilhorn, 1989; Vovk and Prosek, 1997; Ebel and Henkel, 2000). The principal advantages of video densitometry are fast and simultaneous data acquisition from the whole plate, absence

of moving parts, increase in sensitivity by using longer acquisition times, simple instrument design, and compatibility with data analysis of two-dimensional chromatograms that are difficult to scan using conventional slit-scanning densitometers. The ease of storing images electronically as a replacement for photographic documentation and of pasting images into documents is another attractive aspect of video densitometry. Modern instruments provide user-friendly archiving, searching and integration of images (Hahn-Deinstrop *et al.,* 1998; Summanen *et al.,* 1998).

Many groups have reported the use of video densitometry for absorption (Gianelli *et al.,* 1983; Belchamber *et al.,* 1987; Pollack and Schulze-Clewing, 1990; Garcia Sanchez *et al.,* 1993) and fluorescence measurements (Gianelli *et al.*, 1981). A video densitometer was constructed in 1990 which gave better linearity, reproducibility, spatial resolution and enabled faster acquisition than scanning densitometry (Oldham, 1990). Degitar and co-workers used a video system for capture and documentation of images of TLC plates and made a database of the captured images (Degitar *et al.*, 1994). Liang *et al.* (1996) introduced a new CCD-based imaging system for quantitative determination of substances separated on HPTLC plates and showed that the fluorescence background and noise from the plates limited detection.

Slit scanning densitometers and image analysis systems for quantification of TLC separations have been compared by several groups. All the papers report the excellent archiving facility and rapid acquisition of data as advantages of video densitometry. Rapid data acquisition is especially important when there are many samples on one TLC plate. Early CCD systems were expensive and the necessary processing power to fully utilise the technique was not available (Belchamber *et al.,* 1987). Vovk and Prošek (1997) compared slit scanning and video densitometry in reflectance and transmission; slit scanning was found to be more sensitive but video densitometry was found to have a larger dynamic range due to more information being available from inside the layer.

Using a fluorescence quenching method to detect phenolics, Summanen *et al.* (1998) found that there was no significant difference in repeatability between a dual wavelength densitometer and a CCD camera. However, Essig and Kovar (1999) compared video densitometry unfavourably with slit densitometry. They found that the LOD was better with slit scanning (approximately 25 ng) compared with video

densitometry (approximately 35 ng), and the repeatability was also better using slit densitometry.

Simonovska and co-workers used direct fluorescence measurements for the determination of norflaxin (LOD 5 ng) (Simonovska *et al.*, 1999). Test solutions were analysed using the TLC method (using both video and slit densitometry) and with a known HPLC method; comparable accuracy and precision was found in all cases. The linear range was comparable for the HPLC method and slit scanning (10-90 ng). The poorer linear range for video densitometry contrasts with the findings of Vovk and Prošek (1997) in reflectance and transmission measurements.

Video densitometry was performed using a conventional flat bed scanner and commercial software (Mustoe and McCrossen, 2001). Linearity, precision and detection limits were studied for test dyes. The results were compared with those from slit densitometry and it was shown that the two methods gave similar precision but the flat bed scanner had a broader linear range and better sensitivity for the compounds studied.

1.6 Aims and objectives

The aims of this thesis fall into three main categories; (i) to carry out quantitative measurements on wetted thin layer chromatography TLC plates, (ii) to undertake real time imaging of TLC separations, and (iii) to use a CCD camera for UV imaging of TLC separations offline and in real time.

In previous work TLC plates have invariably been imaged dry (Stahl and Mangold, 1966), after the solvent has been evaporated. The main objective of the first part of this work is to find out if it is possible to get quantitative results from a wetted plate using a CCD camera in either reflectance or transmission modes. This will be attempted by taking two images, one before and one during chromatography in order to obtain a two-dimensional array of absorbances and hence peak area values. A secondary objective of imaging wetted plates is to investigate the possibility of obtaining information about the sorbent layer during chromatography.

Work on real-time imaging of chromatographic development on Thin-layer chromatography plates will be undertaken using visible light. Multiple images will be taken during development as bands move along the stationary phase. The possibility of obtaining quantitative results and of improving data by signal averaging will be investigated along with the effect of using different developing solvents. Central to obtaining quantitative results in real-time will be signal referencing in order to compensate for both fixed pattern effects (such as inhomogeneity of light across the plate and imperfections in the plate itself) and the effect of the moving solvent on obtaining reliable absorbance data. Real-time imaging of TLC plates using a CCD camera has been undertaken previously in order to monitor separations as a time saving device (Liang *et al.*, 1996). No quantitative real-time measurements have previously been reported.

CCD chips are solid state devices and as such are not normally sensitive to UV light. It is possible to use a coating to convert the incident UV light into longer wavelengths, which the CCD is more sensitive to (Cowens *et al.*, 1980). However, a lack of UV work undertaken by CCD cameras was reported recently (Prošek *et al.*, 2001). Work on the imaging of TLC plates in UV will be attempted. Quantitative measurements will be undertaken both offline and in real-time.

CHAPTER TWO

Quantitative Measurements on Dry and Wetted TLC Plates Using a CCD Camera

2.1. Introduction

One of the main advantages of planar chromatography over column chromatography is the ability to simultaneously develop many samples on one plate. Scanning densitometry effectively turns this parallel nature into a sequential one. Using video densitometry it is possible to evaluate and compare all the tracks on a plate at once therefore the biggest advantage of TLC (parallel development of standards and samples) is fully supported (Liang *et al.*, 1996).

The output from each sensor pixel on the CCD is a voltage, which is proportional to the intensity of light falling on the sensor and the exposure time. Figure 2.1 shows a voltage applied across the surface of the CCD. When the electron is liberated by the photon it is drawn into the 'well' underneath. CCDs are characterised by the depth of these wells (how may electrons the well can hold), the deeper the wells the greater the dynamic range. A high dynamic range is necessary for absorbance measurements, where light intensities are high.

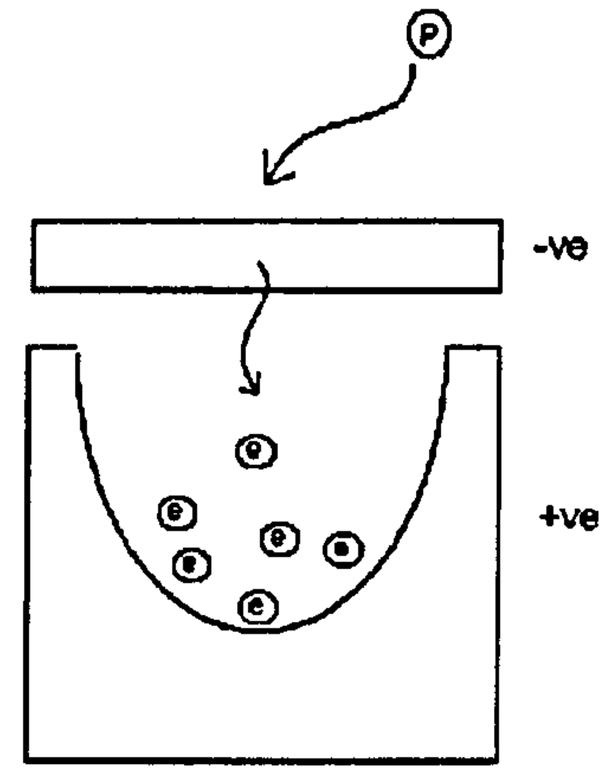

Figure 2.1 One of the sensors comprising a CCD

Generally the plate image is focussed on the CCD by a lens, usually with a filter to increase contrast between the spots and plate background. The CCD output is a series of voltages corresponding to a greyscale for each pixel. As this output is digital it is easy to manipulate the data via a computer.

Application of samples as spots using micro-capillaries is rapid, however, the sample volumes which can be applied are limited if compact spots are to be achieved. The size of initial spots can be minimised if solutions are prepared in the least polar solvent in which the compound of interest will dissolve (Colthup, 1988). Compact spots are then achieved because although the solvent spreads out from the applicator, the dissolved material has an R_f of approximately zero in the solvent and hence remains at or near the origin; the point of application.

However, if samples contain many components it is unlikely that a non-polar solvent will dissolve all of the components, and in this situation a compromise is necessary. Application of small volumes (eg 1 µl) from micro-capillaries results in solvent spread to approximately 5 mm and enables a reasonable amount of material to be applied (1 µg if the solution is 1 mg ml^{-1}). A spot of this size can be reduced to a narrow band by the use of multiple development. The use of micro-capillaries for very small volumes of aqueous samples is, however, less successful, and when samples of this nature are to be applied, use of a sample applicator (eg the Linomat IV from Camag) is more appropriate. Sample applicators are semi-automated instruments for applying samples to TLC plates as bands. The sample is loaded into a syringe and applied onto the plate in a stream of air or nitrogen through a fine nozzle as an aerosol. The aerosol droplets dry rapidly and hence band broadening on sample application is minimised. Sample application is the most critical step for ensuring repeatability in TLC, RSD values of <1% may be realised using automatic spotting (Novakovic, 1999).

The usual detection process in TLC can be considered to be static, as the sample zones are stationary after development is brought to a halt. All information concerning the chromatographic experiment can be made available as a three dimensional array in which the x and y co-ordinates define the position of the spot

pixels and the *z* direction gives the sample amount in each pixel using image analysis techniques (Pollack, 1989). With these data qualitative analysis may be undertaken by the comparison of sample spot co-ordinates with those of standards. Quantitative measurements may be performed by integration of the grey values (*z*) contained in each spot (Jansen *et al.*, 1989).

Very little work has been done involving the imaging of TLC plates whilst still wet with solvent, most workers preferring to attempt measurement after the plate has dried. Indeed, one of the advantages of TLC is the ability to measure separated bands in the absence of solvent or any temporal considerations (Poole and Poole, 1991). This freedom from time constraints allows the use of a variety of techniques to enhance sensitivity and/or specificity, which may be applied sequentially. Detection in TLC is more flexible than in HPLC.

There are two main reasons for looking at plates before drying. Firstly, there is the possibility of finding out information about what happens in the layer during separation or detection. It has been found that analytes migrate into the sorbent layer during chromatography (Vovk *et al.*, 1997) and that a major source of error in TLC quantification is the effect of secondary chromatography during drying (Vovk *et al.*, 1998). Looking at the sorbent layer during chromatography may reveal more about the effects occurring in the depth of the plate, as traditional scanning densitometry is not able to do this (Vovk *et al.*, 1997).

Secondly, the prospect of real time quantitative TLC is an attractive one, however, it is necessary to find out if quantitative measurements may be carried out successfully on wetted TLC plates. This is one of the objectives of the work described in this chapter (Lancaster *et al.*, 2005).

2.1.1 Resolution

There are three types of resolution, which are important in relation to CCD cameras. Namely spatial, temporal and intensity resolution. Spatial resolution in the minimum distance between two objects that can be resolved as separate entities. If the objects are closer than the spatial resolution allows, the photons from the objects will

combine to form charge on one pixel and appear as one object. An imaging system with higher spatial resolution will have finer the detail in the image (Pollack and Schulze-Clewing, 1988).

Temporal resolution is the maximum number of frames per second that the imaging system can handle. High temporal resolution enables images to be acquired more rapidly.

Intensity resolution (or dynamic range) is the range of minimum to maximum intensity values that the system is capable of handling. High intensity resolution produces images with the highest number of grey levels. This enables distinction between two levels close in intensity whereas low intensity resolution would record these two similar grey levels as being the same.

2.1.2 Noise

There are three main sources of noise in a CCD camera, these are photon noise, preamplifier noise and dark current noise. Photon noise or shot noise is a fundamental property of light, it is unavoidable and is present in all imaging systems: this statistical noise is readily calculable from the signal level. Preamplifier noise or read noise is generated by the CCDs output amplifier and can be reduced greatly with the correct operating conditions. Dark current or thermally generated charge can be measured and subtracted from data, but the associated noise cannot be isolated. Cooling the CCD reduces dark current noise to negligible levels.

When under conditions of high light levels, photon statistics are a dominant source of noise and preamplifier noise is not relevant. If photon noise exceeds all other types of noise then the data are said to be photon (or shot) noise limited. Shot noise is dominant in most normal TLC applications (Liang *et al.*, 1996).

2.1.3 Previous work involving scanning densitometry and CCDs

Scanning densitometry is the standard tool for evaluating flat bed separations (Pollak and Schulze-Clewing, 1990). However, this technique is slow (it can take up to twenty minutes to scan a plate) and cannot be used for on-line applications.

Charge Coupled Devices (CCDs), (Sweedler *et al.,* 1988; Epperson *et al.,* 1988) are two-dimensional detectors containing an array of sensors that can image an area in seconds; this makes them ideal for the imaging of TLC plates both off line and online. CCD cameras have been used to evaluate TLC plates quantitatively after drying in several modes, including transmission (Vovk and Prošek. 1997) reflectance (Kowalczuk and Hopkala, 2002) and fluorescence in conjunction with post-run derivatisation (Hayakawa and Hirai, 2003). The archivable properties of CCD images has led to several workers using them for documentation purposes also (Tyaglov *et al.,* 1997; Smolarz and Matysik, 2001; Ponder *et al.,* 2004).

Results using CCD in reflectance mode have been compared with those of scanning densitometry; sensitivities were shown to be similar, but the acquisition times using CCD detection were faster (Degterev *et al.,* 2000; Degtiar *et al.,* 1994; Cosgrove *et al.,* 1989). Relative standard deviation (RSD) values were measured in one study to be < 5%, and r^2 values were > 0.99 (Degterev *et al.,* 1996). Linearity has been demonstrated to be over an order of magnitude, with limit of detection in the range 10-50 ng (Kowalczuk and Hopkala, 2001; Degtiar *et al.,* 2000).

CCD cameras have been used for other analytical applications e.g. to undertake biomonitoring, with picogram limits of detection possible using luminescence on HPTLC plates (Weins and Jork, 1996), as fluorescence detectors in spectroscopy (Epperson *et al.,* 1989) and in capillary zone electrophoresis (Sweedler *et al.,* 1991).

2.2 Experimental

2.2.1 Chemicals

Sudan II (structure shown in figure 2.2) was supplied by Aldrich Chemicals (Poole, UK). The solvents used were HPLC grade hexane, acetonitrile, p-xylene and dichloromethane from Fisher Scientific (Loughborough, UK). A stock solution of Sudan II was prepared by dissolving an accurately weighed amount of dye in hexane. Standards were made by dilution of this stock solution.

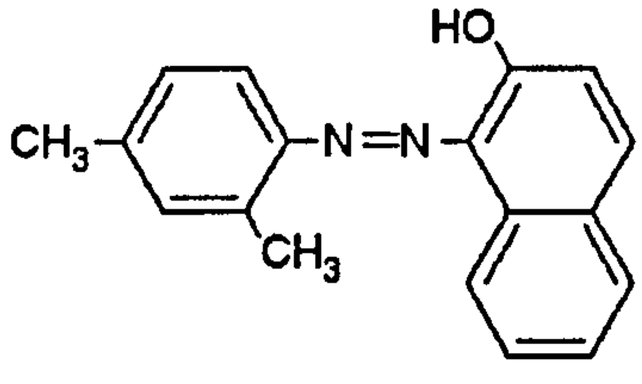

Figure 2.2 Structure of Sudan II dye.

2.2.2 Chromatography

Thin layer chromatography was performed on 5 x 10 cm Silica Gel 60 F_{254} plates from Merck (Darmstadt, Germany), layer thickness 200 μm. Samples were applied as spots approximately 1 cm apart and 0.5 cm from the plate edge by means of 1 μl glass capillaries, supplied by Camlab (Cambridge, UK). Development was performed at room temperature in a 10 x 10 cm horizontal chamber (Camag, Switzerland). A two-step development was chosen, with solvent focusing using acetonitrile before the development proper with dichloromethane.

In the first set of experiments dried plates were imaged. After spotting, the spots were focused with acetonitrile to a distance of approximately 1 cm from the bottom of the plate. The plate was then allowed to dry and an image taken. Subsequently the focused bands were developed for a further 4-5 cm with dichloromethane, after which

the plate was allowed to dry again before imaging in either reflectance or transmission.

In the second set of experiments, the plates were imaged whilst wet with solvent, both before and during chromatography. The blank plate was initially developed up to a predetermined distance (marked on the plate), and an image taken. The plate was allowed to dry and then spotted, focused and dried again. The plate was then developed for a second time and another image taken either in reflectance or transmission, when the solvent front was at the same position as in the first image.

2.2.3 Imaging and processing

Images were taken using an Astromed TE4/A CCD camera (Cambridge, UK) operated to run with maximum dynamic range (5×10^5 electrons per pixel) and at maximum readout rate (80 kHz). Image acquisition was controlled using the associated Imager 2 software. The CCD was fitted with a camera lens (50 mm focal length) from Nikon (Kingston upon Thames, UK) and filters from Edmund Optics (York, UK). A green additive filter (X-52-534) and a blue additive filter (X-52-531) were used.

The wet reflectance experiments were carried out at f 2.8 and 150 ms exposure using the green filter, and at f 2.8 and 200 ms exposure using the blue filter. The wet transmission experiments were carried out at f 8 and 100 ms exposure using the green filter, and at f 4 and 500 ms exposure using the blue filter. Spectral characteristics of the filters, dye and the CCD response are given in Figure 2.3 below.

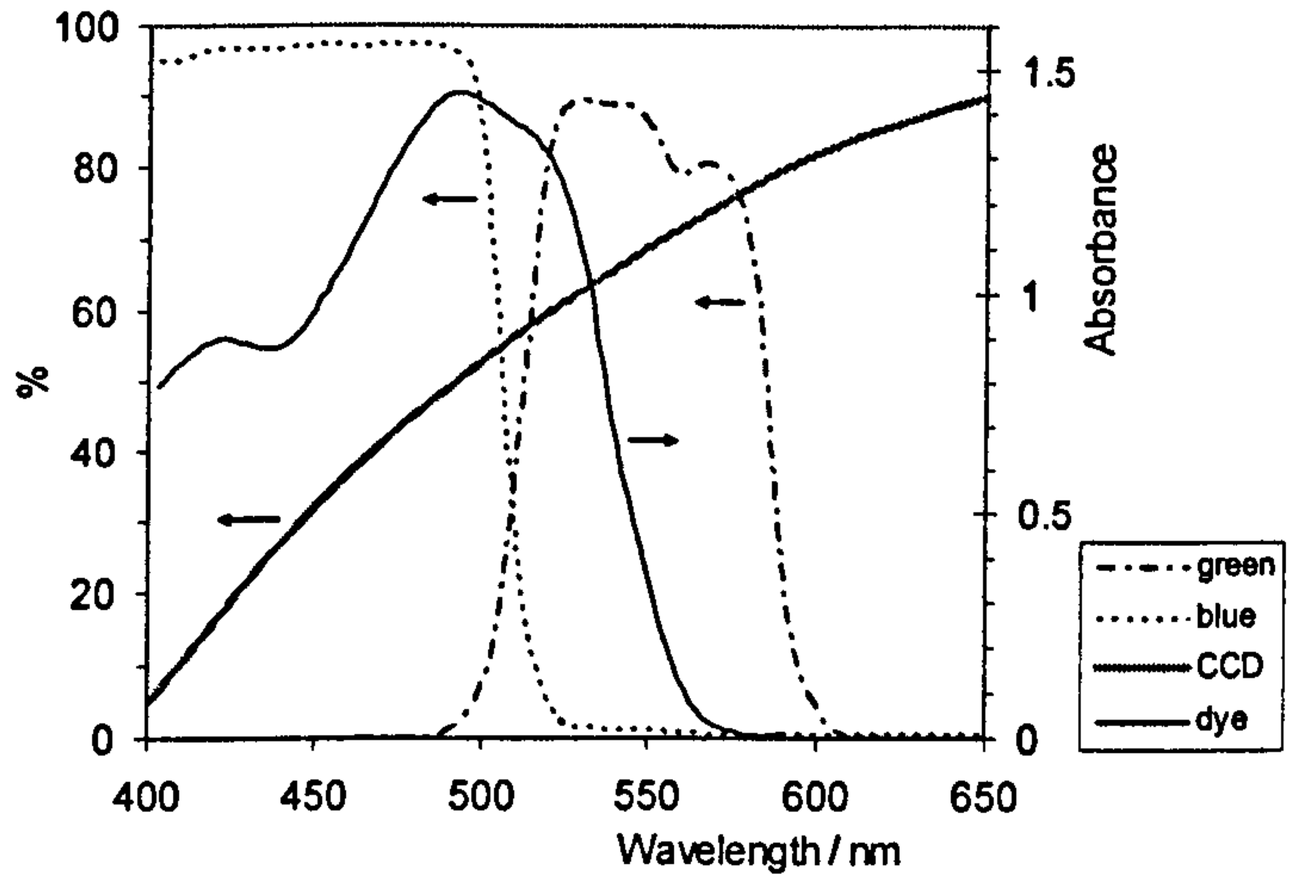

Figure 2.3. Transmittance for the green and blue additive filters, relative sensitivity of CCD (%), and absorption spectrum of Sudan II at 25 mg l^{-1} in dichloromethane in a 1 cm path length cell.

In reflectance mode, the fluorescent strip lights in the laboratory were used to illuminate the plates. In transmission mode, plates were backlit by an 11 W, 250 V fluorescent lamp from CPC (Preston, UK). Centre wavelengths of the emission bands of the phosphor coating of the tubes were measured for both light sources using a calibrated graded interference filter, and found to be 436, 492, 531, 576, 604 and 629 nm. Of these bands, those at 531 and 576 nm overlap with the green filter, whilst those at 436 and 492 nm overlap with the blue filter.

Two images were taken in each experiment, one before and one after chromatography. In the wet plate experiments all images were taken through the glass lid of the tank with the plate still inside. In the transmission experiments any stray light was blanked out between light box and camera using a cover. A schematic diagram of the apparatus is shown in Figure 2.4 below

Signal referencing was accomplished using an in-house program which ratios the signal of each corresponding pixel in two images, and takes the logarithm of this ratio. All images had a blank image (that is one taken with the shutter closed) subtracted.

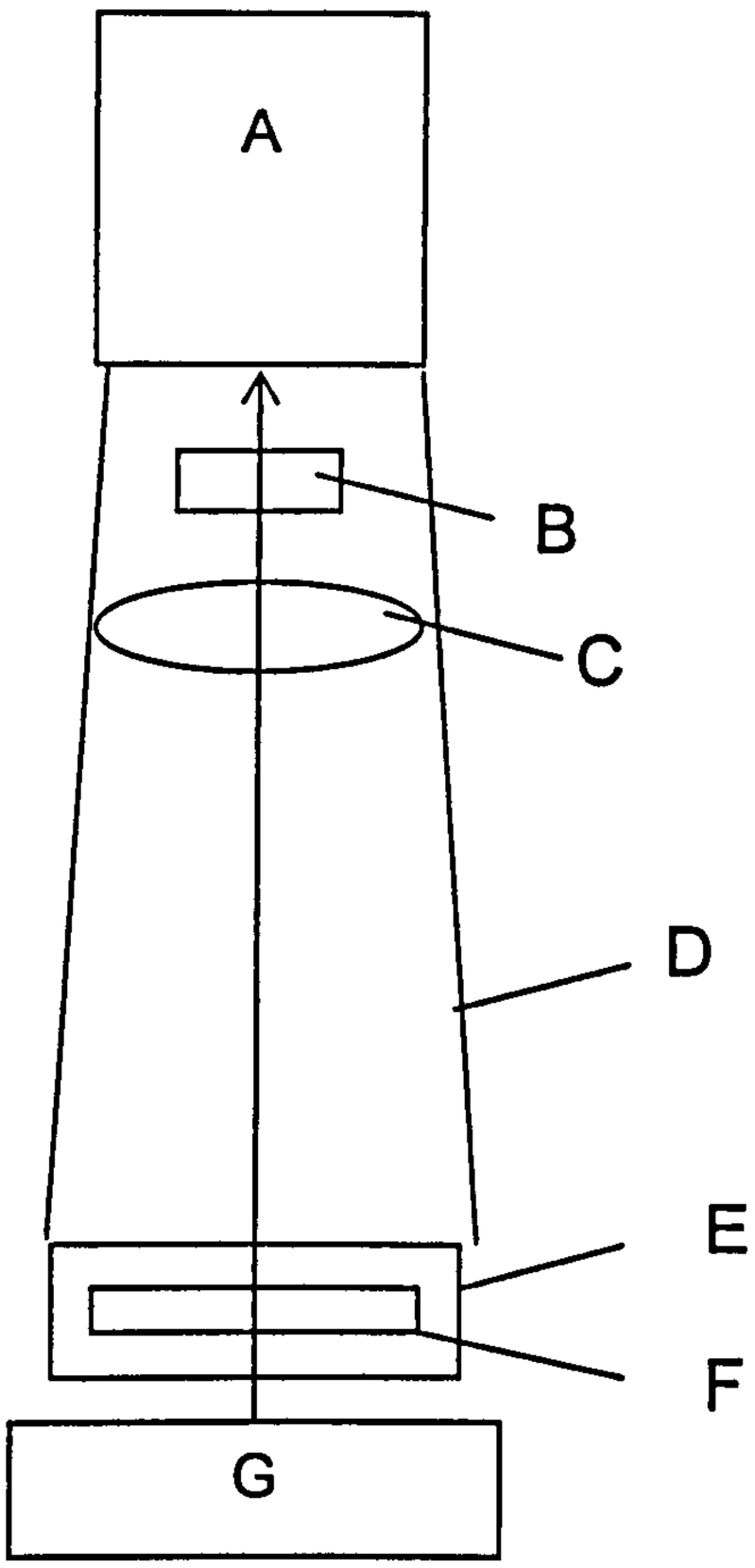

Figure 2.4. Schematic diagram of apparatus to image wet plates in transmission: A, CCD camera, B filter, C lens, D cover, E developing tank, F TLC plate, G light box. The system is enclosed between the top of the developing tank and the CCD to prevent any stray light from entering. For reflectance experiments, the apparatus is the same apart from the removal of the light box and cover.

Further data processing was carried out using Scion Image Beta 4.02 software from Scion Corporation (Maryland, USA) and PeakFit version 4 from Systat Software UK (London, UK).

2.2.4 Spectrophotometry

UV-visible spectrophotometry of Sudan II was carried out using a Shimadzu 1700 spectrophotometer and a quartz cell with a path length of 1 cm. Measurements of absorbance were made between 400 and 650 nm. Sudan II was dissolved in Dichloromethane at a concentration of 25 mg l^{-1} Dichloromethane was also used in the reference cell. The spectrum is given in figure 2.5 below.

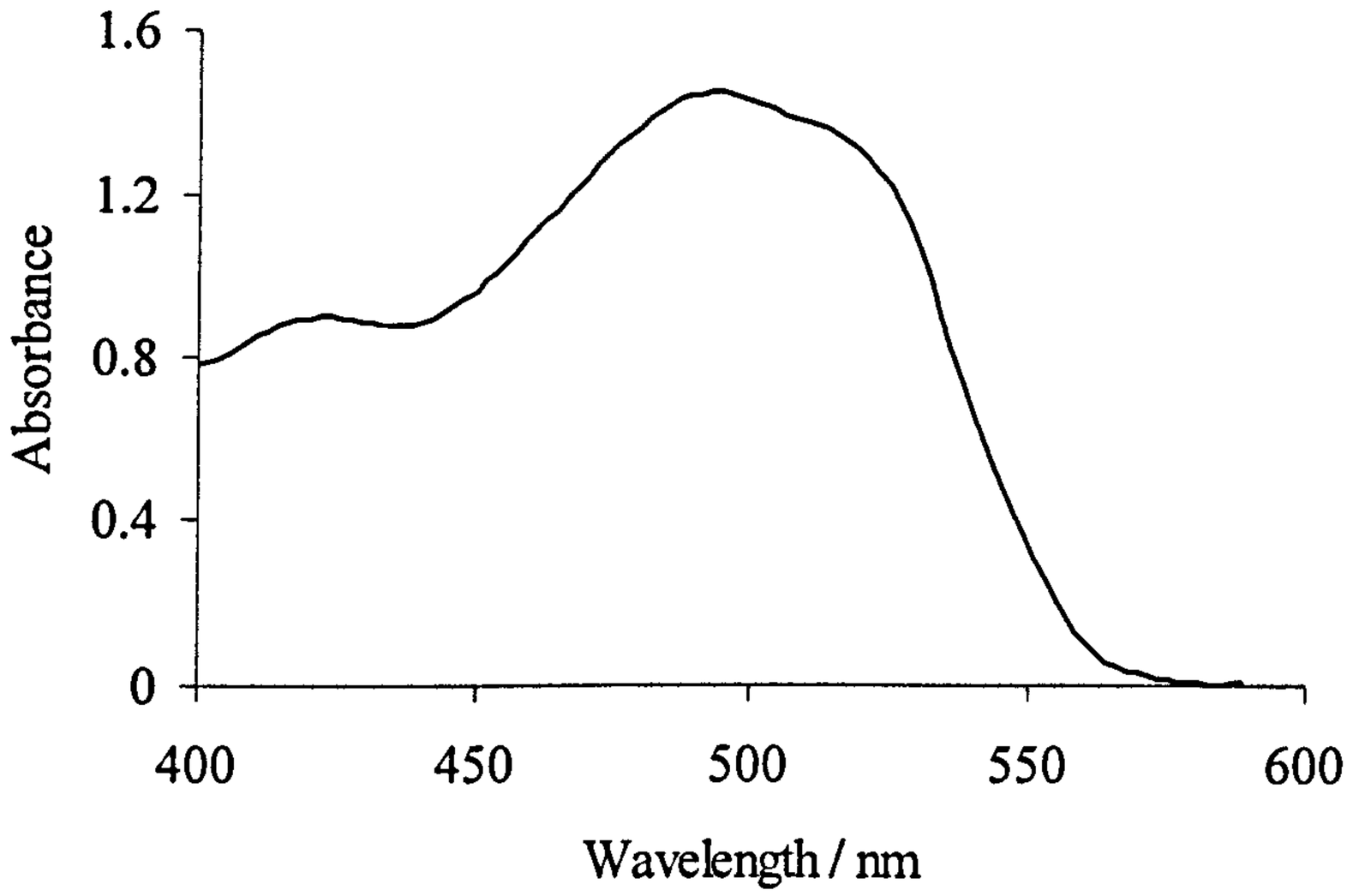

Figure 2.5 UV-Vis spectrum of Sudan II in DCM at 25 mg l^{-1}

2.2.5 Absorbance measurements using cell and CCD camera

Measurements were made using a horizontal quartz cell of path length 0.5 mm in place of a TLC plate beneath the CCD camera. Two images were taken in order to obtain an absorbance. Firstly, of the cell containing solvent only and then with solvent containing Sudan II.

2.3 Imaging parameters

Inside the lens is an adjustable device, the diaphragm, which alters the size of the opening - the aperture. A very small aperture makes everything (background and foreground) in focus. A large aperture makes only the subject focused upon in focus. This zone of acceptably sharp focus (the depth of field) extends both in front of and behind of the point of focus.

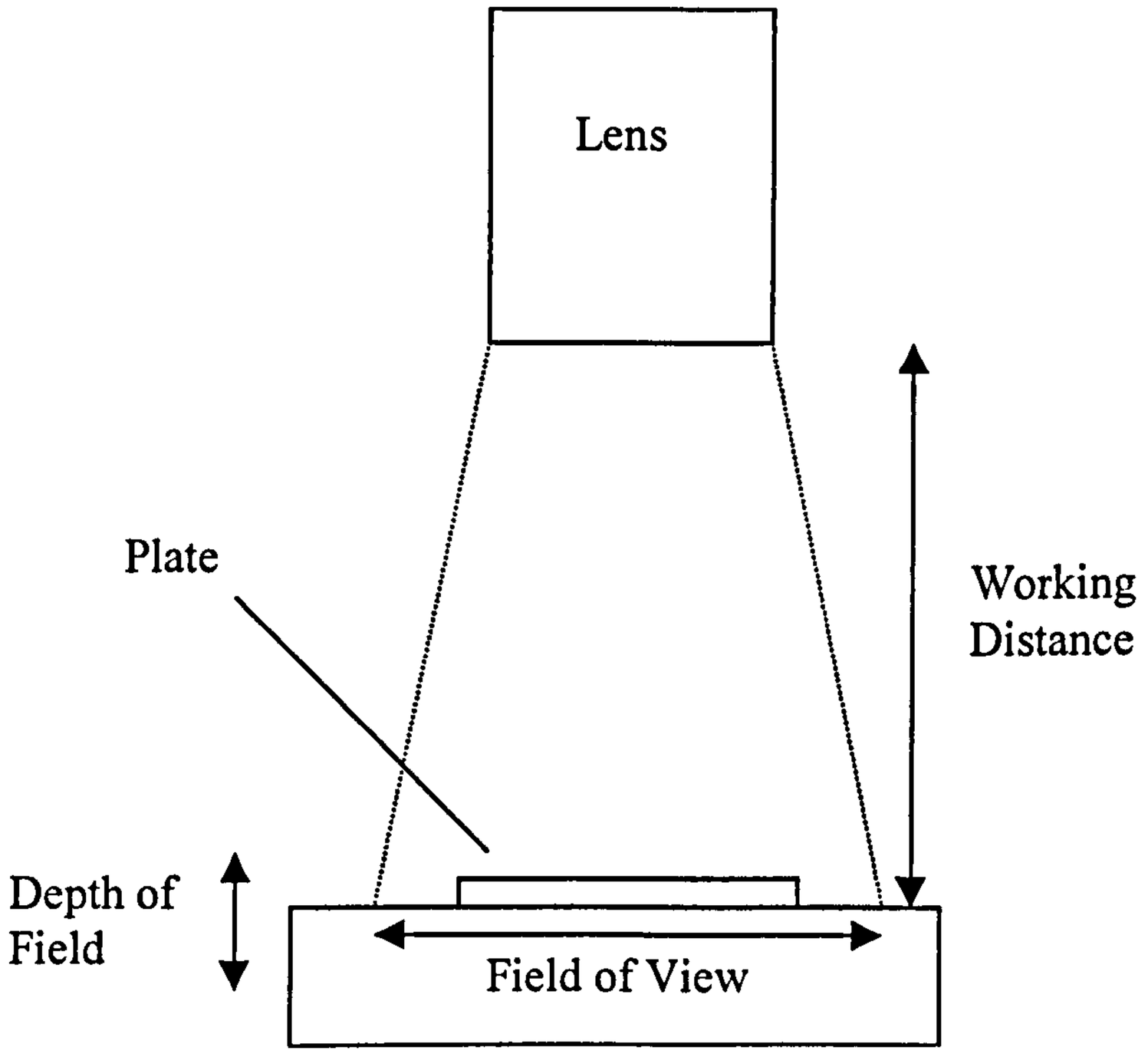

Figure 2.6 Basic terms used in image analysis

The depth of field is affected by three parameters: the size of the aperture; the focal length of the lens; and the distance to the subject focused upon (the focal distance). The first two parameters are combined to give us a field number (f-number or f-stop). The bigger the f-number, the bigger the depth of field (the wider the zone of focus). In TLC, a narrow depth of field is acceptable, as the object being imaged is a planar surface. Some well-known terms used in image analysis are shown in Figure 2.6.

The f-number is the ratio between the diameter of the aperture in the lens and the focal length of the lens (these are usually expressed in millimetres). The smaller the f-number the more light the lens transmits.

In one study of fluorescence quenched CCD detection (Summanen *et al.*, 1998) the largest aperture was found to give the best results, the results being comparable to those obtainable by slit scanning densitometry. Other workers also using fluorescence quenching with CCD detection have suggested that moderately bright images are more repeatable and that they resulted in a lower LOD (Petrović *et al.*, 2000).

The principal source of error in video densitometry is inhomogeneous irradiation of the TLC plate (Petrović *et al.*, 2000a). It is critical to have an even background signal across the plate surface, as gradients will affect the analyte signal. Since the whole plate must be illuminated radiation is usually more inhomogeneous at the edges of the plate with the effect being worse with larger plates (Petrović *et al.*, 2000b). Other workers have also commented on this difficulty (Gianelli *et al.*, 1981; Oldham, 1990; Essig and Kovar, 1999).

Whilst the problem of uneven lighting cannot be fully overcome, it is possible to reduce the effect by a technique known as flat fielding. Flat field correction may be carried out by taking an image of the plate prior to chromatography and ratioing pixel by pixel with an image of the same plate taken after chromatography. Fixed pattern responses in the CCD camera may be eliminated by subtracting (also pixel by pixel) an image taken with the shutter closed as shown in equation 2.1 (Simon *et al.*, 2000).

$$\text{Corrected Image} = \frac{\text{Raw Image - Blank Image}}{\text{Background Image - Blank Image}} \qquad (2.1)$$

Changes in layer thickness and particle size distribution as well as inhomogeneous irradiation of the TLC plate can lead to systematic errors. Short range fluctuations in the surface of the layer or of the particle size distribution are often seen as "plate noise": because this noise is dependent on the texture of the plate and is time-invariant it is termed fixed pattern noise (Kaiser, 1985). Because of its constant nature, plate structure provides a systematic signal error as long as the layer is unaffected by chromatography and remains mechanically sound in the raw and background images. The systematic error may be reduced by subtracting the background texture from the analysis result (Ebel, 1996).

Time dependent noise includes signal noise caused by the light source, electronics. Several authors have described signal referencing in order to eliminate noise and systematic error, in all cases the positioning of the plate before and after chromatography is critical. In order for the referencing to be effective, the plate must

be placed in exactly the same position beneath the camera in both images (Kaiser, 1989), failure to do so may result in systematic errors.

2.4 Beer-Lambert and Kubelka-Munk analysis

To process the data obtained from the CCD camera the Beer-Lambert law was used:

$$\log (I_o / I) = A = \varepsilon dc \qquad (2.2)$$

where A is absorbance, ε is the absorbance coefficient, d is the path length of light through the sample and c is the concentration of the analyte. The quantity of analyte imaged by one pixel is

$$q_i = a_i t c_i, \qquad (2.3)$$

where a_i is the area imaged by pixel i and t_l is the layer thickness. Substituting for c_i and summing over a whole imaged analyte spot gives

$$q = \frac{1}{\varepsilon}\frac{t_l}{d}\sum_i A_i\, a_i = \frac{1}{\varepsilon_{app}}\sum_i A_i\, a_i \qquad (2.4)$$

This equation introduces the term apparent absorbance coefficient, ε_{app}, which is larger than ε by a factor d/t_l due to the increased effective pathlength found in the scattering medium of the TLC layer. The procedure used was to first calculate the absorbance for each pixel using the values for I_0, obtained from the image taken before chromatography, and I from the image taken after chromatography. These absorbance values are then summed to give a signal for the spot, with units AU m^2 that is proportional to the total analyte quantity in the spot.

An example of the signal referencing process is given in Figure 2.7 where 4 spots of 50, 25, 10 and 5 ng loading have been run. The first picture (a) is the raw image direct from the CCD. The second picture (b) shows the data after ratioing with our in house

program in order to correct for fixed pattern effects and also to convert from signal level into absorbance using Eq. 2.2. The fixed pattern contribution is due to the inhomogeneity of light across the plate and also due to irregularities in the plate surface. This is then integrated in the *y* direction using the program Scion Image (Scion Corporation, USA) to produce the peaks seen in the next step plotted as a function of distance in the *x* direction (c). These peaks are integrated a second time using PeakFit from Systat (London, UK) to give results, which can be plotted, as a calibration (d). Very good linearity is observed in the calibration, with correlation coefficient of 0.9989. This validates use of the Beer-Lambert approach over this range of sample loading. Examples of signal referenced plate images are given in Figures 2.8 and 2.9.

The Beer-Lambert approach to signal referencing has also been used by other workers in order to make absorbance measurements on TLC plates (Touchstone *et al.*, 1971; Gianelli *et al.*, 1983; Burns *et al.*, 1986).

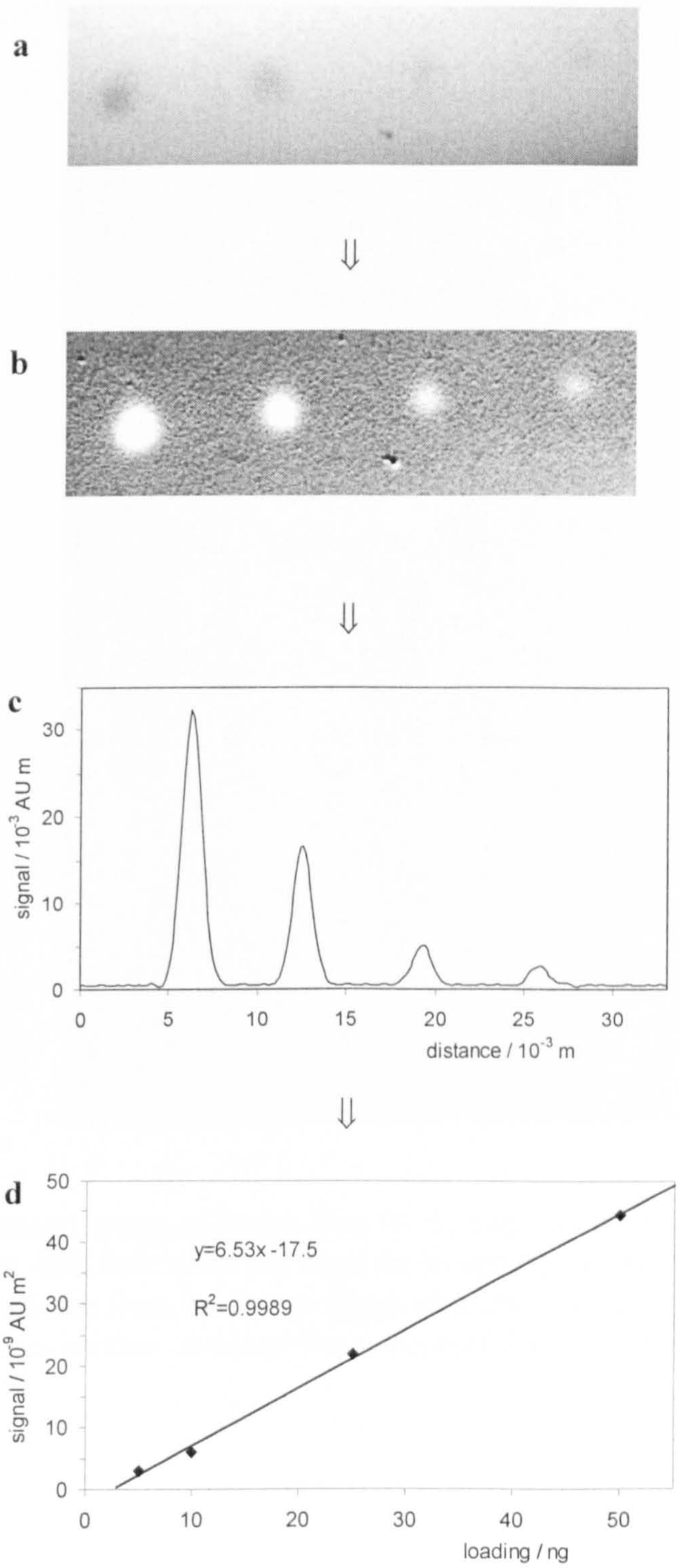

Figure 2.7 Signal referencing and processing for a calibration of Sudan II imaged on wet plates in reflectance with blue filter – 50, 25, 10 and 5 ng spots. a) raw image b) after correction for fixed pattern noise c) after integration in one direction using Scion Image d) calibration plot obtained by integration of c using PeakFit.

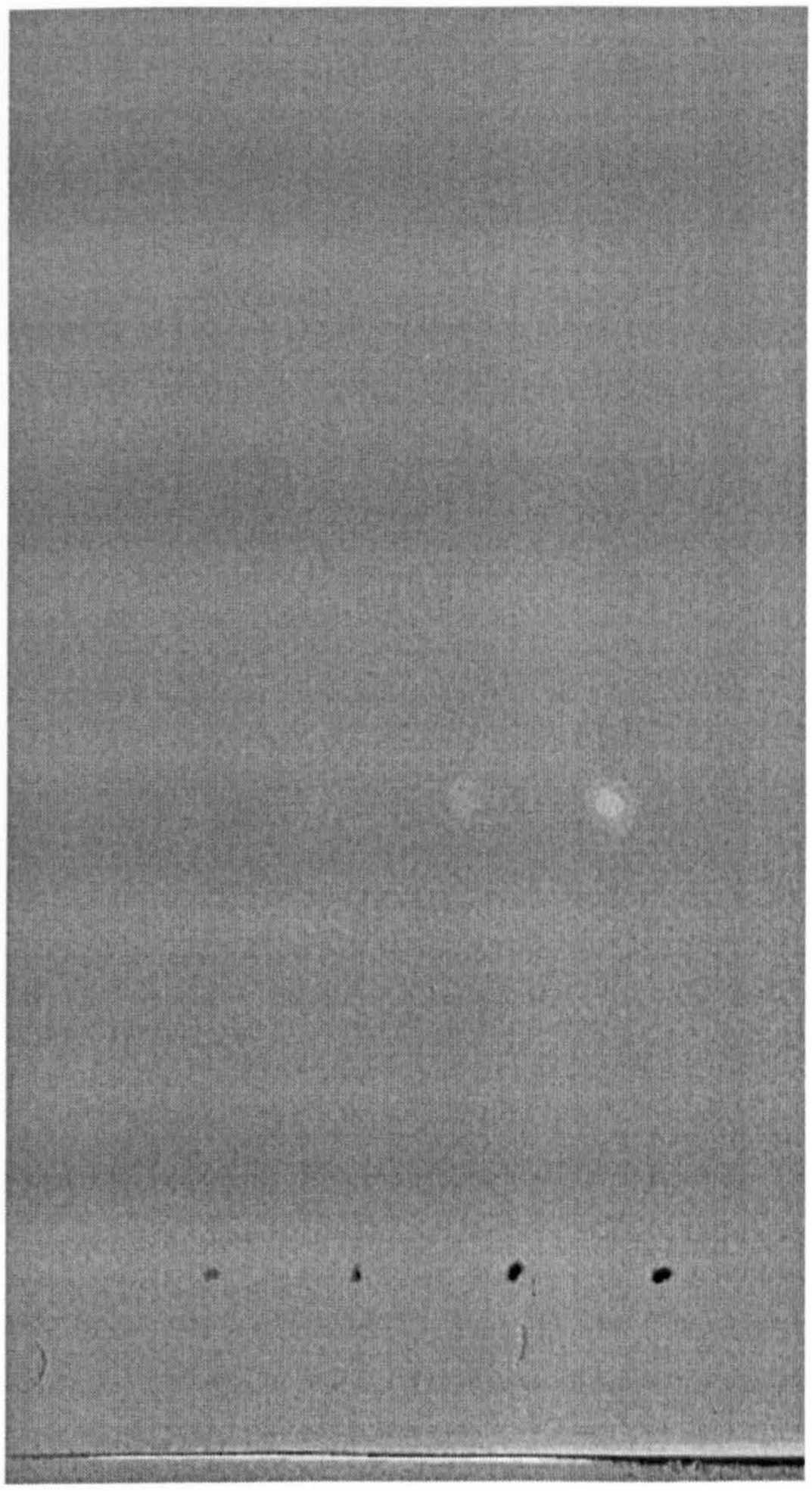

Figure 2.8 Referenced image of Sudan II at 10, 5, 2 and 1 ng on a dry plate with the blue additive filter. The dark spots are from the image taken before chromatography whilst the light spots are from the image taken after chromatography. Notice the smooth, regular plate surface obtained from successful signal referencing.

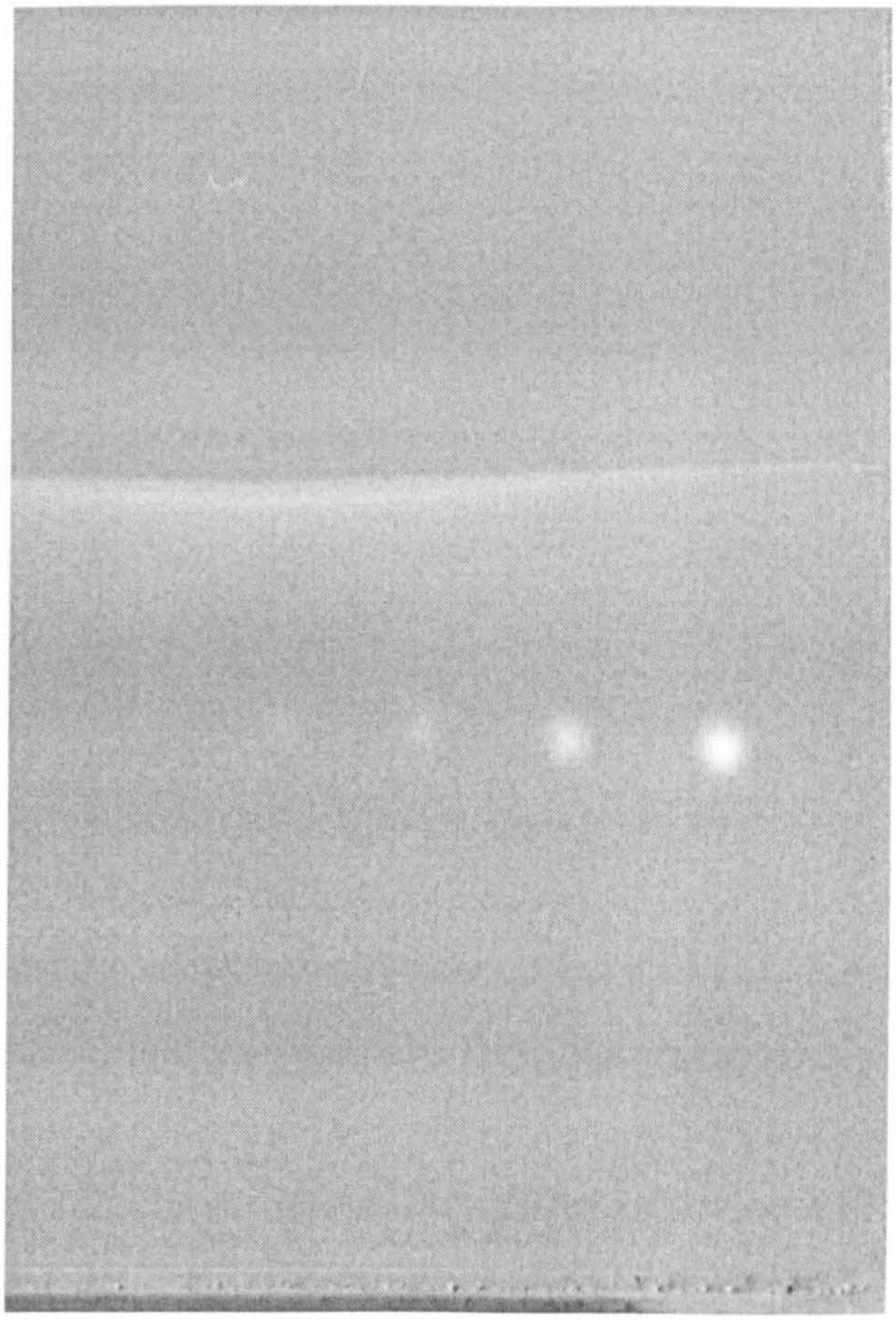

Figure 2.9 Referenced image of Sudan II at 50, 25, 10 and 5 ng on a wet plate run with DCM imaged using the blue additive filter. Only white spots are present as the background image used was of the wet blank plate, not a spotted plate. Notice that the signal referencing at the solvent front produces a white irregular band. This is due to the solvent front being in a slightly different position in both images.

The Beer-Lambert law is normally used to describe absorption in non-scattering media, and since the silica gel of a TLC plate is highly scattering this is not the ideal model. The theory of Kubelka and Munk (1931) has been extensively used to describe the propagation of light in intensely scattering media and in particular to the quantitative analysis in TLC (Goldman and Goodall, 1968; Treiber 1974; Prosek *et al.*, 1996). The equation

$$A_{\text{B-L}} = 2\exp(-2A_0)(A + 0.4A^2) \qquad (2.5)$$

was presented by Goldman and Goodall as a semi-empirical equation approximating the relation between the absorbance expected from the Beer Lambert law ($A_{\text{B-L}}$) and

apparent absorbance measured in transmission, with A_0 the apparent absorbance of the chromatographic adsorbent or layer (Goldman and Goodall, 1968).

$$A_0 = \log \frac{I_0}{I} \qquad (2.6)$$

Where I and I_o are light intensities recorded on the plate with stationary phase and without stationary phase, respectively.

In the case where the sorbent layer does not absorb light at the wavelengths used, A_0 is a measure of its scattering power; the equation holds for $0.7 < A_0 < 1.3$ (Goldman and Goodall, 1968), a range that should include the scattering power of TLC plates. The increased effective pathlength gives an overall enhanced response by the factor $1/[2\exp(-2\ A_0)]$ and the curvature, away from the linear Beer Lambert behaviour, is accounted for by $(A + 0.4A^2)$ (Goldman and Goodall, 1968). In the approach used by Treiber (1974), the constants in the equations derived from Kubelka-Munk theory are obtained empirically. Equation 2.5 was applied to the data shown in Figure 2.10, which covers loadings between 10 and 100 ng, a wider range than that in Figure 2.7. Using A_0 as an empirical variable, the best fit (solid line) to the observed data was obtained with a value for A_0 of 1.2. This lies within the range where the authors proposed that the equation is valid.

The value obtained for A_0 by measuring the reduction in light transmission caused by the presence of the TLC layer is expected to be highly dependent on the nature of the illumination (Stober, 1995), with higher values obtained when a collimated source is used. Measurements of A_0 were made with and without slits to investigate this. Values for A_0 of ~ 0.1 were obtained for wet plates with the highly diffused source in the arrangement of Figure 3, and values of ~1.6 were obtained when a mask with a 1 mm width slit was placed on top of the light box and under the wet plate. This application of the Kubelka-Munk theory accounts for both the slope and curvature of the data shown in Figure 2.10, with a value for A_0 that is within the range measured experimentally. It is also consistent with the observation in the transmission experiments of a smaller absolute loading range and increased apparent absorbance

coefficient for the low loading region that gives an approximately linear response under the conditions of increased scattering in dry plates.

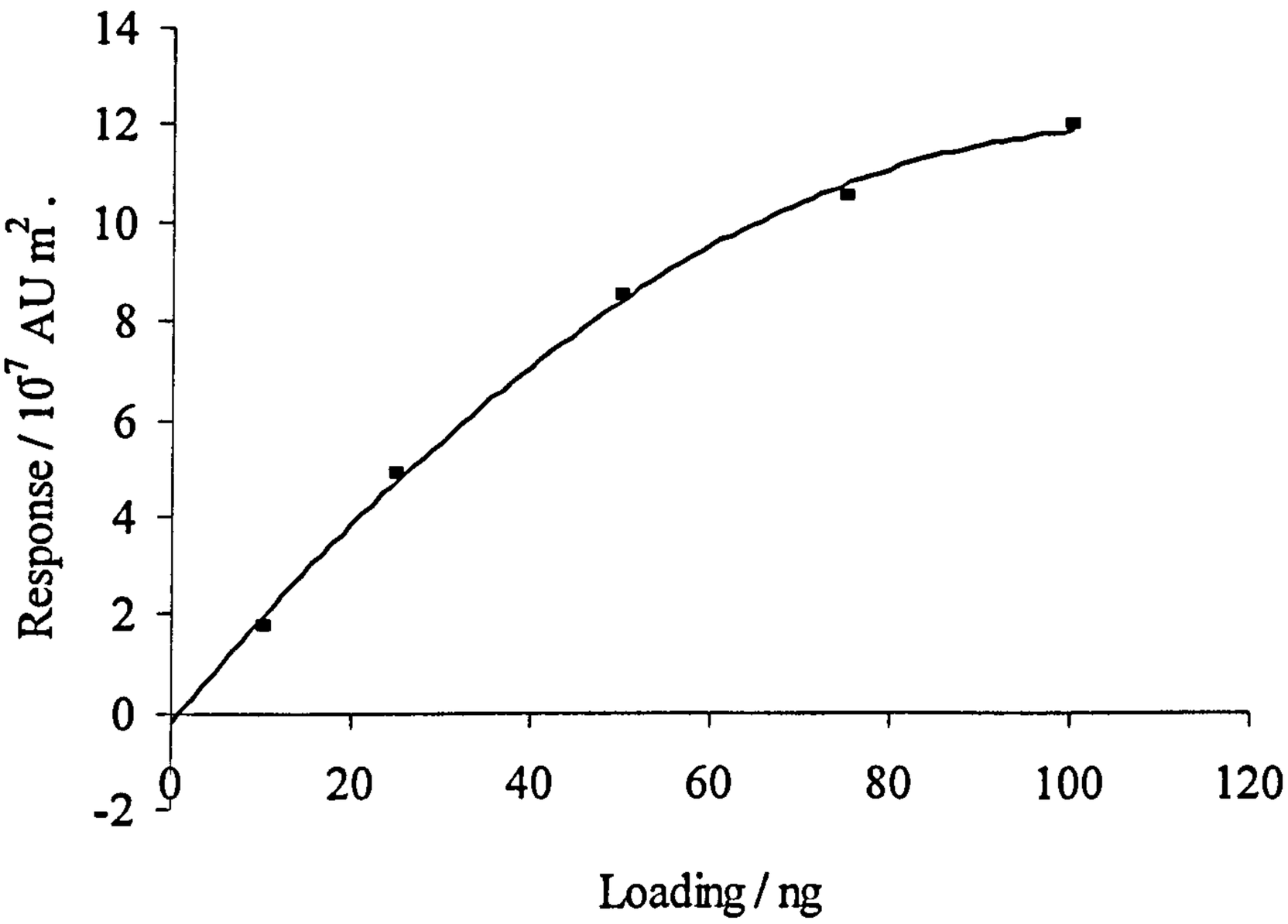

Figure 2.10 A five-point calibration of Sudan II imaged on wet plates in transmission using the blue additive filter – 10, 25, 50, 75 and 100 ng spots.

Calibration ranges were selected after running a wide selection of loadings. Loadings which were outside the linear range (>50 ng on wet plates, Figure 2.10) or too close to the LOD (<5 ng) were discarded for further investigations. Results obtained using sample loadings in the range up to 50 ng and using the Beer-Lambert equation are shown Table 2.1 for transmission on wet plates, Table 2.2 for reflectance on wet plates, and Table 2.3 for transmission on dry plates. Correlation coefficients were greater than 0.995 for linear regression. Intercepts in all calibrations are within experimental error close to zero, but the fact that all intercepts are systematically positive in the transmission data (Table 2.1) and negative in the reflectance calibrations (Table 2.2), rather than being randomly distributed around zero, is consistent with the linear Beer-Lambert fitting being an approximation to reality, as discussed above, this is illustrated in figures 2.11 and 2.12. Causes of non-linearity include; scattering of light due to particles, fluorescence or phosphorescence of the sample, changes in refractive index at high analyte concentration, non-monochromatic radiation (this can be minimised by using a relatively flat part of the

absorption spectrum, such as the maximum of an absorption band), stray light and depth profile of analyte distribution (particularly important for reflectance).

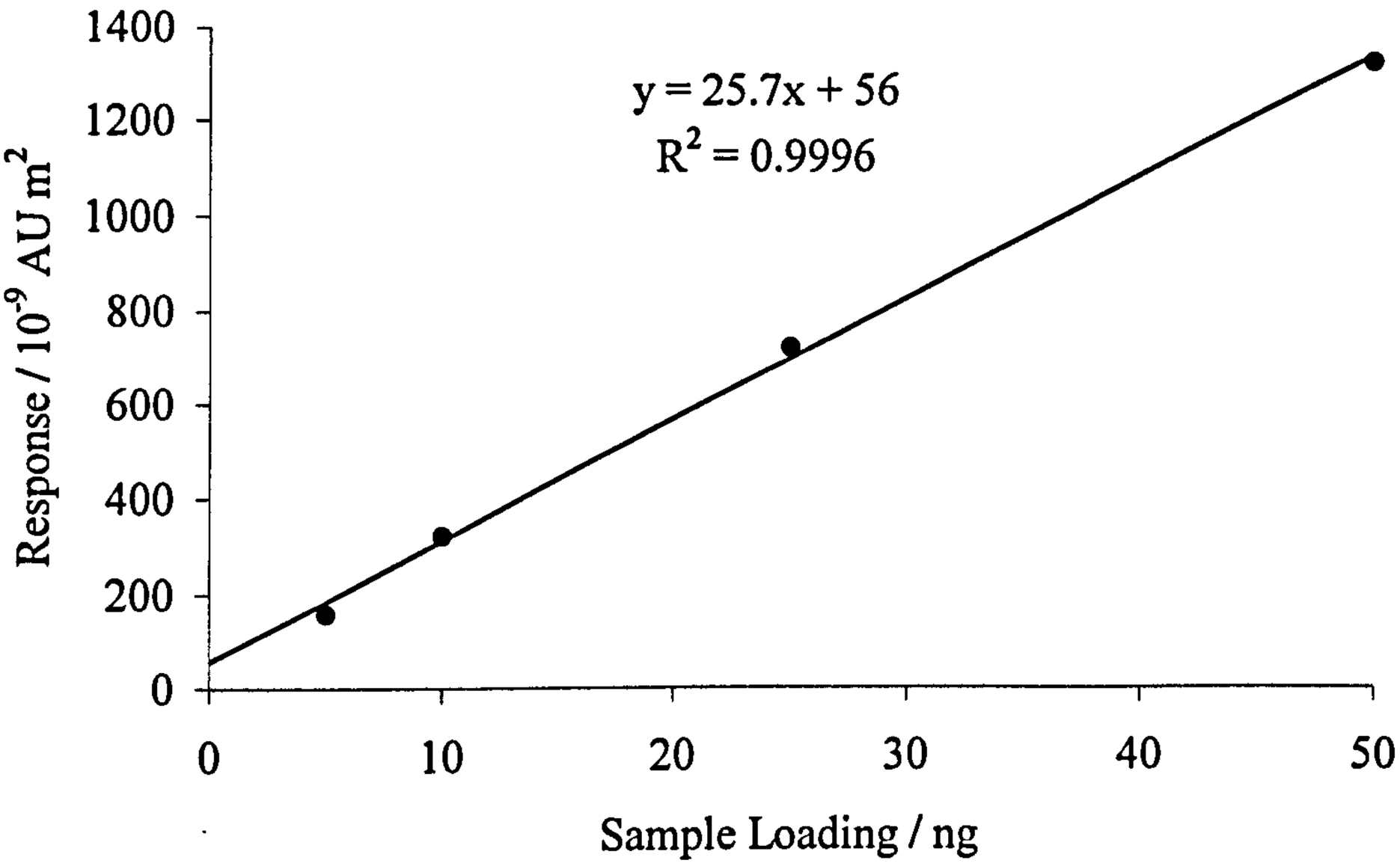

Figure 2.11 Calibration curve of Sudan II at 50, 25, 10 and 5 ng on a wet plate in transmission with the blue additive filter. Note the positive intercept.

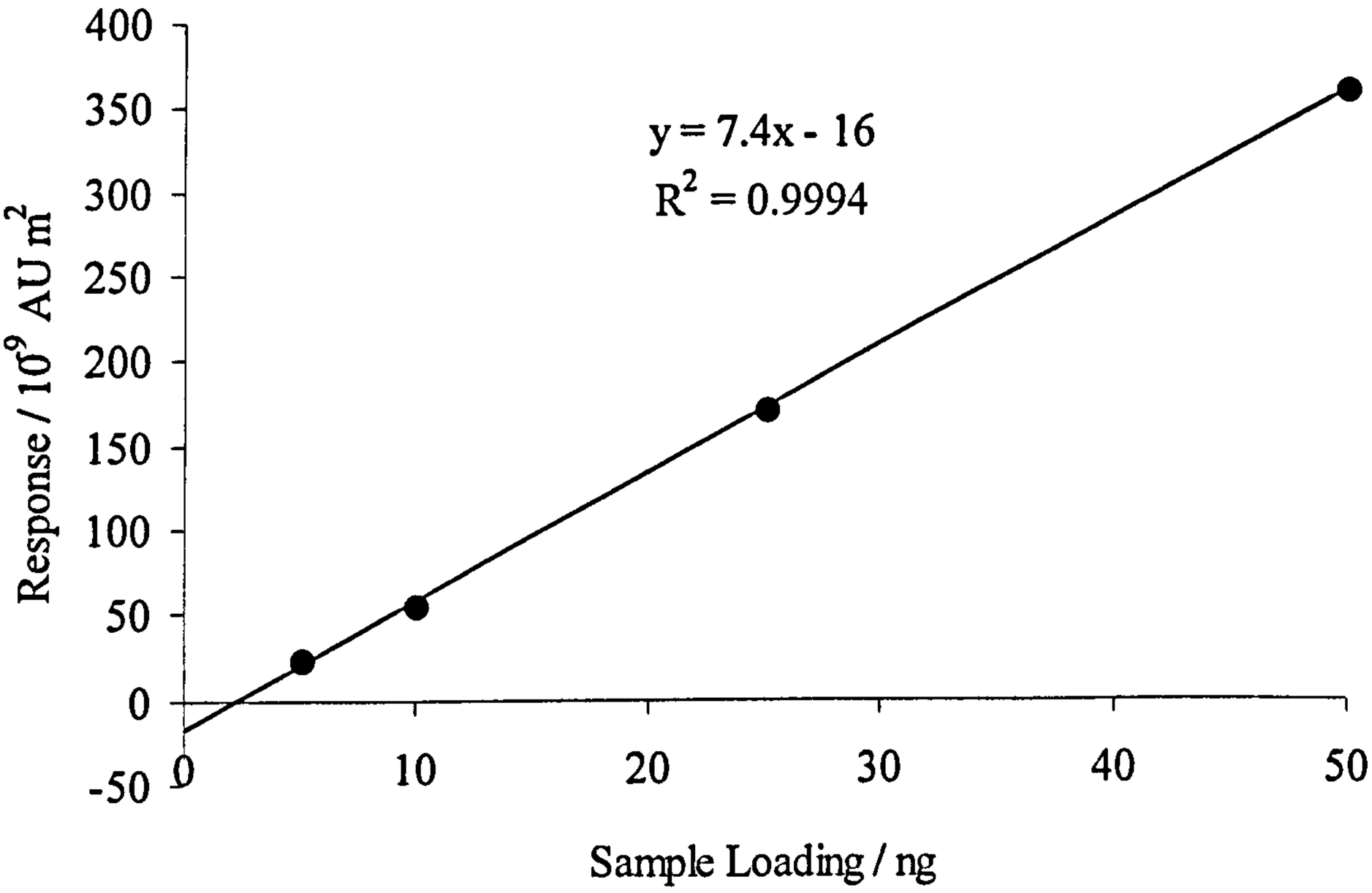

Figure 2.12 Calibration curve of Sudan II at 50, 25, 10 and 5 ng on a wet plate in reflectance with the blue additive filter. Note the negative intercept.

Table 2.1 Calibrations for Sudan II in transmission on wet plates – 5, 10, 25 and 50 ng spots

Calibration	Filter	Gradient / AU m^2 g^{-1}	Intercept / AU m^2	r^2
1	Blue	25.7 ± 1.5	56 ± 42	0.9996
2	Blue	29.8 ± 2.3	30 ± 66	0.9993
3	Blue	27.5 ± 2.0	31 ± 56	0.9994
4	Blue	32.2 ± 1.4	43 ± 40	0.9998
Average		*28.8 ± 2.8*	*40 ± 12*	
5	Green	19.4 ± 1.6	7 ± 44	0.9993
6	Green	23.5 ± 0.4	65 ± 12	0.9999
7	Green	18.9 ± 1.5	33 ± 43	0.9993
8	Green	22.7 ± 2.1	36 ± 59	0.9991
Average		*21.1 ± 2.3*	*35 ± 24*	

Table 2.2 Calibrations for Sudan II in reflectance on wet plates– 5, 10, 25 and 50 ng spots

Calibration	Filter	Gradient / AU m^2 g^{-1}	Intercept / AU m^2	r^2
1	Blue	7.41 ± 1.28	- 16 ± 36	0.9994
2	Blue	7.01 ± 1.18	- 12 ± 34	0.9981
3	Blue	8.75 ± 1.09	- 21 ± 31	0.9993
4	Blue	6.53 ± 0.65	- 17 ± 18	0.9989
Average		*7.42 ± 0.95*	*- 16 ± 4*	
5	Green	4.37 ± 0.35	- 8 ± 25	0.9996
6	Green	4.49 ± 0.72	- 11 ± 20	0.9991
7	Green	3.90 ± 0.52	- 2 ± 15	0.9994
8	Green	5.87 ± 0.82	- 6 ± 23	0.9987
Average		*4.66 ± 0.85*	*- 6 ± 4*	

Table 2.3 Calibrations for Sudan II in transmission on dry plates – 1, 2, 5 and 10 ng spots

Calibration	Filter	Gradient / AU m^2 g^{-1}	Intercept / AU m^2	r^2
1	Blue	49.6 ± 5.0	-8.8 ± 11	0.9989
2	Blue	49.2 ± 4.0	-0.7 ± 23	0.9993
3	Blue	46.1 ± 5.1	6 ± 29	0.9987
4	Blue	45.3 ± 2.9	-1.9 ± 16	0.9996
Average		*47.6 ± 2.2*	*-1.3 ± 6.1*	
5	Green	22.0 ± 4.6	-1 ± 26	0.9954
6	Green	24.1 ± 0.7	-3 ± 4	0.9999
7	Green	23.9 ± 4.7	7 ± 26	0.9959
8	Green	22.4 ± 3.5	-11 ± 20	0.9973
Average		*23.1 ± 1.1*	*-2 ± 7*	

2.5 Apparent absorption coefficient (ε_{app})

The gradients in Tables 2.1, 2.2 and 2.3 are the apparent absorption coefficients, ε_{app} (Eqn. 2.3), and as such they can be compared directly with values for absorption coefficients measured in solution. Measurements for Sudan II in DCM were carried out in three ways: (i) using UV-vis spectrophotometry with a standard 1 cm cell; (ii) using the CCD camera in conjunction with the blue filter, and sample in a 0.5 mm pathlength cell positioned horizontally in place of the TLC plate in Figure 2.3; (iii) as in (ii), but with a narrow-band blue filter centred at 400 nm. All methods gave comparable values of ε: 3.4, 4.0 and 4.1 AU m^2 g^{-1} for (i) (at 400 nm), (ii) and (iii) respectively. This shows that the optical configuration in the present work gives the expected value for absorbance in the absence of any scattering. The value of ε_{app} measured for Sudan II in transmittance through the DCM-wetted TLC plate, 28.8 AU m^2 g^{-1}, is a factor ~7 higher. This increase in value for ε_{app} is consistent with a longer effective pathlength through the scattering medium on the TLC plates, and the effective pathlength in the TLC experiments being considerably greater than the thickness of the sorbent layer. A value of 47.6 AU m^2 g^{-1} for ε_{app} was obtained for Sudan II in transmission on the dry plate with the blue filter which is a factor 1.5 greater than the value on the wet plate and a factor 12 greater than ε in solution which is consistent with a further increase in the effective pathlength under the condition of greater scattering in absence of solvent. The emission band at 576 nm of the light

source used is transmitted by the green filter but is not absorbed by the dye (Figure 2.2) in part accounts for the lower ε_{app} observed for the green filter measurements.

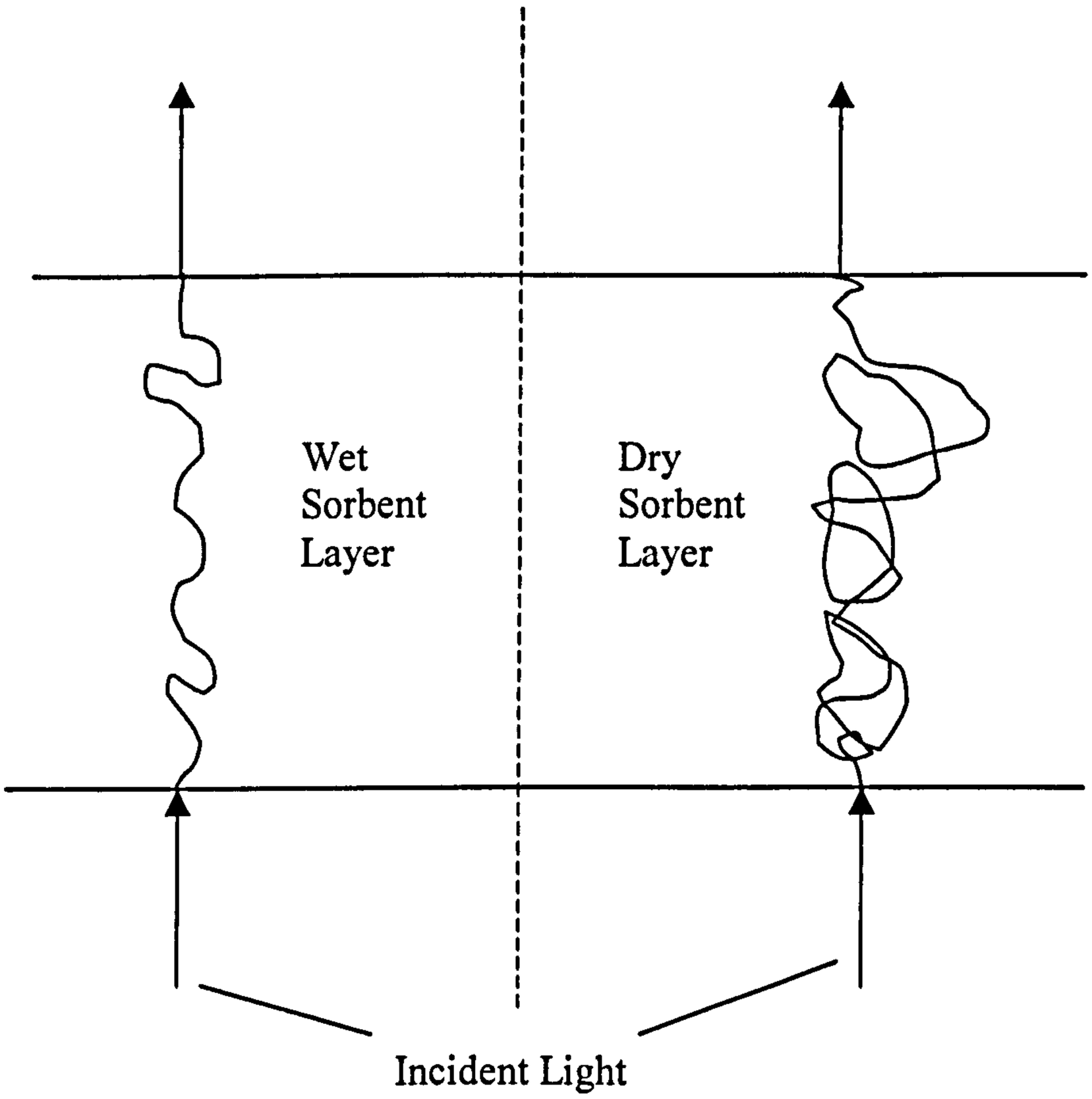

Figure 2.13 Pathways of incident light beams within dry and wet sorbent layers.

Incident light may be reflected in different directions from each particle in the sorbent layer. If analyte is present, absorption will occur. A longer pathlength will lead to more absorption and a higher apparent absorption coefficient. Figure 2.13 shows the effect in transmission, similar behaviour is encountered in reflectance.

2.6 Limit of detection and reproducibility

Four point calibrations were used; this is because of the limited space available on the 5 x 10 cm plates. As discussed in section 2.3.1, the linear range was approximately an order of magnitude, between 1-10 ng on dry plates and 5-50 ng on wet plates. The

relationship between signal and sample loading was found to become non-linear at higher loading; above about 10 ng dry and 50 ng wet (Figure 2.5).

The limit of detection (LOD) was determined using the signal to noise ratio. A typical figure giving raw data is shown in Figure 2.14. The limit of detection is approximately 2 ng on a wetted plate. A loading of 0.5 ng can be easily detected on a dried plate. These figures are significantly better than LODs of 10-50 ng previously reported using reflectance with CCD cameras and dry plates (Degitar *et al.*, 2000; Kowalczuk and Hopkala, 2001). The LOD is higher on a wet than on a dry plate for two reasons. Firstly, there is increased noise due to the presence of solvent, making signal referencing less reproducible. Secondly, the effective absorption coefficient is lower, most probably due to shorter effective pathlength as discussed in the previous section.

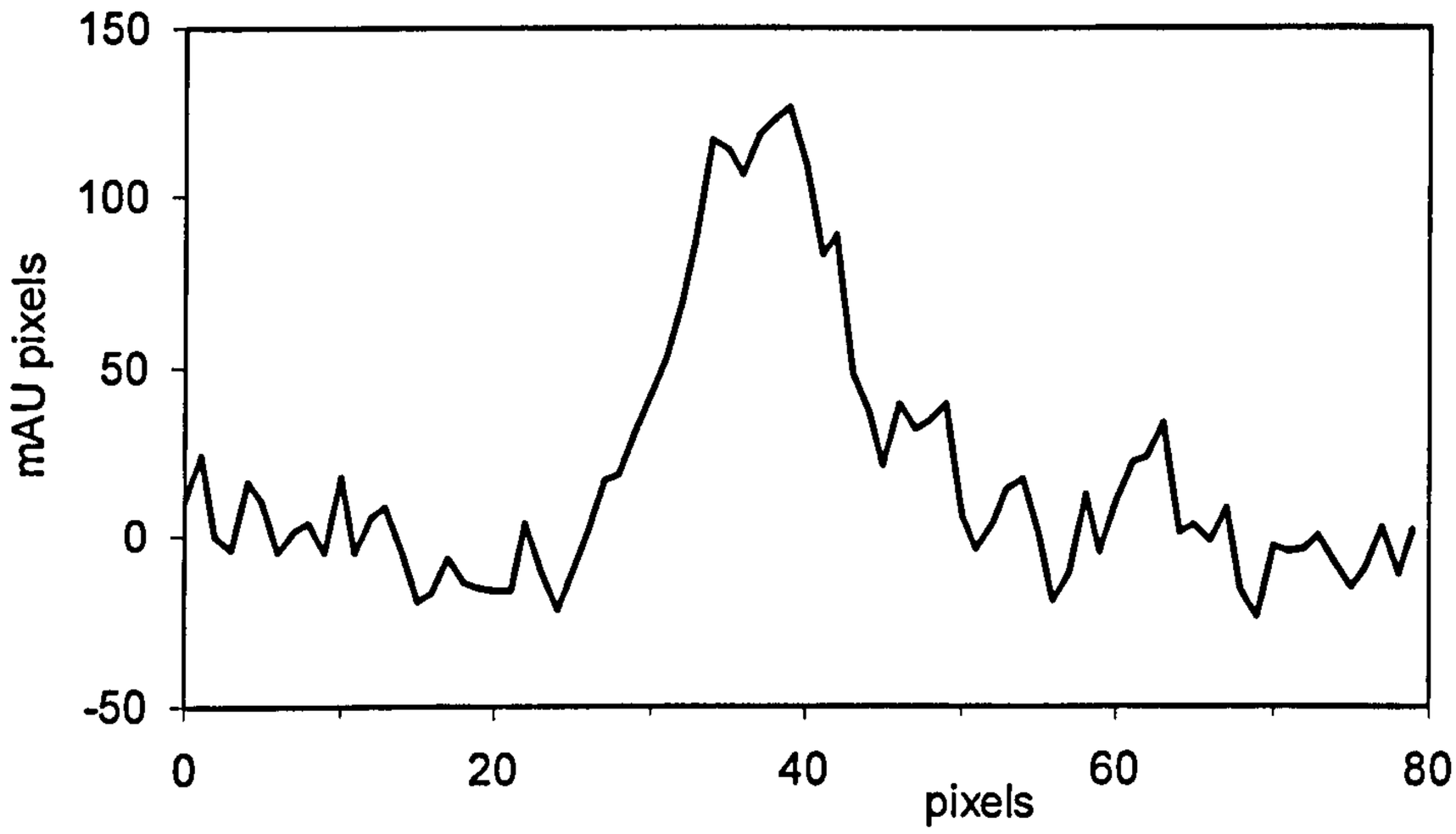

Figure 2.14 Raw data for a 2 ng peak imaged on a wet plate in reflectance with the green filter. The peak-to-peak S/N ratio is approximately 2:1 without any smoothing.

Precision of chromatography and detection was assessed by means of the RSD values between spots of the same loading (Tables 2.4-2.7). Note that all RSD values are for the full analytical process from spotting through to evaluation. Precision was generally good between spots on wet plates in transmission and reflectance (Tables

2.4, 2.5 and 2.6) and also in transmission on dry plates (Table 2.7) with RSD values in the range 1-4%. These are comparable with results previously reported using CCD detection on dry plates and RSDs less than 5% (Degterev *et al.*, 2000). The results were rather poorer between plates as expected (Touchstone and Bobbins, 1983) with RSD values in the range 8-14% for the inter-plate averages of the intra-plate mean values.

Table 2.4 Reproducibility in quantification of peak area of Sudan II after chromatographic development, using transmission on wet plates with the blue additive filter ($n = 4$)

Plate	Loading / ng	Average signal / AU m^2	RSD/ %
1	10	$(2.95 \pm 0.060) \times 10^{-7}$	2.1
2	10	$(3.05 \pm 0.082) \times 10^{-7}$	2.7
3	10	$(2.33 \pm 0.060) \times 10^{-7}$	2.6
4	10	$(2.36 \pm 0.057) \times 10^{-7}$	2.4
Average		*$(2.67 \pm 0.32) \times 10^{-7}$*	*14*
5	50	$(1.32 \pm 0.027) \times 10^{-6}$	2.5
6	50	$(1.09 \pm 0.027) \times 10^{-6}$	2.1
7	50	$(1.16 \pm 0.021) \times 10^{-6}$	1.8
8	50	$(1.21 \pm 0.031) \times 10^{-6}$	2.6
Average		*$(1.19 \pm 0.086) \times 10^{-6}$*	*7*

Table 2.5 Reproducibility of Sudan II in transmission on wet plates with the green additive filter ($n = 4$)

Plate	Loading / ng	Average signal / AU m^2	RSD/ %
1	10	$(1.86 \pm 0.035) \times 10^{-7}$	1.9
2	10	$(2.33 \pm 0.032) \times 10^{-7}$	1.4
3	10	$(2.18 \pm 0.058) \times 10^{-7}$	2.7
4	10	$(2.23 \pm 0.038) \times 10^{-7}$	1.7
Average		*$(2.15 \pm 0.17) \times 10^{-7}$*	*8*
5	50	$(1.05 \pm 0.038) \times 10^{-6}$	3.7
6	50	$(1.04 \pm 0.032) \times 10^{-6}$	3.1
7	50	$(9.88 \pm 0.28) \times 10^{-7}$	2.9
8	50	$(8.61 \pm 0.21) \times 10^{-7}$	2.5
Average		*$(9.84 \pm 0.87) \times 10^{-7}$*	*9*

Table 2.6 Reproducibility of 50 ng spots of Sudan II in reflectance on wet plates (n = 4)

Plate	No of spots	Filter	Average signal / AU m^2	RSD/ %
1	4	Green	$(2.58 \pm 0.075) \times 10^{-7}$	3.0
2	5	Green	$(3.02 \pm 0.11) \times 10^{-7}$	3.2
3	4	Green	$(3.66 \pm 0.097) \times 10^{-7}$	2.7
4	4	Green	$(3.04 \pm 0.11) \times 10^{-7}$	3.7
Average			*$(3.08 \pm 0.44) \times 10^{-7}$*	*14*
5	4	Blue	$(3.89 \pm 0.090) \times 10^{-7}$	2.4
6	5	Blue	$(4.58 \pm 0.061) \times 10^{-7}$	1.2
7	5	Blue	$(4.86 \pm 0.091) \times 10^{-7}$	1.7
Average			*$(4.44 \pm 0.50) \times 10^{-7}$*	*11*

Table 2.7 Reproducibility in transmission on dry plates (n = 5)

Plate	Loading / ng	Filter	Average Signal / AU m^2	RSD / %
1	5	Blue	$(2.07 \pm 0.045) \times 10^{-7}$	2.2
2	5	Blue	$(2.31 \pm 0.040) \times 10^{-7}$	1.7
3	10	Green	$(2.20 \pm 0.070) \times 10^{-7}$	3.2

2.7 Conclusions

It has been shown that quantitative TLC can be carried out with CCD imaging in both transmission and reflectance modes on wetted plates. All data processing was carried out using the Beer-Lambert equation. Curvature at high loadings in the plots of integrated absorbance as a function of sample loading was accounted for using an empirical expression designed for use with the Kubelka-Munk treatment and apparent absorbance of the chromatographic sorbent layer due to scattering.

Results are consistent with an effective pathlength significantly longer than the thickness of the sorbent layer when apparent absorbance coefficients are compared with absorbance coefficients obtained from spectrophotometry and from using a horizontal cell placed beneath the CCD. The value of ε_{app} measured for Sudan II in

transmittance through the DCM-wetted TLC plate is a factor ~7 higher than the values obtained from both spectrophotometry and use of the horizontal cell. The horizontal cell and the spectrophotometer gave comparable results for absorbance of Sudan II. This shows that the optical configuration gives the expected value for absorbance in the absence of any scattering. A value for ε_{app} was obtained for Sudan II in transmission on the dry plate with the blue filter which is a factor 1.5 greater than the value on the wet plate and a factor 12 greater than ε in solution. This is consistent with a further increase in the effective pathlength, probably owing to greater scattering in absence of solvent.

The limit of detection was 2 ng and the linear range was between 5 and 50 ng in both transmission and reflectance on wetted plates. Linearity was very good over this limited range, with r^2 values of > 0.995 obtained. Intra-plate RSD values were between 1 and 4 %, whilst inter-plate RSD values were higher (8-14%) due to plate-to-plate variability. Results for a similar system evaluated in transmission, after the plate had been dried, gave a better limit of detection of < 0.5 ng and a linear range between 1 and 10 ng. Intra-plate RSD values (1-3 %) were comparable with those obtained for wet plates.

The increased noise due to the solvent is a factor adversely affecting the LOD on wet plates compared to that of dry plates. Another factor affecting LOD is the reproducibility of the background correction procedure. The solvent may not behave in exactly the same way in the two runs necessary for signal referencing to be carried out. This can be seen as a white band at the solvent front in figure 2.9. The difference between the two images is far less of a problem when imaging dry plates so long as the usual care is taken to ensure lighting conditions and the spatial register of the plate is the same in both cases.

Values for N_{obs} and H_{obs} were calculated from the data in Figure 2.8 using equations 1.15 and 1.16 respectively (section 1.1.7.5). N_{obs} was found to be 1376 and H_{obs} was 3.7×10^{-5} m. Values for N_{real} and H_{real} were calculated from the data in Figure 2.8 using equations 1.17 and 1.18 respectively (section 1.1.7.5). N_{real} was found to be 2601 and H_{real} was 2.0×10^{-5} m. These values fall in the expected range for TLC

(section 1.1.7.5). The benefit of including the initial spot width may be seen in the increase in plate number from 1376 to 2601.

The separation number (SN) was calculated from the data in Figure 2.8 using equation 1.24 (section 1.1.7.6) and found to be 16. This is also in the normal range for TLC (section 1.1.7.6).

CHAPTER THREE

Real-time Image Acquisition for Absorbance Detection and Quantification in Thin-layer Chromatography

3.1 Introduction

Scanning densitometry is the standard tool for evaluating planar separations (Pollack and Schulze-Clewing, 1990). However, this technique is slow (it can take up to twenty minutes to scan a plate) and is only suitable for offline applications where the sample spots are stationary. According to a review of planar chromatography, image analysis is likely to become the preferred method of densitometric evaluation in the future (Poole, 1999).

In previous work TLC plates have normally been imaged dry, after the solvent has been evaporated. The objective of this work is to find out if it is possible to get quantitative results from real-time measurements using a CCD camera during chromatographic development. CCD cameras have been used to evaluate TLC plates after drying in several modes, including transmission (Kowalczuk and Hopkala, 2002), reflectance (Vovk and Prošek, 1997) and fluorescence in conjunction with post-run derivatisation (Degterev *et al.*, 2000). Results using CCD cameras in reflectance mode have been compared with those of scanning densitometry; sensitivities were shown to be similar, but the acquisition times using CCD detection were faster (Cosgrove and Bilhorn 1989; Degtiar *et al* 1994; Degterev *et al* 1996)..

The benefits of real-time image acquisition using CCD cameras have previously been demonstrated in capillary-based separations, for example capillary zone electrophoresis (Bergström *et al.*, 1999) and capillary isoelectric focussing (Wu *et al.*, 1995). In the former case, this allowed enhancement of sensitivity whilst maintaining spectral resolution, and in the latter case the analytes were imaged in situ obviating the need for any mobilisation step. In both these examples absorbance was measured with spatial resolution in one dimension. In work described in this chapter (Lancaster *et al.*, 2005b), absorbance has to be measured with spatial resolution in both dimensions of the planar

TLC plate. The benefits are similar to those already demonstrated in previous 1D separations, namely in situ measurements and potential gains in sensitivity through signal averaging.

Some online work has been carried out in TLC. Firstly, diode array detection has been used, with a second detector for signal referencing (Nyiredy, 2002). Secondly, a CCD camera has been used to monitor a TLC separation of aflotoxins using UV excitation and fluorescence detection (Liang *et al.,* 1996). No quantitative measurements were made in either case.

3.2 Experimental

3.2.1 Chemicals

Sudan II was supplied by Aldrich Chemicals (Poole, UK). The solvents used were HPLC grade hexane, acetonitrile and dichloromethane from Fisher Scientific (Loughborough, UK). A stock solution of Sudan II of concentration 250 μg ml^{-1} was prepared by dissolving an accurately weighed amount in hexane. Standards were made by dilution of this stock solution, to give spotted weights in the range 1- 50 ng.

3.2.2 Chromatography

Thin layer chromatography was performed on 5 x 10 cm Silica Gel 60 F_{254} standard TLC plates and 10 x 10 cm Silica Gel 60 HPTLC plates from Merck (Darmstadt, Germany), glass backed, layer thickness 200 μm. Samples were applied as spots approximately 1 cm apart and 0.5 cm from the plate edge by means of 1 μl glass capillaries, supplied by Camlab (Cambridge, UK). Development was performed at room temperature in a 10 x 10 cm horizontal chamber (Camag, Switzerland).

A two-step development was chosen, with solvent focusing using acetonitrile before the development with dichloromethane. After spotting, the spots were focused with acetonitrile to a distance of approximately 1 cm from the bottom of the plate. The plate was then allowed to dry and then the focused bands were developed for a further 4-5 cm with dichloromethane. The camera was set up to take images continuously as development occurred. One image was taken every 6 s.

3.2.3 On-chip charge binning

The normal procedure for reading out the electric charge pattern stored in a CCD pixel by pixel was described in chapter one. In this procedure, a single parallel transfer places the accumulated charges from one row of pixels into the serial output register. The output register is then emptied by transferring the charge from each element of the register to the output amplifier and reading the amount of charge in each. However, if one parallel transfer is immediately followed by others (without reading the output register first) then the charges in the second or subsequent rows are added to the charges already in the output register.

The addition of charges in this way is known as charge binning or sometimes simply just binning. Binning the parallel transfer electrodes is known as parallel binning (Figure 3.1) and binning the serial transfer electrodes is known as serial binning (Figure 3.2). Any parallel binning factor may be combined with any serial binning factor. Figures 3.1 and 3.2 illustrate 2 × 2 charge binning. That is to say a sequence of two parallel transfers followed by a serial readout where pairs of pixels are transferred to the CCD output node to me measured together. The binning of a charge pattern is a noiseless process and leads to higher signal levels in the output register and also significantly reduces the readout time, which is important in some applications, especially where there may be temporal considerations and constraints.

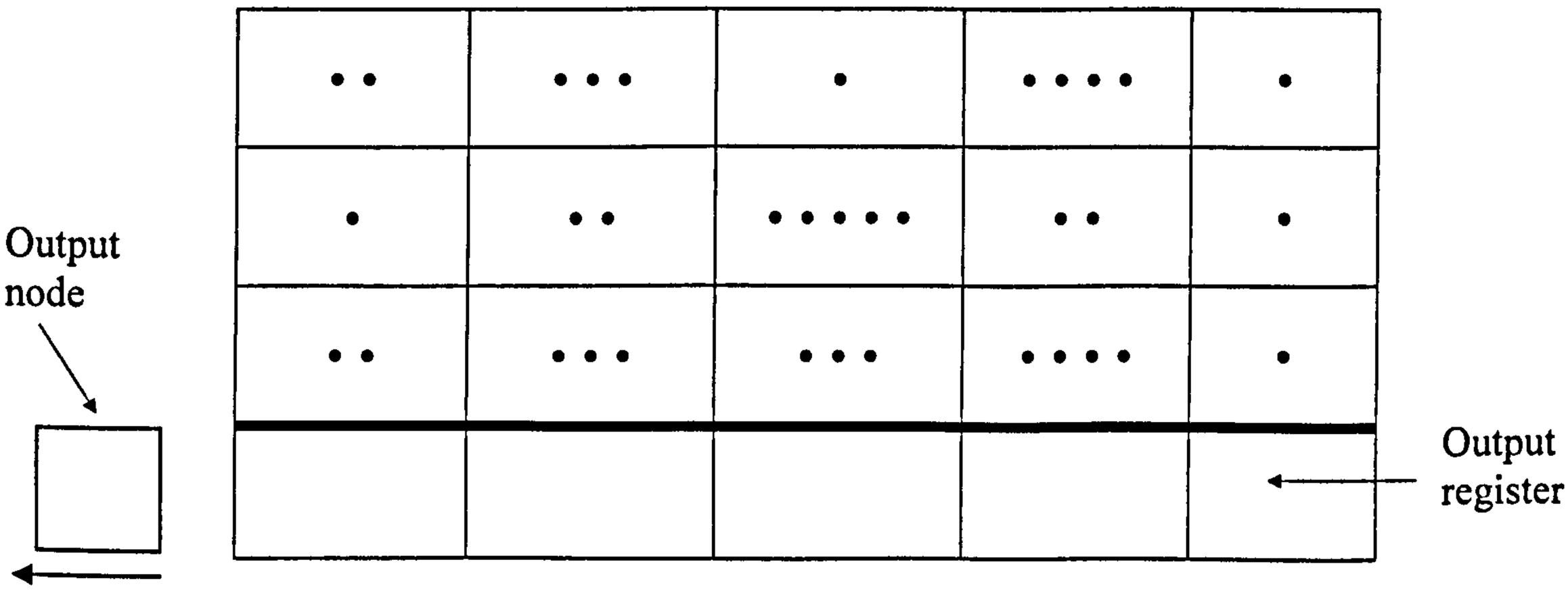

A. Charge pattern stored in pixels after exposure. The output register and output node are both empty.

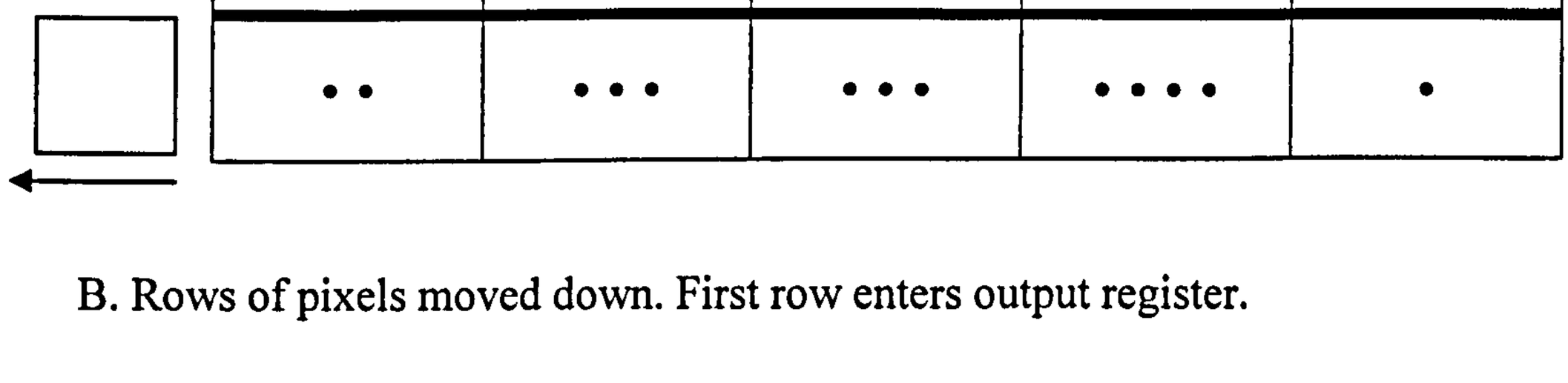

B. Rows of pixels moved down. First row enters output register.

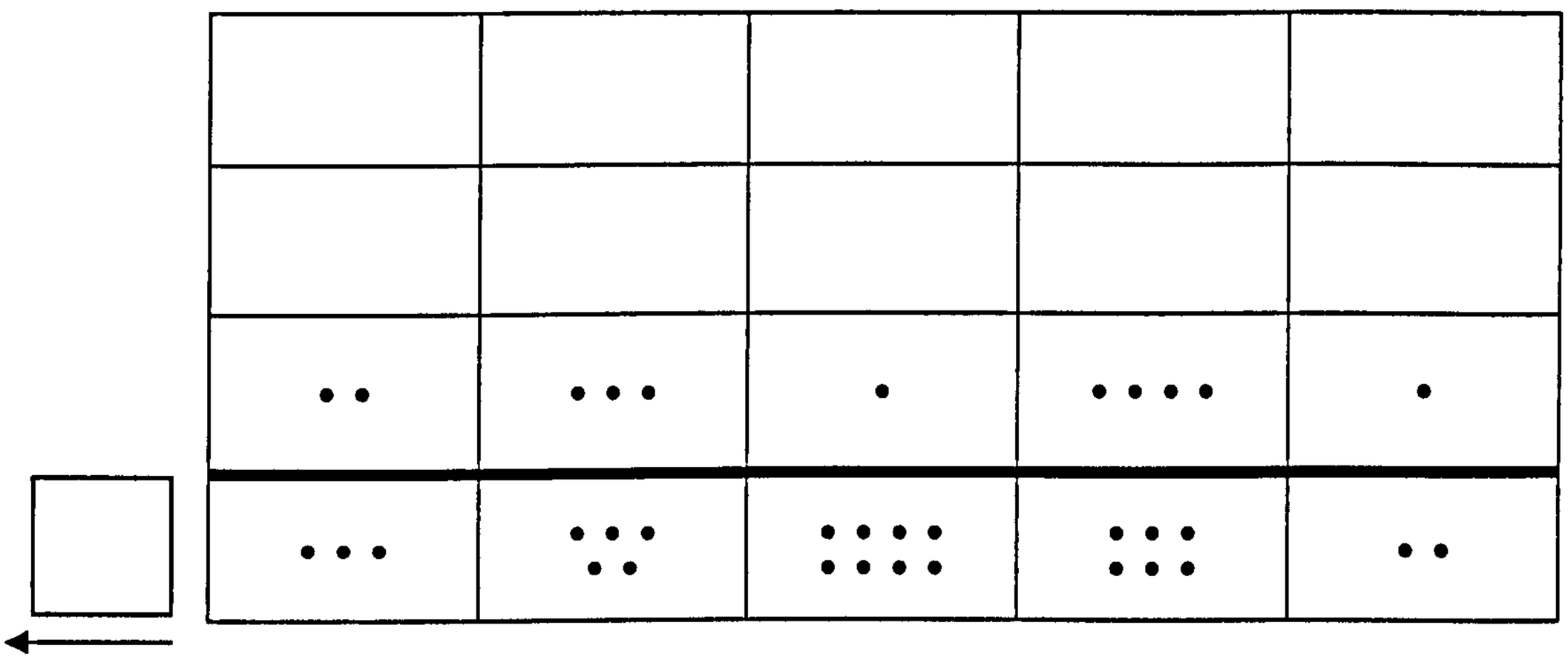

C. Second row of pixels added to first in output register.

Figure 3.1 Adding charges in the parallel registers of a CCD.

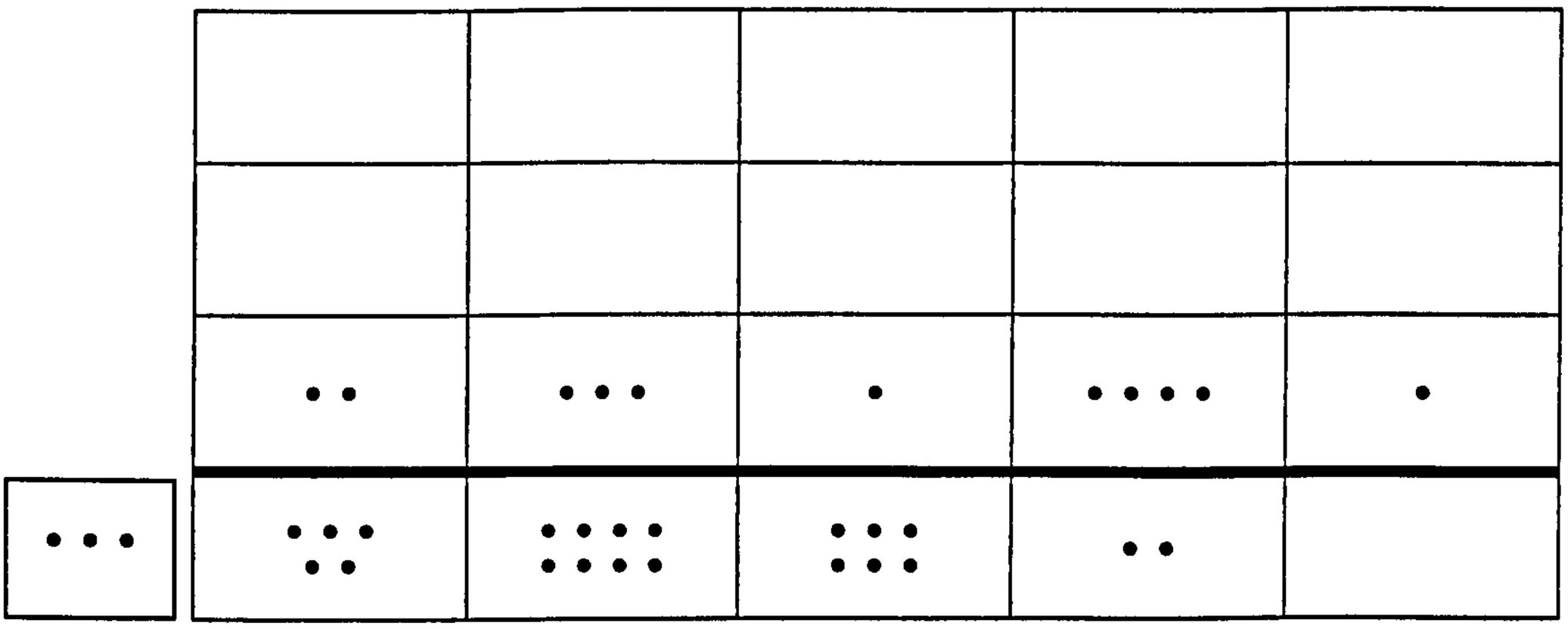

A. Output register moved left. First pixel held in output node.

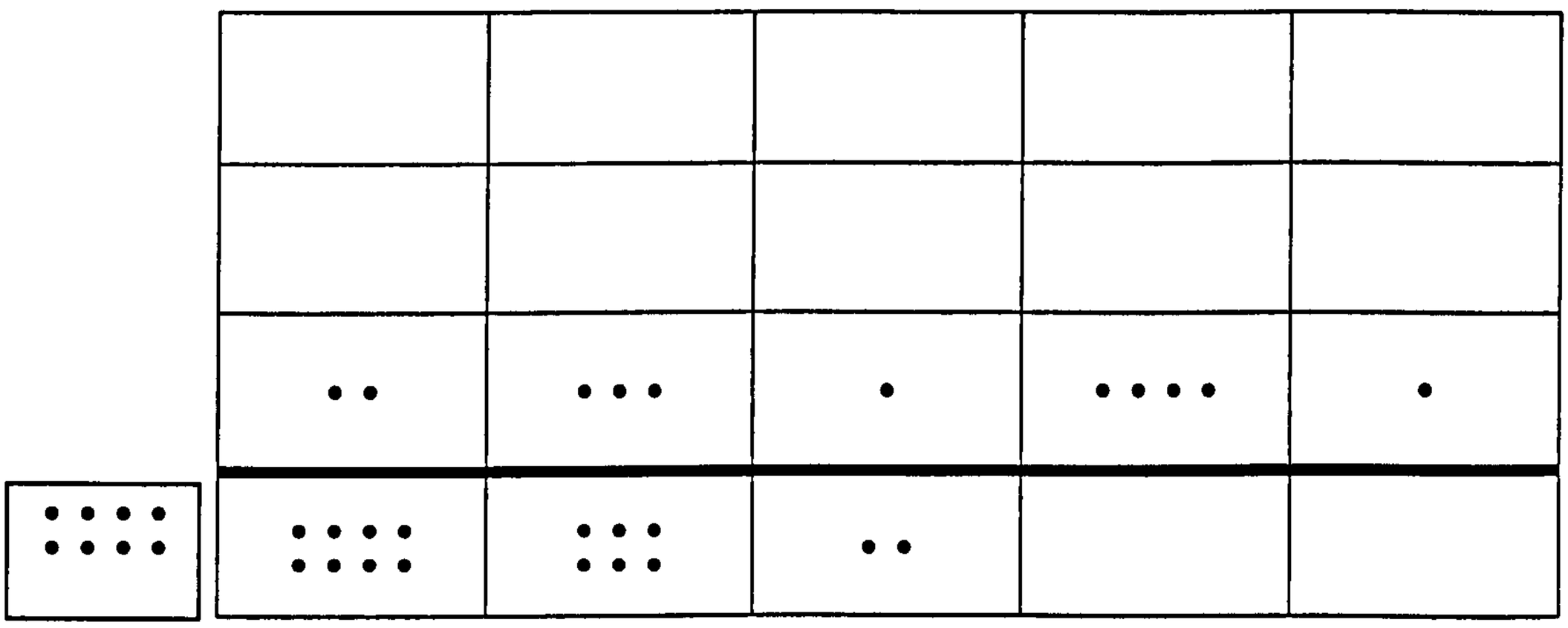

B. Output register moved left, summing first two pixels in output node.

Figure 3.2 Adding charges in the serial register of a CCD.

With a CCD camera designed for low light level applications the best performance is achieved with fairly slow readout rates (20-50,000 pixels per second). The time taken is to allow the signal processing to occur on each pixel read out. The time taken to transfer and add charges is very small in comparison and may be done very rapidly, as it is noiseless. Performing a 2 × 2 charge binning of a CCD will produce only a quarter of the number of output pixels. Therefore the entire electric charge pattern in the CCD can be read out in roughly a quarter of the time as that taken to read out the same pattern with no binning.

Currents in the CCD output amplifier generate the readout noise level, which provides the lower limit to the sensitivity of a CCD camera system. One of the advantages of charge binning is that the number of readout operations, and hence the readout noise, is reduced.

In this way the CCD may be operated to allow n rows to be added into the serial output register and for m serial output register elements (corresponding to CCD columns) to be added into the output amplifier. This is described as binning $n \times m$ pixels on-chip, and the readout of this signal (which will be nm times the signal in a single pixel for uniform illumination) will only have one unit of readout noise associated with it from the output amplifier.

There are advantages and disadvantages in binning the CCD image on-chip by $n \times m$. The advantages are that readout noise is reduced, signals will be larger and the readout time will be much shorter (almost in proportion to the number of elements read out). The main disadvantage of on-chip binning is obviously that the image resolution is degraded (by $n \times m$) and there is a trade-off between this and other factors, particularly readout rate. On-chip charge binning allows the speed disadvantages inherent in any slow-scan CCD camera system to be at least partially overcome at the cost of (some) spatial resolution.

3.2.4 Imaging and processing

The imaging apparatus used was the same as outlined in section 2.2.3, a picture of the set up is shown in Figure 3.3. All plate images had a blank image (taken with the shutter closed) subtracted and then 2×2 binning was carried out, giving effective pixels that each represent an area of 0.163 mm × 0.163 mm on the TLC plate. The conversion factor is thus 1 effective pixel = 2.66×10^{-8} m^2. The experimental set up for the reflectance experiments was the same as for the transmission experiments except that the light box was switched off, the cover removed and the laboratory lights used for illumination.

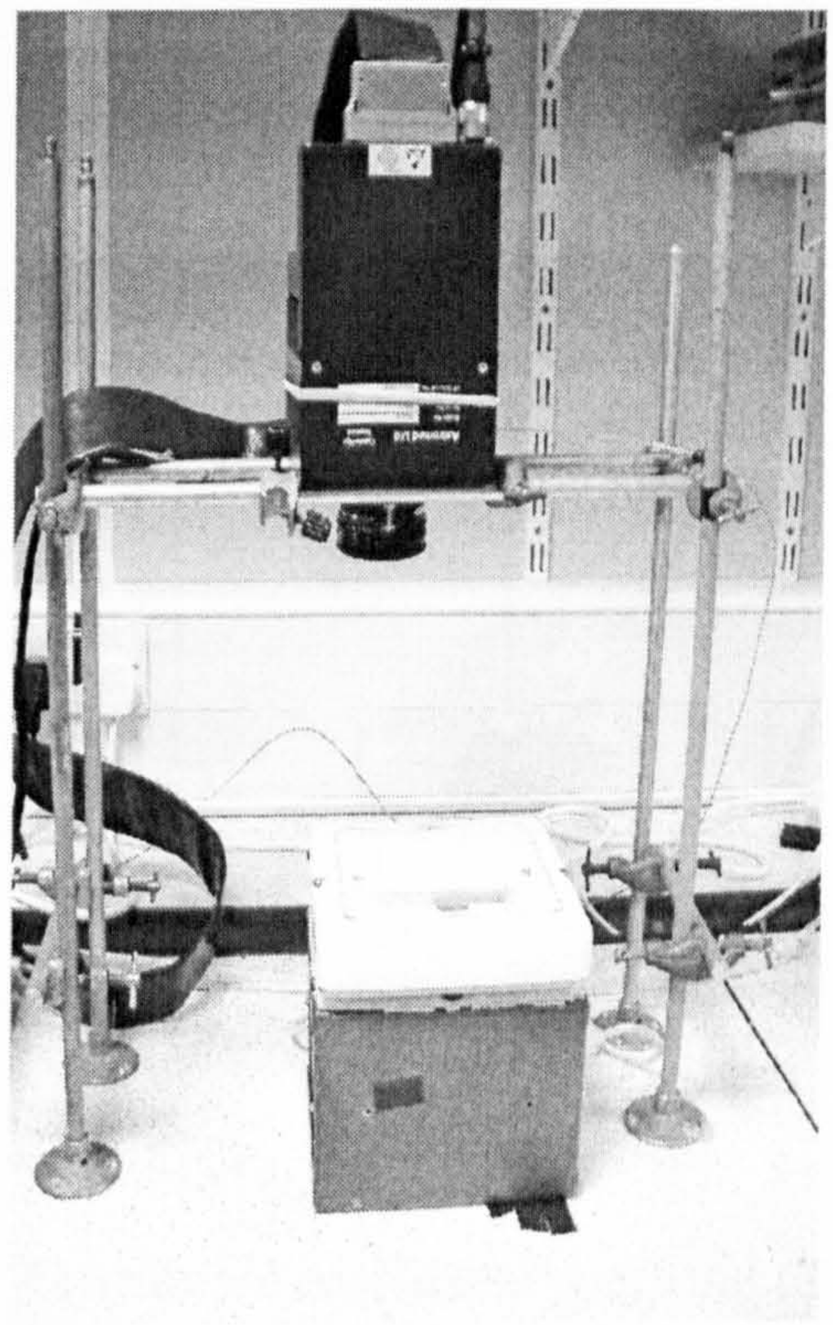

(A) CCD camera
(B) Filter
(C) Lens
(D) Cover
(E) Developing tank
(F) TLC plate
(G) Light box

Figure 3.3 Experimental set-up. The cover has been removed in the photograph.

Spectral characteristics of the filter, dye, CCD response and of the lamp used are given in Figure 3.4. The figure shows that the detection signal obtained in these studies arises predominantly from the absorbance of light centred at 485 nm emitted by the phosphor-coated fluorescent lamp.

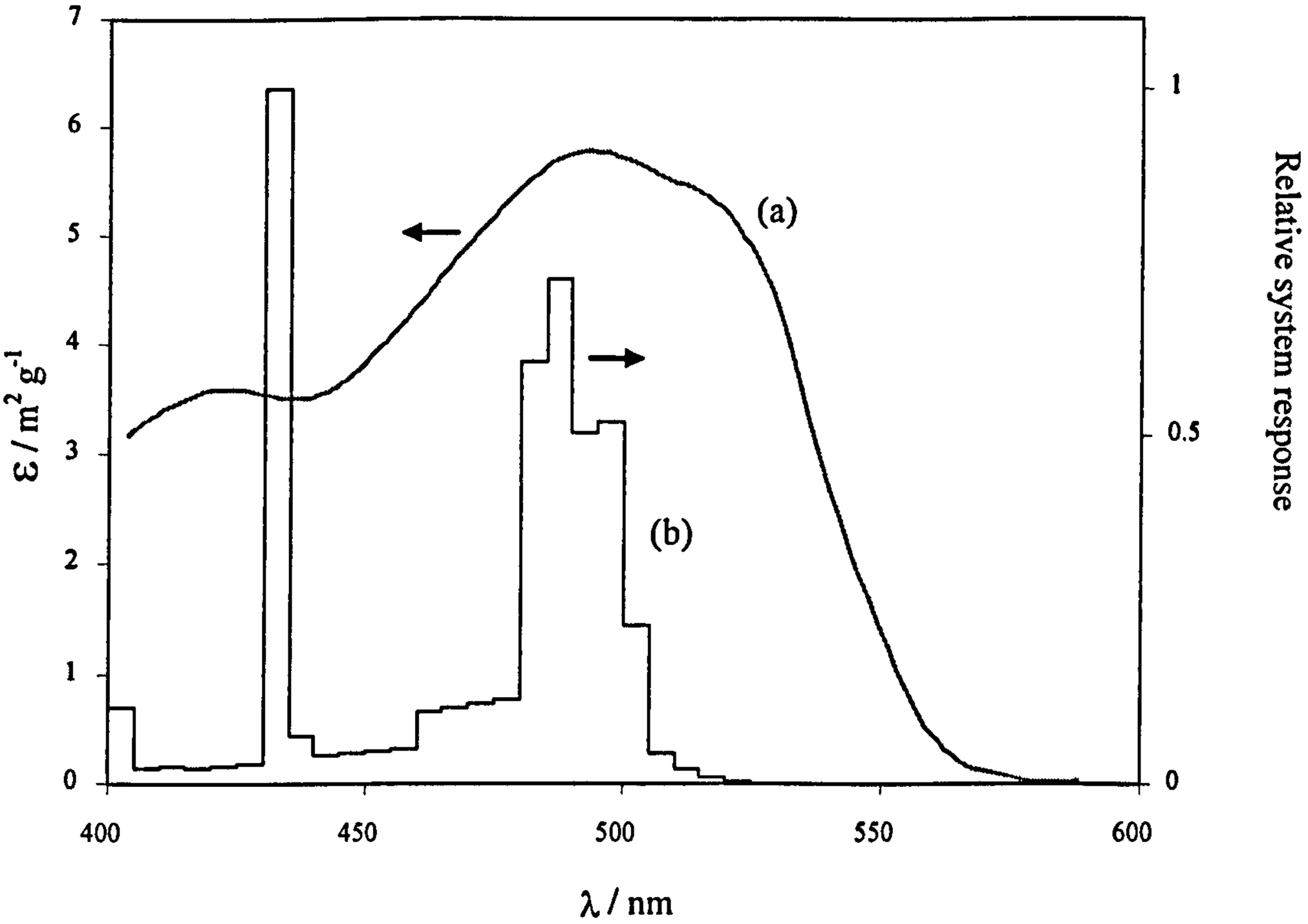

Figure 3.4 (a) Absorbance coefficient spectrum of Sudan II measured using a 25 mg l^{-1} solution in dichloromethane in a 1 cm cell. (b) Overall relative spectral response of the detection system calculated from the CCD responsivity, filter transmission and the lamp spectral power distribution.

3.3 Signal referencing

The output from the CCD camera is a series of images, each taken at regular intervals during the chromatographic development. These images need to be corrected for fixed pattern and solvent effects. Several raw images taken in transmission during chromatography are presented in Figure 3.5 (parts A-D).

Image A is the first image taken during the chromatographic development. The plate has been spotted with four 10 ng spots of Sudan II, chromatography has just begun and the solvent front has not yet reached the spots. Image B is the tenth image in the series and shows the spots just behind the solvent front, which has moved further along the plate. Image C is the fortieth image in the series and shows that the spots have migrated further along the plate, as has the solvent front. The wet part of the plate appears bright in the image; this is because more light is transmitted through the wetted portion. Image

D is the sixtieth image in the series; the spots are now much further behind the solvent front. Some band broadening is evident in the relative size of the spots between the images as the chromatographic development progresses, the spots being much more diffuse in Image D than in Image B.

Whilst it was still possible to compensate for fixed pattern noise in the same way as for offline experiments, the presence of moving solvent prevents signal referencing being carried out in the same way as in offline measurements (Lancaster *et al* 2005a).

In order to compensate for the presence of moving solvent, the plate is divided into lanes of pixels; the sample lane (lane containing the sample spot) and reference lanes (lanes that include no spot), used to provide reference signals. The width of the sample lane was chosen such that it encompassed the whole of the spot when at its most diffuse at the end of the chromatographic run. The reference lanes were selected far enough away from the sample lane so that the spot did not interfere with them. The lanes are assigned after chromatography, as shown in Figure 3.6. Typically 20 contiguous columns of effective pixels make up the sample lane, and five contiguous columns of effective pixels were used for the reference lanes, one either side of the sample lane.

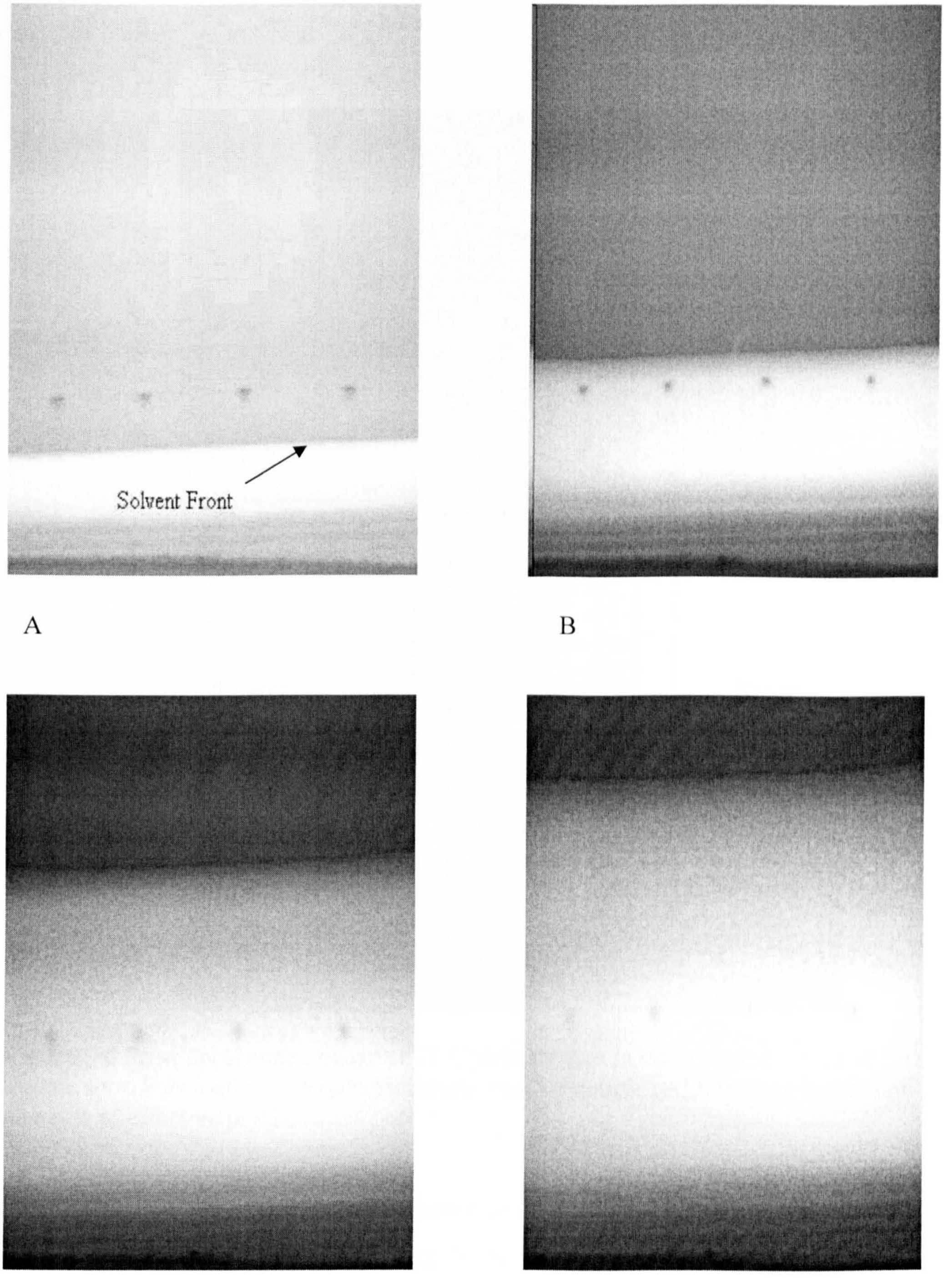

A B

C D

Figure 3.5 (A-D) Four images from a series taken during chromatography are shown. All are raw, uncorrected images with no signal referencing. The spots are all 10 ng imaged in transmission. A is the 1st image, B the 10th, C the 40th and D the 60th in the series.

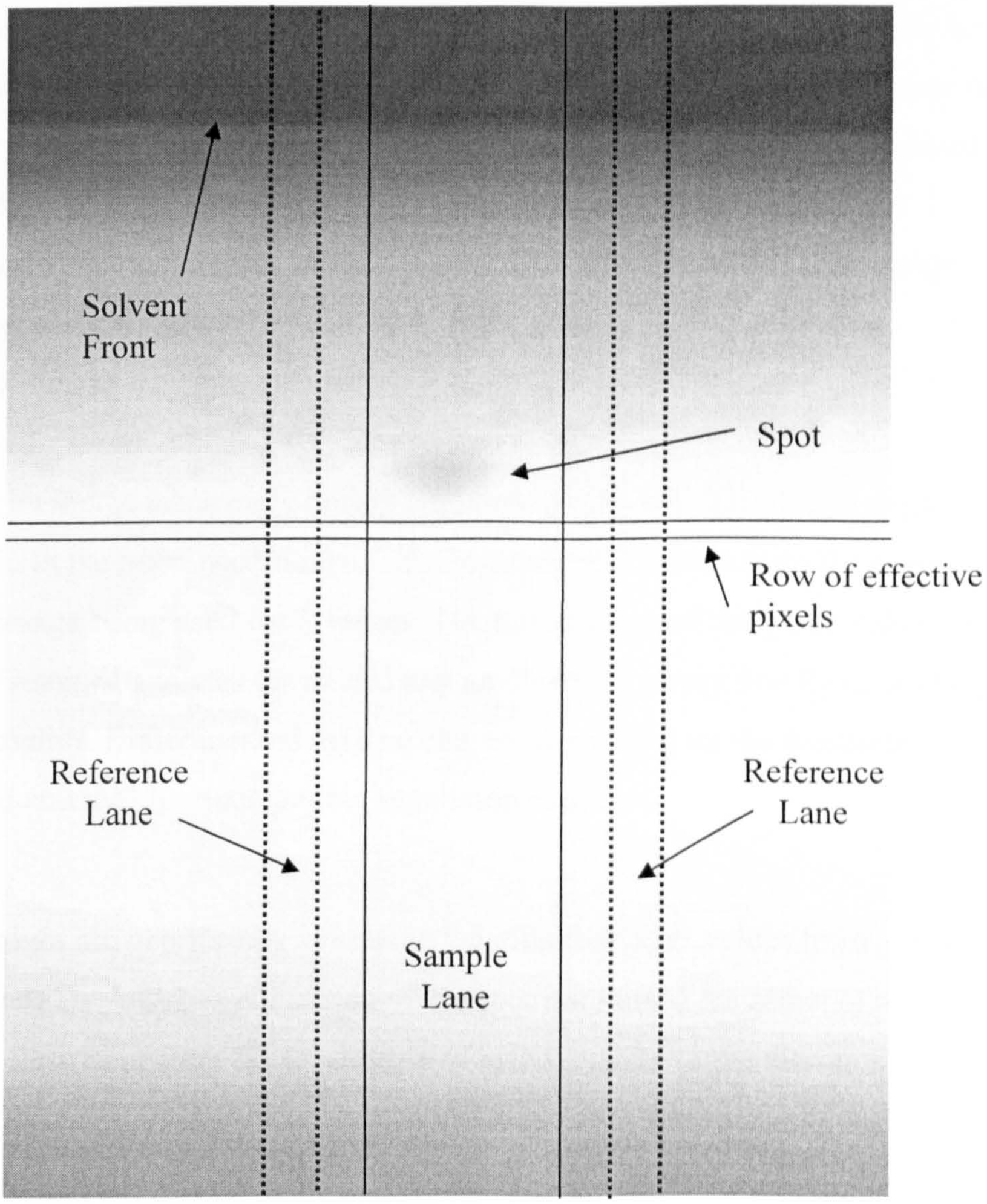

Figure 3.6 Raw, uncorrected image of TLC plate imaged in transmission with a 10 ng sample spot. Schematic shows superimposed areas of sample and reference lanes, and also row of effective pixels.

After the assignment of sample and reference lanes, signal referencing of images was carried out by an in-house program using the equation given below to obtain the corrected absorbance A_{corr} for each sample effective pixel address

$$A_{corr} = \log\left(\frac{(I_o / I)_s}{(I_o / I)_{ref}}\right) \tag{3.1}$$

where I = value for effective pixel, and the subscripts are as follows: ref denotes reference lane, s effective pixel from sample lane, and o initial image.

To obtain the initial image, giving values of I_0 for each pixel, either the dry, blank plate may be imaged prior to chromatographic development (Figure 3.7A), or an image taken early in the chromatographic run (before the solvent reaches the sample spots) may be used (Figure 3.7B). There are advantages associated with either method. If the plate is to be imaged dry then the plate will have to be removed for spotting and then replaced for chromatography with the possibility of introducing an error if the plate is not positioned in exactly the same place in each image. This error is avoided if an image taken early in the chromatographic run is used, as the plate is not moved during chromatography.

However, using an image taken early during chromatography will introduce a negative peak at the origin in the referenced image. This negative peak comes from the presence of a spot in the image being used for I_0 values. The introduction of this peak makes the measurement of retained analytes (or indeed any analyte with a very low R_f value) very difficult or impossible. Either method may be chosen, depending on the demands of the analysis required and the chromatographic separation expected.

The reference values are obtained by averaging the effective pixel values from a row in the reference lanes. Use of lanes either side of the spot minimised the effect of any distortion of the flow front from the ideal angle of orthogonality to the direction of flow. For each row in the sample lane, values of A_{corr} are summed to give a signal, S_a, with units of AU pixels

$$S_a = \sum_{i}^{n} A_{corr} \tag{3.2}$$

where n is the number of columns in the sample lane. The need for reference lanes to be well separated from the sample lane means that fewer spots than normal can be fitted onto a plate; no more than four spots could be fitted onto one end of a 5 × 10 cm plate.

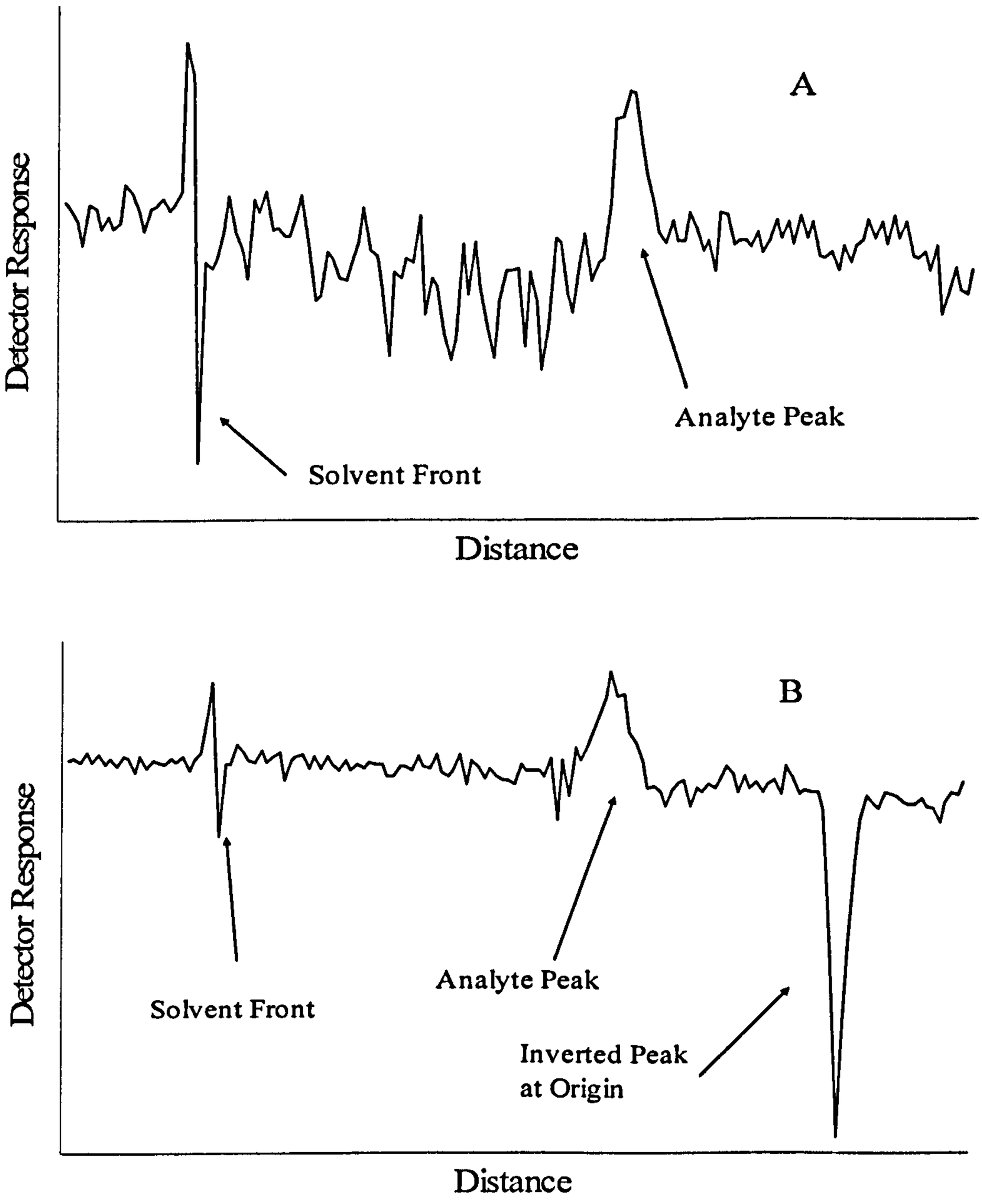

Figure 3.7 Comparison of different methods of compensating for fixed pattern noise. In A, an image of blank, dry plate was used to compensate for fixed pattern effects. In B, an image taken early in chromatographic run was used to compensate for fixed pattern effects. The compensation is more successful in B at the cost of loss of information from the origin.

Figure 3.8 shows data from one of a series of images taken as a separation progresses. The figure illustrates the signal referencing procedure, which compensates for fixed pattern and solvent effects.

$$\sum_{i}^{n} I_s$$

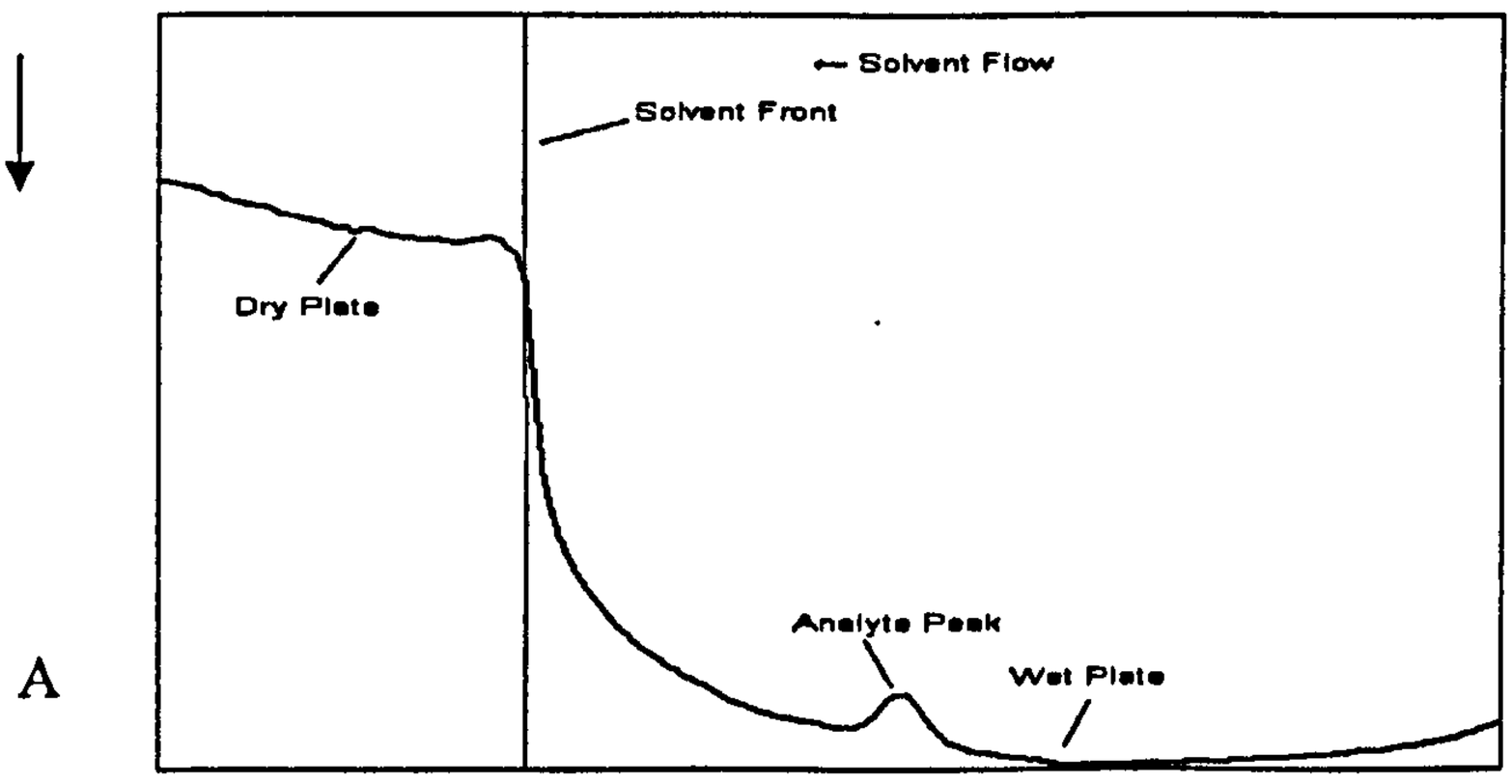

A

$$\sum_{i}^{n} \log\left(\frac{I_o}{I_s}\right)$$

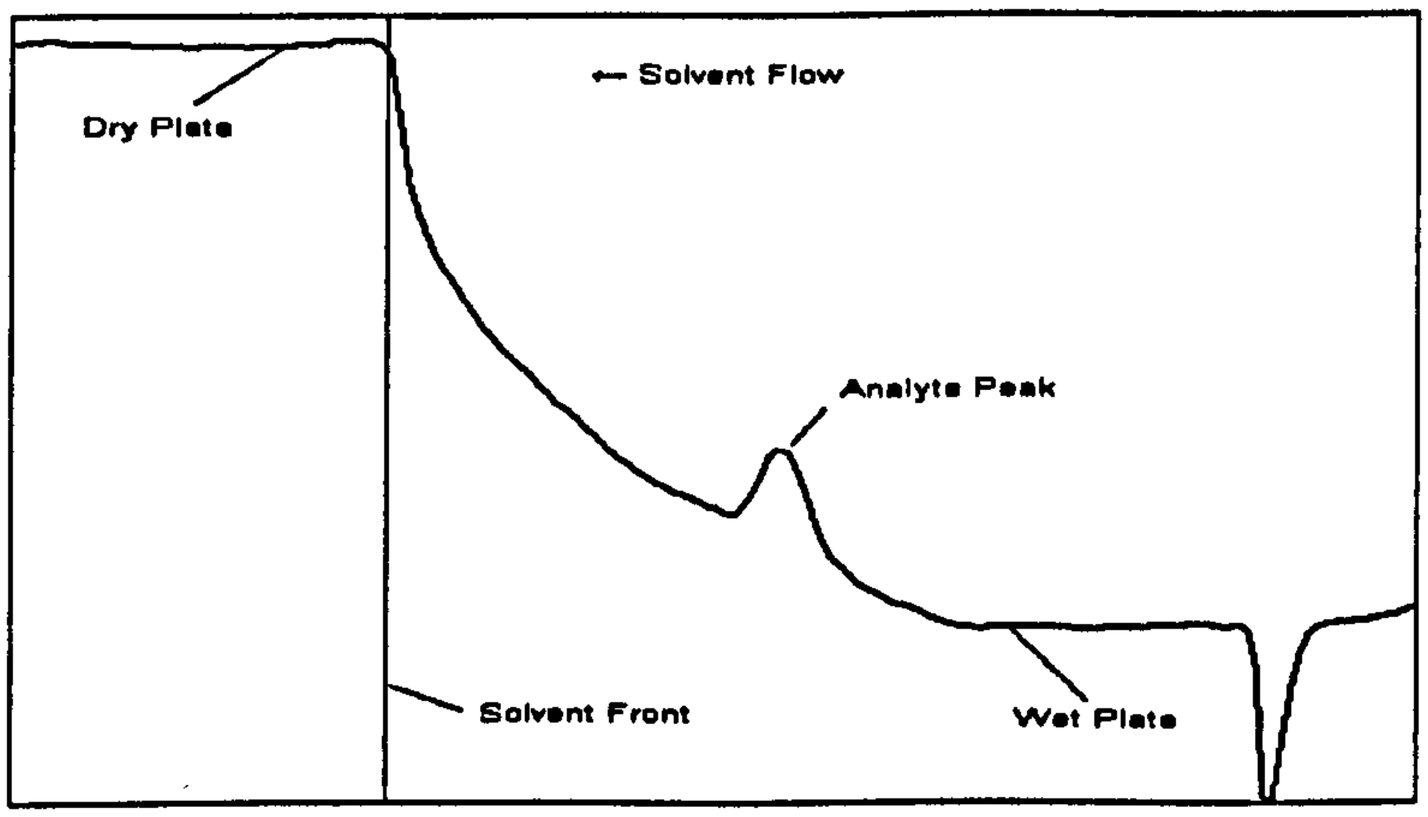

B

$$\sum_{i}^{n} \log\left(\frac{(I_o / I)_s}{(I_o / I)_{ref}}\right)$$

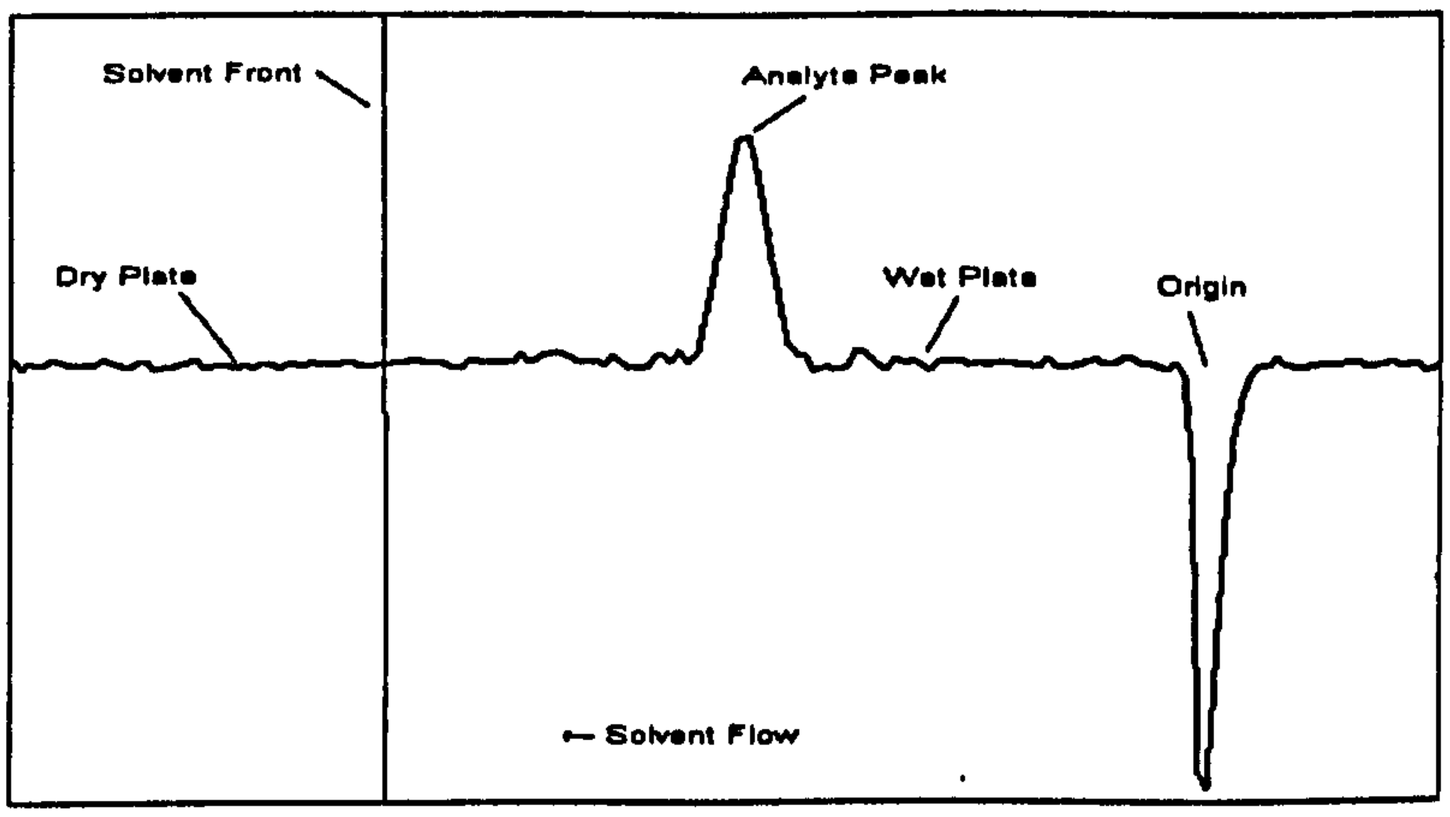

C

Distance

Figure 3.8. Signal referencing online in TLC with dichloromethane as developing solvent. A, raw uncorrected data for a 10 ng Sudan II peak imaged in transmission; B, data corrected for fixed pattern noise; C, data corrected for plate and light variations and also for solvent effects.

The fixed pattern contribution evident in Figure 3.8 A from the variation in light level with distance along the plate is due to the inhomogeneity of light transmitted through the plate, arising partly from irregularities in the sorbent layer. Correction for this contribution was accomplished by ratioing with the initial image taken prior to chromatographic development. The background correction for fixed pattern effects (as in offline results in chapter two) results in flat baselines in the dry and fully solvated portions of the plate. The apparent peak at the origin in Figure 3.8 B is a consequence of the background correction.

In Figure 3.8 B the straight horizontal portion to the left of the solvent front corresponds to the dry area of the TLC plate. The horizontal portion at lower apparent absorbance is assumed to show the fully wetted area. This is consistent with more light being transmitted through the plate when the sorbent layer is wet. It is likely that the curve between the two horizontal portions is correlated to the degree of solvent permeation into the pores of the stationary phase. This is the first example of real-time observation of the effect of differential wetting of the TLC plate.

If it were necessary to examine a spot close to the origin, the inverted peak in Figures 3.8 B and 3.8 C could be removed by ratioing using a blank plate for the initial image, before spotting, instead of a spotted plate. Ratioing with a blank plate could introduce some error, because after the initial image was taken, the plate would have to be removed for spotting and then replaced for chromatography. If the plate is not replaced in exactly the same location then the correction will be imperfect.

Figure 3.8 C shows data from the sample lane in Figure 3.8 B corrected for solvent effects using signals from the reference lanes in the same row. This leads to a flat baseline, with no discontinuity at the point of the solvent front.

Figure 3.9 shows the absorbance along the plate obtained at several times during chromatographic development. The raw images (as in Figure 3.8 B) have been ratioed with another image in order to correct for fixed pattern effects such as inhomogeneity of light and plate effects but not for solvent effects. It can be seen that the background level on the dry portion of the plate is effectively constant, as is the absorbance on the fully solvated part. The absorbance of the fully wetted part of the plate is lower than that of the dry part. This is likely to be due to the wetted part letting through more light

because of less scattering at the solid/liquid than the solid/air interface. Scattering depends on the refractive index difference between the particle and the medium, and this difference is greater when the medium is liquid rather than air. The absorbance in between varies with time, the slope between the dry and wet parts becoming shallower as the separation progresses.

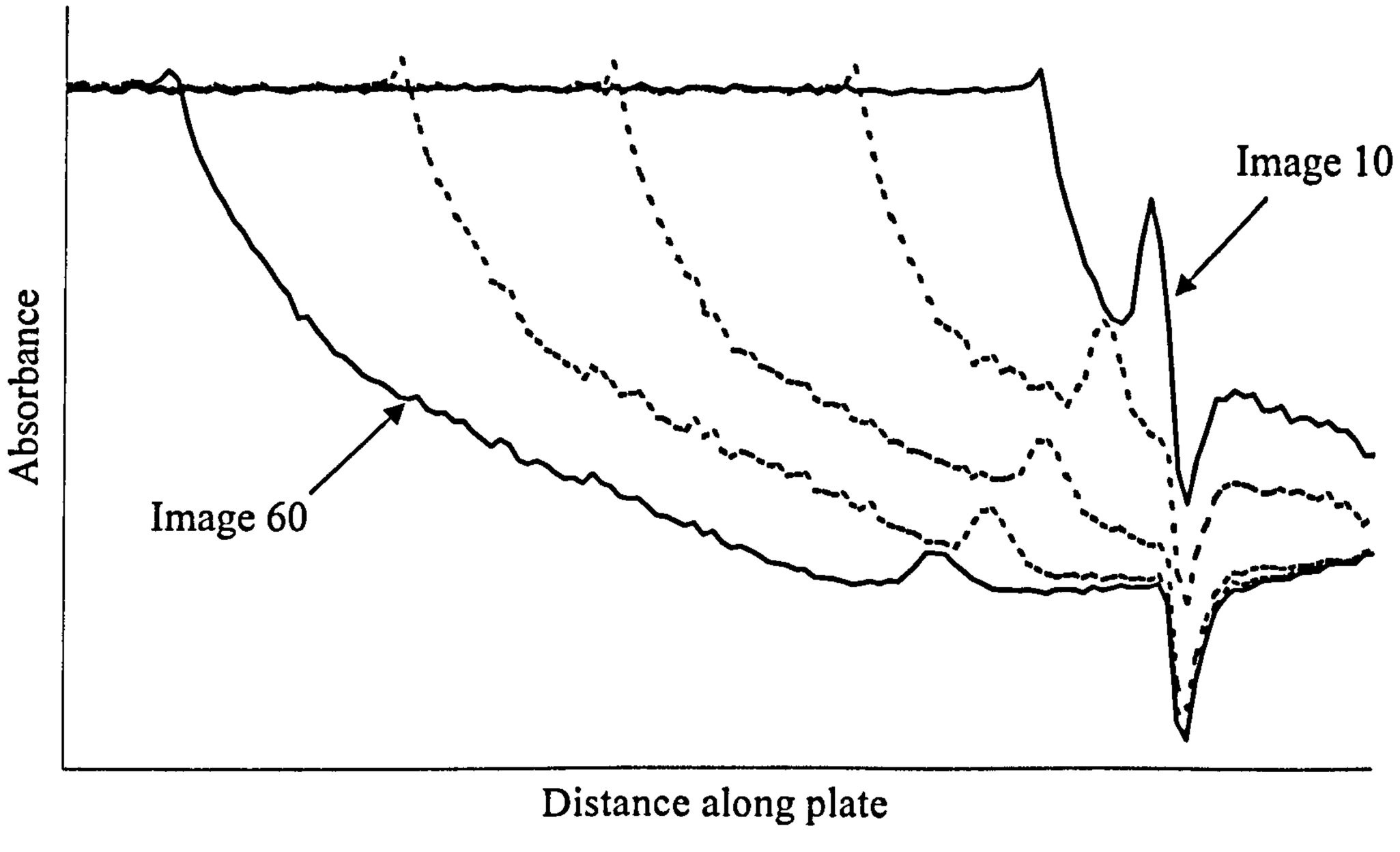

Figure 3.9 Absorbance plotted as a function of distance along plate for a 10 ng spot of Sudan II imaged in transmission at several points during chromatographic development.

3.4 Signal averaging

Since many snapshots can be taken throughout the chromatographic development, it is possible to combine the information from a number of images to improve the sensitivity and dynamic range. Figure 3.8 C shows the spot profiles obtained from 14 of the 70 images of a Sudan II spot taken during a 7 minute development with dichloromethane.

The peaks in Figure 3.10 are at five exposure intervals of 6 s, with the first peak from the left being the fifth exposure taken 30 s after starting chromatography, the second at the tenth exposure (60 s) and so on.

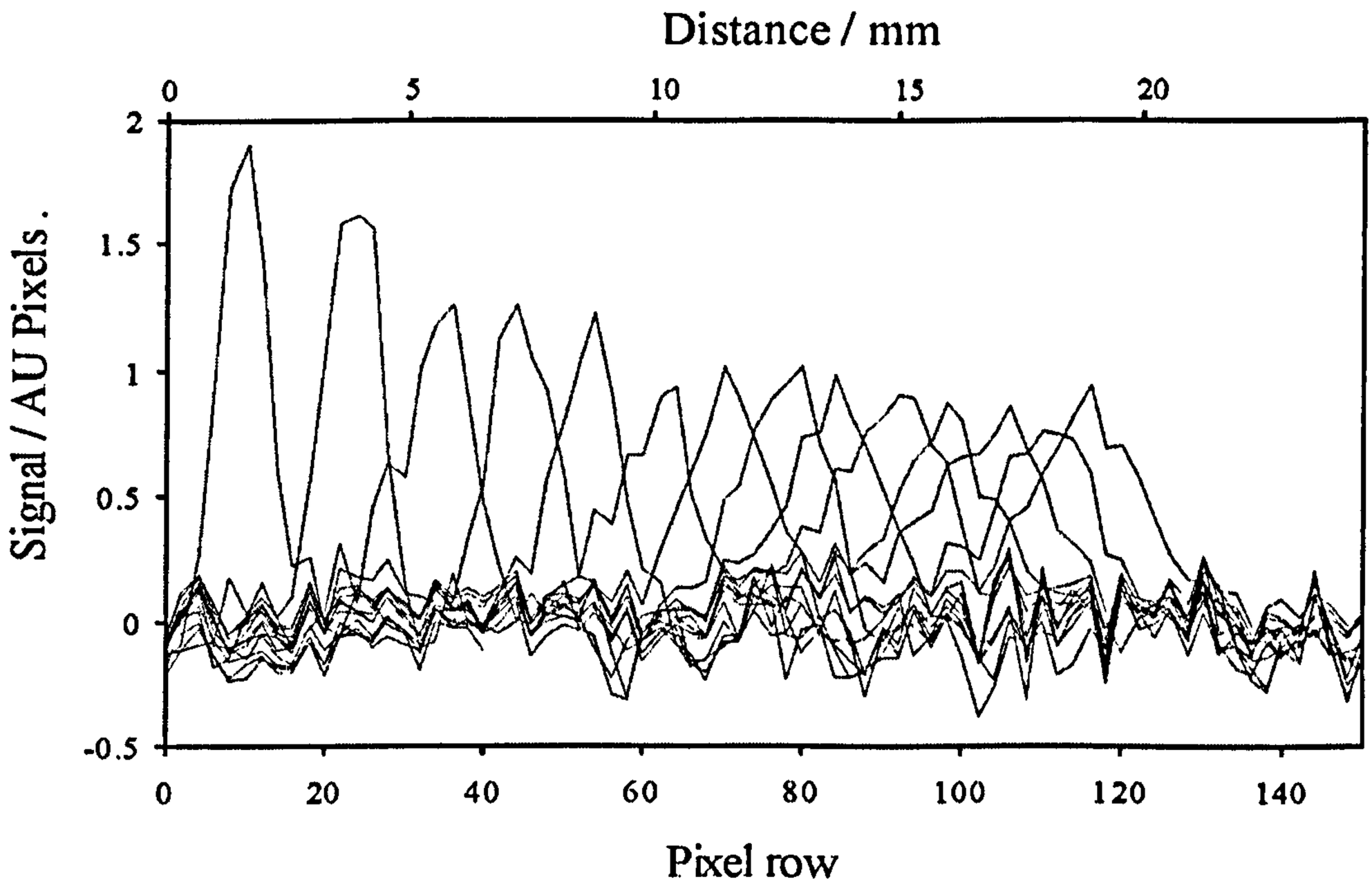

Figure 3.10 Snapshots of a spot moving during chromatographic development, taken in transmission mode at 30 s intervals.

In making quantitative measurements, it is necessary to show that there is no systematic change in peak area in a sequence of images. The peak areas from successive images can then be combined by simple addition in order to improve the signal to noise (S/N) ratio. Such averaging is most effectively carried out when the peaks are aligned to a common centre. Figure 3.11 shows peak area as a function of exposure number, for all 70 images acquired during the run shown in Figure 3.10. Data from the same experiment is also given in Table 3.1.

The peak area is obtained by integrating the signal over all rows containing the peak, and is reported with units of AU m^2 after conversion from the area of the effective pixel to m^2. In this run the distance moved by the analyte peak between the first and last exposure is ~ 2 cm. The areas from the first few points in all runs were not used in subsequent analysis. These points cover the time before the analyte band is separated from the solvent front, and are subject to artefacts. The data points p, from $p = 15 - 70$

were found to be randomly distributed about the mean value over this range, and it is evident that within experimental error, for $p \geq 15$, the peak area is time independent.

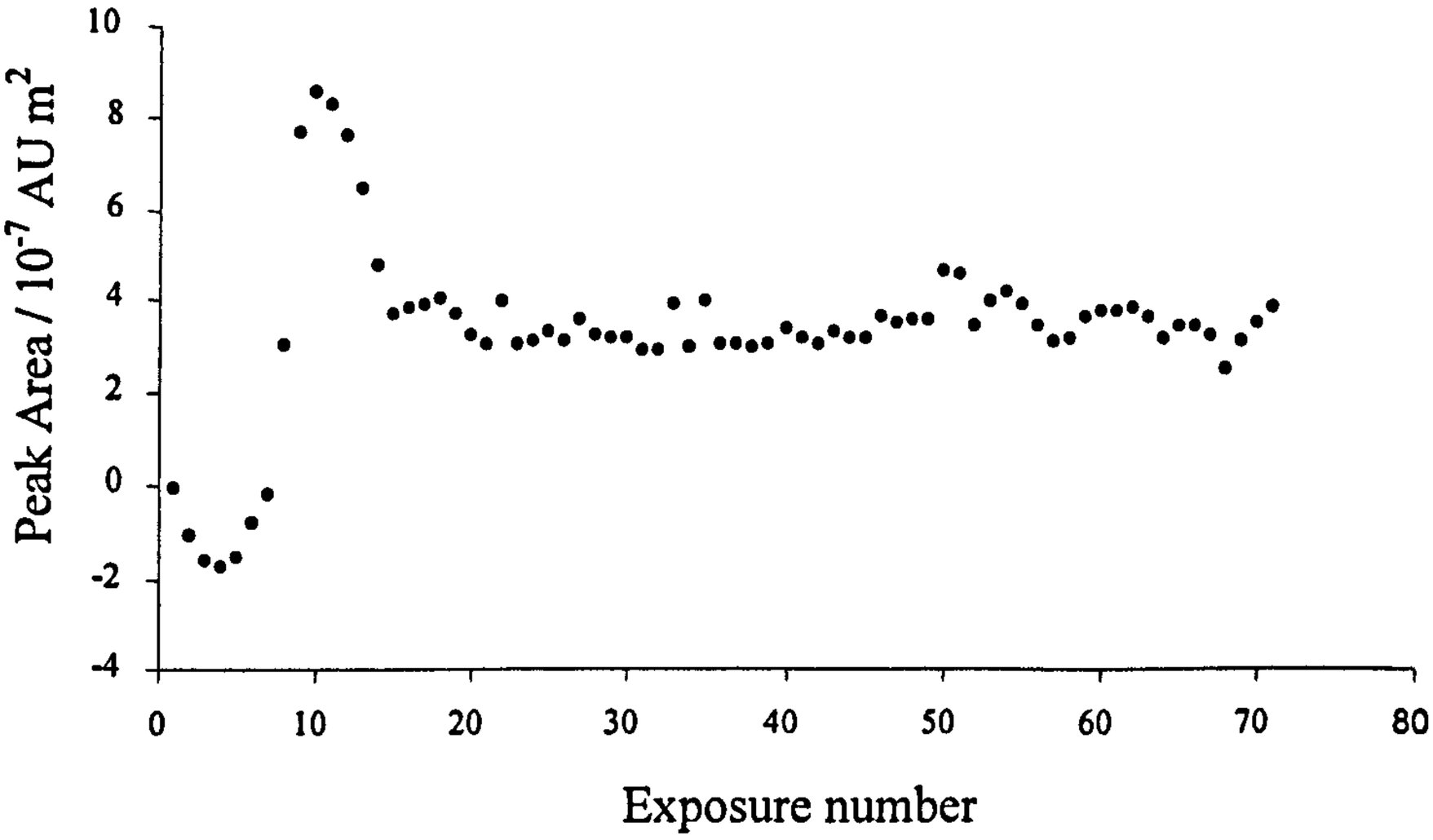

Figure 3.11 Graphical representation of peak area versus exposure number during chromatographic development. Time between each exposure is 6 s.

Table 3.1 Integrated signal as a function of exposure number during elution of a 10 ng peak of Sudan II in transmittance. Ten exposures are averaged in each case.

Exposures	Signal / AU m^2
20-29	3.23×10^{-7}
30-39	3.17×10^{-7}
40-49	3.45×10^{-7}
50-59	3.70×10^{-7}
60-69	3.38×10^{-7}

This finding allows the images obtained in transmission to be averaged. The pixel address shift necessary to achieve this was calculated using the following relationship (shown in Equation 3.3) between solvent front position and time, which is well established for TLC (Kowalczuk and Hopkala, 2001)

$$Z_f = \sqrt{k_v t} \qquad (3.3)$$

where Z_f is the distance migrated by the solvent, k_v the velocity constant, and t the time after solvent makes contact with the layer. Since the retardation factor linking the analyte position to the solvent front is a constant, it follows that the relationship between distance migrated by the analyte and time should also take the form of Equation 3.3. This was indeed found to be the case, and is visibly evident in Figure 3.10. Equation 3.3 was used through adjusting k_v to minimise the peak width obtained from the summed images during alignment of peaks to a common centre.

Features can be seen after averaging many images that cannot be seen in one image, as shown in Figure 3.12. In Figure 3.12 A the 1 ng peak cannot be seen in a single exposure, but after averaging 55 images (Figure 3.12 B) the peak could be clearly identified and quantified with a S/N ratio (peak to peak noise) of about 3.

In experiments using a 50 ng loading, the S/N in peak area from summed images was found to scale with the square root of the number of images averaged, n_i, over the range $n_i = 1 - 60$, giving a value of the S/N (peak to peak) of $(8.86 \pm 0.24)\sqrt{n_i}$ with $R^2 =$ 0.977. The data is given in Table 3.2 and the relationship is illustrated in Figure 3.13.

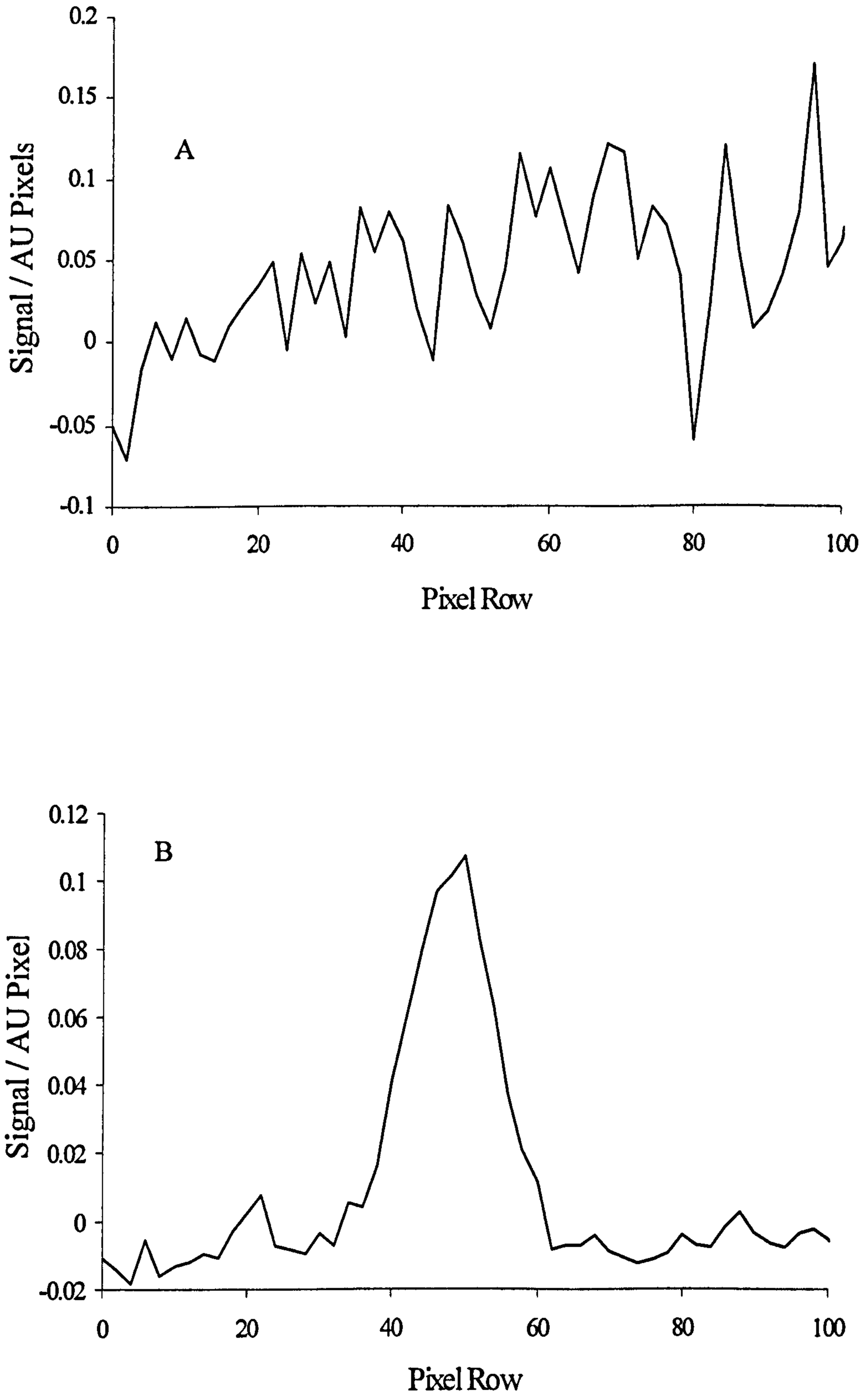

Figure 3.12 Profiles from: A, a single image; B, the average of 55 images. The sample loading is 2 ng.

Table 3.2 Variance of signal to noise ratio with number of images averaged (n_i) of a 50 ng peak of Sudan II.

n_i	$\sqrt{n_i}$	S/N
1	1	8
3	1.73	14
10	3.16	25
20	4.47	36
30	5.48	54
40	6.32	60
50	7.07	63
60	7.75	65

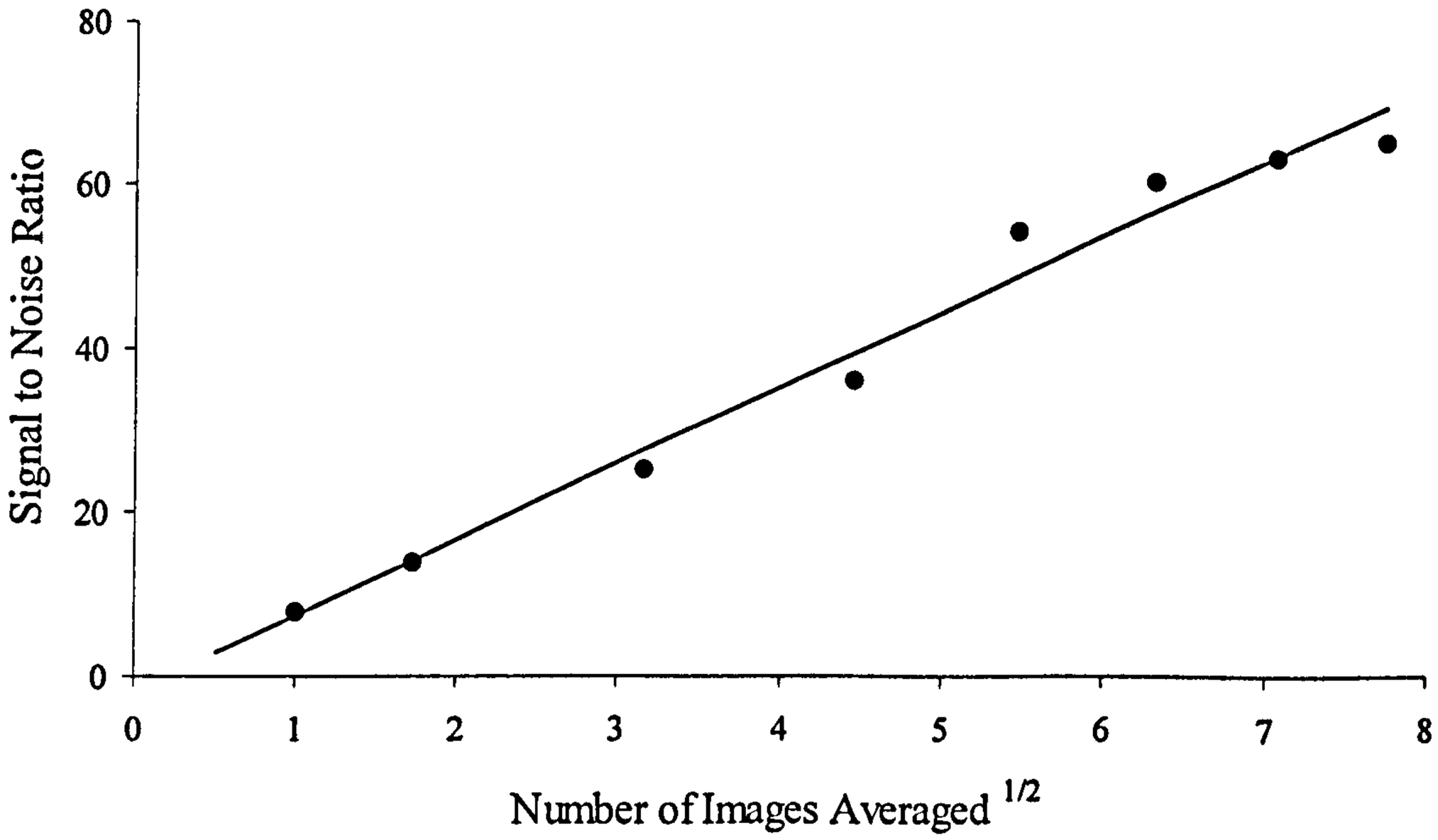

Figure 3.13 Plot of signal to noise ratio against the square root of the number of images averaged as given in table 3.1. The r^2 value is 0.977, the slope is 9.16 ± 1.35 and the intercept is –1.72 ± 7.01.

Table 3.3 gives values for LODs obtained in the present real-time imaging study and a comparison with results from offline CCD imaging. In comparison with the LOD that was obtained using a single image, there is a factor 5 improvement in LOD after averaging 55 images. The LOD of 1 ng obtained after signal averaging lies between the values of 0.5 and 2 ng obtained for dry and wet plates respectively in offline

measurements (Lancaster *et al.*, 2005a). The LOD of 5 ng obtained from a single image in real-time is greater than the value of 2 ng obtained for Sudan II in a wet plate offline using the same exposure parameters (100 ms, f 4) and light intensity. This suggests that the method of correcting for the moving solvent front is not as complete as in the offline experiments. Close inspection of Figure 3.10 reveals the presence of systematic noise in the baseline, which is consistent with these findings. The benefit of signal averaging in the real-time measurements with the correction for peak position shift is that such systematic noise features are attenuated.

Table 3.3 Detection limits (S/N = 3) and RSD values (n = 4) for Sudan II in TLC with dichloromethane as developing solvent and various modes of imaging detection. [a] 10 ng spots, [b] 50 ng spots. [c] (Lancaster *et al* 2005).

Mode	LOD / ng	RSD / %	Inter-plate RSD / %
Real-time no averaging	5	3.5 [a]	16 [a]
Real-time averaged	1	1.9 [a]	5 [a]
Real-time averaged HPTLC	1	1.6 [a]	3 [a]
Wet offline transmission [c]	2	2.4 [a]	14 [a]
Dry transmission [c]	0.5	3.1 [b]	9 [b]
Dry reflectance [c]	1	3.2 [b]	14 [b]

Table 3.3 also documents the improvement in reproducibility of results by averaging many exposures. For averaging real-time images of four eluting 10 ng spots, the RSD values for the integrated peak areas are below 2%. In all other modes higher RSDs are obtained, in the range 2.4 – 3.5%. When comparing intra-plate RSD values, the two best results are seen when using the averaged real-time imaging data. The lowest intra-plate RSD is with the HPTLC plates, which would be consistent with reproducibility in manufacture being greater than with standard TLC plates.

Table 3.4 presents calibration curves for Sudan II using four spots with different loadings on a single plate. Calibrations were carried out over two overlapping ranges, each spanning an order of magnitude variation in sample loading: 1, 2, 5, 10 and 5, 10, 20, 50 ng respectively. Regression analysis was carried out to equations with two independent variables. Over the range 1-10 ng a linear fit was found to be satisfactory,

using r^2 values. The intercept in a plot of integrated area versus loading, the term in x^0, is within experimental error equal to zero. The x^0 term was consequently set equal to zero for fitting the data over the range 5 – 50 ng loading to an equation with x^1 and x^2 terms. The coefficient for the x^1 term is seen to be the same within the limits of uncertainty for the two calibration ranges, with averaging over results from four separate plates giving values of 38.7 ± 4.2 and 36.1 ± 5.2 AU m^2 g^{-1} for the 1-10 and 5-50 ng calibration ranges respectively. In the higher calibration range, the systematic negative curvature in the calibration curve is consistent with results obtained in other studies (Belchamber *et al.*, 1987; Vovk *et al.*, 1997; Lancaster *et al.*, 2005) and is fitted satisfactorily using the x^2 term.

Table 3.4 Coefficients in four-point calibrations for Sudan II, with results from transmission images for four TLC plates at each of two calibration ranges. Values in italics are averages and standard deviations of the mean values of the coefficients from the four plates.

Calibration Range / ng	x^0 / AU m^2	x^1 / AU m^2 g^{-1}	x^2 / AU m^2 g^{-2}	r^2
1-10	$-(0.5 \pm 2.5) \times 10^{-8}$	(39.5 ± 4.3)	-	0.9987
	$(1.1 \pm 1.7) \times 10^{-8}$	(35.2 ± 3.0)	-	0.9992
	$(0.2 \pm 1.9) \times 10^{-8}$	(44.8 ± 3.3)	-	0.9994
	$(0.5 \pm 1.4) \times 10^{-8}$	(35.8 ± 2.4)	-	0.9995
	$(0.3 \pm 0.6) \times 10^{-8}$	*(38.7 ± 4.2)*		
5-50	-	29.1 ± 1.5	$-(1.47 \pm 0.33) \times 10^8$	0.9981
	-	35.2 ± 0.9	$-(2.56 \pm 0.20) \times 10^8$	0.9993
	-	40.1 ± 2.5	$-(3.44 \pm 0.54) \times 10^8$	0.9946
	-	40.0 ± 1.8	$-(2.65 \pm 0.40) \times 10^8$	0.9980
		(36.1 ± 5.2)	*$-(2.51 \pm 0.70) \times 10^8$*	

Table 3.5 shows the results of a study of the reproducibility of online imaging results. Reproducibility was assessed by means of the RSD values between four spots of equal sample loading on the same plate. All RSD values quoted are for the full analytical procedure from spotting to measurement. Results are given for RSD values calculated from peak areas obtained from one image (the last in the sequence) and also from peak areas obtained from 40 averaged images. It can be seen that averaging of images

resulted in a lowering of relative standard deviation between the peak areas obtained for the four spots.

Table 3.5 Reproducibility of 4 x 10 ng spots of Sudan II in transmission imaged online using dichloromethane as solvent.

Plate	Signal from last image/ AU m^2	RSD of last image / %	Average signal after averaging 40 images / AU m^2	RSD after averaging 40 images / %
1	$(4.01 \pm 0.17) \times 10^{-7}$	4.2	$(3.88 \pm 0.08) \times 10^{-7}$	2.0
2	$(4.08 \pm 0.12) \times 10^{-7}$	2.9	$(4.20 \pm 0.07) \times 10^{-7}$	1.8
3	$(4.40 \pm 0.14) \times 10^{-7}$	3.3	$(4.45 \pm 0.08) \times 10^{-7}$	1.9
Average	*$(4.16 \pm 0.14) \times 10^{-7}$*	*3.4*	*$(4.16 \pm 0.08) \times 10^{-7}$*	*1.9*

3.5 Effect of different developing solvents

All results discussed in previous sections were obtained using dichloromethane as the developing solvent. As the measurements are made in the presence of the developing solvent, different solvents may affect the quantitative result in different ways. Table 3.6 shows data from online experiments carried out using xylene as the developing solvent. As with dichloromethane, linearity over the range studied is very good with r^2 values >0.99. Intercepts are comparable with those obtained with dichloromethane and are zero within experimental error. However, the signals in xylene are consistently lower than the corresponding signals in dichloromethane by a factor of about 25%.

It was found that this lowering of signal was not due to a change in the optical properties of Sudan II when dissolved in different solvents. Similar absorbance values were obtained when Sudan II was measured in different solvents using the spectrophotometer. Another explanation would be a change in the plate properties in the presence of different solvents, more scatter resulting in a longer path through the layer and hence a higher signal. Differences in the indices of the solvents used may also result in differential scatter of light. The closer the refractive indices of plate and solvent are to one another, the less scattering results.

Table 3.6 Calibrations for Sudan II in transmission imaged online – 10, 5, 2 and 1 ng spots. Xylene was used as the developing solvent, 40 images were averaged.

Calibration	Gradient / AU m^2 g^{-1}	Intercept / AU m^2	r^2
1	31.1 ± 3.5	(- 6 ± 20) × 10^{-9}	0.9986
2	26.4 ± 1.0	(- 4 ± 6) × 10^{-9}	0.9999
3	25.9 ± 2.7	(0 ± 15) × 10^{-9}	0.9988
4	27.5 ± 2.2	(- 15 ± 19) × 10^{-9}	0.9992
Average	*27.7 ± 2.0*	*(-5 ± 6) × 10^{-9}*	

Results from reproducibility experiments with xylene as the developing solvent are given in Tables 3.7 and 3.8. Once again, averaging of images improves the RSD values obtained between the peak areas measured. The RSD obtained for 1 ng spots was higher than that obtained for 10 ng spots. This is due to the higher S/N ratio that results from higher sample loadings.

Table 3.7 Reproducibility of 4 x 10 ng spots of Sudan II imaged online in transmission on HPTLC plates using xylene as solvent, 40 images averaged.

Plate	Signal from last image/ AU m^2	RSD of last image / %	Average signal after averaging 40 images / AU m^2	RSD after averaging 40 images / %
1	(2.95 ± 0.061) x 10^{-7}	2.1	(2.83 ± 0.03) x 10^{-7}	1.0
2	(2.80 ± 0.088) x 10^{-7}	3.1	(2.85 ± 0.04) x 10^{-7}	1.6
3	(2.99 ± 0.075) x 10^{-7}	2.5	(2.96 ± 0.04) x 10^{-7}	1.5
4	(2.78 ± 0.078) x 10^{-7}	2.8	(2.91 ± 0.05) x 10^{-7}	1.6
Average	*(2.8 ± 0.11) x 10^{-7}*	*3.7*	*(2.88 ± 0.05) x 10^{-7}*	*1.8*

Table 3.8 Reproducibility of 4 x 1 ng spots of Sudan ii in transmission on wet plates using xylene as solvent, 40 images averaged.

Signal from last image/ AU m^2	RSD of last image / %	Average signal after averaging 40 images / AU m^2	RSD after averaging 40 images / %
(5.35 ± 0.29) x 10^{-8}	5.5	(5.24 ± 0.21) x 10^{-8}	4.0

3.6 Reflectance experiments

In transmission experiments it was found that the signal of a chromatographic peak was independent of time and distance moved. This was not found to be the case for reflectance experiments, where a more complex relationship between signal and time was discovered. Nevertheless, it was still possible to obtain quantitative results from real time experiments in reflectance mode.

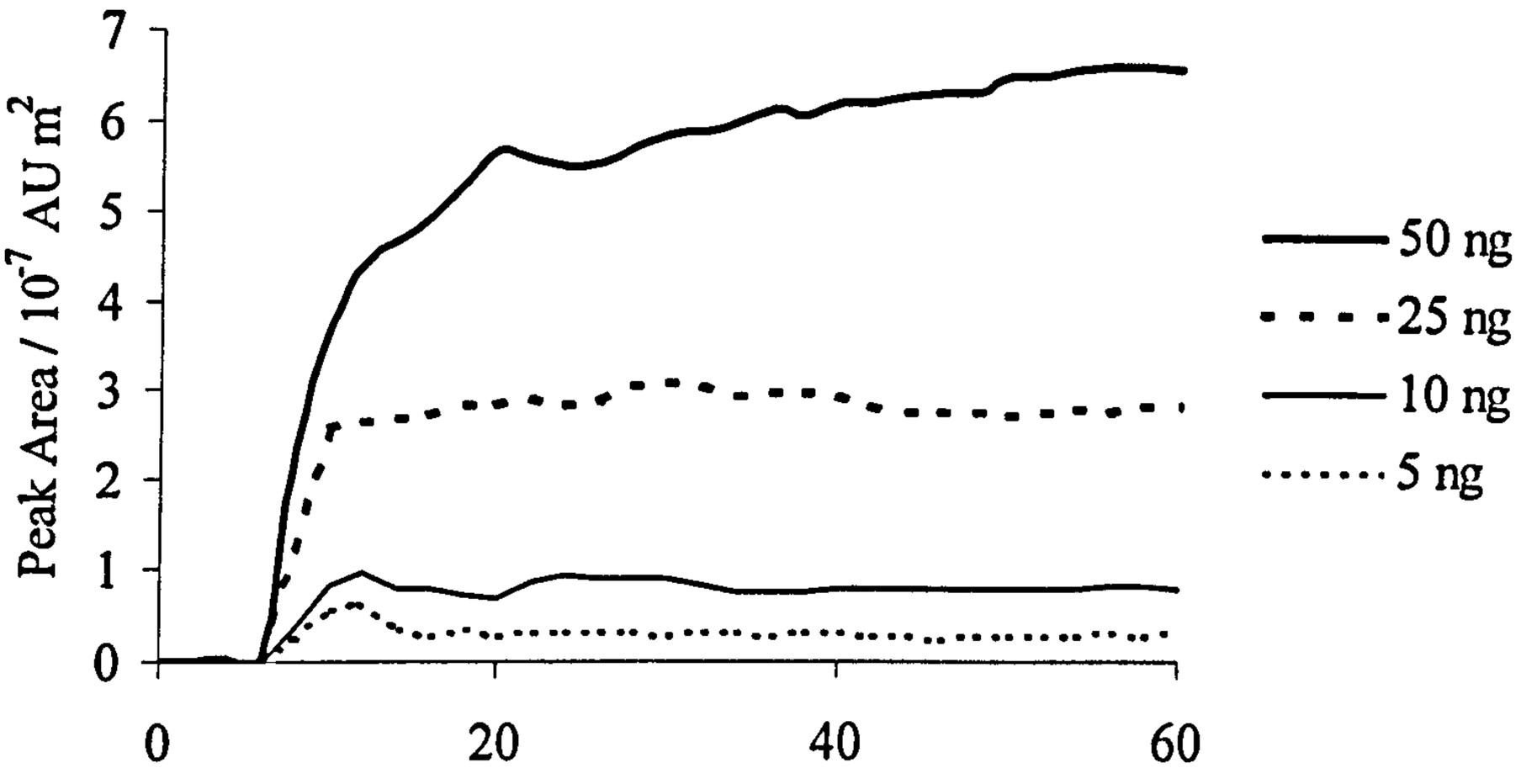

Figure 3.14 Graph of peak area against time for several loadings of Sudan II imaged online in reflectance.

It can be seen from Figure 3.14 that the peak areas for spots of lower sample loadings (5-25 ng) are time independent after the first 15 exposures. However, this is not the case for the 50 ng spot. The peak area for the 50 ng spot continues to increase with time as the development progresses.

An explanation for this phenomenon could be that the apparent absorbance of an analyte is a non-linear function of its concentration, with absorbance curving towards the loading axis at higher sample loading (Figure 1.11). As the spot becomes more diffuse during development then it is less likely to be highly concentrated at its centre and consequently the overall absorbance is less likely to be attenuated. The spot may

then give a higher signal as development progresses (up to some optimum value) owing to this effect.

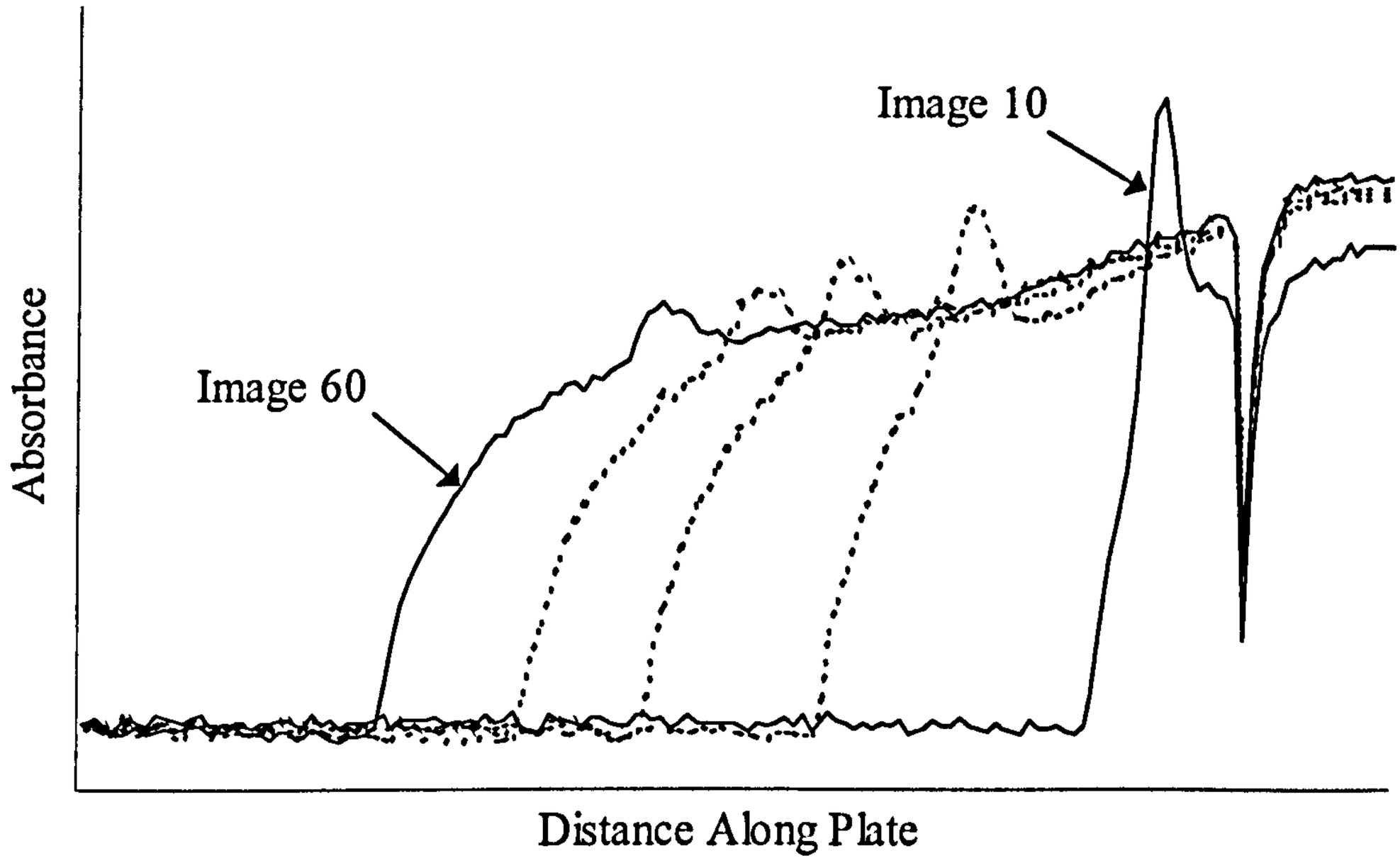

Figure 3.15 Absorbance plotted against distance along plate for a 10 ng spot of Sudan II imaged in reflectance at several points during chromatographic development: corrections made for fixed-pattern effects only.

Figure 3.15 shows the absorbance along the plate obtained in reflectance at several times during chromatographic development. It is analogous to Figure 3.9 but with the detector on the same side of the plate as the light source. In deriving Fig 3.15, the raw images (Figure 3.16) have been ratioed with another image in order to correct for fixed pattern effects such as inhomogeneity of light and plate effects but solvent effects remain uncorrected. The absorbance is higher on the solvated part of the plate as this transmits more and reflects less light, and therefore appears darker than the dry part of the plate in reflectance. The absorbance in the section between the fully wet and dry parts of the plate varies with time, the slope becoming shallower as the development progresses.

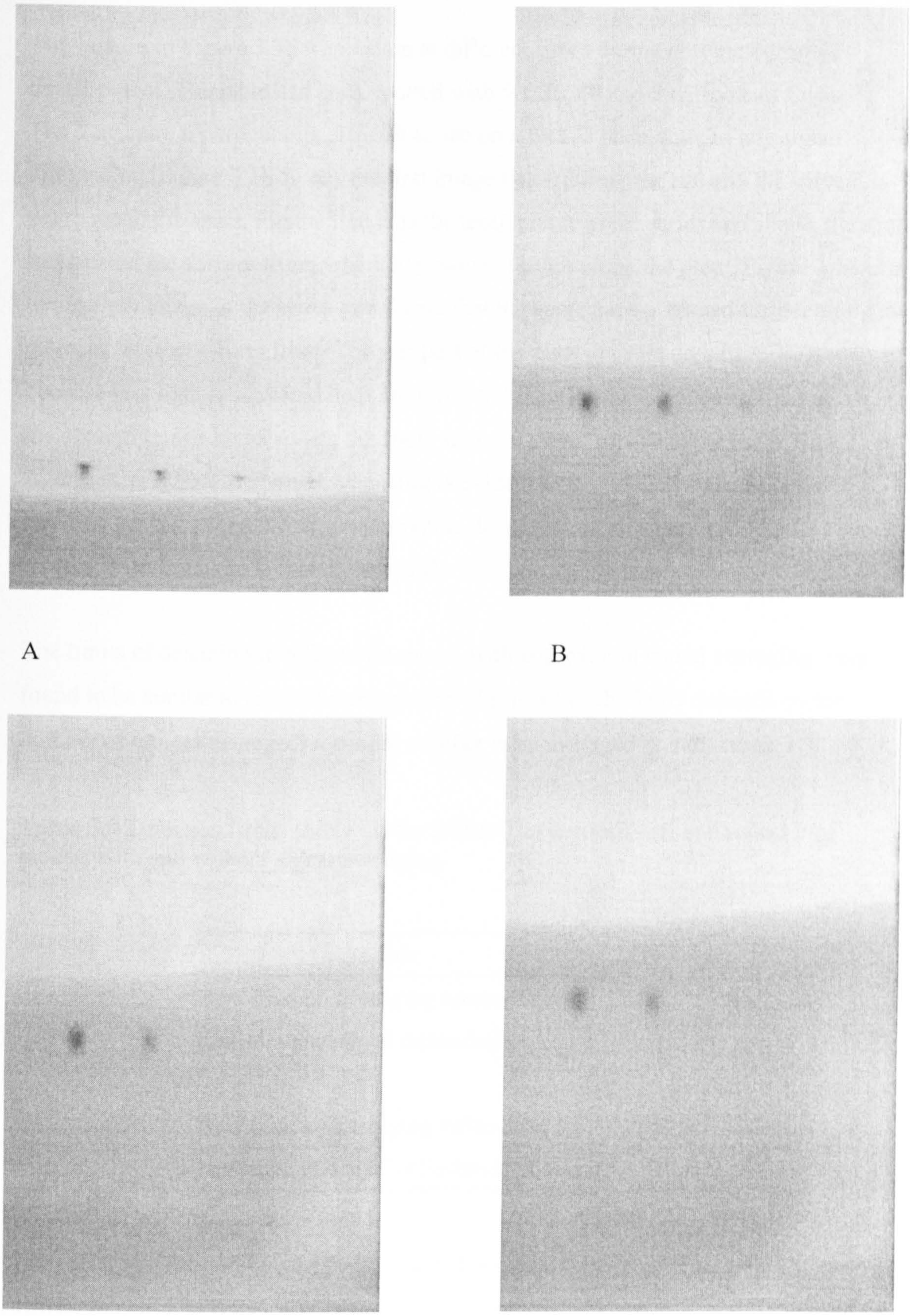

A

B

C

D

Figure 3.16 (A-D) Four images from a series taken during chromatography are shown. All are raw, uncorrected images with no signal referencing. The spots are 50, 25, 10 and 5 ng Sudan ii imaged in reflectance. A is the 1st image, B the 10th, C the 40th and D the 60th in the series.

The images in Figure 3.16 were taken at different times during chromatographic development. The plate had been spotted with 50, 25, 10 and 5 ng spots of Sudan II. The 5 ng spot in particular is difficult to see on a wetted plate without any signal referencing. Figure 3.16 A was the first image taken during the run and the solvent is yet to reach the spots. Figure 3.16 B is the tenth image in the series and shows the spots just behind the solvent front, which has moved further along the plate. Figure 3.16 C is the fortieth image in the series and shows that the spots have migrated further along the plate, as has the solvent front. The wet part of the plate appears dark in reflectance because less light is scattered back from the wet than from the dry part. Figure 3.16 D is the sixtieth image in the series; the spots are now even further behind the solvent front. Again, as in Figure 3.5 band broadening is evident in the relative size of the spots between the images as the chromatographic development progresses, the spots being more diffuse in Image D than in Image B.

The limits of detection in reflectance mode, with and without signal averaging were found to be similar to those in transmission (Table 3.9). The LOD depends on the number of images averaged; a similar number were averaged in both cases.

Table 3.9 Detection limits (S/N = 3) for Sudan II in transmission and reflectance modes, with and without signal averaging.

Mode	LOD / ng
Real-time no averaging transmission	5
Real-time averaged transmission	1
Real-time no averaging reflectance	5
Real-time averaged reflectance	2

The effect shown in Figure 3.14 may mean that calibrations are not reliable over wider sample loadings as the 50 ng peak area is not time independent. It was still possible, however, to obtain reasonable r^2 values from calibrations at lower loadings (Table 3.10). RSD values between spots on the same plate in reflectance were not as good as those in transmission but were consistently <3% after the averaging of 40 images (Table 3.11). The absolute values of peak areas for the spots in AU m^2 were not as high as

those obtained in transmission. This is most likely due to the effective pathlength being shorter, with some reflected light not travelling far into the depth of the plate. In transmission, all light must travel through the full thickness of the sorbent layer.

Table 3.10 Coefficients in four-point calibrations for Sudan II, with results for four TLC plates at loadings of 25, 10, 5 and 2 ng using dichloromethane as developing solvent and imaging in reflectance.

Calibration	Gradient / AU m^2 g^{-1}	Intercept / AU m^2	r^2
1	9.05 ± 0.86	$-(0.6 \pm 2.3) \times 10^{-8}$	0.9986
2	9.49 ± 1.13	$-(1.2 \pm 1.9) \times 10^{-8}$	0.9993
3	8.38 ± 1.21	$-(0.8 \pm 1.8) \times 10^{-8}$	0.9987
4	9.82 ± 1.15	$-(1.5 \pm 1.6) \times 10^{-8}$	0.9992
Average	*9.19 ± 0.62*	*$-(1.0 \pm 0.4) \times 10^{-8}$*	

Table 3.11 Reproducibility of 4 x 10 ng spots of Sudan II imaged online in reflectance on HPTLC plates using dichloromethane as developing solvent, 40 images averaged.

Plate	Average signal / AU m^2	RSD / %	
1	$(1.96 \pm 0.04) \times 10^{-7}$	2.0	
2	$(2.16 \pm 0.04) \times 10^{-7}$	2.2	
3	$(2.03 \pm 0.05) \times 10^{-7}$	2.5	
4	$(1.95 \pm 0.05) \times 10^{-7}$	2.6	
Average	*$(2.02 \pm 0.10) \times 10^{-7}$*		*4.8*

The difference between the LODs and absorption coefficients in transmission versus those in reflectance may be explained by the different sampling depths of the two techniques. The ability to probe analyte close to the bottom of the layer, away from the light source and detector in reflectance is limited as light is either absorbed by the silica or glass support, with relatively little being reflected back up to the detector. This is not a problem in transmission, which does not rely on the light having to be reflected back in the opposite direction, hence it is more sensitive and delivers lower LODs.

3.7 Conclusions

This work provides the first quantitative demonstration of real-time imaging TLC during chromatographic development. Central to these measurements using a CCD camera is signal referencing, after assigning pixels to lanes including either the sample spot or just solvent. Absorbance is referenced to the apparent absorbance of the solvent in lanes to either side of the sample lane and in the same row of effective pixels orthogonal to the direction of travel of the solvent front. This procedure corrects for differences in scattering due to differential wetting of the stationary phase by solvent as chromatography progresses. The integrated peak area is found to be independent of time and distance moved. Averaging of 55 images acquired during a single run gives limits of detection better than those from offline measurements on wetted TLC plates, and within a factor of two of the values for offline measurements on dried plates. Reproducibility in calibration curves is also better than in offline studies. All results suggest that use of real-time imaging is fully capable of providing quantitative TLC measurements.

In principle, signal referencing and all data processing could be done in real-time. A relatively slow CCD camera, with readout rate 80 kHz, was used in this study. Such cameras are optimised for low-noise readout and fluorescence studies and a faster CCD or other active pixel sensor with readout rate of MHz should allow considerable enhancement in S/N. This work could provide further development towards automated real-time TLC analysis. This work has enabled a better understanding of the important parameters and constraints in real-time quantitative measurements in situ in the presence of the stationary as well as the mobile phase. Using this as a foundation the principles could be applied to LC type situations where the whole chromatographic column and sample components could be studied during the separation process. Chen and Horvath have shown with single-point detection the potential for on-column UV absorption in capillary HPLC (Chen and Horvath, 1995). These results demonstrate the benefits of multi-point imaging detection in TLC, and these should also be applicable to on-column detection in HPLC since averaging of snapshots of a moving analyte band yields significant gains in signal to noise, due to attenuation of systematic noise features arising from local non-uniformities of the stationary phase packed bed.

The effect of using different developing solvents was investigated, with xylene being use in place of dichloromethane. It was established that the developing solvent has an effect on the analytical result. Good quantitative measurements were still possible but the overall performance was not as good as with dichloromethane, possibly due to less scattering of light and hence a shorter effective pathlength.

Some experiments were carried out in reflectance mode. The relationship between peak area and sample loading was found to be not as simple as that in transmission. However, reasonable results were obtained at low sample loading (2-25 ng) with r^2 values >0.99 and reproducibility <3% although imaging in reflectance is not as sensitive as in transmission mode.

Finally, imaging in real time gives an insight into the properties of the solvent as it migrates along the plate as can be seen in Figures 3.11 and 3.17. Such transmission and reflectance measurements may provide information on the degree of solvent permeation into the stationary phase as a function of time and of distance from the solvent front, which could be useful for TLC method development. It may be possible to find out more about depth distribution of analytes in the layer (Poole, 2003) and secondary chromatography (Vovk and Simonovska, 2001) using real time imaging. Also there is the possibility with real time imaging of measuring some peak parameters such as the amount of band broadening during chromatography (Poole and Poole, 1991). This could lead to a better understanding of the kinetics of capillary driven Thin Layer Chromatography as well as forced flow methods.

CHAPTER FOUR

Ultra-Violet Image Acquisition and Quantification in Thin-layer Chromatography using CCD Detection

4.1 Introduction

Making quantitative measurements in the ultra-violet region of the electromagnetic spectrum is important because so many compounds absorb in this region. There is no problem with making UV measurements using scanning densitometry as the photomultiplier tubes used for detecting photons are UV sensitive (Pollack and Schulze-Clewing, 1988). Indeed there are many reports of quantitative UV measurements being made by scanning densitometry (Vujic *et al.*, 2003; Habdas and Matysik, 2003). Generally, UV scanning densitometry gives good precision, linearity, linear range and LOD (Petrović and Kaštelan-Macan, 1999; Wuladari and Indrayanto, 2003).

CCD cameras are generally not sensitive to UV light, with response greatly reduced below 400 nm (Burt, 1980). Whilst this might be thought to cause problems for imaging UV absorbing compounds, the problems have been surmounted by the use of UV sensitive coatings which absorb then re-emit light at wavelengths amenable to CCD detection (Samson, 1967; Blouke *et al.,* 1980; Cowens *et al.,* 1980).

A CCD system fitted with UV and visible light sources in order to illuminate a planar surface has been reported (Touchstone, 1993); however, the demand for UV sensitive CCD sensors has not yet justified the large-scale production of phosphor coated devices, which are therefore still very expensive (Pollack *et al.,*

1992). Perhaps this is at least part of the reason why a lack of ultraviolet CCD work was identified recently (Prošek *et al.*, 2001).

Absorption of ultraviolet light can be determined on plates containing a fluorophore. However, this method (known as fluorescence quenching or just quenching) is limited to compounds having a very strong absorption in the ultra violet region. For fluorescence quenching, the compounds must absorb near the wavelength necessary to activate the fluorophore. Moving bands of analytes that absorb ultraviolet light in the range of the activating light of the fluorophore will prevent fluorescence of the plate region into which they migrated, and absorption will be to a degree indicative of the quantity of analyte present in the band (Touchstone *et al.*, 1971).

Quenching is a common method of detecting UV absorbing compounds used with both scanning densitometry (Gries and Jork, 1989) and CCD detection (Hopkala and Pomykalski, 2003). Reversed phase plates containing a fluorophore are available and fluorescence quenching has been reported on reversed-phase TLC plates with videodensitometry (Misztal *et al.*, 2003; Hopkala and Pomykalski, 2004). LODs associated with fluorescence quenching are generally in the 50 ng region, with linear range of approximately one order of magnitude and precision <3%, which is comparable with LC results for the same analytes (Gumieniczek *et al.*, 2002). Quantitative evaluation of fluorescence quenched, two-dimensional chromatograms has also been reported (Petrović *et al.*, 1998).

Several authors have compared scanning densitometry with fluorescence quenched videodensitometry in quantitative analysis of pharmaceuticals in tablets (Campbell and Sherma, 2003; Hopkala *et al.*, 2003; Skibiński and Misztal, 2004). In all cases the two methods were found to give similar results. Early reports comparing video integration and scanning densitometry showed the image analysing system to be less precise and accurate (Ebel, 1990) results, however, indicate that in the UV region, scanning densitometry and video integration produce analytical results that are equivalent in accuracy and precision (Renger, 1998).

Direct UV absorbance measurements by CCD camera would result in greater specificity than fluorescence quenched measurements; however, there are no reports of this in the literature.

The main aims of the work in this chapter are i) to make quantitative measurements on wetted TLC plates in the UV using a CCD camera, ii) to make quantitative real-time measurements in the UV on TLC plates using a CCD camera, iii) to investigate the ability of the system to deal with multiple analyte mixtures.

4.2 Experimental

4.2.1 Chemicals

Methyl 4-hydroxybenzoate, benzophenone, niacinamide, and 3-hydroxybenzaldehyde (structures shown in Figure 4.1) were supplied by Aldrich Chemicals (Poole, UK). The solvents dichloromethane, p-xylene, hexane and acetonitrile were all HPLC grade and supplied by Fisher Scientific (Loughborough, UK). Stock solutions of benzophenone, niacinamide, methyl 4-hydroxybenzoate, 3-hydroxybenzaldehyde and (all 200 mg dm^{-3}) were prepared accurately in DCM, and standards were made by dilution.

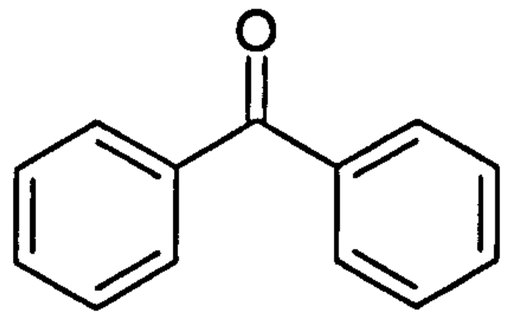

benzophenone

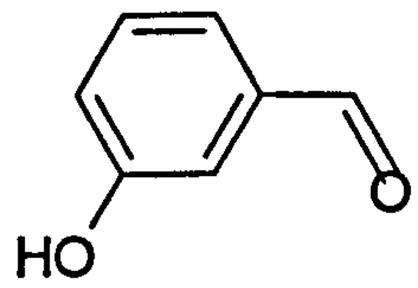

3-hydroxybenzaldehyde

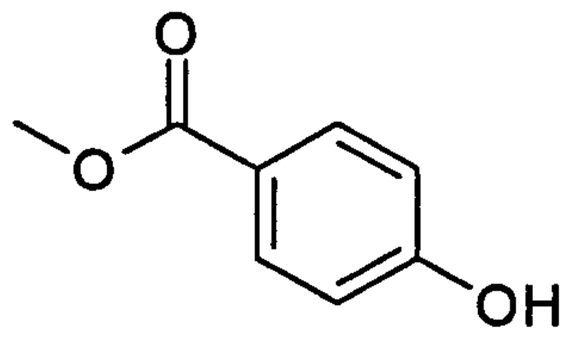

methyl-4-hydroxybenzoate

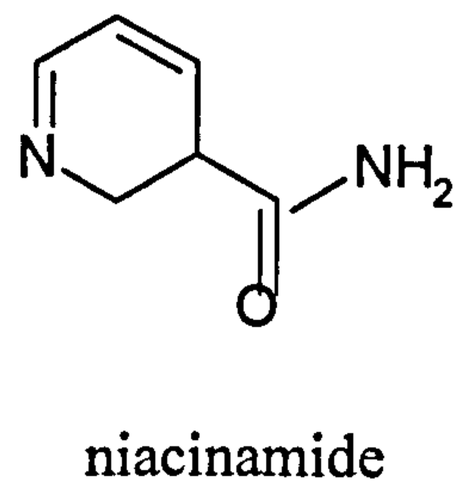

niacinamide

Figure 4.1 Structures of compounds used in UV work

4.2.2 Chromatography

Thin layer chromatography was performed on 5 x 10 cm Silica Gel 60 F_{254} TLC plates, 5 x 10 cm Silica Gel 60 TLC plates (glass and aluminium backed varieties were used), layer thickness 200 μm. High performance thin layer chromatography was performed on 5 x 10 cm Silica Gel 60 F_{254} HPTLC plates, 5 x 10 cm Silica Gel 60 HPTLC plates (glass and aluminium backed varieties were used), layer thickness 200 μm and 100 μm. All plates were supplied by Merck (Darmstadt, Germany). Samples were applied as spots approximately 1 cm apart and 0.5 cm from the plate edge by means of 1 μl glass capillaries, supplied by Camlab (Cambridge, UK). Development was performed at room temperature in a 10 x 10 cm horizontal chamber (Camag, Switzerland).

4.2.3 Imaging and Processing

The images were taken using an Antares Duo, LSR AstroCam CCD camera (Cambridge, UK). The camera was fitted with an EEV CCD05-20 CCD chip; this has 770 by 1152 pixels each 22.5 μm square. The camera head cools the chip thermoelectrically to -40 °C.

The UV sensitive phosphor coating is called 'Astrochrome 90', this is a Lumogen coating which is an organic phosphor that is excited below 400 nm and emits at 520-580 nm. The quantum efficiency of Lumogen coated devices below 400 nm is approximately 25% (Cowens *et al*, 1980).

The CCD was fitted with an A4869, 50 mm focal camera lens (Hamamatsu Photonics UK Limited, Welwyn Garden City, UK). The camera was operated at maximum dynamic range and readout rate (165 kHz). Images were acquired using Imager 2 software. All images had a blank image (taken with the shutter closed) subtracted, to compensate for camera dark current. The xenon lamp was fitted with a P/ACE 254 nm narrow bandpass filter (Beckman, High Wycombe, UK). A Chance OX7 filter (Chance-Pilkington, St. Asaph, UK) was employed to block non-UV light in experiments using plates containing fluorophore. The spectral characteristics of the blocking filter are given in Figure 4.2.

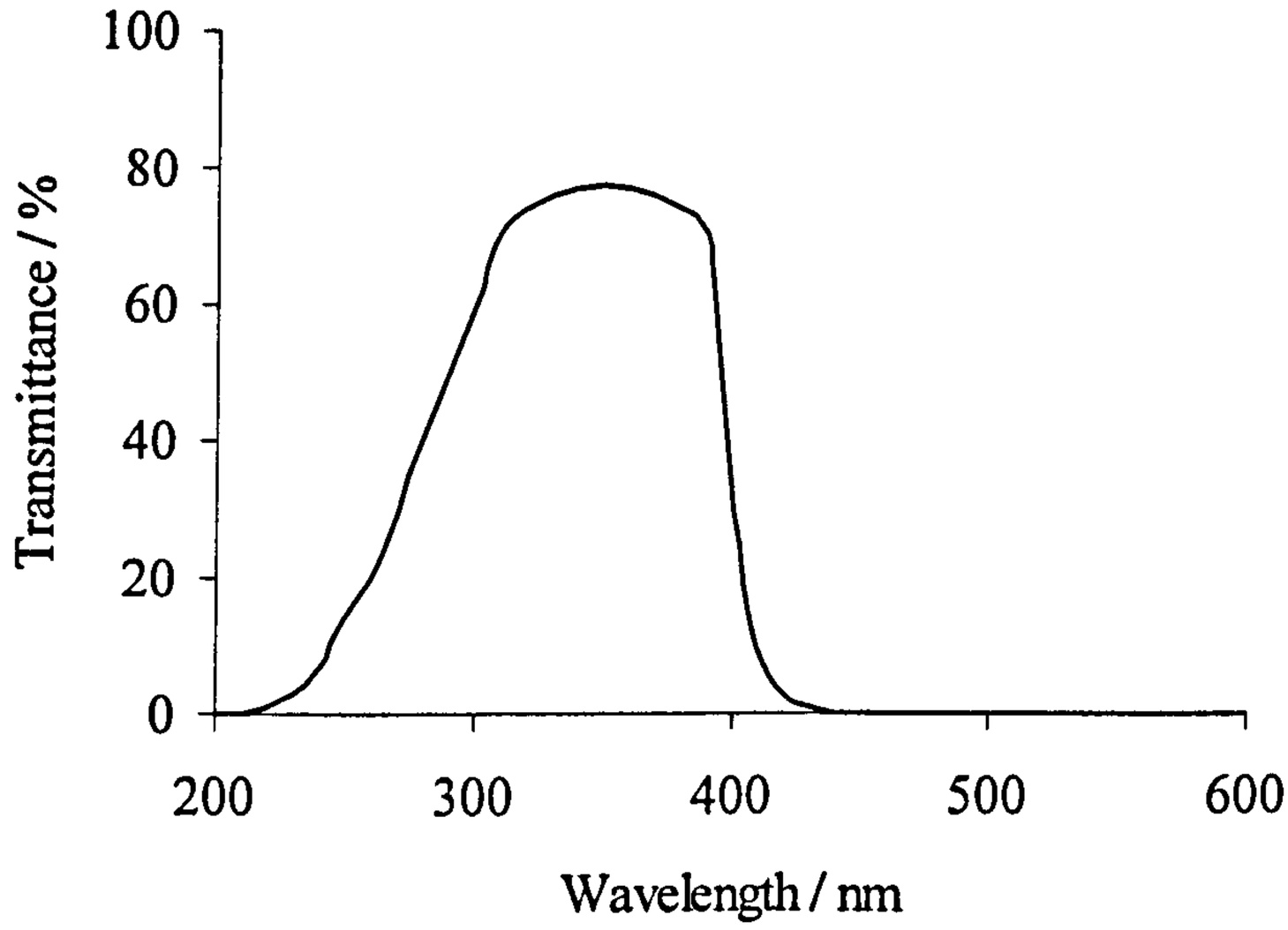

Figure 4.2 Transmittance of the UV pass filter used with plates containing fluorophore.

The UV light was delivered from either a 75 W xenon source LPS 251 SR (Spectral Energy Corporation, Westwood, USA) via a 0.5 m fused silica optical fibre with 1 mm core diameter (CeramOptec GmbH, Bonn, Germany) or a 2 x 8 W 254/366 nm mercury lamp (Camag, Switzerland). Schematic diagrams of the apparatus for both xenon and mercury lamp experiments are given in Figures 4.3

and 4.4 respectively. Xenon lamp experiments were carried out with the aperture at f 3.5 and an exposure time of 10 s. The mercury lamp experiments were carried out with the aperture at f 3.5 and an exposure time of 200 ms. The intensity of the UV sources were measured using a UV sensitive photodiode, and found to be 10 $\mu W\ cm^{-2}$ for the xenon lamp and 600 $\mu W\ cm^{-2}$ for the mercury lamp. Both measurements were made at a distance of 20 cm from the source.

Offline image processing was achieved using Scion Image Beta 4.02 software (Scion Corporation, Maryland, USA). Data smoothing and quantification was accomplished using Peak Fit version 4 (Systat Software, London, UK) as in Chapter 2.2.3.

4.2.3.1 Xenon Lamp Experiments

In the xenon lamp experiments dried plates were imaged in the UV. After spotting, the spots were focused with acetonitrile to a distance of approximately 1 cm from the bottom of the plate. The plate was then allowed to dry and an image taken. Subsequently the focused bands were developed for a further 4-5 cm with solvent, after which the plate was allowed to dry again before imaging in reflectance.

4.2.3.2 Mercury Lamp Offline Experiments

Using the mercury lamp at 254 nm, offline experiments were undertaken on dried plates and also on wetted plates. The dry plate experiments were carried out in the same way as the xenon lamp experiments described in section 4.2.3.1 above. In the wet plate experiments, an image was taken of the blank plate and then the plate was developed up to a predetermined distance (marked on the plate), and another image taken. The plate was allowed to dry and then spotted, focused and dried again. The plate was then developed for a second time and another image taken in reflectance, when the solvent front was at the same position as in the first image. Finally the plate was allowed to dry and imaged again. In this way two sets of results (wet and dry) were obtained for the same spots on the same plate as in Chapter 2.2.2.

4.2.3.3 Real Time Experiments

In the real-time experiments (using the mercury lamp for illumination) a two-step development was also chosen, with solvent focusing using acetonitrile before the development proper. After spotting, the spots were focused with acetonitrile to a distance of approximately 1 cm from the bottom of the plate. The plate was then allowed to dry and then the focused bands were developed for a further 4-5 cm. The camera was set up to take images continuously as development occurred. One image was taken every 6 s.

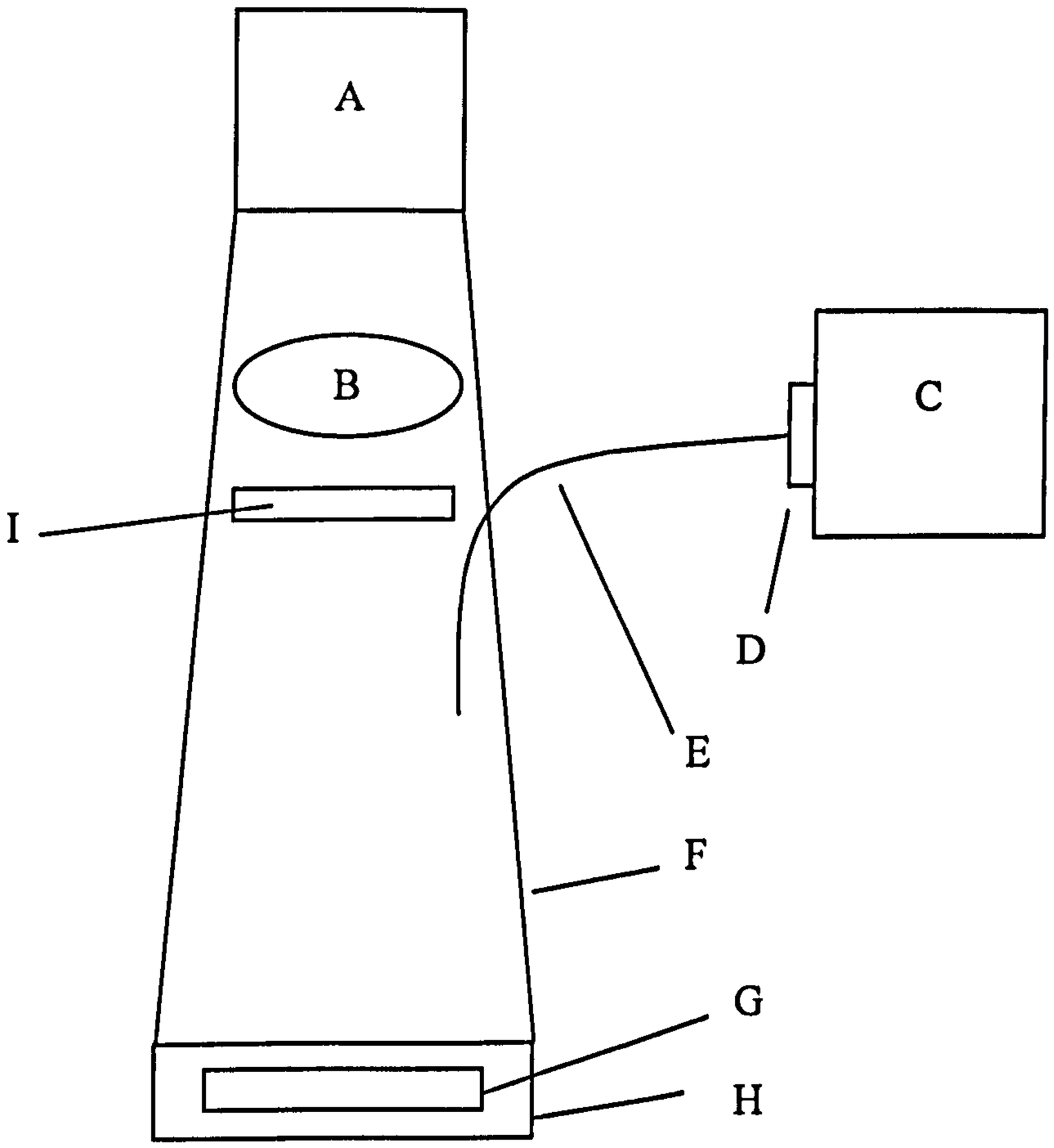

Figure 4.3 Schematic diagram of apparatus to image plates in UV in reflectance mode using a xenon lamp: A, CCD camera; B, UV lens; C, xenon lamp; D, 254 nm filter; E, optical fibre; F, cover; G, TLC plate; H, Developing Tank. I, UV pass filter.

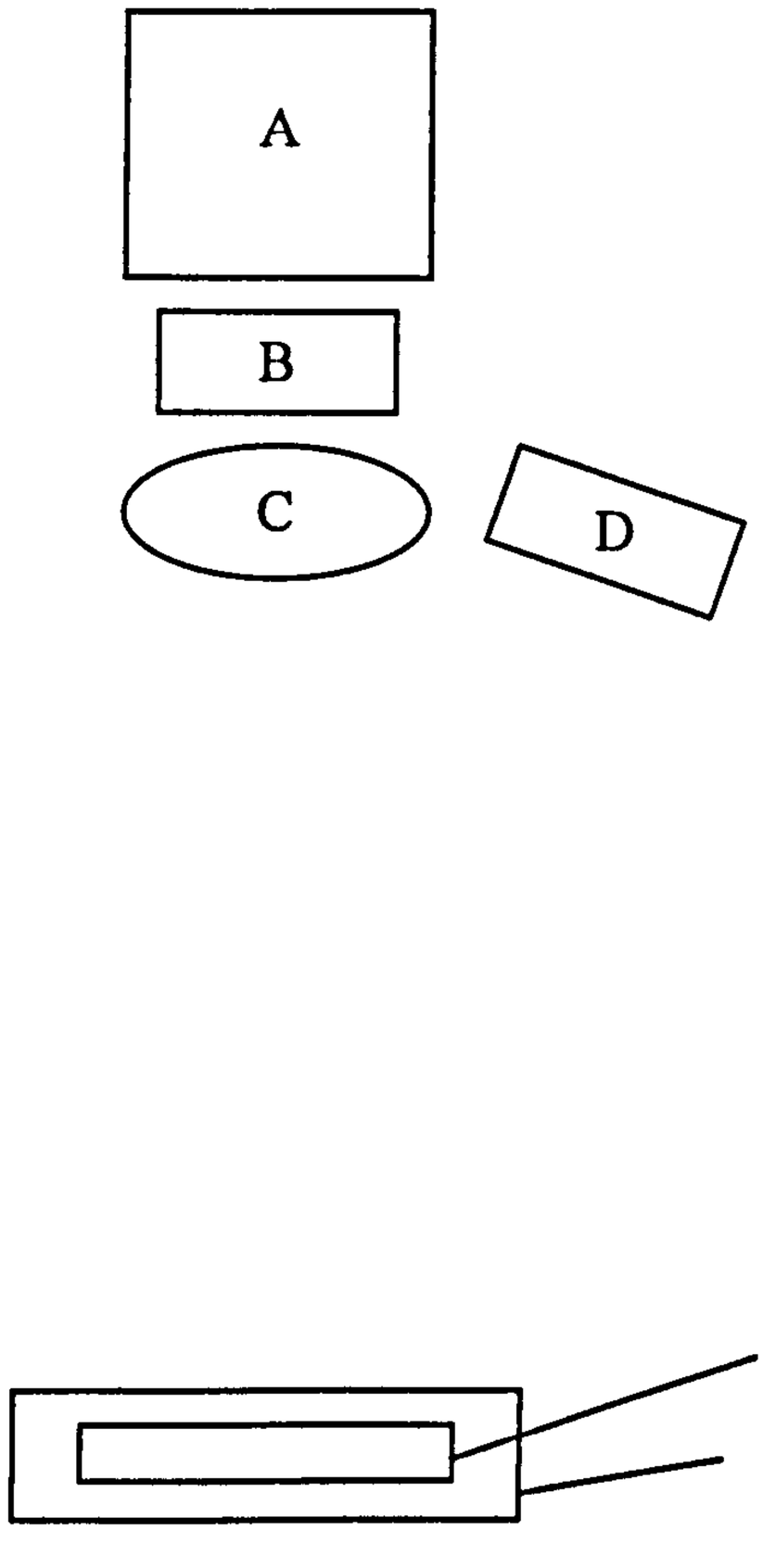

Figure 4.4 Schematic diagram of apparatus to image plates in UV in reflectance mode with mercury lamp: A, CCD camera; B, UV pass filter; C, UV lens; D, mercury lamp; E, TLC plate; F, developing tank (fitted with UV transparent window). The whole system is enclosed to prevent any stray light from entering.

4.2.4 Spectrophotometry

UV-visible spectrophotometry of methyl 4-hydroxybenzoate, benzophenone, niacinamide, and 3-hydroxybenzaldehyde was carried out using a Shimadzu 1700 spectrophotometer and quartz cells with a path length of 1 cm. Measurements of

absorbance were made between 200 and 400 nm. The compounds were dissolved in dichloromethane at a concentration of 25 mg l^{-1}, and diluted by a factor 2 if necessary to bring the absorbance to below 2 AU at peak maximum. Dichloromethane was also used in the reference cell. Absorbance data are given in Table 4.1 and the spectra are given in Figures 4.5-4.8 below.

Table 4.1 Absorbance at 254 nm of methyl 4-hydroxybenzoate, benzophenone, niacinamide, and 3-hydroxybenzaldehyde (at 12.5 or 25 mg l^{-1} in DCM) and corresponding absorption coefficients.

Compound	Absorption at 254 nm / AU	ε / AU m^2 g^{-1}
methyl 4-hydroxybenzoate	1.7	13.3
benzophenone	1.1	8.6
niacinamide	0.4	1.5
3-hydroxybenzaldehyde	1.9	7.3

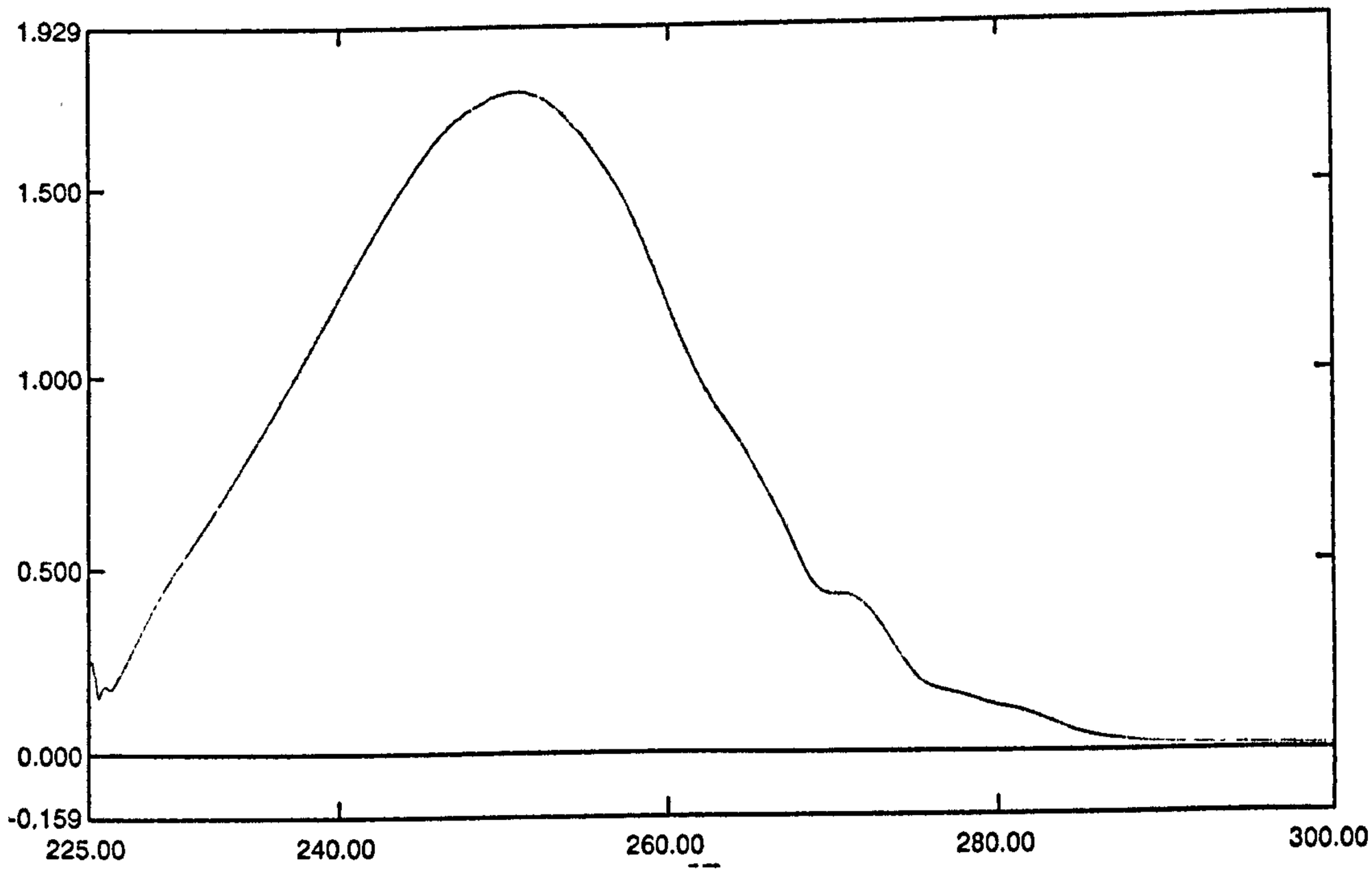

Figure 4.5 UV-vis spectrum of methyl 4-hydroxybenzoate at 12.5 mg l^{-1} in DCM.

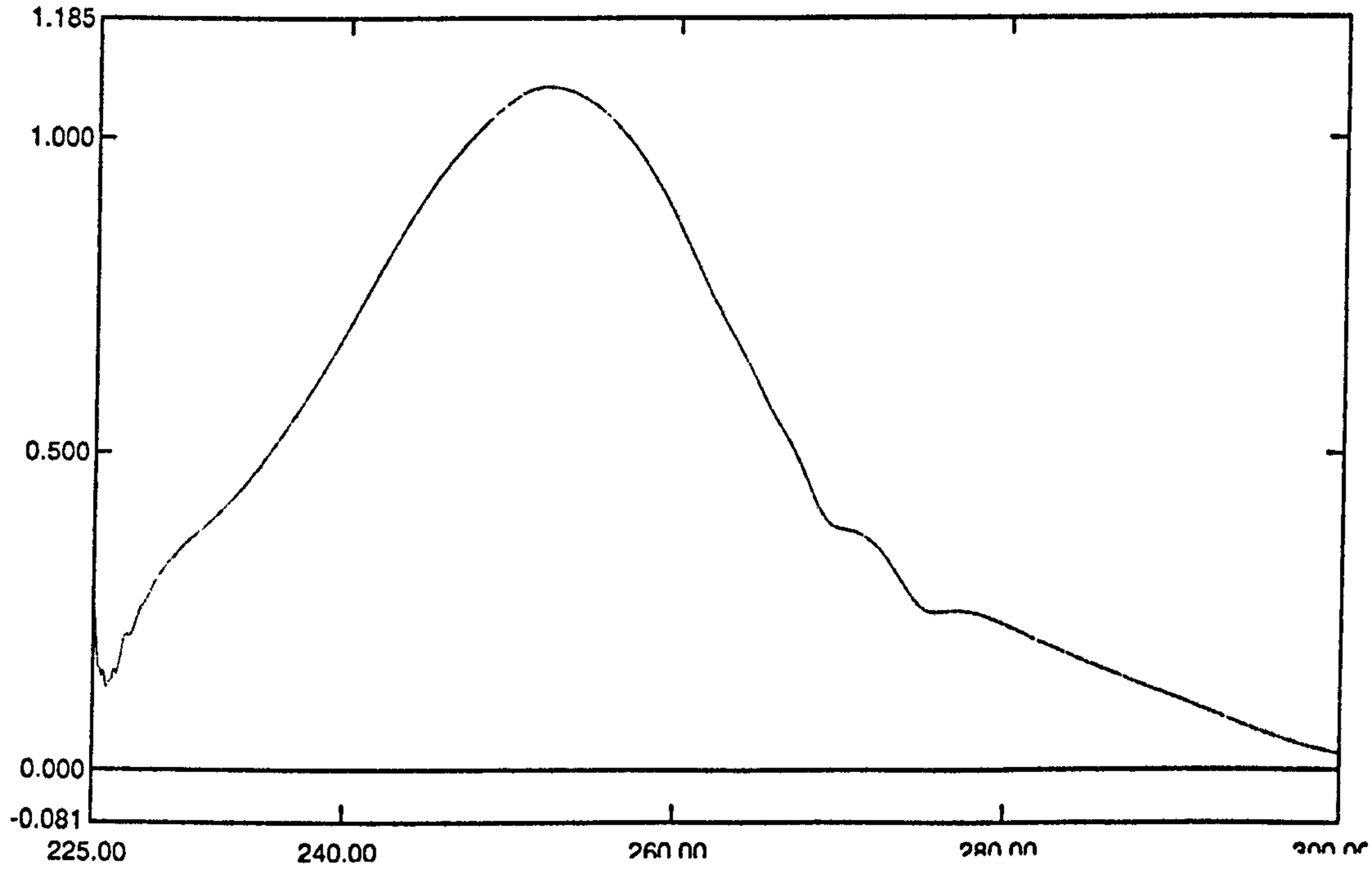

Figure 4.6 UV-vis spectrum of benzophenone at 12.5 mg l^{-1} in DCM

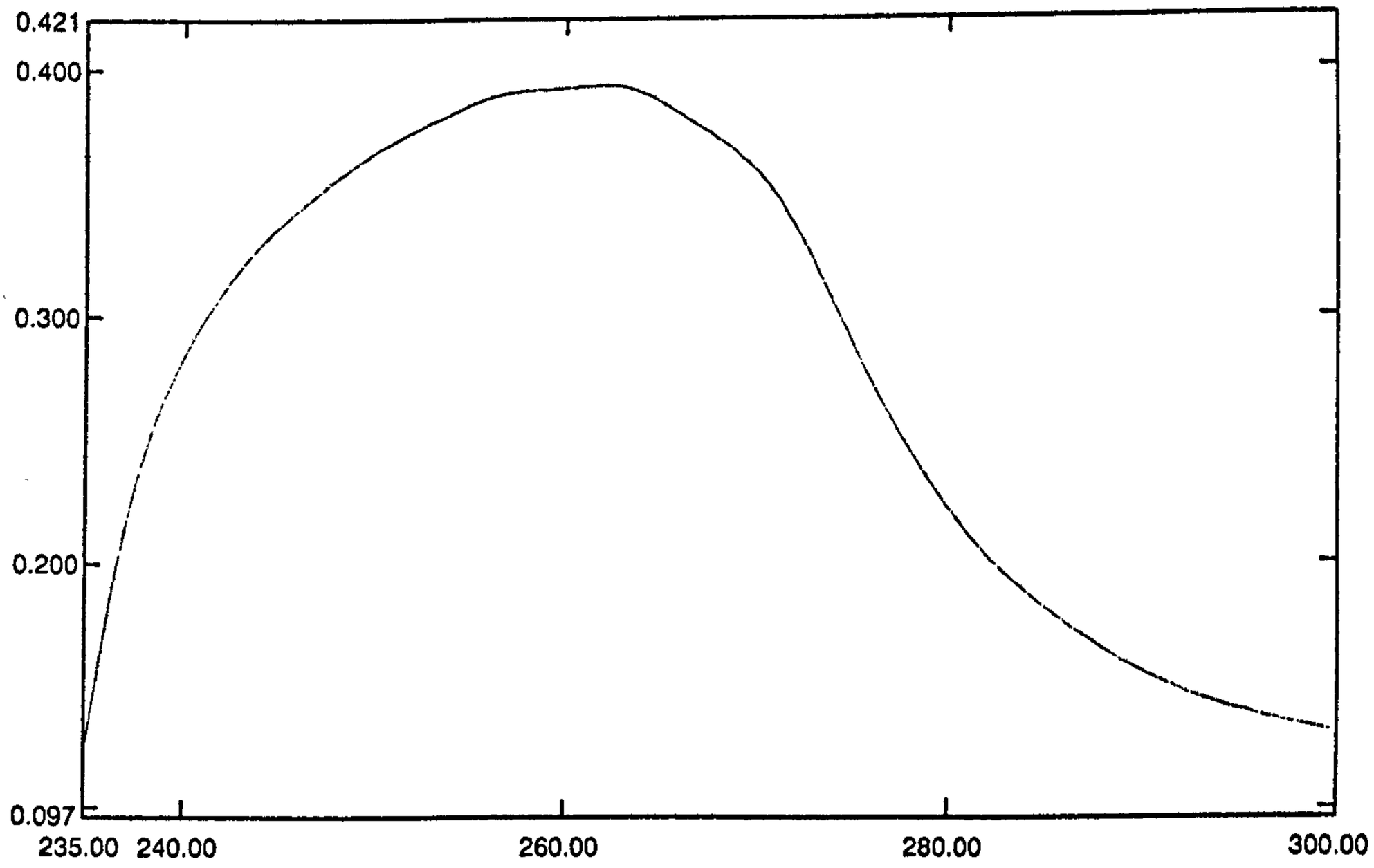

Figure 4.7 UV-vis spectrum of niacinamide at 25 mg l^{-1} in DCM.

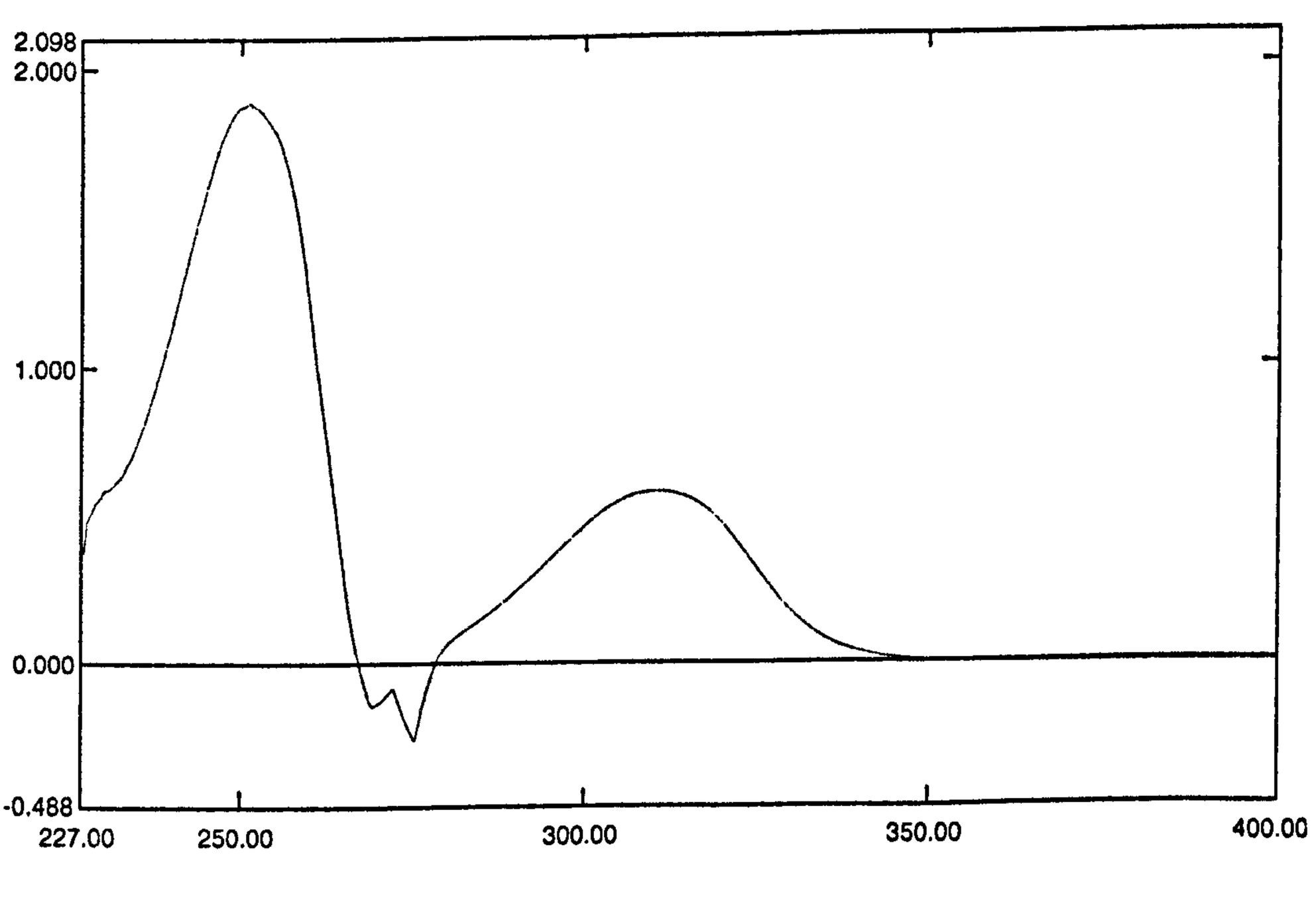

Figure 4.8 UV-vis spectrum of 3-hydroxybenzaldehyde at 25 mg l^{-1} in DCM.

4.2.5 UV transparent plates

Thin-layer chromatography plates backed with UV transparent glass are not currently available commercially. It was necessary to make our own plates in-house. Two pieces (50 × 50 × 1 mm) of Spectrosil b quartz (Edmund Optics, York, UK), which has no significant absorbance above 200 nm, were coated with a Silica gel slurry. The slurry was made by suspending 10 g of silica gel from Merck (Darmstadt, Germany) in 20 ml of water. Any air bubbles were removed by applying a partial vacuum in a Buchner flask. The slurry was then poured on the glass pieces. An aluminium jig was used, which allowed the glass plates to be given a sorbent layer of known thickness by means of a scraper (Fig 4.9). The end shown in the figure was open in order for the plate to be slid in and out; the other end was closed so that the plate could be held stationary. The plates were then removed from the jig and left to dry overnight at room temperature.

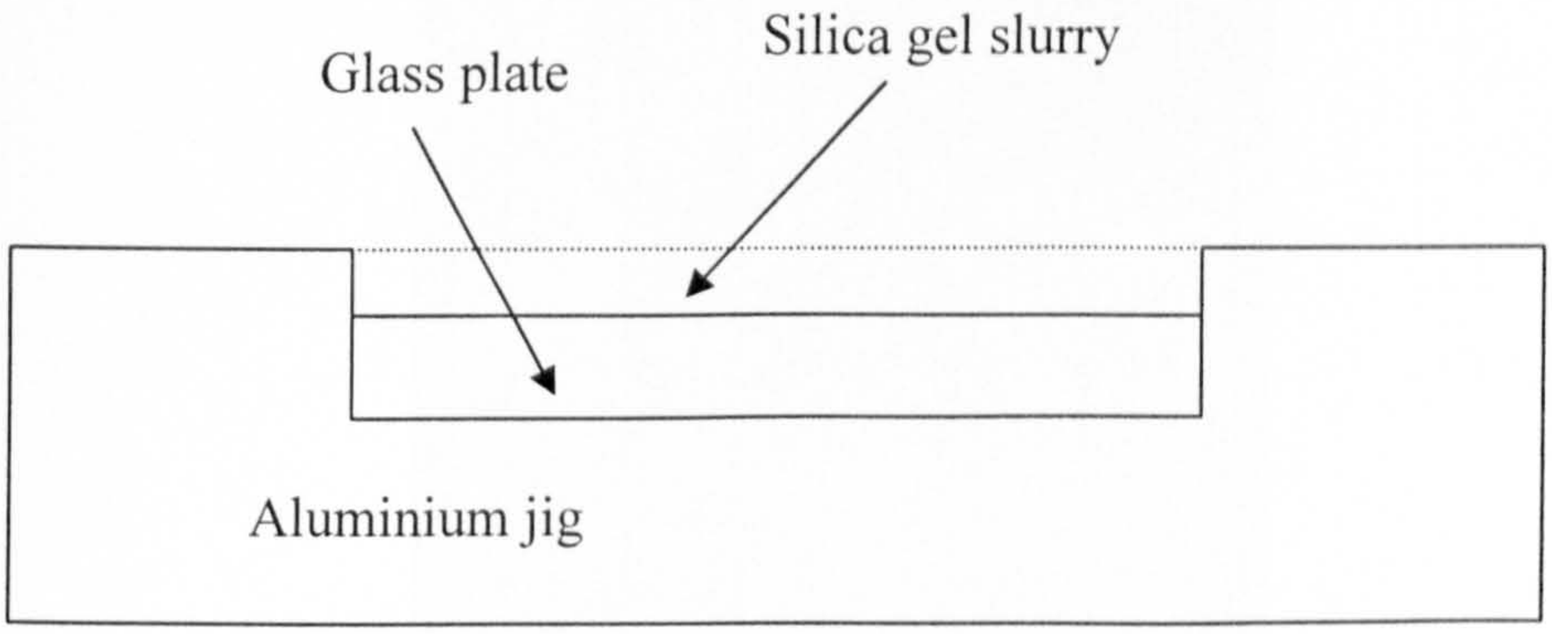

Figure 4.9 Cross section of the aluminium jig used in the coating of home made plates.

4.3 Xenon Lamp Results

The first attempts to image UV absorbing compounds were carried out with a xenon lamp fitted with a 254 nm narrow bandpass filter. This produced a circular illuminated area upon the TLC plate (shown in Figure 4.10). The illumination was very uneven. However, a lot of the unevenness could be compensated for by signal referencing as discussed in Chapter 2 (compare Figures 4.10 and 4.11) and reasonable measurements could then be made.

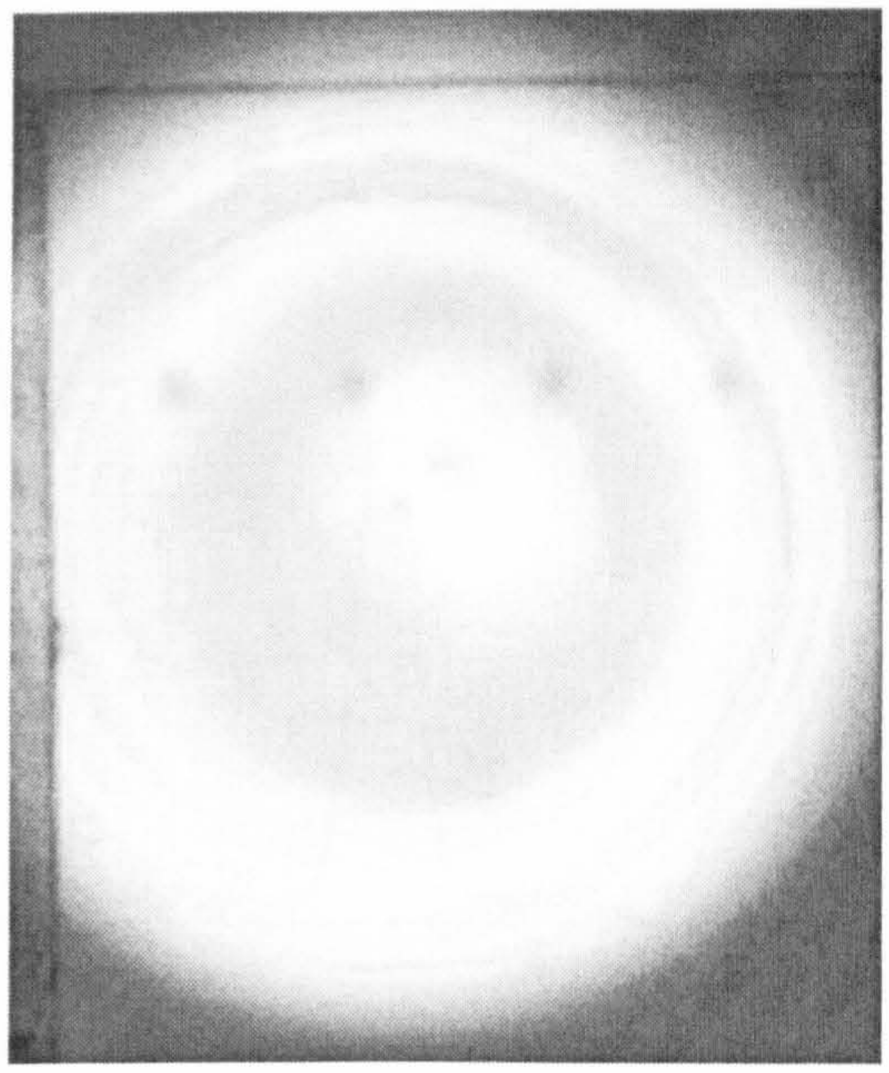

Figure 4.10 Raw image of four 50 ng spots of benzophenone

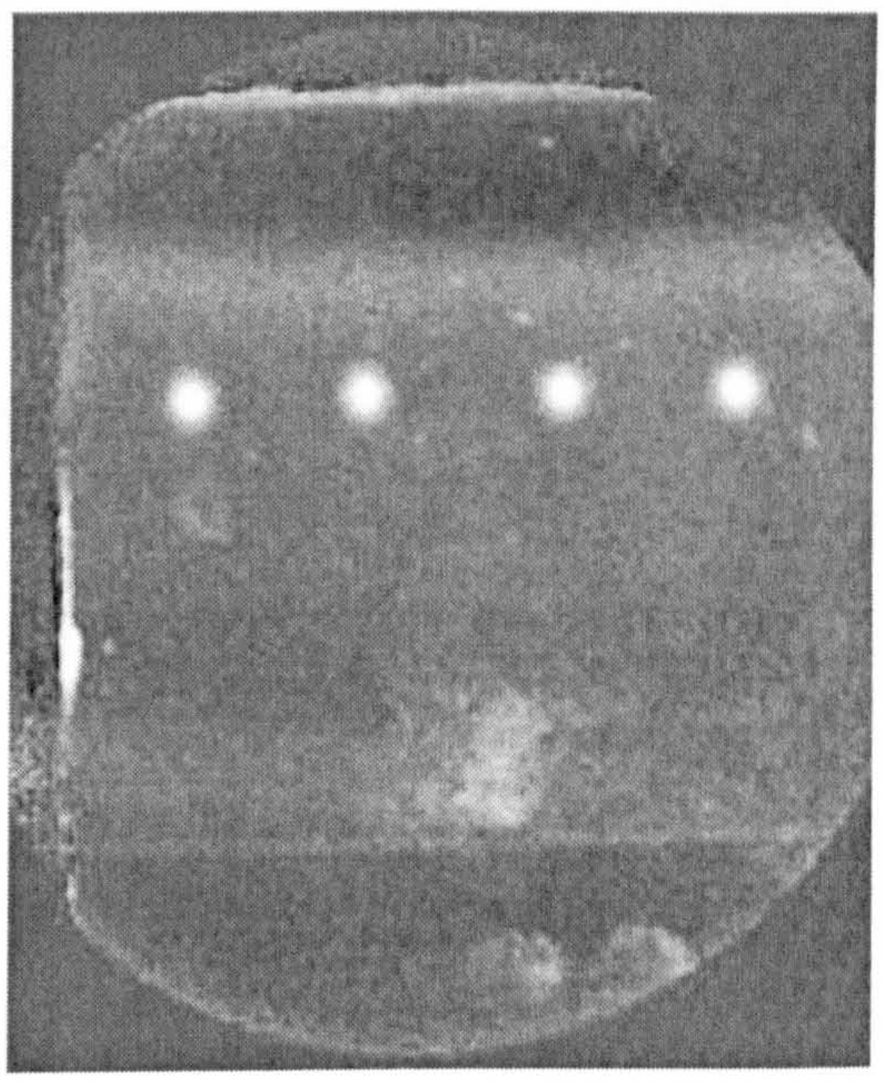

Figure 4.11 Figure 4.10 above corrected for fixed pattern effects by signal referencing.

Precision was assessed by measuring four spots of the same loading after chromatography. A chromatogram of four 50 ng spots of benzophenone is given in Figure 4.12. The results are given in Table 4.2.

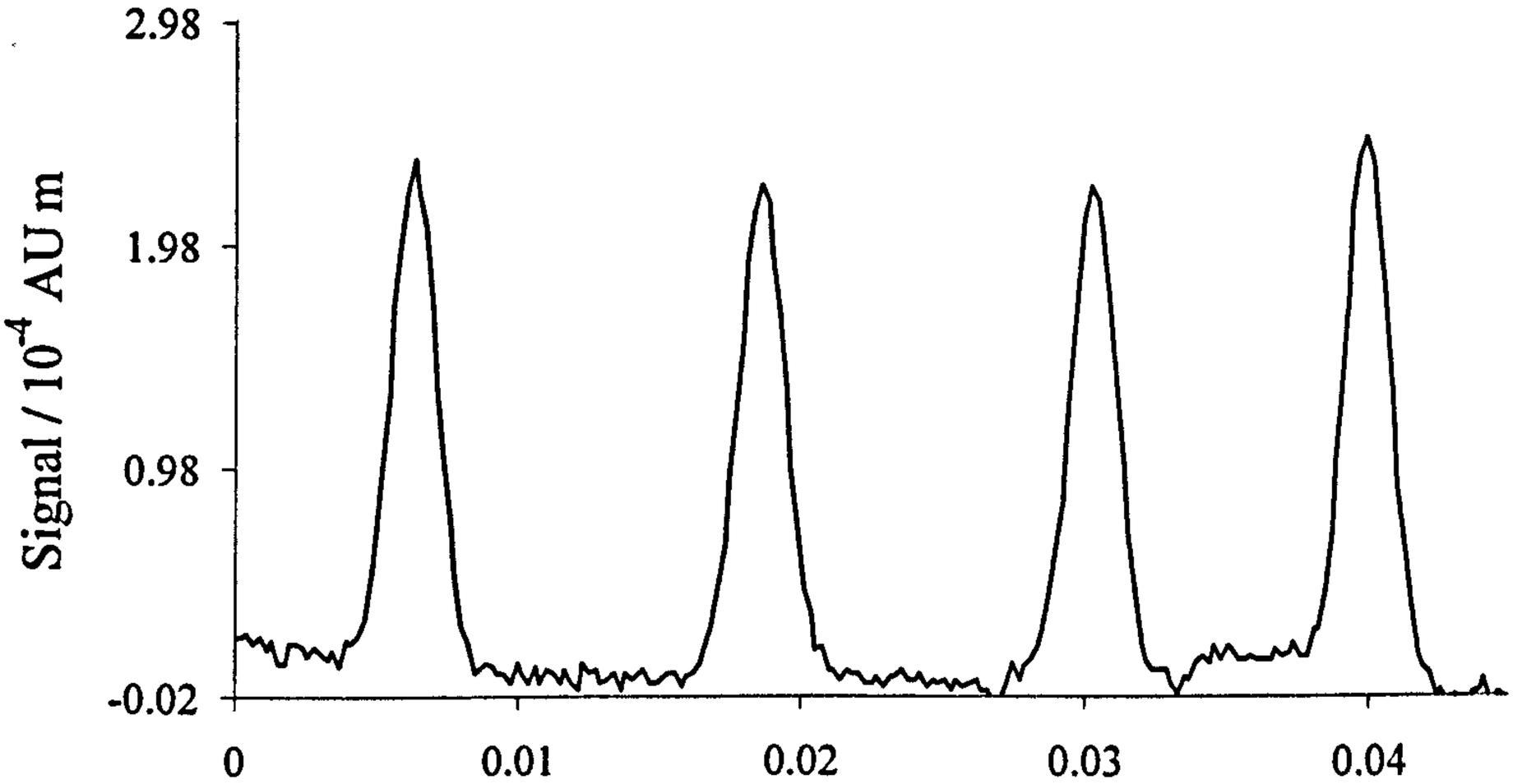

Figure 4.12 Spots in Figure 4.11 integrated in the direction of chromatography.

Table 4.2 Reproducibility of 4 x 50 ng benzophenone run with 50:50 DCM/xylene, imaged offline in reflectance with xenon lamp.

Plate	Average signal / 10^{-7} AU m^2	RSD / %
1	3.78 ± 0.14	3.8
2	3.63 ± 0.10	2.7
3	3.71 ± 0.11	3.0
4	4.19 ± 0.16	3.9
5	4.36 ± 0.0	1.3
6	4.25 ± 0.10	2.4
7	4.37 ± 0.06	1.5
8	4.51 ± 0.08	1.7
9	4.33 ± 0.07	1.6
10	4.07 ± 0.04	1.1
Average	*(4.17 ± 0.10) x10^{-7}*	Inter-plate RSD = 6.8

The RSD between spots on the same plate was between 1.1 and 3.9%. The inter plate RSD, taking all the results, was found to be greater at 6.8%. These results fall within the normal range for TLC (Degterev *et al.*, 1996; Goodall, 1972). The intra-plate RSD is more important, as unknown samples and standards are usually

developed using the data pair method on the same plate (Betheke and Frei, 1974; Huynh and Leipzig-Pagani, 1996). Calibrations were performed using this system. The normal working range was 5-50 ng but experiments at a lower range of 2-25 ng were also undertaken. Raw and corrected images from the lower range are show in Figures 4.13 and 4.14 below.

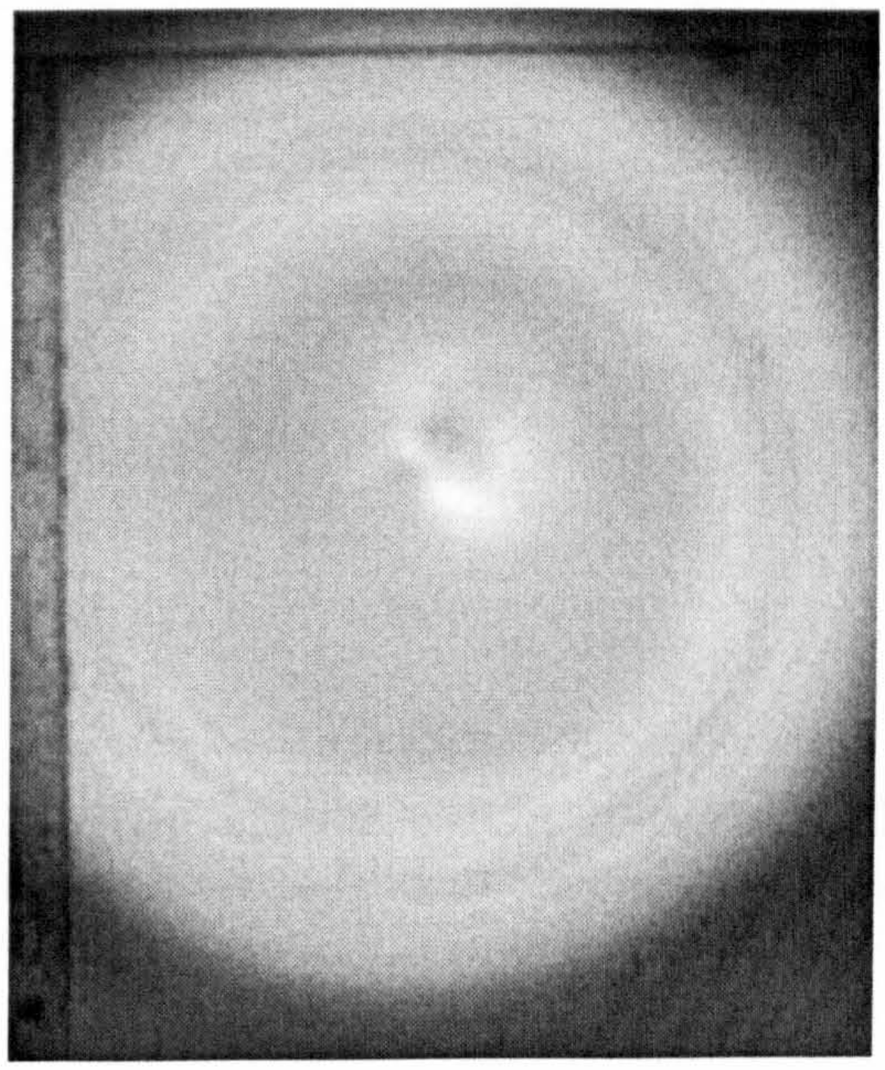

Figure 4.13 Raw image of four spots of benzophenone (2, 5, 10 and 25 ng). Only the 25 ng spot is visible in this uncorrected image.

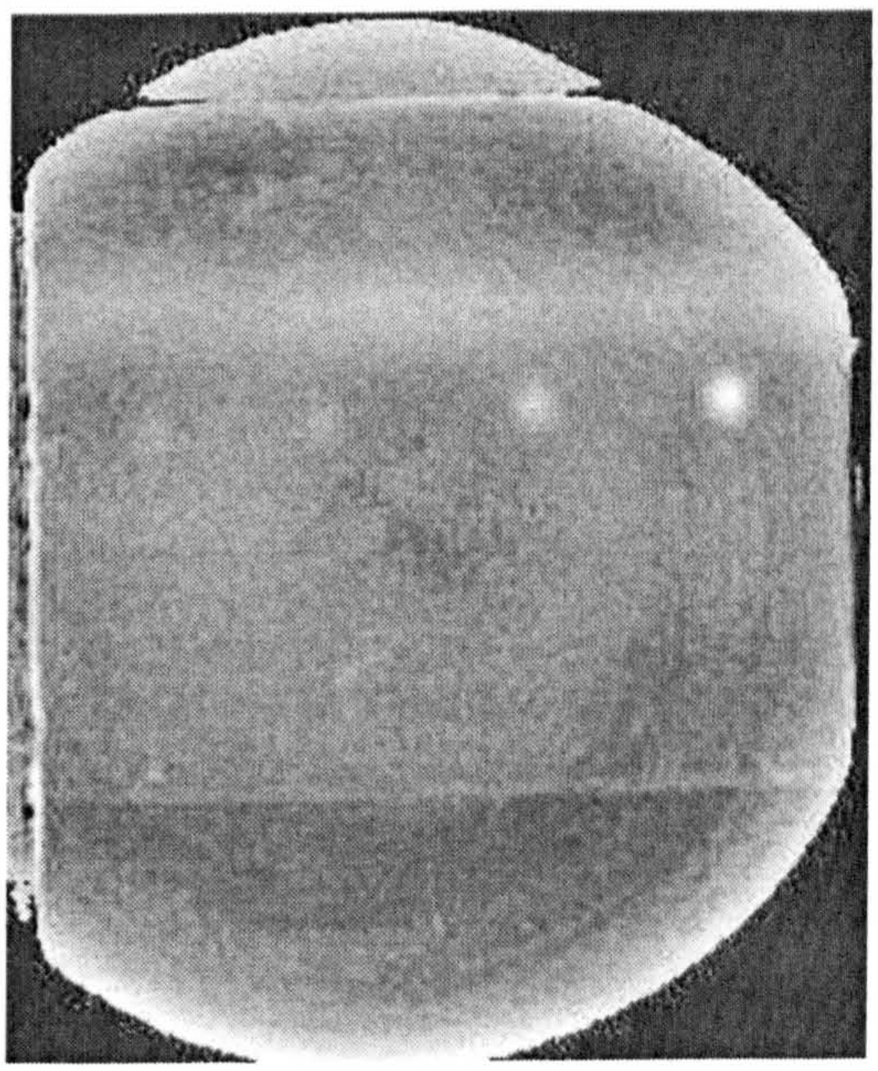

Figure 4.14 Figure 4.13 above corrected for fixed pattern effects. All four spots are now visible.

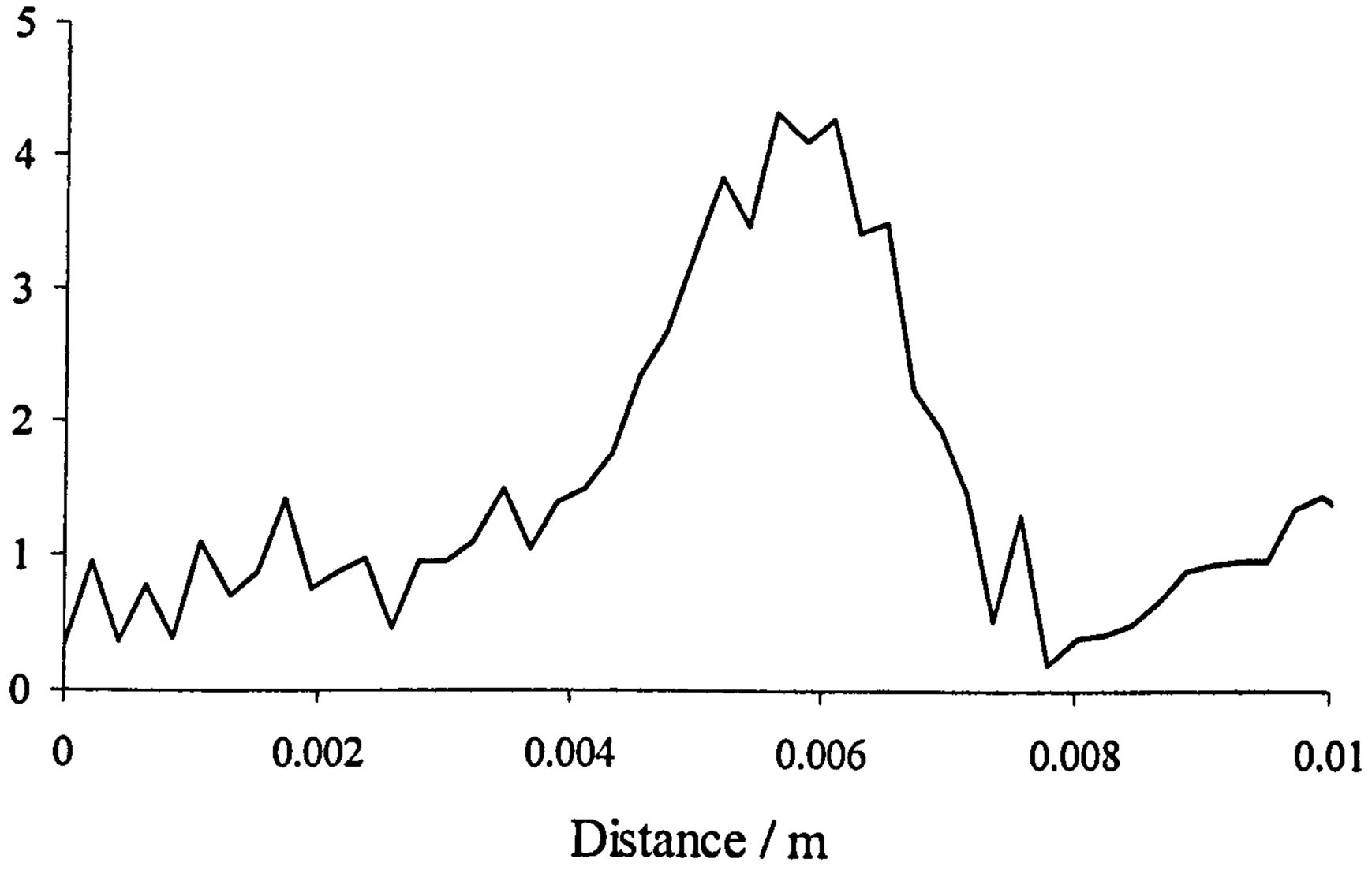

Figure 4.15 The 2 ng benzophenone spot from Figure 4.14 integrated in the direction of chromatography. The peak can clearly be distinguished from the noise, the S/N ratio being 4:1.

The UV light was delivered by means of an optical fibre; any slight movement of the apparatus between the taking of the two images severely affected the referencing and increased the noise, making detection more difficult. It was possible to see 2 ng of benzophenone and obtain a calibration. However, this was not easy and most attempts failed even after the fibre was strongly secured to a retort stand. Delivery of the UV light by means of mirrors, in an attempt to make illumination of the plate more homogeneous and the set up more robust, was tried but without any improvement in the results.

In Table 4.3 below, the gradient (x^1 coefficient) is equivalent to the effective absorption coefficient ε_{eff} in AU $m^2 g^{-1}$. The slopes of the 5-50 ng loading experiments show good repeatability, with intercepts around zero within experimental error. The average gradient of 7.9 ± 0.5 AU $m^2 g^{-1}$ in Table 4.3 is in good agreement with the spectrophotometer value for benzophenone of 8.6 AU $m^2 g^{-1}$ at 254 nm quoted in section 4.2.4. Comparison of the 5-50 ng results with the 2-25 experiment shows that the slope is slightly steeper over the lower range of concentrations, consistent with a positive intercept on average obtained from

linear regressions and slight downward curvature at the highest loading. This accords with observations from measurements in the visible region reported in Chapter 3.

Table 4.3 5, 10, 25 and 50 ng benzophenone run with 50:50 DCM/xylene imaged in reflectance mode. Last result 2, 5, 10 and 25 ng used.

Calibration Range / ng	x^0 / 10^{-8} AU m^2	x^1 / AU m^2 g^{-1}	r^2
5-50	2.3 ± 2.7	7.7 ± 0.9	0.9984
	0.8 ± 4.2	7.9 ± 1.5	0.9966
	2.4 ± 3.7	7.7 ± 1.3	0.9969
	1.9 ± 3.6	7.8 ± 1.3	0.9971
	1.5 ± 1.6	7.0 ± 0.5	0.9994
	0.2 ± 2.9	8.4 ± 1.0	0.9985
	1.4 ± 3.5	7.7 ± 1.2	0.9973
	-0.5 ± 2.4	8.8 ± 0.9	0.9989
	-0.2 ± 0.6	8.1 ± 0.2	0.9989
	1.1 ± 1.1	*7.9 ± 0.5*	
2-25	1.3 ± 1.5	9.4 ± 1.1	0.9985

An exposure time of 10 s was used in these experiments. Obviously this is too long to use in an online experiment, and it would be necessary to use a shorter exposure in order to give a sharp image. This would only be possible if the light level were higher, for example by using a brighter arc lamp or by obtaining a lamp with higher power over a larger radiant area.

Furthermore, the use of an optical fibre to deliver UV light in these experiments was not ideal. It was necessary to move the plate between taking background images and taking images after chromatography in order for the plate to be spotted. Severe difficulties were encountered in making the two images compatible, owing to the nature of the light delivered by the fibre and the fibre itself. The light delivered was not uniform and was altered significantly by any

slight movement of the apparatus in a way that was not evident in previous experiments with more robust apparatus. To meet these requirements of power and robustness a mercury lamp was used for all further experiments.

4.4 Mercury Lamp Offline Results

4.4.1 Dry imaged mercury lamp results

The first experiments undertaken using the mercury lamp were on dry plates in reflectance. Reproducibility and linearity of results were investigated on dry glass backed plates initially. The lamp was operated at 254 nm and light levels were much more satisfactory than with the xenon lamp as was the robustness and user-friendliness of the set up as a whole.

All images were taken with a filter (see Figure 4.2) in place in order to block out non-UV light, particularly that produced by the fluorophore in the plates. This ensured that the images were true direct UV measurements. Signal referencing was carried out in the same way as for all other offline work. Examples of dry plate images using the mercury lamp for illumination are given in Figures 4.16 and 4.17 below.

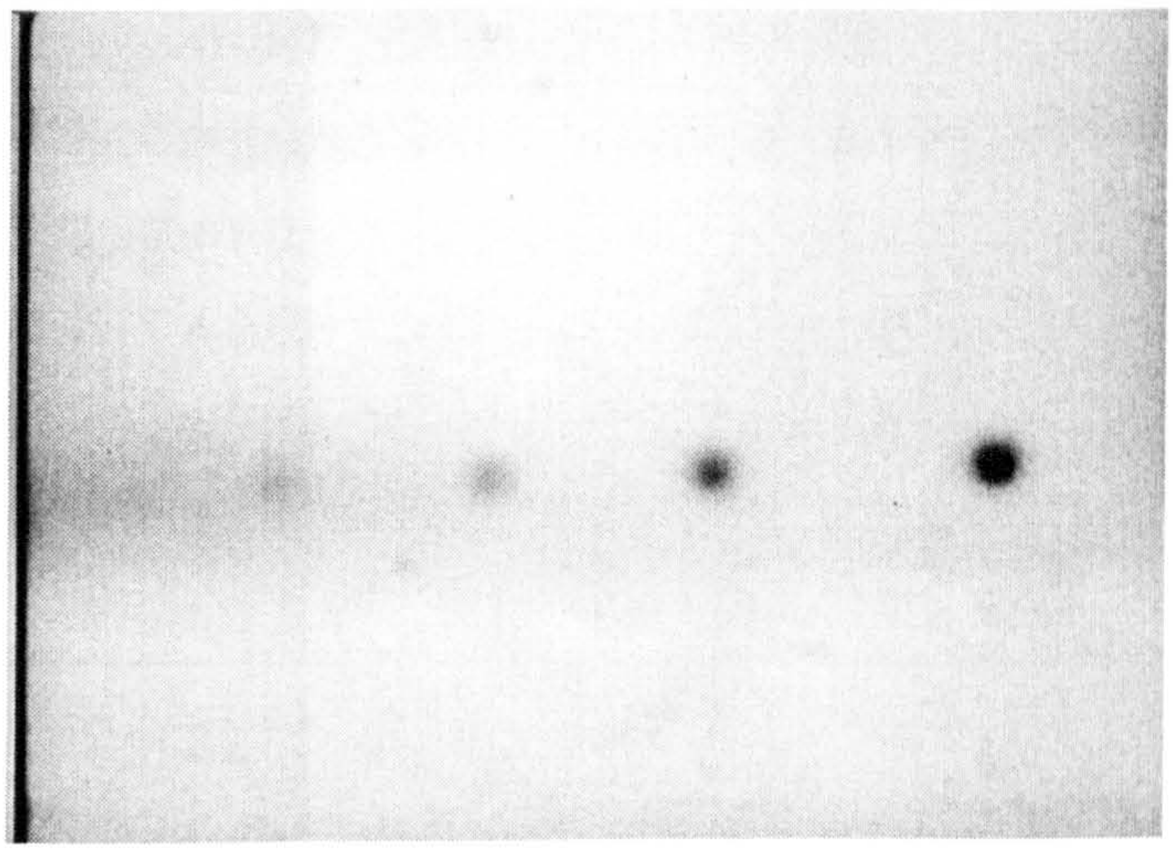

Figure 4.16 Raw, uncorrected image of a benzophenone calibration (5, 10. 25 and 50 ng) on a dry plate using the mercury lamp for illumination. Compare the evenness of the illumination with Figure 4.10.

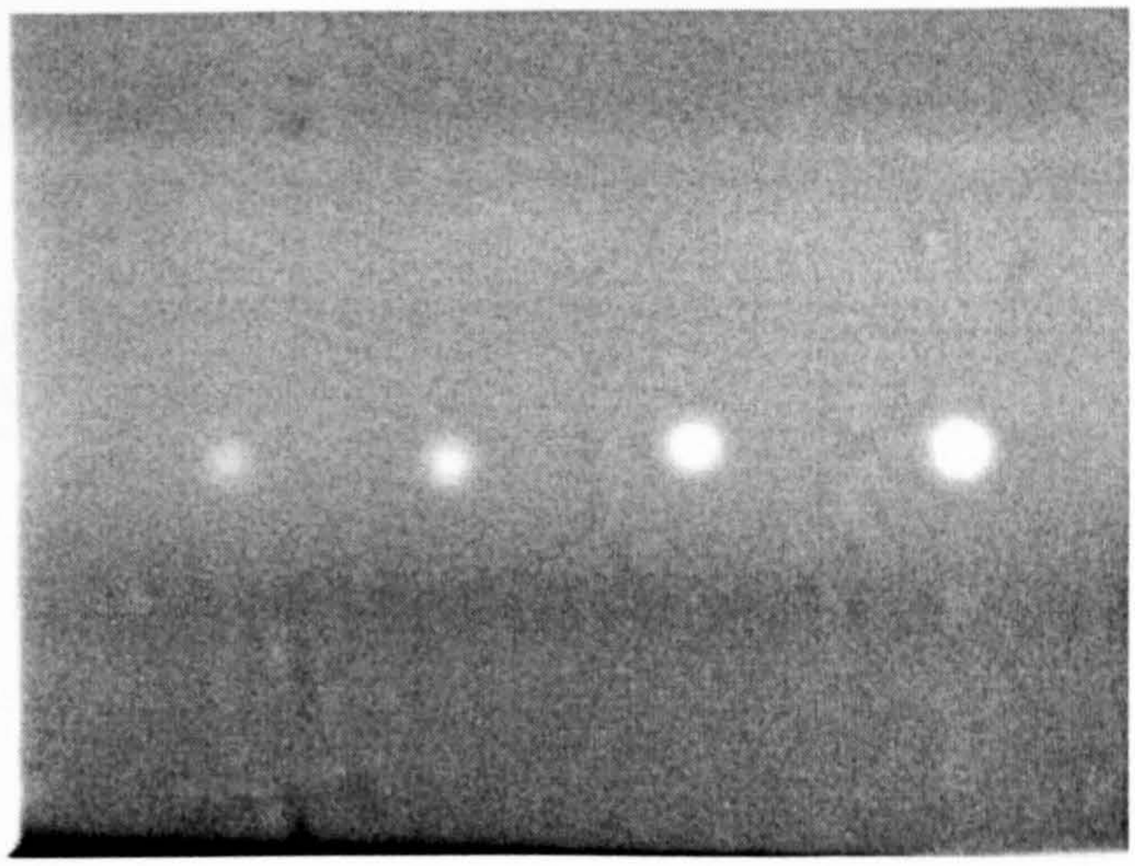

Figure 4.17 Figure 4.16 above corrected for fixed pattern effects.

Results obtained are given in Tables 4.4 – 4.7 below. Reproducibility and linearity were assessed for two different layer thicknesses (100 and 200 μm). Different calibration ranges were also studied.

Table 4.4 Average signals of 4 × 25 ng benzophenone spots run with 50:50 DCM/hexane, imaged offline in reflectance using a mercury lamp for illumination. Glass backed Silica Gel 60 F_{254} TLC plates used (200 μm layer thickness).

Average signal / 10^{-7}AU m^2	RSD / %
1.67 ± 0.05	3.1
2.06 ± 0.06	3.0
1.71 ± 0.02	1.2
1.99 ± 0.02	1.0
Average 1.86 ± 0.20	Interplate RSD = 11 %

Table 4.5 Average signals of 4 × 25 ng benzophenone run with 50:50 DCM/hexane, imaged offline in reflectance using a mercury lamp for illumination. Glass backed Silica Gel 60 F_{254} HPTLC plates with a layer thickness of 100 μm used.

Average signal / 10^{-7}AU m^2	RSD / %
1.83 ± 0.01	0.5
1.70 ± 0.04	2.4
1.38 ± 0.02	1.4
1.49 ± 0.02	1.3
Average 1.60 ± 0.20	Interplate RSD = 13 %

RSDs quoted in the right hand columns of tables 4.4 and 4.5 above are between four spots on one plate for the full analytical procedure from spotting to evaluation. The RSD values obtained on both layers were satisfactory (<5% in all cases), with the HPTLC layer performing slightly better than the standard layer in terms of intra-plate RSDs (0.5 – 2.4 % as against 1.0 – 3.1%). Inter-plate RSDs were comparable for the TLC and HPTLC plates.

The average signal was found to be lower on the 100 μm layer (1.60×10^{-7} AU m^2) than on the 200 μm layer (1.86×10^{-7} AU m^2), though statistically the difference is not substantial given the standard deviation on each value of 0.20×10^{-7} AU m^2. This is in contrast to results reported previously (Poole *et al.*, 1990) in which a higher signal was observed for the thinner layer. However, the results in Table 4.4 above were not obtained on HPTLC plates and this would be expected to have a significant effect on the signal obtained due to the smaller particle size and tighter particle size distribution.

Table 4.6 Calibrations of benzophenone run with 50:50 DCM/hexane imaged offline in reflectance using a mercury lamp for illumination. Glass backed Silica Gel 60 F_{254} TLC plates used (200 μm layer thickness).

Calibration	Range / ng	x^0 / 10^{-8} AU m^2	x^1 / AU m^2 g^{-1}	r^2
1	2-25	1.8 ± 3.0	9.0 ± 0.7	0.9994
2		1.0 ± 4.9	7.6 ± 1.7	0.9947
3		4.2 ± 4.8	9.1 ± 1.7	0.9964
4		2.5 ± 2.9	9.6 ± 0.9	0.9991
	Average	*2.4 ± 1.4*	*8.8 ± 0.9*	
1	5-50	-0.7 ± 2.3	7.9 ± 1.7	0.9951
2		-0.4 ± 1.5	7.9 ± 1.0	0.9979
3		-0.4 ± 1.4	7.1 ± 1.0	0.9979
4		0.1 ± 2.4	7.4 ± 1.7	0.9942
	Average	*-0.4 ± 0.3*	*7.6 ± 0.4*	

Table 4.7 Calibrations of benzophenone (2, 5, 10 and 25 ng) run with 50:50 DCM/xylene imaged offline in reflectance mode on glass backed Silica Gel 60 F_{254} HPTLC plates with a layer thickness of 100 μm.

Calibration	x^0 / 10^{-8} AU m^2	x^1 / AU m^2 g^{-1}	r^2
1	1.0 ± 2.1	6.0 ± 1.5	0.9934
2	1.1 ± 2.1	5.7 ± 1.5	0.9923
3	-0.8 ± 1.3	6.1 ± 1.0	0.9968
4	0.5 ± 1.4	6.4 ± 1.2	0.9972
Average	*0.5 ± 0.9*	*6.1 ± 0.3*	

In Tables 4.6 and 4.7 above, the gradient (x^1 coefficient) is equivalent to the effective absorption coefficient ε_{eff} in AU m^2 g^{-1}. The slopes from all the experiments show good repeatability, with intercepts (x^0 coefficient) around zero within experimental error. Comparison of the 5-50 ng results with the 2-25 results in Table 4.6 shows that the slope is once again slightly steeper over the lower range of concentrations, consistent with slight downward curvature at the highest

loading. This is in good agreement with measurements in the visible region reported in Chapter 3 and also xenon lamp UV measurements reported in section 4.4. The average ε_{eff} values from Table 4.6 agree well with the spectrophotometer value previously quoted (8.6 AU $m^2 g^{-1}$).

The slopes in Table 4.6 are steeper than those for the same loading range in Table 4.7. This is consistent with observations from the absolute values in the reproducibility experiments (Tables 4.4 and 4.5), with the thicker layer giving a higher signal.

4.4.2 UV imaging on wet glass backed plates

An attempt was made to undertake wet offline experiments as in Chapter 2 but with the imaging being done in the UV. Initial experiments were carried out on glass backed plates with similar sample loadings to those in Section 4.4.1, but no peaks were visible when the plates were solvated. The peaks became visible if the plates were allowed to dry and were of a similar size to those reported in the previous section.

Further attempts were made at higher loadings until detection was possible, with 500 ng spots giving a S/N ratio of approximately 4:1 as illustrated in Figures 4.18 and 4.19.

The average result of 1.8×10^{-7} AU m^2 for the 500 ng peaks in Figure 4.18 corresponds to a ε value of 0.36 AU $m^2 g^{-1}$. This value is a factor ~ 20 lower than those obtained from dry plates (6-10 AU $m^2 g^{-1}$), as well as being unexpected after our visible light investigations with Sudan ii.

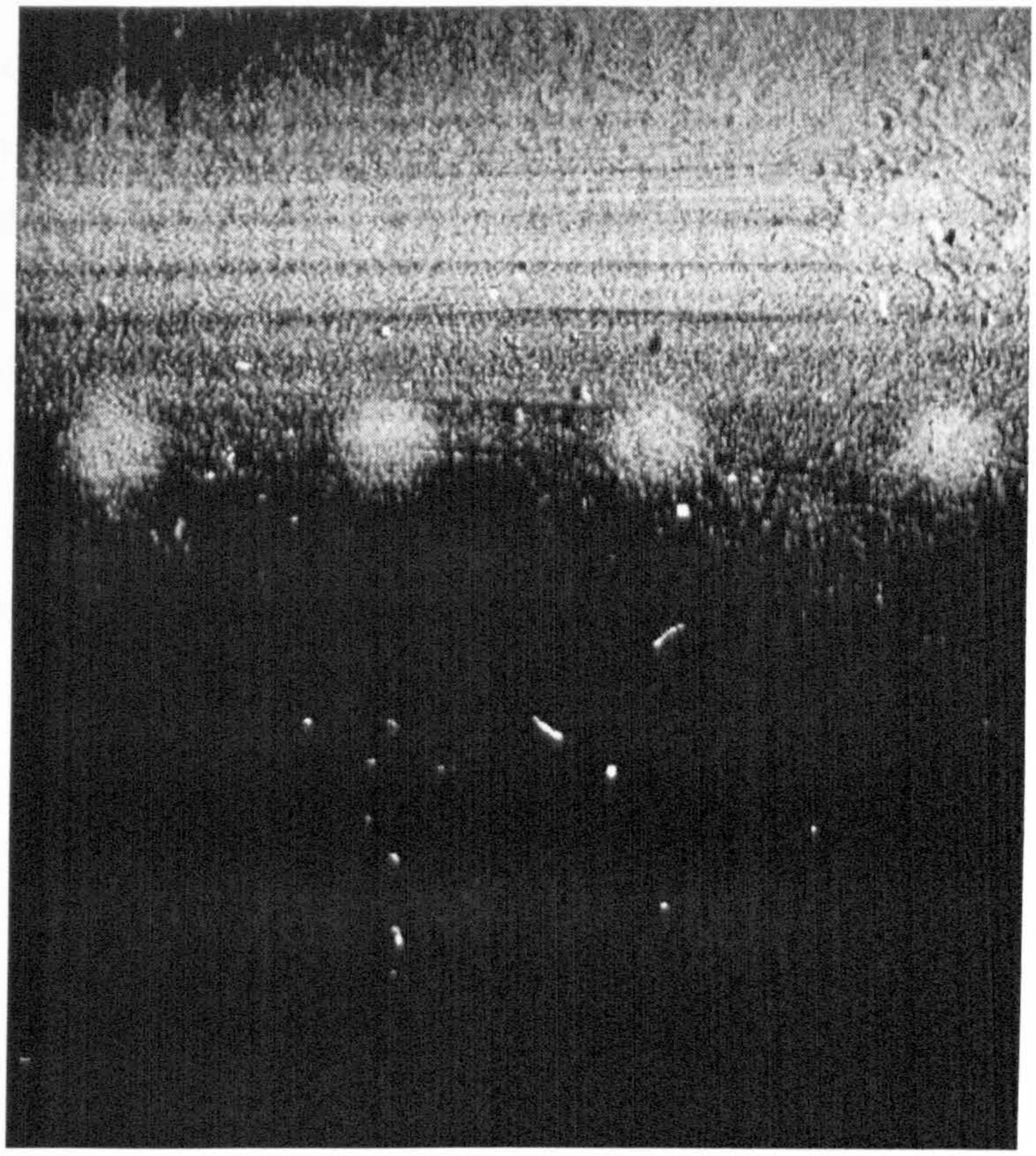

Figure 4.18 A corrected image of four 500 ng spots of benzophenone, imaged wet on a glass backed Silica Gel 60 F_{254} TLC plate.

Figure 4.19 Peak obtained from a 500 ng spot of benzophenone imaged on a wet glass backed Silica Gel 60 F_{254} TLC plate and integrated in the direction of chromatography. The S/N ratio is approximately 4:1.

An investigation was made into effective absorbance values by employing home made plates with a UV transparent support (spectrosil b quartz, section 4.2.5). Absorbance measurements were made in reflectance with the tank lined with polished aluminium in order to increase reflection and also with the tank lined with black felt in order to decrease reflection. Measurements were made on the same spots wet and dry. A high sample loading (500 ng) was used because the layers we produced were not as reproducible as commercially available layers. The results are given in Table 4.8.

Table 4.8 Apparent absorption coefficients of 500 ng benzophenone measured on TLC plates backed with UV transparent fused silica.

	ε_{eff} / AU m^2 g^{-1}	
	Aluminium lined tank	Felt lined tank
Dry	10.4	6.5
Wet	5.5	3.6

The first thing to note is that all values of the effective absorption coefficients are a factor 10 or greater than those from images with the wet glass backed plate. This suggests that when the plate is wet, UV light traverses the whole of the layer and is absorbed by the glass. Using the fused silica plate, which does not absorb UV light, the effective absorption coefficient for benzophenone measured with the dry plate in the felt lined tank is comparable to the values reported in previous tables. It can be seen that lining the tank with reflective or absorbent material has a significant effect on the effective absorbance coefficients obtained, both wet and dry. The reflective conditions of the aluminium lined tank results in higher values (10.4 dry and 5.5 wet) than when using black felt as a liner (6.5 dry and 3.6 wet). It is likely that more light is being reflected back up through the fused silica plate and the sorbent layer when aluminium is used to line the tank. The increased reflection results in higher effective absorbance coefficients as the effective pathlength through the layer is increased.

4.4.3 Wet and dry imaged plates

It was found that a good signal could be obtained on wetted plates from absorbance experiments by using aluminium backed plates instead of the usual glass backed plates. The aluminium backed plates were not quite as robust as the glass-backed variety and more care had to be taken with them but no serious problems were encountered.

It was possible to obtain both wet and dry result from the same spots, during and after chromatography. Two types of plate were used: aluminium backed Silica Gel 60 F_{254} and aluminium backed Silica Gel 60 TLC plates, with and without fluorophore respectively. The filter for blocking non-UV light (Figure 4.2) was used in experiments with all plates containing fluorophore. Linearity and precision were investigated using benzophenone and the results are given in Tables 4.9 - 4.12 below.

Table 4.9 Average signals of 4 x 25 ng benzophenone runs with 75:25 DCM/hexane imaged wet and dry offline in reflectance with the mercury lamp. Aluminium backed Silica Gel 60 F_{254} TLC plates used in conjunction with a filter used to block non-UV light.

Average signal / 10^{-7}AU m^2		RSD / %	
Wet	Dry	Wet	Dry
2.82 ± 0.13	2.16 ± 0.07	4.4	3.5
2.63 ± 0.11	1.95 ± 0.07	4.1	3.7
2.44 ± 0.12	1.91 ± 0.06	4.9	3.1
2.18 ± 0.09	1.68 ± 0.05	4.1	2.8
2.52 ± 0.27	*1.93 ± 0.20*	Interplate = 11 %	Interplate = 10 %

Table 4.10 Average signals of 4 × 25 ng benzophenone runs with 75:25 DCM/hexane imaged wet and dry offline in reflectance with the mercury lamp. Aluminium backed Silica Gel 60 TLC plates (no fluorophore) used.

Average signal / 10^{-7}AU m^2		RSD / %	
Wet	Dry	Wet	Dry
3.88 ± 0.18	1.74 ± 0.04	4.6	2.3
3.37 ± 0.12	2.34 ± 0.07	3.4	2.9
3.00 ± 0.14	2.11 ± 0.02	4.8	0.9
3.61 ± 0.16	2.42 ± 0.06	4.5	2.3
3.47 ± 0.37	*2.15 ± 0.30*	Interplate = 11 %	Interplate = 14 %

Good precision (<5% RSD) was obtained from wet and dry plates, with dry plates being the more repeatable of the two as expected. Higher signals were obtained from the plates without fluorophore. This may be due at least in part to the fluorophore containing plates absorbing some UV at 254 nm.

It is clear from Tables 4.9 and 4.10 that the signal obtained is higher on wetted plates than for dry plates on aluminium backed plates. This is in contrast to glass backed plates, where dry plates gave a higher signal than wet plates (Section 2.4, Tables 2.1-2.3). In discussion of the previous results, it was thought that increased scatter (and hence longer effective path length) on dry layers was responsible for the higher signal. It is probable that light is being reflected back up from the aluminium backing of the plate, and that this reflection is more pronounced under wet conditions, as the sorbent layer becomes less opaque. This would be consistent with the higher signal being obtained on wet plates. This would not be the case for glass backed plates, especially when UV light was being used, as the glass would tend to absorb the light, not reflect.

The results for the calibration experiments are given in Tables 4.11 and 4.12. Consistent with the higher signals observed on wet than on dry plates for 25 ng loadings, the slopes of the calibration plots were greater for wet (12.6 AU m^2 g^{-1}

without fluorophore and 10.0 AU m^2 g^{-1} with fluorophore) than on dry plates (8.2 AU m^2 g^{-1} without fluorophore and 5.5 AU m^2 g^{-1} with fluorophore). Higher slopes were obtained from plates with no fluorophore. All intercepts were positive, though the error bounds of all intercepts from experiments on individual plates encompassed zero. However, the low error bounds on the averages from all plates suggested that the intercepts were in fact significantly different from zero. Linearity was good with r^2 values >0.99 in all cases.

Table 4.11 Calibrations of benzophenone (5, 10, 25 and 50 ng) run with 75:25 DCM/hexane imaged wet and dry offline in reflectance mode. Aluminium backed Silica Gel 60 F_{254} TLC plates used in conjunction with a filter used to block non-UV light.

Plate	Dry			Wet		
	x^0 / 10^{-8} AU m^2	x^1 / AU m^2 g^{-1}	r^2	x^0 / 10^{-8} AU m^2	x^1 / AU m^2 g^{-1}	r^2
1	1.8 ± 2.1	4.8 ± 0.6	0.9981	4.5 ± 7.3	10.2 ± 2.6	0.9932
2	1.2 ± 1.4	5.0 ± 0.5	0.9989	1.5 ± 3.1	9.9 ± 1.1	0.9987
3	1.2 ± 4.5	6.3 ± 1.6	0.9935	3.6 ± 7.4	10.3 ± 2.6	0.9930
4	1.4 ± 1.9	5.9 ± 1.1	0.9979	2.4 ± 3.4	9.5 ± 1.7	0.9971
Average	*1.4 ± 0.3*	*5.5 ± 0.7*		*3.0 ± 1.3*	*10.0 ± 0.4*	

Table 4.12 Calibrations of benzophenone (5, 10, 25 and 50 ng) run with 75:25 DCM/hexane imaged wet and dry offline in reflectance mode. Aluminium backed Silica Gel 60 TLC plates (no fluorophore) used.

Plate	Dry			Wet		
	x^0 / 10^{-8} AU m^2	x^1 / AU m^2 g^{-1}	r^2	x^0 / 10^{-8} AU m^2	x^1 / AU m^2 g^{-1}	r^2
1	2.7 ± 5.2	7.3 ± 1.8	0.9933	5.3 ± 6.4	11.3 ± 2.3	0.9958
2	1.6 ± 5.2	9.1 ± 1.8	0.9957	1.6 ± 4.7	11.4 ± 1.7	0.9977
3	1.0 ± 5.8	9.9 ± 2.0	0.9955	2.7 ± 4.5	13.7 ± 1.6	0.9986
4	1.7 ± 2.4	6.6 ± 0.8	0.9982	3.1 ± 5.4	13.9 ± 1.9	0.9980
Average	*1.8 ± 0.7*	*8.2 ± 1.5*		*3.2 ± 1.6*	*12.6 ± 1.4*	

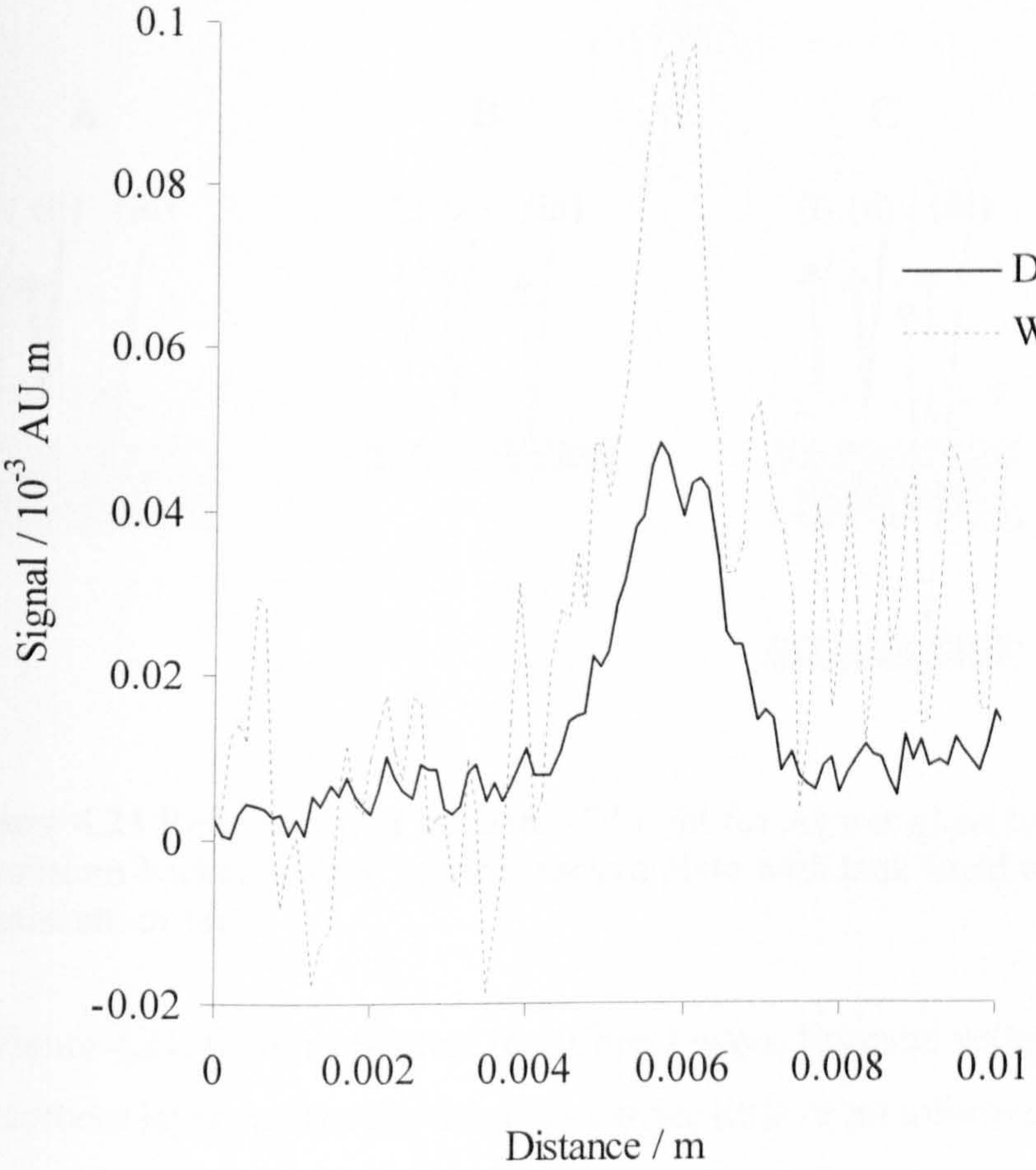

Figure 4.20 The same 5 ng benzophenone peak imaged wet (during chromatography) and dry (after chromatography).

It is evident from Figure 4.20 that a higher signal is obtained from a wet image than from a dry image. However, the noise associated with the measurement is also clearly higher, the result being that the S/N ratio is higher (and the LOD lower) for the dry imaged peak. The S/N for the dry peak is approximately 5:1, whilst the S/N for the wet peak is approximately 3:1. The wet 5 ng peak is approximately at the limit of detection, whereas it should be possible to detect <5 ng on a dry plate by this method.

UV results in reflectance with an aluminium backing layer give an effective absorption coefficient of 12.6 AU m^2 g^{-1} which is similar to but somewhat higher than straightforward spectrophotometer experiments (8.9 AU m^2 g^{-1}). Thus, effectively this becomes in some respects comparable to a transmission type of measurement.

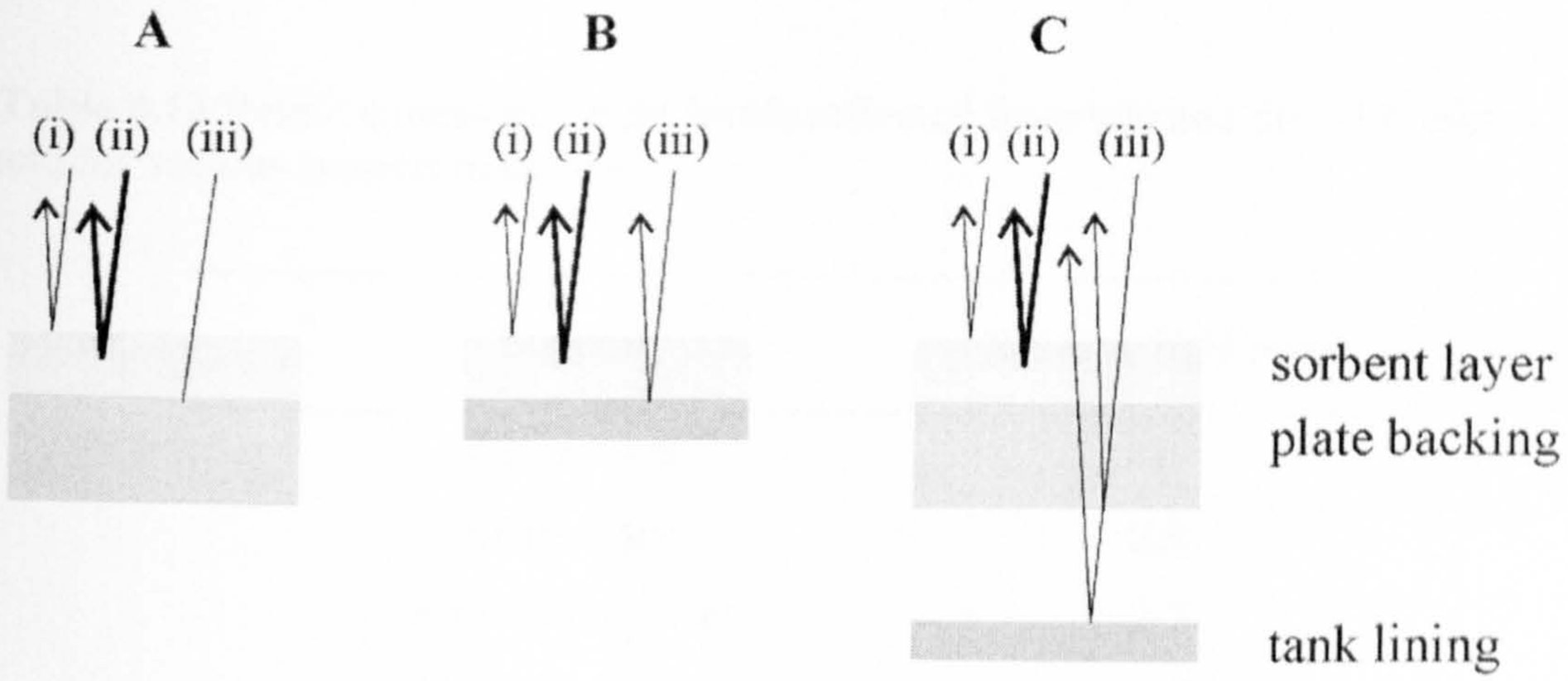

Figure 4.21 Reflectance of incident UV light for A) wet glass backed plate B) wet aluminium backed plate C) quartz backed plate with tank lined with either aluminium or felt.

In Figure 4.21, light is reflected in different ways. Specular reflection occurs at the sorbent layer surface (i); this light carries little or no information about any analyte present. Light is reflected or scattered back from the stationary phase (ii); this light does provide information about analyte present. Light is also reflected from other interfaces (iii) particularly those with large refractive index differences. For a wet plate these are air/mobile phase at the top surface and mobile phase/aluminium, silica or air at the bottom surface. The effective pathlength will depend on the relative proportions of these light paths.

For a wet glass backed plate (as in Figure 4.21 A), ε is very low so most of the light reaching the detector must be from the top surface resulting in a short apparent pathlength. Light levels relative to this are given in Table 4.13. Figure 4.21 B shows light reflected from the mobile phase/aluminium interface of an aluminium backed plate.

Wet quartz with a felt lined tank gives a higher reflected light level and apparent pathlength consistent with light reflected from the lower plate surface (Figure 4.21 C). With an aluminium lined tank both reflected light level and pathlength are

increased further. Dry plates all have similar reflectance levels as the dominant effect is light reflected and scattered from the sorbent layer

Table 4.13 Relative measured light levels reflected from wet and dry TLC plates and for various support materials.

Support	Relative light level
Glass - wet	1
Glass - dry	2.4
Aluminium - wet	2.7
Aluminium - dry	2.5
Quartz with felt lining - wet	1.3
Quartz with Aluminium lining - wet	2.4

The sorbent layer on aluminium backed plates does not extend to the full width of the backing. Reflection from the exposed aluminium surface at the plate edges, gave rise to a bright band caused by the unscattered reflection of the lamp. However, the sorbent layer itself was not any brighter at this angle; this is consistent with multiple paths within the sorbent layer and reflection from the top surface being dominant.

Table 4.14 shows refractive index values of silica and solvents at visible (500 nm) and UV (254 nm) wavelengths. Closer matching between the two values results in less scattering of light from within the sorbent layer. It can bee seen that both sets of values for DCM are close to those of silica at the corresponding wavelength. This means that there would be little scattering of light when the plate was solvated. At 254 nm the light would pass through the layer and be absorbed by the glass support. At 500 nm light would not be absorbed by the glass support and some would be reflected back up off the glass air interface and from the bottom of the tank and result in a higher effective pathlength. This is the main reason why poor results were obtained using glass backed plates in UV compared with those using visible light. Additionally, the RI values are even better matched at 254 nm

than they are at 500 nm therefore more scattering would be expected in the sorbent layer at 254 nm also resulting in a lower apparent pathlength.

Table 4.14 Refractive indices of silica gel and solvents at 500 and 254 nm.

Wavelength / nm	Acetonitrile[1]	hexane[1]	DCM[2]	Silica[3]
500	1.3458	1.3795	1.4349	1.4623
254	1.4755	1.4255	1.4985	1.5075

1 Kozma *et al.*, 2005
2. Samoc, 2003 values for RI dispersion of chloromethane used, scaled by refractive index ratio of DCM to chloromethane at sodium D line.
3. http://www.sciner.com/Opticsland/FS.htm

Both acetonitrile and hexane have refractive indices which are not as well matched with silica as that of DCM. These solvents would be expected to give rise to longer effective pathlengths and larger analyte signals than DCM. This is the case in Table 4.30 although the comparison is not a direct one as a HPTLC layer was used for the mixed solvents compared with standard TLC used with DCM alone.

4.4.4 Multi-component offline experiments

So far we have looked at chromatographic development involving only one analyte. It would be useful to examine some separations involving more than one analyte in order to test the performance of the system under conditions more likely to be met in a normal working laboratory.

Four UV absorbing organic compounds, methyl 4-hydroxybenzoate, benzophenone, niacinamide and 3-hydroxybenzaldehyde were investigated. Using aluminium backed Silica Gel 60 F_{254} TLC plates in conjunction with a filter to block non-UV light and 75:25 DCM/hexane as solvent it was possible to resolve the benzophenone and niacinamide peaks with R_f values of 0.8 and 0 respectively (Figures 4.22 and 4.23). Effecting separation of the methyl 4-hydroxybenzoate and the 3-hydroxybenzaldehyde peaks was more problematic and after several solvent systems had been tried it was decided to use results for the unresolved

peaks (R_f = 0.5, Figures 4.23 and 4.24) and comparison with spectrophotometric measurements for a mixture of the two analytes (Table 4.18). The masses of the two analytes were added to give the x axis value.

Experiments were carried out in reflectance mode on both wet and dry aluminium backed plates and the results are for the same spots during and then after chromatography. Tables 4.15 –4.17 show results for the different analytes separated on the same plates (Plate 1 results in each Table are taken from the same plate).

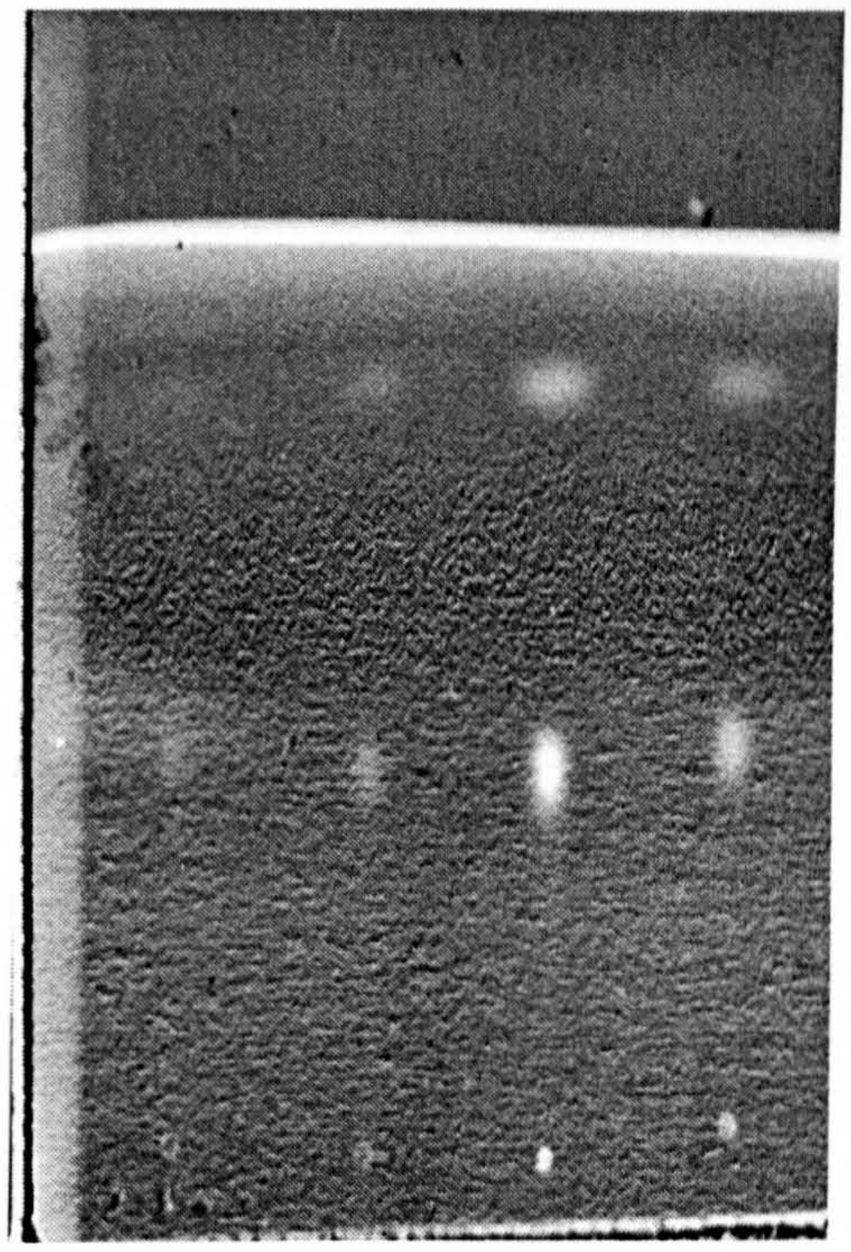

Figure 4.22 Calibration of UV mixture (benzophenone (1.58, 3.16, 15.8 and 7.9 ng), methyl 4-hydroxybenzoate (1.32, 2.63, 13.15 and 6.58 ng), 3-hydroxybenzaldehyde (1.05, 2.1, 10.53 and 5.26 ng) and niacinamide (1.05, 2.1, 10.53 and 5.26 ng)) on a wet Silica gel F_{254} TLC plate. The solvent was 75:25 DCM/hexane.

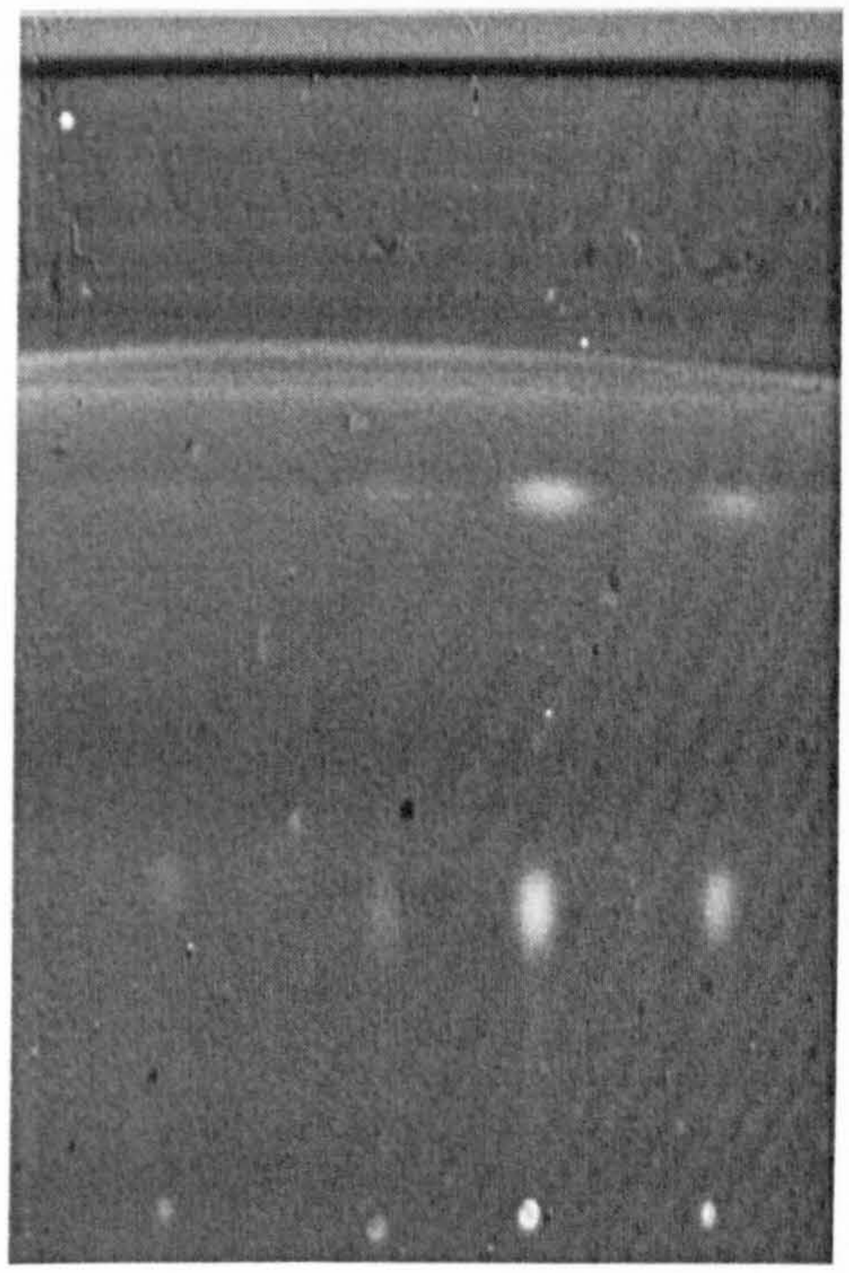

Figure 4.23 Calibration of UV mixture (benzophenone (1.58, 3.16, 15.8 and 7.9 ng), methyl 4-hydroxybenzoate (1.32, 2.63, 13.15 and 6.58 ng), 3-hydroxybenzaldehyde (1.05, 2.1, 10.53 and 5.26 ng) and niacinamide (1.05, 2.1, 10.53 and 5.26 ng)) on a dry Silica gel F_{254} TLC plate. The solvent was 75:25 DCM/hexane.

Table 4.15 Calibrations of benzophenone in reflectance on both wet and dry Silica gel F_{254} TLC plates. The sample loadings used were 1.58, 3.16, 15.8 and 7.9 ng. The solvent was 75:25 DCM/hexane.

Plate	Dry			Wet		
	x^0 / 10^{-9} AU m^2	x^1 / AU m^2 g^{-1}	r^2	x^0 / 10^{-9} AU m^2	x^1 / AU m^2 g^{-1}	r^2
1	-0.08 ± 0.54	3.79 ± 0.22	0.9932	-0.04 ± 0.63	8.68 ± 0.52	0.9930
2	-0.04 ± 0.20	4.57 ± 0.09	0.9993	0.24 ± 0.75	10.66 ± 0.60	0.9935
3	-0.02 ± 0.52	4.73 ± 0.21	0.9960	-0.61 ± 0.98	11.58 ± 0.80	0.9905
4	-0.06 ± 0.45	5.25 ± 0.18	0.9977	-0.07 ± 0.52	10.40 ± 0.42	0.9967
Average		*4.59 ± 0.60*			*10.33 ± 1.21*	

Table 4.16 Calibrations of unresolved spots of methyl 4-hydroxybenzoate (1.32, 2.63, 13.15 and 6.58 ng) and 3-hydroxybenzaldehyde (1.05, 2.1, 10.53 and 5.26 ng) in reflectance on both wet and dry Silica gel F_{254} TLC plates. The solvent was 75:25 DCM/hexane.

Plate	Dry			Wet		
	x^0 / 10^{-9} AU m^2	x^1 / AU m^2 g^{-1}	r^2	x^0 / 10^{-9} AU m^2	x^1 / AU m^2 g^{-1}	r^2
1	-0.36 ± 0.62	7.03 ± 0.25	0.9974	-0.41 ± 1.41	10.65 ± 0.26	0.9997
2	-0.41 ± 0.42	6.97 ± 0.17	0.9988	0.75 ± 1.82	11.43 ± 0.31	0.9986
3	0.28 ± 0.46	8.72 ± 0.19	0.9991	-0.02 ± 1.53	12.11 ± 0.66	0.9941
4	-0.11 ± 0.46	7.80 ± 0.19	0.9988	-0.02 ± 0.94	12.13 ± 0.43	0.9975
Average	*7.63 ± 0.82*			*11.58 ± 0.70*		

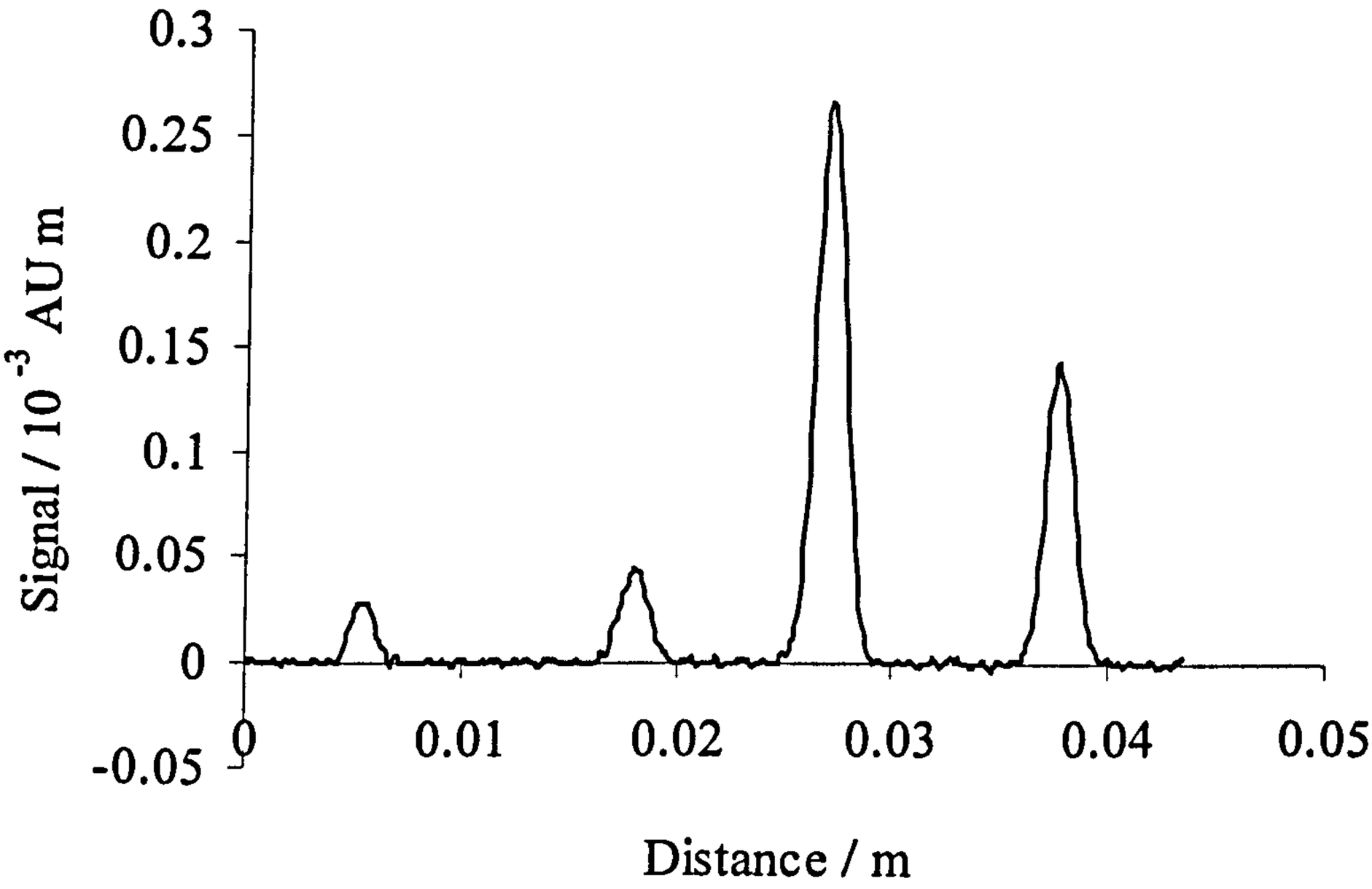

Figure 4.24 Unresolved peaks of methyl 4-hydroxybenzoate (1.32, 2.63, 13.15 and 6.58 ng) and 3-hydroxybenzaldehyde (1.05, 2.1, 10.53 and 5.26 ng) imaged on a dry plate and integrated in the direction of chromatography.

The results for benzophenone and the unresolved peak of methyl 4-hydroxybenzoate and 3-hydroxybenzaldehyde all demonstrate good linearity between peak area and sample loading, with r^2 values > 0.993 for dry plates and 0.990 for wet plates. The fact that the r^2 values from the wet plates were lower in

comparison to the dry plates is probably due to the contributions from the presence of solvent, resulting in more noise and hence a lower S/N ratio.

Table 4.17 Calibrations of niacinamide in reflectance on both wet and dry Silica gel F_{254} TLC plates. The sample loadings used were 1.05, 2.1, 10.53 and 5.26 ng. The solvent was 75:25 DCM/hexane.

Plate	Dry			Wet		
	x^0 / 10^{-9} AU m^2	x^1 / AU m^2 g^{-1}	r^2	x^0 / 10^{-9} AU m^2	x^1 / AU m^2 g^{-1}	r^2
1	4.6 ± 0.4	1.31 ± 0.13	0.9744	0.21 ± 0.03	1.39 ± 0.11	0.9868
2	15 ± 3.5	1.39 ± 0.14	0.9803	19.41 ± 1.72	1.30 ± 0.07	0.9942
3	0.4 ± 0.1	1.42 ± 0.15	0.9791	4.41 ± 8.88	1.49 ± 0.04	0.9988
4	6.7 ± 0.4	1.88 ± 0.15	0.9892	10.23 ± 4.28	1.87 ± 0.18	0.9826
Average		*1.50 ± 0.31*			*1.51 ± 0.25*	

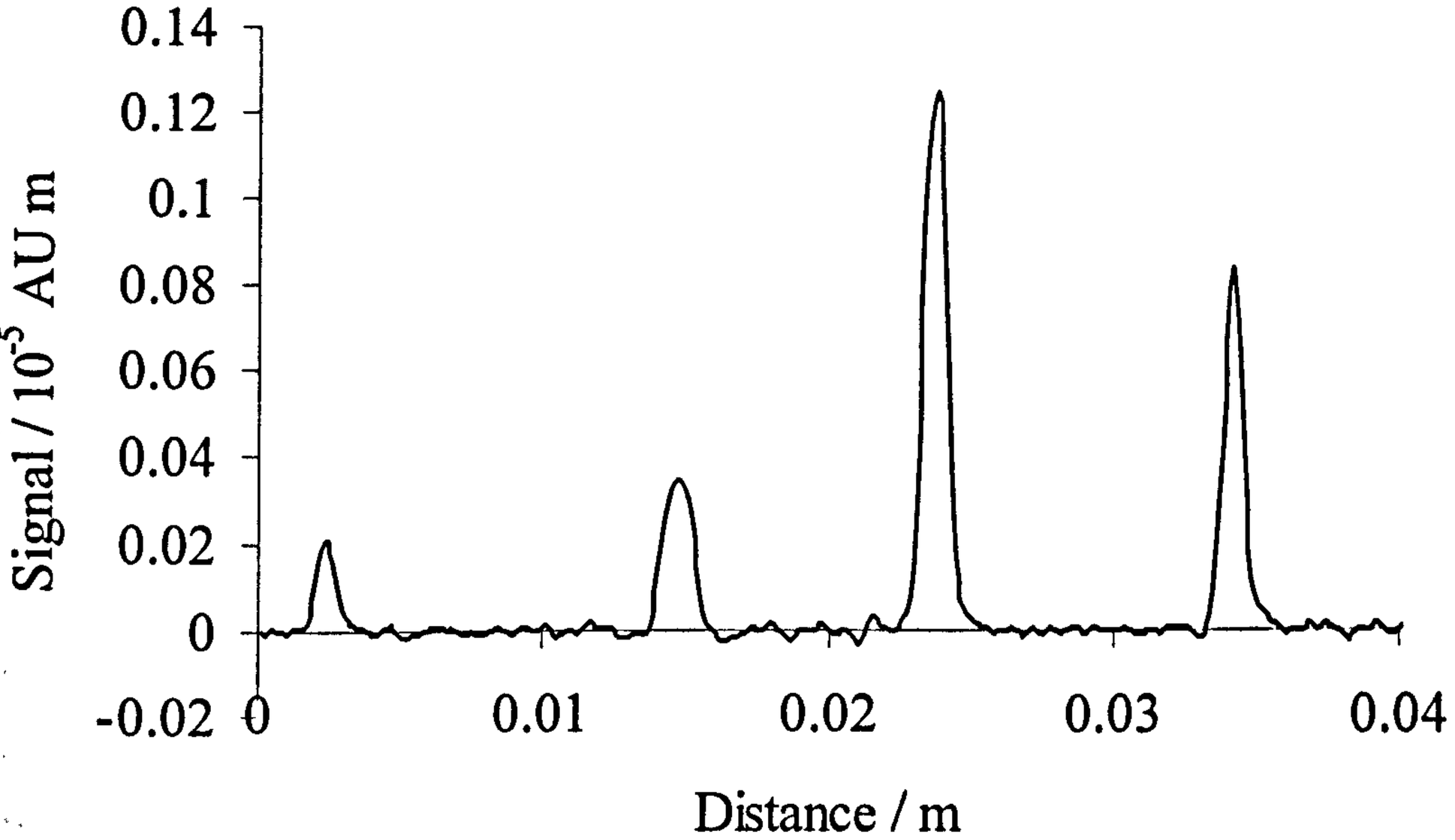

Figure 4.25 Niacinamide peaks (1.05, 2.1, 10.53 and 5.26 ng) imaged on a wet plate integrated in the direction of chromatography.

The intercepts for benzophenone and the unresolved peak of methyl 4-hydroxybenzoate and 3-hydroxybenzaldehyde were equal to zero within experimental error. The linear plots and zero intercepts demonstrate that the benzophenone and the unresolved peak obey the Beer-Lambert law within the range of sample loadings used.

Niacinamide displays correlation coefficients significantly worse than those for the other analytes: r^2 values for niacinamide are 0.974 on dry plates and 0.983 on wet plates. This could be because the niacinamide spots underwent little or no diffusion, causing the analyte to remain concentrated onto a small area on the plate (Figure 4.25) and giving much sharper peaks compared with the other compounds. These concentrated bands may be more affected by the essentially non-linear relationship between concentration and sample loading than more diffuse spots with linearity breaking down at higher concentrations. On average, the intercepts are slightly positive for niacinamide. This suggests that at high concentrations linearity does not prevail, and the results would be consistent with the relationship between absorbance and concentration only holding in dilute solutions.

Benzophenone on dry plates has an average gradient of 4.59 AU $m^2 g^{-1}$, the unresolved peak has gradient 7.63 AU $m^2 g^{-1}$, and niacinamide 1.52 AU $m^2 g^{-1}$. Benzophenone on wet plates has an average gradient of 10.33 AU $m^2 g^{-1}$, the mixture 11.58 AU $m^2 g^{-1}$ and niacinamide 1.51 AU $m^2 g^{-1}$. The unresolved peak has the highest slope value. Interestingly, the wet and dry results for niacinamide are identical, possibly a result of no diffusion occurring (as $R_f = 0$). The benzophenone results agree reasonably well with those in Table 4.11 given that a different solvent system is in use. The slope values above are compared in Table 4.18 to molar absorption coefficients at 254 nm determined by spectrophotometry (Table 4.1). For niacinamide, ε_{254} is identical to the two ε_{app} values obtained on-plate. The wet benzophenone result is in reasonable agreement with the spectrophotometer value, with the dry value being lower. A mixture of methyl 4-hydroxybenzoate and 3-hydroxybenzaldehyde of the same ratio as in the plate experiments was also studied by spectrophotometry. The result was in reasonable agreement with the wet plate value, with the dry value once again being lower.

Table 4.18 Comparison of absorption coefficients in DCM at 254 nm from UV spectrophotometry and apparent absorption coefficients determined from CCD imaging of peak areas as a function of loading.

Analyte	ε_{254} / AU $m^2 g^{-1}$	ε_{app} / AU $m^2 g^{-1}$	
		wet	dry
benzophenone	8.5	10.3	4.6
niacinamide	1.5	1.5	1.5
methyl 4-hydroxybenzoate	13.4	-	-
3-hydroxybenzaldehyde	7.3	-	-
mixture of methyl 4-hydroxybenzoate and 3-hydroxybenzaldehyde	10.1	11.6	7.6

Having a non-moving component in the analyte mixture is beneficial, as there is great interest in monitoring and quantifying all components in a mixture and this is possible using TLC. By contrast, in HPLC niacinamide, with $R_f = 0$, would not have been eluted from the column (Poole, 1999). For benzophenone the LOD was found to be approximately 1 ng wet and < 1 ng dry. The limit of detection was

estimated as the loading giving S/N = 3. For the unresolved peak of methyl 4-hydroxybenzoate and 3-hydroxybenzaldehyde the LOD was about 0.5 ng wet and < 0.5 ng dry. In the case of niacinamide the LODs were determined as approximately 0.5 ng wet and < 0.5 ng dry. For all analytes the LODs are higher on wet plates as there is increased noise due to solvent. In comparison with the other analytes, the narrower band of niacinamide compensates for the lower absorbance and the net result is a similar LOD. Images of bands from 4 spots of benzophenone and niacinamide are shown in Figures 4.25 and 4.26 respectively. These figures clearly demonstrate the influence of band broadening during analyte elution in the case of benzophenone, and the relative sharpness of the niacinamide peak, which remains at the position of spotting on the plate.

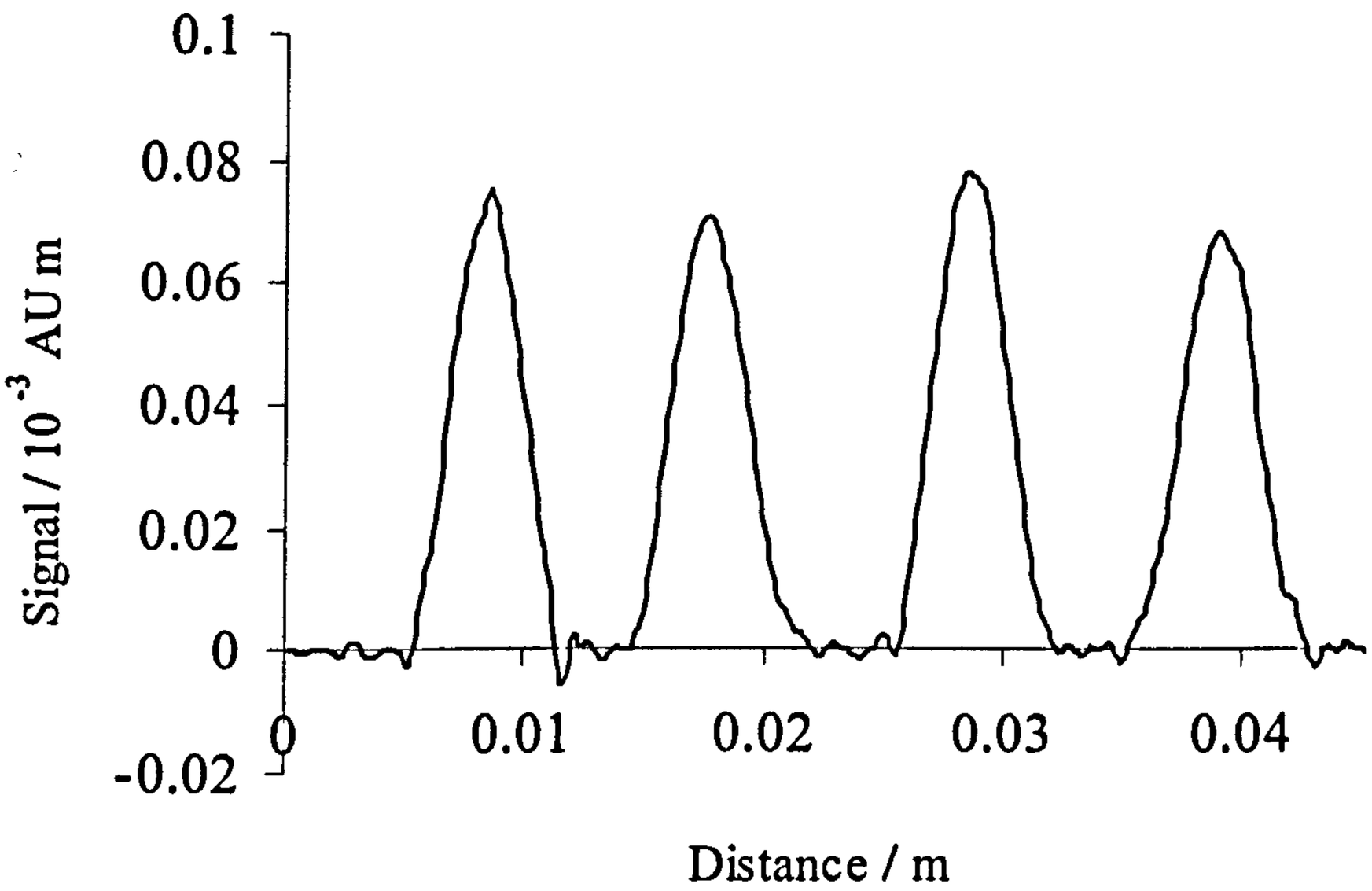

Figure 4.26 Benzophenone peaks (15.8 ng) imaged on a wet plate and integrated in the direction of chromatography

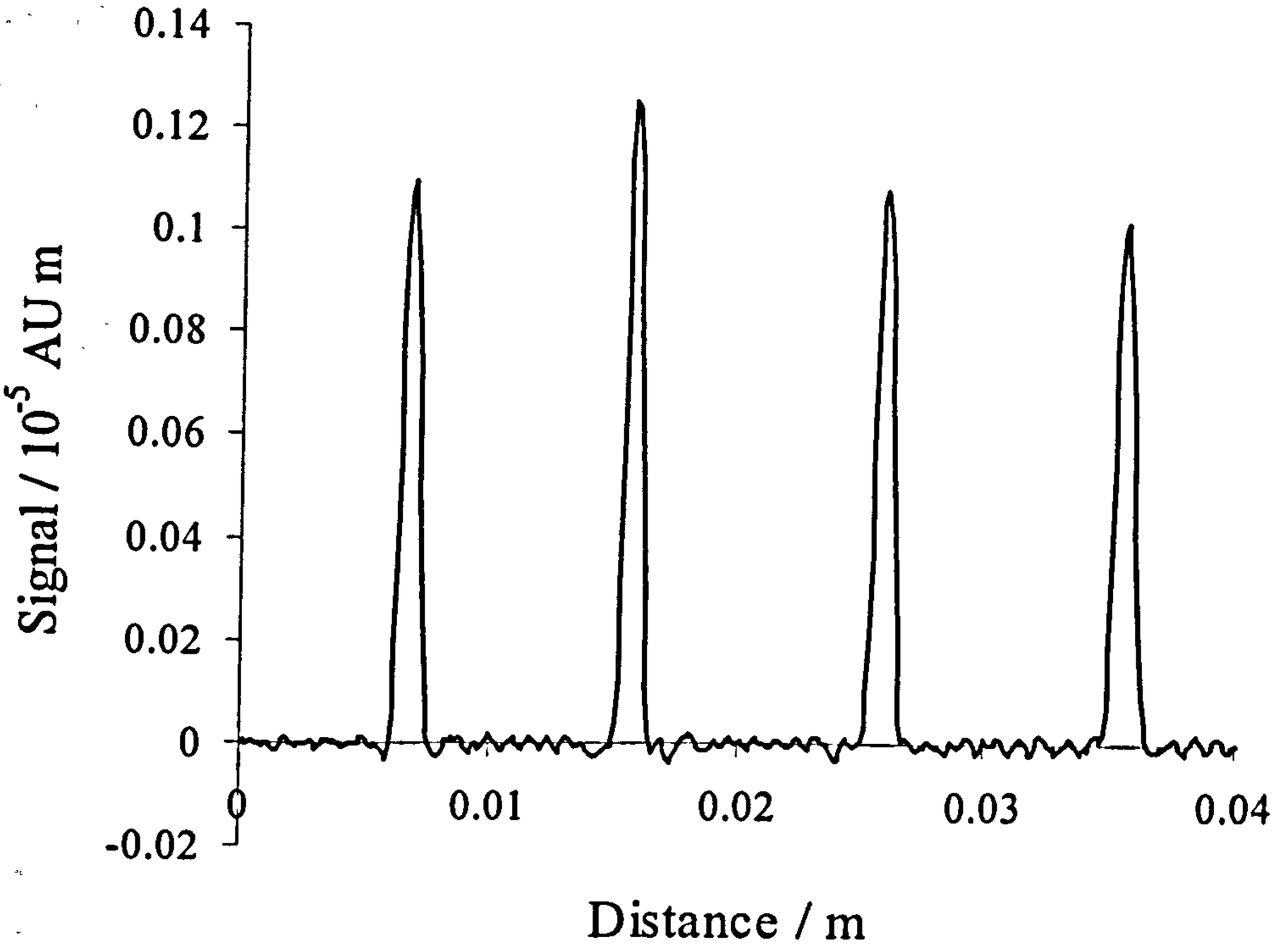

Figure 4.27 Niacinamide peaks (10.53 ng) imaged on a wet plate and integrated in the direction of chromatography.

Results for signal reproducibilities at fixed loadings for the various analytes are given in Tables 4.19, 4.20 and 4.21. RSD values for all of the compounds are seen to be below 5%, which accords with results from previous work on inter-spot reproducibility on a TLC plate (Liang *et al.*, 1998). Benzophenone on dry plates had RSD values of $\leq 4.4\%$ and $\leq 5.0\%$ on wetted plates (Table 4.19). The unresolved peak of methyl 4-hydroxybenzoate and 3-hydroxybenzaldehyde had RSDs $\leq 3.8\%$ on dry plates and on wetted plates $\leq 4.0\%$ (Table 4.20). Niacinamide on dry plates had values $\leq 3.0\%$ and on wet plates $\leq 4.6\%$ (Table 4.20).

RSD values for wet plates were higher than the corresponding value for dry plates due to the increased noise resulting from the presence of solvent. The RSD values between plates were rather poor, as expected. All RSD values are for the full analytical process from spotting to evaluation.

Table 4.19 Reproducibility of 4 × 15.8 ng spots of benzophenone in reflectance on both wet and dry plates.

	Dry		Wet	
Plate	Average signal / 10^{-7} AU m^2	RSD / %	Average signal / 10^{-7} AU m^2	RSD / %
1	2.04 ± 0.08	4.0	1.90 ± 0.08	4.2
2	1.85 ± 0.08	4.4	2.13 ± 0.11	4.9
3	2.69 ± 0.10	3.9	2.08 ± 0.08	3.7
4	2.27 ± 0.08	3.4	2.62 ± 0.09	3.5
Average	*2.21 ± 0.36*	*16*	*2.18 ± 0.31*	*14*

Table 4.20 Reproducibility of four unresolved spots of methyl 4-hydroxybenzoate (13.2 ng) and 3-hydroxybenzaldehyde (10.53 ng) in reflectance on both wet and dry plates.

	Dry		Wet	
Plate	Average signal / 10^{-7} AUm^2	RSD / %	Average signal / 10^{-7} AU m^2	RSD / %
1	2.98 ± 0.07	2.4	4.92 ± 0.07	1.36
2	3.15 ± 0.05	1.5	5.11 ± 0.20	3.99
3	3.60 ± 0.11	3.0	5.27 ± 0.16	3.06
4	3.31 ± 0.13	3.8	5.29 ± 0.16	2.96
Average	*3.26 ± 0.26*	*8*	*5.15 ± 0.17*	*3*

Table 4.21 Reproducibility results of four 10.53 ng spots of niacinamide in reflectance on both wet and dry plates.

Plate	Dry		Wet	
	Average signal / 10^{-9} AUm^2	RSD / %	Average signal / 10^{-9} AU m^2	RSD / %
1	6.73 ± 0.18	2.7	7.14 ± 0.29	4.1
2	4.67 ± 0.14	3.0	6.89 ± 0.31	4.5
3	5.07 ± 0.13	2.5	6.81 ± 0.29	4.3
4	6.34 ± 0.17	2.7	6.01 ± 0.18	2.9
Average	*5.70 ± 0.99*	*17*	*6.71 ± 0.49*	*7*

4.5 Real Time UV Studies

4.5.1 Benzophenone experiments

Real time experiments in the visible part of the electromagnetic spectrum were reported in Chapter 3. Further real time experiments were carried out in the ultraviolet using the same signal referencing procedure as reported in Section 3.3 and the same signal averaging as reported in Section 3.4.

Further to our findings in Section 4.5, aluminium backed plates were used in all real time UV experiments in order to give a reasonable analyte signal. This meant that all UV real time imaging had to be carried out in reflectance mode. 100 images were taken during every chromatographic run, of which the last 80 were used for signal averaging purposes.

Benzophenone alone and then a mixture of analytes were studied. Reproducibility and linearity (over different calibration ranges) were assessed. Results obtained are presented in Tables 4.22 – 4.30.

Reproducibility was assessed by running four 25 ng spot on the same plate. The precision was then calculated from the four peak areas in the final image taken during the chromatographic development and also from the last 80 images averaged. It may be seen from Table 4.22 that the RSD values obtained after signal averaging are invariably lower than those obtained from a single image. This demonstrates one of the benefits of signal averaging. Inter-plate RSD values are substantially higher than intra-plate values, as expected, at 8 and 10% for averaging and no averaging respectively.

It is also evident from Table 4.22 that the averaged signal from the four 25 ng peaks is slightly higher in a single image than after signal averaging of 80 images, though the difference lies within the error bounds. If this difference were substantiated in further studies, it could be indicative of a change in apparent pathlength. This change could be due to either the change in angle of incidence of illumination as the analyte migrates along the plate or a change in the degree of wetting of the sorbent layer at the analyte position.

Table 4.22 Results from the averaging of 80 images and from the last image only for 4 × 25 ng benzophenone runs with 75:25 DCM/hexane imaged online in reflectance. Aluminium backed Silica Gel 60 TLC plates used.

Plate	Signal / 10^{-7}AU m^2		RSD / %	
	Averaged	Last	Averaged	Last
1	3.79 ± 0.08	3.94 ± 0.13	2.0	3.4
2	3.30 ± 0.10	3.14 ± 0.12	3.1	3.7
3	4.03 ± 0.12	4.03 ± 0.15	2.9	3.8
4	3.57 ± 0.13	4.19 ± 0.37	3.6	8.9
5	3.26 ± 0.13	3.73 ± 0.32	3.9	8.6
Average	*3.59 ± 0.29*	*3.81 ± 0.37*	*8*	*10*

Benzophenone calibrations were run at different sample loadings in the range 5-50 ng and are presented in Table 4.23. As with the reproducibility work in Table

4.22, results obtained from a single image (the last taken during the run) and after signal averaging (of the last 80 images) are shown.

Table 4.23 Calibrations of benzophenone (5, 10, 25 and 50 ng) run with 75:25 DCM/hexane imaged online in reflectance mode on aluminium backed Silica Gel 60 TLC plates.

Plate	x^0 / 10^{-8} AU m^2		x^1 / AU m^2 g^{-1}		r^2	
	Averaged	Last	Averaged	Last	Averaged	Last
1	6.8 ± 7.8	3.1 ± 3.2	10.1 ± 2.7	11.5 ± 11.1	0.9921	0.9076
2	3.2 ± 6.5	2.8 ± 8.7	15.7 ± 2.3	15.7 ± 3.1	0.9977	0.9959
3	4.1 ± 12	1.1 ± 1.3	16.3 ± 4.0	19.3 ± 4.6	0.9934	0.9938
4	6.2 ± 10	2.1 ± 3.8	12.7 ± 3.6	14.6 ± 0.8	0.9912	0.9997
5	5.3 ± 6.3	4.8 ± 3.3	13.9 ± 1.9	15.4 ± 9.9	0.9981	0.9572
Average	*5.3 ± 1.4*	*3.1 ± 1.3*	*13.7 ± 2.2*	*15.3 ± 2.5*		

The r^2 values are generally better for the averaged results and the slope values (x^1) are lower (13.7 AU m^2 g^{-1}) than for the single image (15.3 AU m^2 g^{-1}), supporting the suggestion of a systematic temporal variability as discussed above. The mean values of all intercepts are positive. Though the standard deviations for values obtained from individual plates in most cases suggest that results could be within experimental uncertainty equal to zero, the narrow spread around the averages of the mean values of the intercepts show that these are indeed significantly different from zero. The intercept after signal averaging is higher than that from the single image.

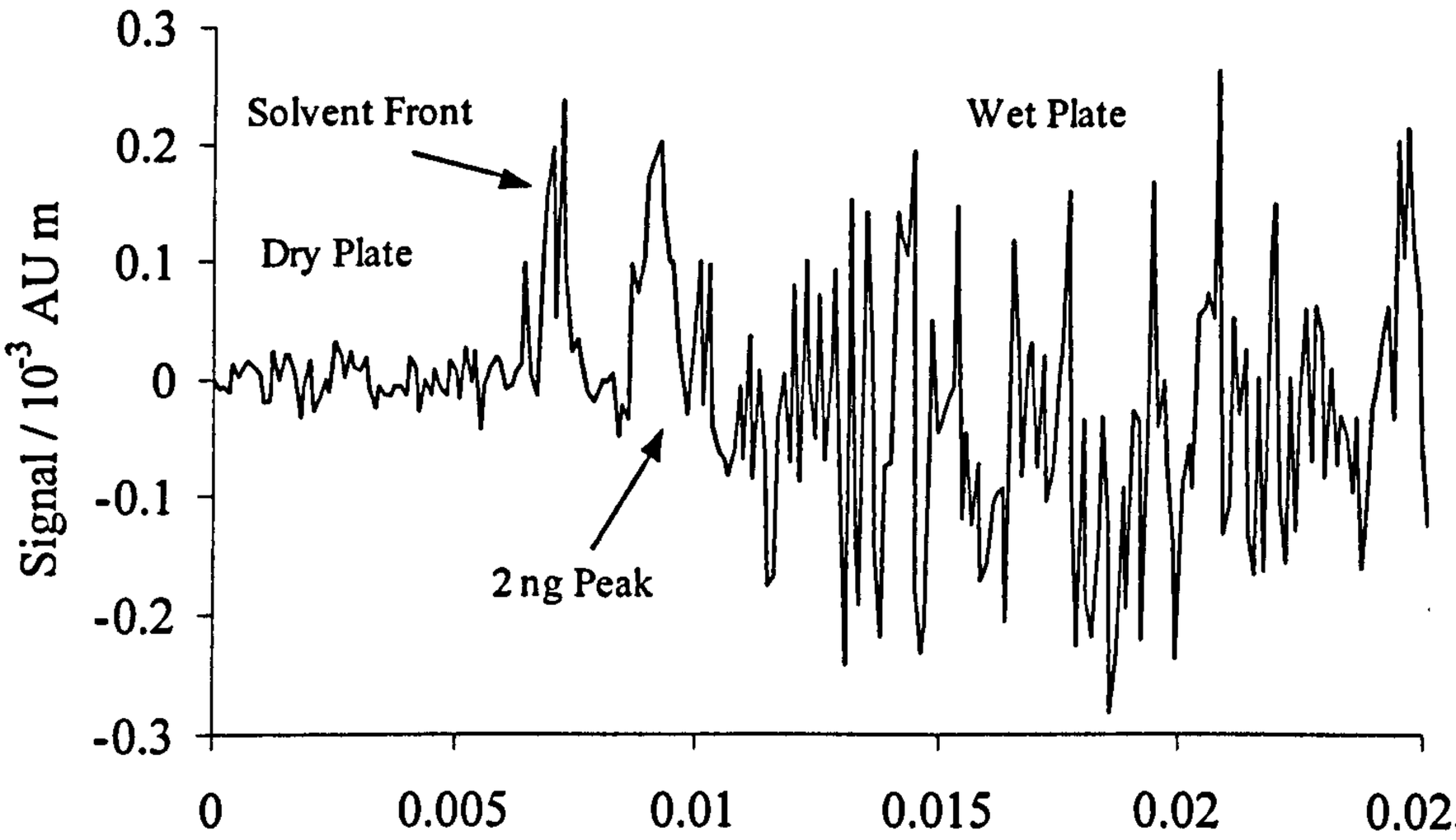

Figure 4.28 Integrated data from a single image taken during development of a 2 ng peak of benzophenone.

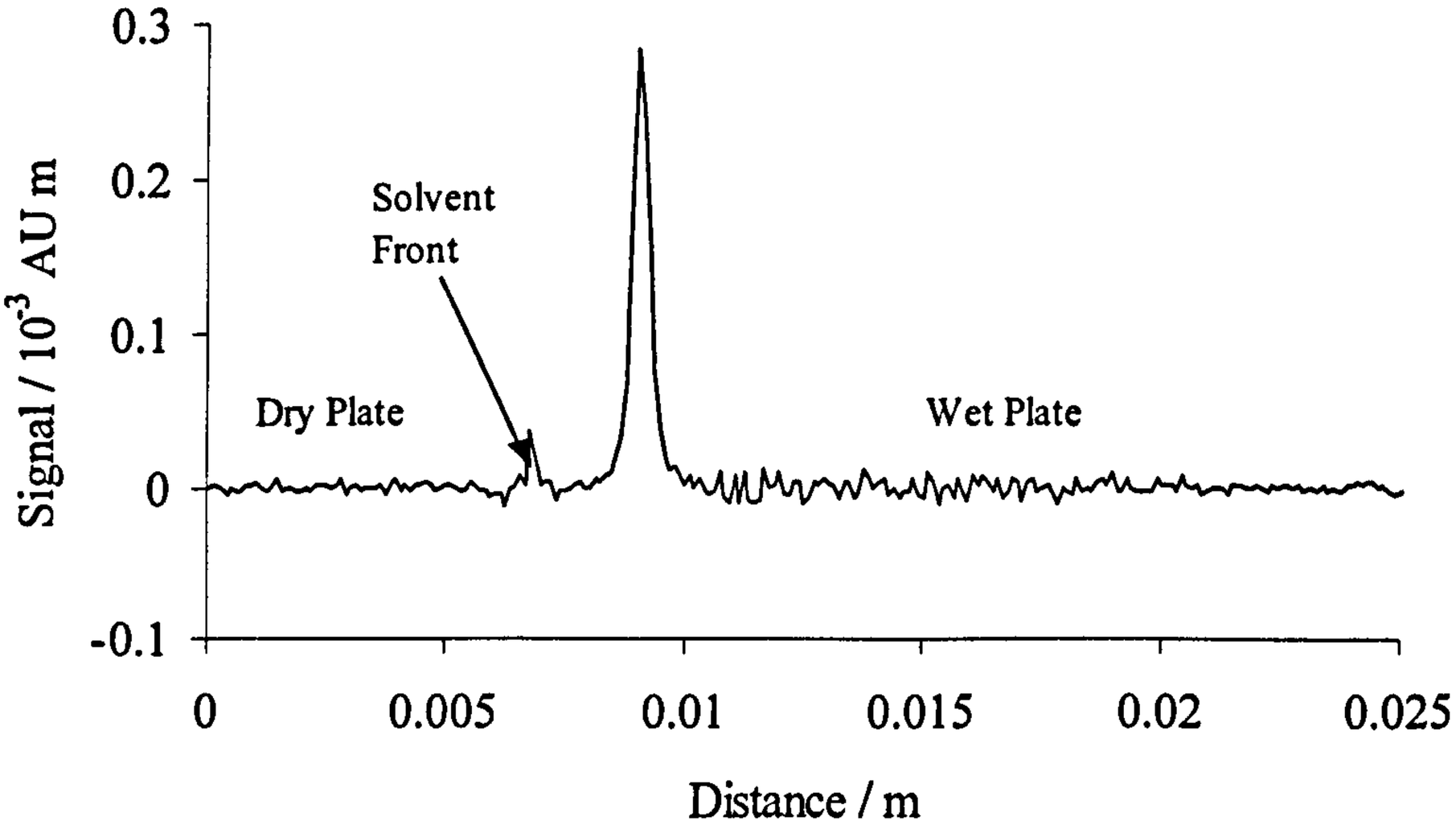

Figure 4.29 The same 2 ng peak in Figure 4.27 above after integration in the direction of chromatography and signal averaging of 80 images.

The greatest benefit from signal averaging is demonstrated by the experimental results at low loadings. A single image from a real time experiment at loading of 2 ng is shown in Figure 4.28 and results after signal averaging in Figure 4.29. Looking at Figure 4.28, it is clear that the wet portion of the plate is far noisier than the dry part. Comparing Figs 4.29 and 4.28, noise from the wet and dry parts

of the plate has been significantly reduced along with the contribution from the solvent front. The LOD of benzophenone using a *single image from a real time* experiment is approximately 2 ng (see Figure 4.28), whereas a far better S/N ratio is obtained after signal averaging thereby enabling detection at lower loadings.

Results obtained at loadings of 0.5 ng are shown in Figures 4.30 and 4.31, which reinforce the power of signal averaging. The 0.5 ng spot of benzophenone is not detectable from a single image (Figure 4.30) but after averaging 80 images, the peak can clearly be seen (Figure 4.31) with a S/N ratio of approximately 4:1. The LOD (S/N ratio 3:1) is thus 0.4 ng.

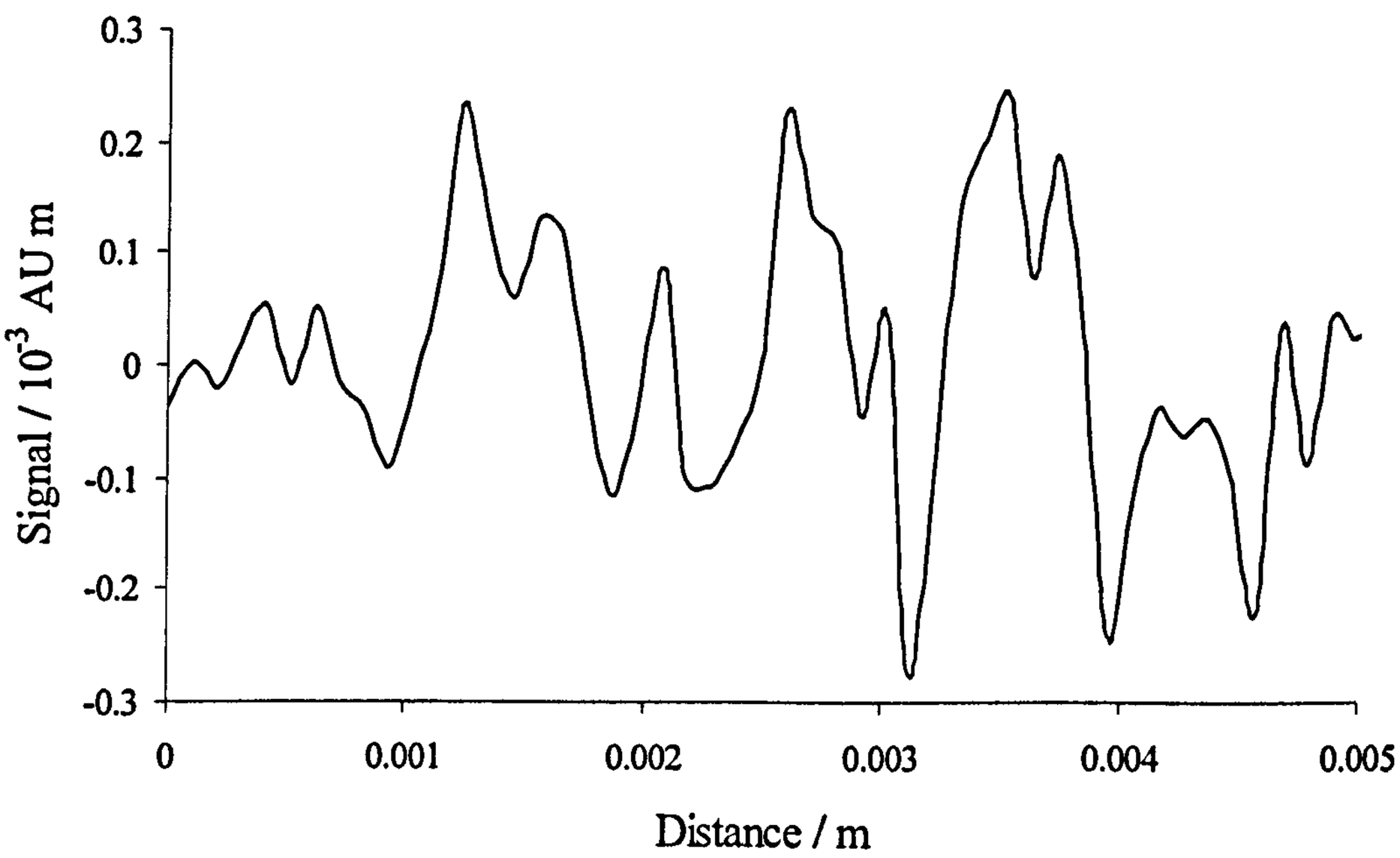

Figure 4.30 Integrated data from a single image taken during development of a 0.5 ng spot of benzophenone.

Having established that by using signal averaging the LOD is less than 0.5 ng, calibrations were carried out over the range of loadings 0.5 – 5 ng. Results are shown in Table 4.24, and it should be stressed that the range is a factor 10 lower than the range 5 – 50 ng of Table 4.22. Using signal averaging of many images acquired in real time it was possible to detect peaks at concentrations lower than those found under the best conditions on dry plates.

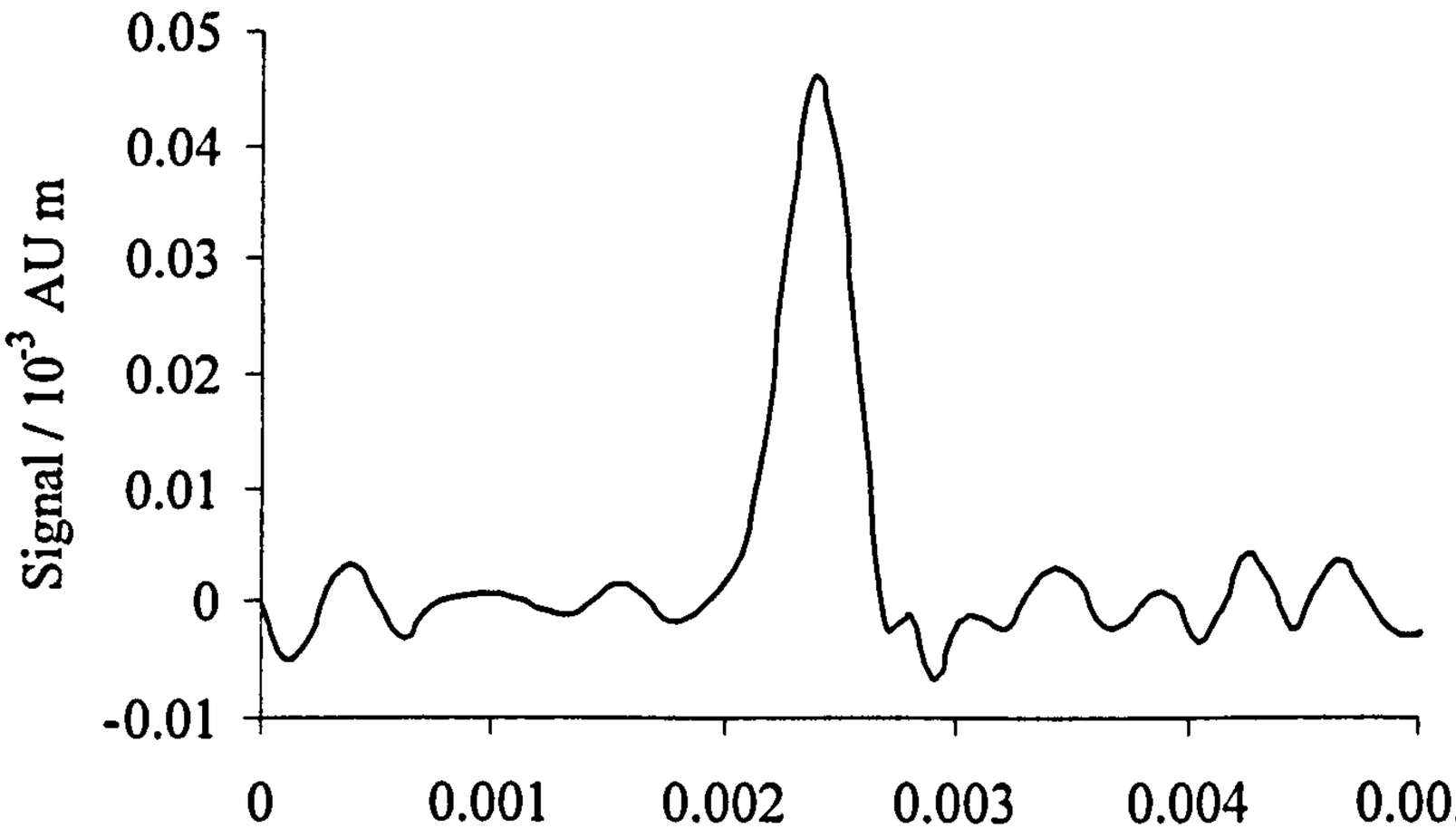

Figure 4.31 After integration in the direction of chromatography and signal averaging of 80 images, the 0.5 ng peak is resolved from the baseline with a S/N ratio of approximately 4:1.

Table 4.24 Calibrations of benzophenone (0.5, 1, 2 and 5 ng) imaged online in reflectance mode on aluminium backed Silica Gel 60 TLC plates. Two solvent systems investigated, DCM and DCM/ acetonitrile 40:1.

Plate	Solvent	x^0 / AU m^2	x^1 / AU m^2 g^{-1}	r^2
1	DCM	$(0.9 \pm 7.1) \times 10^{-9}$	23.8 ± 1.2	0.9997
2		$(0.3 \pm 5.9) \times 10^{-9}$	24.8 ± 2.4	0.9990
3		$(0.1 \pm 1.1) \times 10^{-8}$	17.6 ± 1.8	0.9988
4		$(0.1 \pm 1.1) \times 10^{-8}$	18.4 ± 2.0	0.9987
Average		*$(0.8 \pm 0.3) \times 10^{-9}$*	*21.2 ± 3.2*	
1	DCM/ Acetonitrile 40:1	$(0.7 \pm 1.8) \times 10^{-8}$	11.7 ± 2.6	0.9948
2		$-(3.7 \pm 4.7) \times 10^{-9}$	11.5 ± 2.2	0.9962
3		$(0.1 \pm 0.5) \times 10^{-8}$	16.0 ± 4.2	0.9927
4		$(1.5 \pm 5.5) \times 10^{-9}$	15.1 ± 3.9	0.9926
Average		*$(1.5 \pm 3.8) \times 10^{-9}$*	*13.6 ± 2.0*	

The two sets of results in Table 4.24 were obtained using slightly different solvent systems yet are significantly different. The first solvent system used was simply DCM alone, the second a 40:1 mixture of DCM and acetonitrile. The addition of a small amount of acetonitrile reduced the average slope value (coefficient of x^1) from 21.2 to 13.6 AU m^2 g^{-1}; the R_f value of benzophenone was also changed from 0.4 to 0.8. It was not clear if this difference were caused by a change in refractive index (and hence scatter) or if the different angle between UV source, analyte spot and detector at different R_f values resulted in a different effective path length through the sorbent layer.

In order to investigate the possibility of an angular dependence of the signals an experiment was devised in which a 1 mm slit was placed over the mercury lamp in order to brightly illuminate a small strip of the plate orthogonal to the direction of chromatography. Developments of 4 x 50 ng benzophenone spots were then carried out in two different positions under the camera. In the first run the plate was positioned directly beneath the lens (as usual), and in the second the whole developing tank was moved 5 cm in the direction of chromatographic development. The experiments were carried out in real time with 80 images being averaged and the results are presented in Table 4.25.

Table 4.25 Benzophenone (4 x 50 ng) runs with DCM/hexane 75:25 on aluminium backed TLC plates at two plate positions.

Plate position	Average signal / $\times 10^{-7}$AU m^2	RSD / %
1	4.75 ± 0.09	2.0
2	4.79 ± 0.08	1.7

Results from two runs are identical, even under lighting conditions designed to bring out differences between the two runs in angles of incidence of light traversing the analyte band and reflected off the backing aluminium plate towards the CCD detector. It must therefore be concluded that the different angles between

UV source, analyte spot and detector at different R_f values in a normal development has no significant effect on absorbance results.

4.5.2 Multi-component real time experiments

In Section 4.4.4 we looked at separations of four analytes offline. In this section, the same mixture (methyl 4-hydroxybenzoate, benzophenone, niacinamide and 3-hydroxybenzaldehyde) was examined in real time in order to evaluate the performance of real-time UV detection with a mixture rather than a single analyte. The same signal referencing and averaging techniques were used as discussed in Sections 3.3 and 3.4 respectively. Once again, separation of the methyl 4-hydroxybenzoate and the 3-hydroxybenzaldehyde peaks was not effected and it was decided to use results for the unresolved peak ($R_f = 0.40$) as before, the masses for the two analytes were added to give the x axis value. Experiments were carried out in reflectance mode on aluminium backed plates with different solvent systems and plates investigated. During every chromatographic run, 100 images were taken, the last 80 of which were used for signal averaging purposes.

Firstly, the mixture was run with DCM/hexane 75:25 on Silica Gel 60 TLC plates. Results are given in Tables 4.26 and 4.27, with plate 1 being the same actual plate in both instances. Results were obtained for benzophenone and for the unresolved peak but it was not possible to detect niacinamide at the loadings used (0.42, 1.05, 2.11, and 5.26 ng). It is evident that signal averaging of a non-migrating peak is not as effective as for a moving peak. This is because fixed pattern effects due to local inhomogeneities in the sorbent layer tend to be averaged out when placing moving peaks about a common centre. The analyte signal for a moving peak occurs at a different point in each image and centring the signals tends to average out plate structure contributions (see discussion in Section 3.4). This is obviously not the case for a retained analyte as the peak occurs at the same point in every image.

Good linearity between peak area and sample loading ($r^2 > 0.99$) was obtained for benzophenone and the unresolved peak over the range of loadings investigated. The intercepts for benzophenone and the unresolved peak were equal to zero

within experimental error. The linear plots and zero intercepts demonstrate that the Beer-Lambert law holds for benzophenone and the unresolved peak within the range of sample loadings used.

Table 4.26 Dependence of peak area on loading for benzophenone (0.63, 1.58, 3.16 and 7.9 ng) in an analyte mixture run with DCM/hexane 75:25 on aluminium backed TLC plates.

Plate	x^0 / 10^{-8} AU m^2	x^1 / AU m^2 g^{-1}	r^2
1	0.1 ± 5.6	17.6 ± 5.1	0.9910
2	0.7 ± 1.8	17.3 ± 2.0	0.9986
3	0.1 ± 1.9	17.6 ± 2.1	0.9985
4	-1.0 ± 2.3	18.3 ± 2.5	0.9980
Average	*0.2 ± 0.3*	*17.7 ± 0.4*	

Table 4.27 Dependence of peak area on loading for the unresolved peak of methyl 4-hydroxybenzoate (0.53, 1.32, 2.63 and 6.58 ng) and 3-hydroxybenzaldehyde (0.42, 1.05, 2.10 and 5.26 ng) in an analyte mixture run with DCM/hexane 75:25 on aluminium backed TLC plates.

Plate	x^0 / AU m^2	x^1 / AU m^2 g^{-1}	r^2
1	$(4.3 \pm 9.3) \times 10^{-8}$	48 ± 14	0.9911
2	$(0.1 \pm 1.1) \times 10^{-7}$	51 ± 16	0.9900
3	$(2.3 \pm 5.8) \times 10^{-8}$	45 ± 10	0.9961
4	$(0.3 \pm 1.2) \times 10^{-7}$	49 ± 18	0.9957
Average	*$(1.7 \pm 1.7) \times 10^{-8}$*	*48 ± 2*	

The same mixture of analytes was then investigated on Silica Gel 60 HPTLC plates using two solvent systems, DCM/hexane 75:25 (as in Tables 4.26 and 4.27), and DCM/acetonitrile 40:1. The results are given in Tables 4.29 and 4.29. The R_f of benzophenone in DCM/hexane 75:25 is 0.8, whilst in DCM/acetonitrile 40:1 it is 0.5. The R_f of the unresolved peak in DCM/hexane 75:25 is 0.5; in DCM/acetonitrile 40:1 it is 0.3.

Again, linearity between peak area and sample loading was good (r^2 >0.99) over the loadings investigated using both solvent systems. All intercepts for benzophenone and the unresolved peak were equal to zero within experimental error. As previously noted using the TLC plates and solvent DCM/hexane 75:25, it was not possible to detect niacinamide on HPTLC plates at the loadings used.

The average slope value for benzophenone obtained using DCM/hexane 75:25 was higher on HPTLC plates (20.1 AU m^2 g^{-1}) than that obtained using standard TLC plates (17.7 AU m^2 g^{-1}). The layer thickness was 200 microns in both cases. This difference in slope may be due to a difference in the scatter in the HPTLC layer owing to the smaller particle size of the silica. Increased scatter would be expected to result in a longer effective pathlength through the layer. The same effect is observed with the unresolved peak (53 AU m^2 g^{-1} in HPTLC, compared with 48 AU m^2 g^{-1} in TLC).

Table 4.28 Dependence of peak area on loading for benzophenone (0.63, 1.58, 3.16 and 7.9 ng) in an analyte mixture run on aluminium backed HPTLC plates.

Plate	Solvent	x^0 / AU m^2	x^1 / AU m^2 g^{-1}	r^2
1	DCM / acetonitrile	$-(3.7 \pm 7.0) \times 10^{-9}$	14.3 ± 1.6	0.9986
2		$(1.0 \pm 1.2) \times 10^{-8}$	15.1 ± 2.9	0.9907
3		$-(0.9 \pm 1.8) \times 10^{-8}$	14.5 ± 2.0	0.9979
4		$(0.1 \pm 2.2) \times 10^{-8}$	15.0 ± 2.5	0.9924
Average		*$-(0.4 \pm 0.6) \times 10^{-8}$*	*14.7 ± 0.3*	
1	DCM/ hexane	$-(1.6 \pm 3.5) \times 10^{-8}$	21.8 ± 3.9	0.9966
2		$-(0.5 \pm 4.8) \times 10^{-8}$	19.6 ± 5.3	0.9922
3		*$(1.7 \pm 3.0) \times 10^{-8}$*	20.3 ± 1.5	0.9976
4		$(2.7 \pm 3.0) \times 10^{-8}$	21.4 ± 1.6	0.9986
Average		*$-(0.6 \pm 1.7) \times 10^{-8}$*	*20.1 ± 0.9*	

The average slope values obtained using the two different solvent systems are also significantly different, with a higher value being obtained in DCM/hexane than in DCM/acetonitrile for both analyte peaks. This solvent effect has been discussed previously (Section 3.5).

It is clear from Table 4.30 that the *in situ* ε_{app} values for the non-retained analytes are much higher than the spectrophotometer values. The highly scattering sorbent layer increases the effective path length, resulting in a higher effective absorbance as discussed in a previous section (2.5), this is increased further with aluminium backed plates (section 4.4.3). The results with DCM/hexane and DCM/acetonitrile were obtained on HPTLC plates. This may account for the high results obtained as the scattering conditions would be significantly different than in experiments using standard TLC plates.

Table 4.29 Dependence of *peak area on loading* for the unresolved peak of methyl 4-hydroxybenzoate (0.53, 1.32, 2.63 and 6.58 ng) and 3-hydroxy*benzaldehyde* (0.42, 1.05, 2.10 and 5.26 ng) in an analyte mixture on aluminium backed HPTLC plates.

Plate	Solvent	x^0 / AU m^2	x^1 / AU m^2 g^{-1}	r^2
1	DCM / acetonitrile	$(1.0 \pm 2.5) \times 10^{-8}$	39.4 ± 7.7	0.9959
2		$(0.1 \pm 1.0) \times 10^{-7}$	47.6 ± 3.5	0.9914
3		$-(1.9 \pm 5.5) \times 10^{-8}$	44.4 ± 8.1	0.9965
4		$-(1.2 \pm 3.4) \times 10^{-8}$	42.4 ± 6.6	0.9965
Average		*$-(0.3 \pm 1.3) \times 10^{-8}$*	*43.5 ± 3.0*	
1	DCM/ hexane	$(1.2 \pm 3.2) \times 10^{-8}$	55.4 ± 3.1	0.9915
2		$(3.5 \pm 7.3) \times 10^{-8}$	50.5 ± 8.1	0.9924
3		$-(1.5 \pm 4.5) \times 10^{-8}$	54.1 ± 6.2	0.9969
4		$-(1.9 \pm 3.8) \times 10^{-8}$	52.4 ± 6.7	0.9975
Average		*$(0.3 \pm 2.2) \times 10^{-8}$*	*53.1 ± 1.8*	

The LODs for benzophenone and the unresolved peak were both found to be < 0.5 ng after averaging 80 images. The LODs from a single image were found to be in the low nanogram range (1-2 ng). Niacinamide could not be detected at 10 ng.

Table 4.30 Comparison of absorption coefficients at 254 nm from UV spectrophotometry (in DCM) and apparent absorption coefficients determined from CCD imaging of peak areas as a function of loading.

Analyte	ε_{254} / AU m^2 g^{-1}	ε_{app} / AU m^2 g^{-1}			
		DCM	DCM/ hexane	DCM/ acetonitrile	dry
benzophenone	8.5	10.3	20.1	14.7	4.6
niacinamide	1.5	1.5	-	-	1.5
methyl 4-hydroxybenzoate	13.4	-	-	-	-
3-hydroxybenzaldehyde	7.3	-	-	-	-
mixture of methyl 4-hydroxybenzoate and 3-hydroxybenzaldehyde	10.1	11.6	53.1	43.5	7.6

RSD values for benzophenone and the unresolved peak were investigated by evaluating four spot of the same sample load on the same plate. The RSD values are seen to be well below 5% after signal averaging of 80 images (Table 4.31). Niacinamide was present at 10 ng but not detectable. All RSD values are for the full analytical process from spotting to evaluation.

Table 4.31 Benzophenone (4 x 15.8 ng) and unresolved peak (4 x 11.85 ng) run with DCM/acetonitrile 40:1 on aluminium backed HPTLC plates.

Plate	Signal / $\times 10^{-7}$ AU m^2		RSD / %	
	Benzophenone	Unresolved Peak	Benzophenone	Unresolved Peak
1	2.35 ± 0.04	6.40 ± 0.12	1.6	1.9
2	2.14 ± 0.04	6.10 ± 0.06	1.9	1.0
3	2.23 ± 0.06	6.21 ± 0.07	2.6	1.1
4	2.15 ± 0.05	5.78 ± 0.08	2.3	1.4
Average	*2.22 ± 0.08*	*6.12 ± 0.22*	*5*	*4*

4.6 Scanning Densitometry

In order to gain a direct comparison between our CCD work in this chapter and scanning densitometry, a series of experiments were undertaken using a Camag TLC scanner 3 at 254 nm. The scanning conditions were s follows - slit 5 x 0.1 mm, speed 5 mm s^{-1}, resolution 25 μm $step^{-1}$. Generally, five tracks of 5 mm each were employed. A mixture containing niacinamide, methyl 4-hydroxybenzoate and benzophenone was sprayed (1 μl) onto various plates using a Camag ATS 4 spraying device. The stock solution contained 100 mg l^{-1} of each analyte. All plates were run with DCM/hexane 75:25 as developing solvent. Glass backed plates were use initially, and then aluminium backed plates, in order to investigate the relative responses obtained. Linearity, LOD and reproducibility of a UV mixture containing niacinamide, methyl 4-hydroxybenzoate and benzophenone were investigated. The results are presented in Tables 4.32-4.35.

Table 4.32 Reproducibility of 5 x 50 ng of each analyte on a glass backed Silica Gel 60 F_{254} plate (200 micron layer thickness).

Substance	R_f	Average signal	RSD / %
Niacinamide	0.00	1769 ± 64	3.6
Methyl 4-hydroxybenzoate	0.05	3228 ± 68	2.1
Benzophenone	0.48	2559 ± 61	2.4

Table 4.33 Calibration of 5, 10, 25 and 50 ng of each analyte on a glass backed Silica gel 60 F_{254} plate (200 micron layer thickness).

Analyte	x^0 / area counts	x^1 / area counts ng^{-1}	r^2
Niacinamide	24 ± 66	39 ± 2	0.9996
Methyl 4-hydroxybenzoate	61 ± 252	47 ± 8	0.9966
Benzophenone	197 ± 207	41 ± 7	0.9966

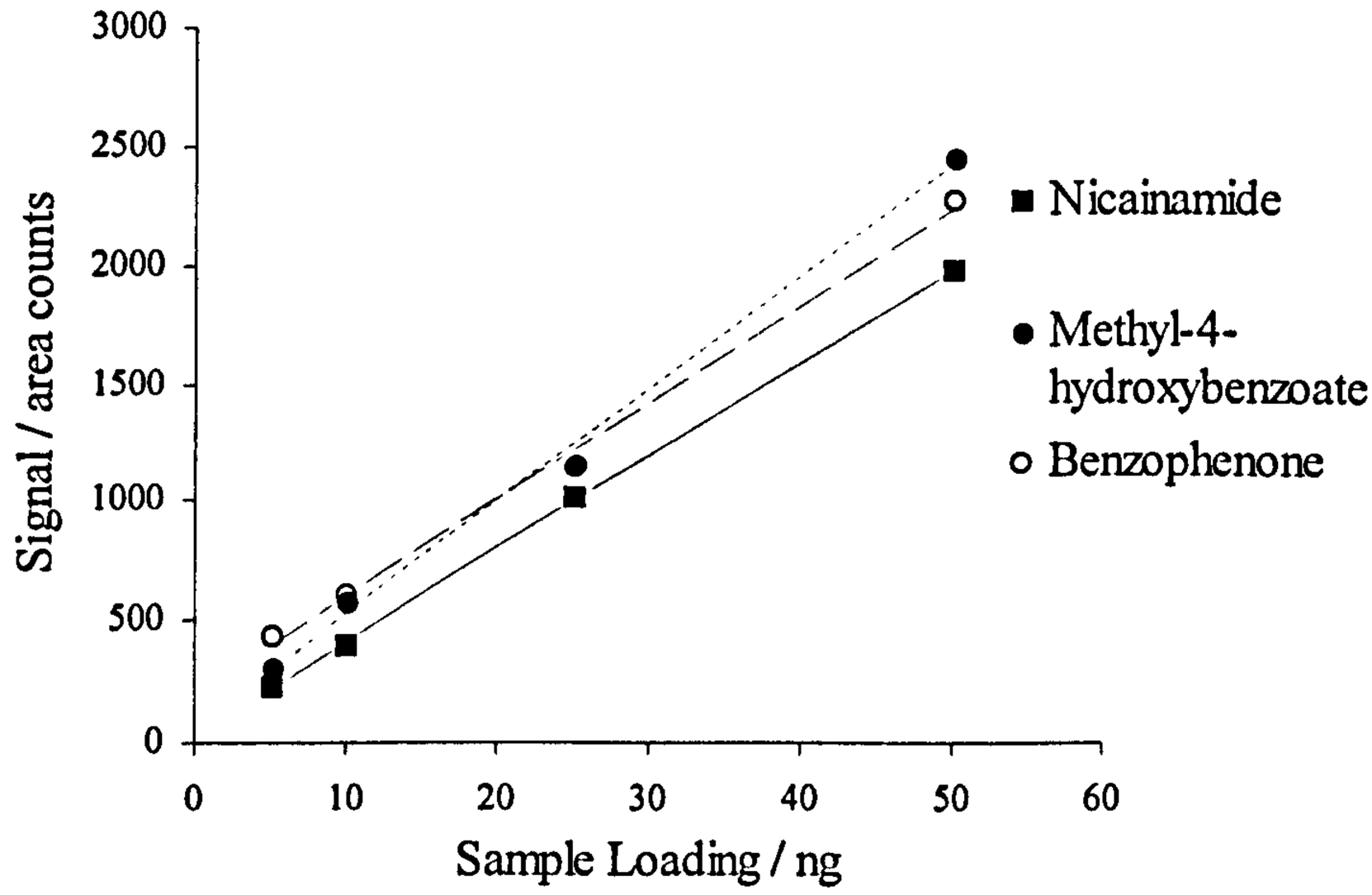

Figure 4.32 Calibration curves from Table 4.31.

From Table 4.32, the RSD values are all < 5%, with the two moving components <3%; this is in the expected range. Methyl 4-hydroxybenzoate and benzophenone both gave a higher response than niacinamide as expected as both have stronger absorbance at 254 nm.

Calibrations from Table 4.33 (and shown in Figure 4.32) were run on a glass backed Silica Gel 60 F_{254} plate (200 micron layer thickness). Sample loadings used were 2, 5, 10, 25 and 50 ng for each analyte. The 5 ng peak had a S/N ratio of approximately 4, and the 2 ng peak was not detectable. The r^2 values were good, > 0.99 in all cases, and all intercepts were zero within experimental error.

Unfortunately it is not possible to make a direct comparison of slope values with the CCD work as results are quoted with units of area counts, not AU m^2.

Table 4.34 Reproducibility of 5 x 50 ng analyte mixture on an aluminium backed Silica Gel 60 F_{254} plate (200 micron layer thickness).

Substance	R_f	Average signal	RSD / %
Niacinamide	0.00	2435 ± 112	4.6
Methyl 4-hydroxybenzoate	0.05	4621 ± 129	2.8
Benzophenone	0.43	6016 ± 138	2.3

Table 4.35 Calibration of analyte mixture (5, 10, 10, 25 and 50 ng) on an Al backed Silica Gel 60 F_{254} plate (200 micron layer thickness).

Analyte	x^0 / area counts	x^1 / area counts ng^{-1}	r^2
Niacinamide	-297 ± 1030	84 ± 37	0.9801
Methyl-4-hydroxybenzoate	-473 ± 2570	182 ± 90	0.9745
Benzophenone	-578 ± 3360	232 ± 120	0.9732

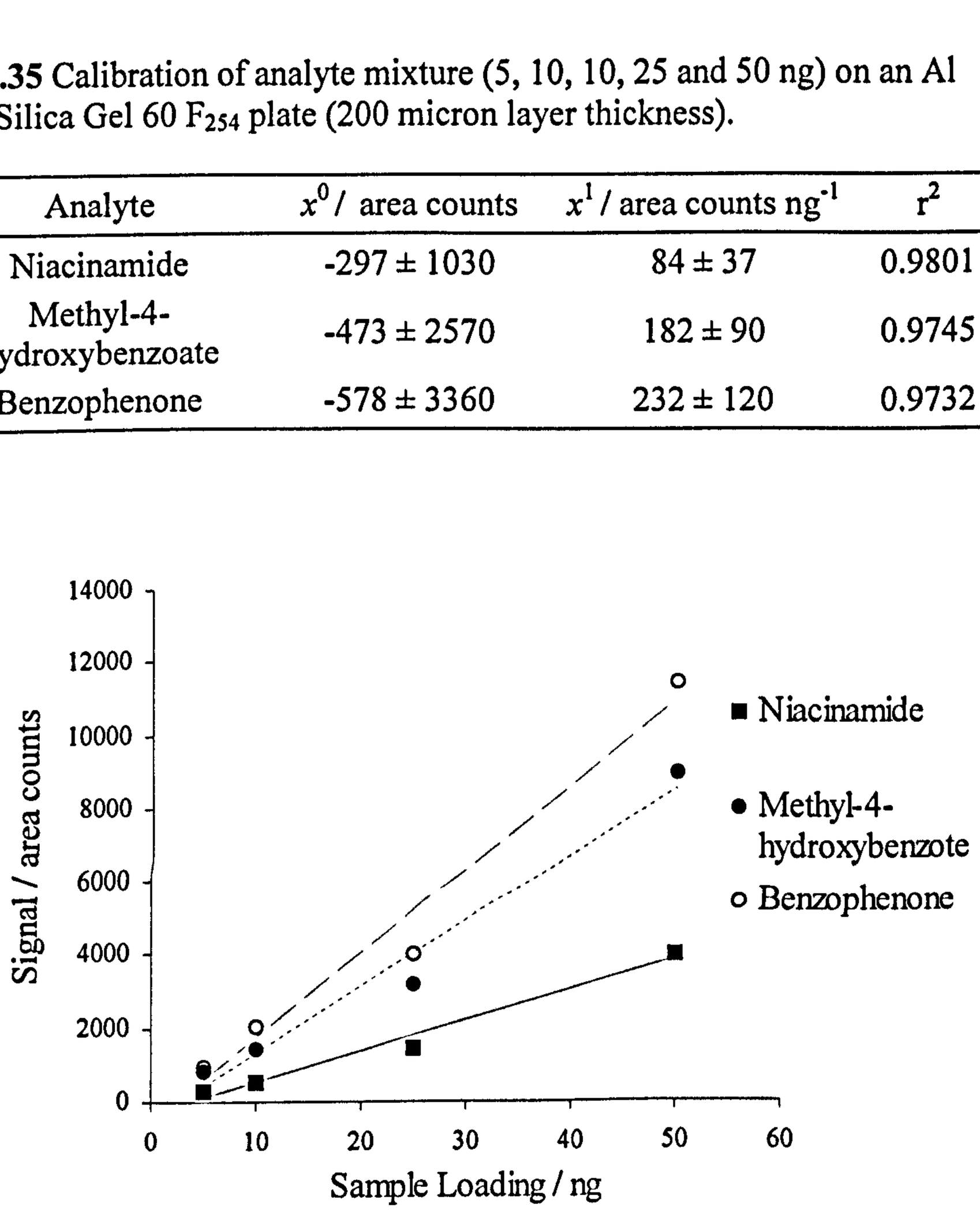

Figure 4.33 Calibration curves from Table 4.33

From Table 4.34, the RSD values are all < 5%, with values for the two moving components < 3%, as with the results from glass backed plates. Once again, methyl 4-hydroxybenzoate and benzophenone both gave a higher response than

niacinamide as well as lower RSD values. The responses obtained on aluminium backed plates were all higher than those obtained on glass backed plates

Calibrations from Table 4.35 (and shown in Figure 4.33) were run on an aluminium backed Silica Gel 60 F_{254} plate (200 micron layer thickness). Sample loadings used were 5, 10, 25 and 50 ng. The 5 ng peak had a S/N ratio of approximately 5; the 2 ng peak was not detectable and therefore not used in constructing the calibration curves. Intercepts were zero within experimental error, and the r^2 values (0.97-0.98) were poorer than those obtained from glass backed plates.

These results show that aluminium plates have the potential to deliver lower LODs than the more commonly used glass backed plates, as they give a higher response for all analytes studied by scanning densitometry. This appears to be at the cost of reproducibility and linearity. Aluminium backed plates are not as robust as the glass backed variety due to the thinness of the support. Consequently the chromatographic bed is often not as flat with aluminium backing and this would have an effect on the results obtained. Perhaps a thicker aluminium support would provide the required robustness and enable the potential advantages of aluminium backed plates to be realised without loss of performance in reproducibility and linearity.

The lowest detectable loading of benzophenone was 5 ng by scanning densitometry. A loading of 0.5 ng benzophenone was detectable after averaging 80 images using real time CCD. Real-time UV imaging offers an improvement of an order of magnitude in limit of detection in comparison with current scanning densitometry *detection methods*. The linearity and precision were similar using both techniques.

4.7 Conclusions

In this work, the key achievement is novel UV imaging of the TLC separation process. Quantitative TLC has been carried out using UV light both offline and online in the presence of solvent, with good linearity, precision and sensitivity. A xenon lamp was initially used for illumination and gave good results for benzophenone offline. Online experiments were not possible, however, due to the excessive exposure time needed because of the limited power of the lamp. A mercury lamp was employed for all subsequent work giving good results both offline and in real time. Benzophenone was used initially as a single analyte and then a more complex mixture was studied. There was good agreement between the results obtained with the xenon lamp (Section 4.3) and the dry imaged results with the mercury lamp (Section 4.4.1).

Wet offline experiments were carried out using the mercury lamp (Section 4.4.2) as had previously been done using visible light in Chapter 2. Interestingly, the glass backed plates used initially gave very poor results. When aluminium backed plates were tried the results were much improved. The value obtained for the slope of the calibration curve (equivalent to the apparent absorption coefficient) increased by an order of magnitude from < 1 to 10 AU m^2 g^{-1} by the use of reflective backing, consistent with significant amount of incident light being transmitted through the layer and reflected back up through the chromatographic band. Using a glass backed plate, all the UV light is absorbed on transmission through the layer. The hypothesis about absorption was tested and confirmed using a non-absorbing fused silica plate to support the sorbent layer. The spectrophotometric value obtained for the absorption coefficient of benzophenone was 8.6 AU m^2 g^{-1}, which is in reasonable agreement with the value of the apparent absorption coefficient determined from the slope of the calibration curve obtained using the aluminium backed plate.

The aluminium backed plates were used in reflectance only and good results were obtained in calibration and reproducibility experiments. Good precision was obtained from the same spots imaged wet (<5% RSD) and dry (<4%RSD). The linearity was over an order of magnitude with r^2 values >0.99 and intercepts zero

within experimental error for all moving components. The niacinamide results were not as good, with positive intercepts and poorer r^2 values (Table 4.17). This is probably owing to the lack of movement from the spotting position. The migration and diffusion experienced by the moving spots would probably have a tendency to average out any inhomogeneities in the applied band.

A comparison between absorption coefficients obtained by different methods was presented in Table 4.17. The spectrophotometric ε values were in good agreement with ε_{app} values obtained from results of offline imaging of wet plates. The dry imaged results were lower in general, consistent with the layer being less opaque when dry and reflection occurring from the aluminium support assisting in increasing the effective pathlength.

Real time experiments were undertaken on aluminium backed plates. This work provides the first quantitative demonstration of real-time imaging using ultraviolet *light of* TLC during chromatographic development. Central to these measurements using a CCD camera is signal referencing, *as described in Chapter* 3, Section 3.3. More images (80) were averaged than in the visible work as the readout rate of the camera was faster enabling more images to be taken during the chromatographic run. The results are very encouraging and suggest that use of real-time imaging is capable of providing quantitative TLC measurements in the UV, where most analytes absorb light.

The averaging of many images was shown to improve the LOD greatly from that available from one image. The explanation for this is as discussed in Chapter 3, Section 3.4. The analyte signal for a moving peak occurs at a different point in each image and centring the signals tends to average out plate structure contributions to the fixed pattern noise. This was shown not the case for a retained analyte, niacinamide, as the peak was located at the same point in every image. A loading of 0.5 ng benzophenone was detectable after averaging 80 images. From the scanning densitometry results presented in Section 4.6, the lowest detectable loading of benzophenone was 5 ng. Thus the real-time UV imaging offers an

improvement of an order of magnitude in limit of detection in comparison with current scanning densitometry detection methods.

CHAPTER FIVE

Conclusions and Further Work

The main aims of this thesis were threefold. Firstly, the study of online imaging of wetted TLC plates in order to see if quantitative results could be obtained and also to investigate properties of the sorbent layer. Secondly, the study of real-time imaging of TLC plates in order to obtain quantitative results and investigate the benefits of multi-point detection and signal averaging. Thirdly, the study of UV detection on TLC plates both offline and in real-time using CCD detection. These aims have been realised using novel signal averaging techniques and good quantitative results have been obtained in all cases.

5.1 Quantitative Measurements on Dry and Wetted TLC Plates Using a CCD Camera

Quantitative TLC was carried out with CCD imaging in both transmission and reflectance modes on dry and wetted plates as described in Chapter two. Signal referencing in order to compensate for both fixed pattern and solvent effects is central to this work. A novel signal referencing technique outlined in section 2.2.2 was used. This gave reproducible quantitative results for both dry and wet plates. The dry imaged results were comparable to those that might be expected from scanning densitometry. For a similar system evaluated in transmission, after the plate had been dried, a limit of detection of < 0.5 ng and a linear range between 1 and 10 ng with r^2 values of > 0.995 were obtained. Intra-plate RSD values were between 1 and 3 %.

The wetted plate results were slightly poorer owing to increased noise due to the presence of solvent. The limit of detection was 2 ng and the linear range was between 5 and 50 ng in both transmission and reflectance. Linearity was very good

over this range, with r^2 values of > 0.995 obtained. Intra-plate RSD values were between 1 and 4 %.

The increased noise due to the solvent adversely affects the LOD on wet plates compared to that of dry plates. The reproducibility of the background correction procedure also affects the LOD, as the solvent may not behave in exactly the same way in the two runs necessary for signal referencing to be carried out. Good practice such as ensuring that the plate is equilibrated will increase reproducibility and lessen (but not prevent) the possibility of background correction errors. This effect can be seen in Figure 2.9.

The Beer-Lambert equation was used to carry out all data processing. Curvature at high loadings in the plots of integrated absorbance as a function of sample loading was accounted for using an empirical expression designed for use with the Kubelka-Munk treatment and apparent absorbance of the chromatographic sorbent layer due to scattering.

It was possible to directly compare apparent absorbance coefficients obtained from on-plate observations with those from solution-phase samples, using either a spectrophotometer or the optical setup in the TLC experiments and a horizontal sample cell in the position of the TLC plate. The horizontal cell and the spectrophotometer gave comparable results for absorbance of Sudan II. This shows that in the absence of any scattering the optical configuration gives the expected value for absorbance. The value of ε_{app} measured for Sudan II in transmission through the DCM-wetted TLC plate was a factor ~7 higher than the values obtained from both spectrophotometry and use of the horizontal cell. These results are consistent with an effective pathlength significantly longer than the thickness of the sorbent layer.

A value for ε_{app} was obtained for Sudan II in transmission on a dry plate which is a factor 1.5 greater than the value on the wet plate and a factor 12 greater than ε in solution. This is consistent with a further increase in the effective pathlength, probably owing to greater scattering by the sorbent layer in the absence of solvent.

The presence of solvent does not, however, prevent the use of absorbance measurements for the quantitative detection of analytes on TLC plates.

5.2 Real-time Image Acquisition for Absorbance Detection and Quantification in Thin-layer Chromatography

In Chapter three, the first quantitative demonstration of online imaging TLC during chromatographic development was carried out. Once again, signal referencing was central to these measurements. The signal referencing employed in Chapter two was not suitable, as the moving solvent has to be compensated for in fully online work. A different method of signal referencing was used in which absorbance is referenced to the apparent absorbance of the solvent in lanes to either side of the sample lane and in the same row of effective pixels orthogonal to the direction of travel of the solvent front. This procedure corrects for differences in scattering due to differential wetting of the stationary phase by solvent as chromatography progresses. Fixed pattern effects such as those due to variations of optical responses from the various signal pixels were also corrected for.

The integrated peak area was found to be independent of time and distance moved in transmission experiments. In reflectance mode, the relationship between peak area and sample loading is not as simple as that in transmission, with the signal for higher sample loadings actually increasing as the development progresses. However, reasonable results were obtained at low sample loading (2-25 ng) with r^2 values >0.99 and reproducibility <3% although imaging in reflectance was not as sensitive as in transmission mode.

Averaging of images acquired during a single run gave limits of detection better than those from offline measurements on wetted TLC plates, and within a factor of two of the values for offline measurements on dried plates. It was found that the more images that were used for averaging, the greater the improvement in S/N ratio and hence LOD.

These results demonstrate the benefits of multi-point imaging detection in TLC, since averaging of snapshots of a moving analyte band yields significant gains in signal to noise, due to attenuation of systematic noise features arising from local non-uniformity of the stationary phase packed bed.

It was established that the developing solvent does have an effect on the analytical result, with xylene and dichloromethane being investigated. Good quantitative measurements were possible with both solvents but the overall performance was not as good as with dichloromethane, possibly due to less scattering of light and hence a shorter effective pathlength through the layer.

This work has enabled a better understanding of real-time quantitative measurements *in situ* in the presence of the stationary as well as the mobile phase. The results show that use of real-time imaging is capable of providing quantitative TLC measurements.

5.3 Ultra-Violet Image Acquisition and Quantification in Thin-layer Chromatography using CCD Detection

In Chapter 4 a quantitative study of the imaging of TLC plates using UV light was carried out both offline (dry and wet) and in real time. Good linearity, precision and sensitivity were obtained in all cases. A xenon lamp was initially used for illumination and gave good offline results. The limited power of the xenon lamp in a narrow wavelength range meant that it was not suitable for wet offline or real-time work due to the excessive exposure times needed. A mercury lamp, with high output power at 254 nm, was employed for all subsequent work. This enabled a suitably short exposure time to be used in order to work offline and in real time, and gave good results with both techniques.

In Chapters 2 and 3, simple, single component standards were spotted on to the plates. In Chapter 4 benzophenone alone was used initially and then more complex

mixtures were studied. It was possible to apply the signal averaging techniques of Chapter 3 to each separate chromatographic band (after signal averaging). Non migrating bands ($R_f = 0$) were also investigated: however, the signal averaging was less successful as fixed pattern noise was not attenuated as in the case for peaks that migrate ($R_f > 0$).

Wet offline experiments were initially carried out using glass-backed plates, which gave very poor results. When aluminium backed plates were used the results were much improved. The value obtained for ε_{app} was increased over tenfold in comparison with solution phase measurements, from <1 to 10 AU m^2 g^{-1}. This indicates a greater effective pathlength in the TLC situation, and is consistent with a significant amount of incident light being transmitted through the layer and reflected at the aluminium surface back up through the chromatographic band to the detector. The aluminium-backed plates could only be used in reflectance and good results were obtained in calibration and reproducibility experiments. The linearity was over an order of magnitude, with r^2 values >0.99 and intercepts zero within experimental error for all moving analytes. The results for the analyte which remained stationary, niacinamide, were not as good, with positive intercepts and poorer r^2 values. This is believed to be due to the inability to remove systematic and fixed pattern effects, as discussed previously.

The work presented in Chapter 4 provides the first quantitative demonstration of real-time imaging using ultraviolet light of TLC during chromatographic development. Real time experiments were also undertaken on aluminium backed plates. More images (80) were averaged than in the real-time visible work, as the readout rate of the UV camera was faster. The results were encouraging and suggest that use of real-time imaging is capable of providing quantitative TLC measurements in UV with performance comparable to existing techniques and the potential for improvements.

A comparison with scanning densitometry results was made in section 4.6 on Chapter four. A loading of 0.5 ng benzophenone was detectable after averaging 80 images using the real-time technique. By contrast, benzophenone was not detectable at 2 ng by scanning densitometry. This improved limit of detection demonstrates one

of the benefits of real-time analysis over traditional scanning densitometry. Other benefits include potential time savings due to faster acquisition of results and the ability to halt development as soon as separation has been effected.

5.4 Future Work

After results on wetted glass backed plates imaged in UV were found to be poor, it was found that aluminium backed plates gave much better performance. A direct comparison could be made between the two supports. It would be interesting to see if similar effects were observed between the two supports using Sudan II and visible light. Does the use of a different support improve analytical sensitivity? Furthermore, there is the possibility of looking at support materials other than the currently available glass and aluminium such as polished or mirrored metal or plastics. A thin aluminium coating on a plastic backing, for example as used in food packaging, could offer combined benefits of reflectance, robustness at very low cost.

The solvent system used does affect the analytical result. It would be interesting to investigate this further in order to get a better understanding of why this is the case. A wider variety of solvents (and solvent mixtures) than the ones we looked at could be investigated. Amongst the properties of the solvent for more detailed investigation are the following. Firstly, the refractive index, which affects the light scattering and hence the effective absorption coefficient of the analyte. Secondly, the solvent strength, which determines where the analyte travels relative to the solvent front. Thirdly, the solvent composition in mixed solvent systems, which would allow not only solvent strength but also any differential wetting effects to be investigated.

The CCD cameras used in the experiments presented were of a relatively slow readout rate (80 kHz). It follows that a camera with a high readout rate would provide better results, as it would be possible to collect more images during a chromatographic development. A faster CCD with readout rate of MHz should allow considerable enhancement in S/N, since the S/N ratio scales with the square root of the number of snapshots taken during the chromatographic development. A factor

100 improvement in readout rate is possible, using current generations of *either* CCDs or active pixel sensors. Each exposure would have to be shortened in order to accommodate the greater number of frames, and the light intensity increased correspondingly. This could readily achieved by using a mercury arc lamp and a lens to collimate the beam.

The UV lens used in the present work was very expensive, largely because this was a complex lens with many elements in order to minimise chromatic aberration. By concentrating on work at a single wavelength, 254 nm, a less expensive lens could possibly be specified since one would not have to worry about chromatic aberration effects. The use of reflective optics could also be investigated, to image plates of typical TLC plate dimensions (5x5 cm) onto sensors used in current compact imagers, for example those used in mobile phones where the imager area is less than 1x1 cm.

Fully real-time analysis could be carried out. In principle, signal referencing and all data processing could be done in real-time with results being constantly updated as development progresses. This work could provide further development towards automated real-time TLC analysis.

All work presented in this thesis made use of capillary forces to drive development. Forced flow TLC enables optimum flow rates, whether for increased separation efficiency or to meet time constraints. There would, in principle, be no problem in utilising different types of forced flow planar chromatography in conjunction with real-time detection.

Using real-time detection may give information about depth distribution of analytes in the layer and it may also be possible to investigate secondary chromatography using real time imaging. Furthermore, there is the possibility of measuring some peak parameters such as band broadening during chromatography. This could lead to a better understanding of the kinetics of capillary driven TLC as well as forced flow methods.

Finally, direct comparison of the performance of real-time imaging with other detection methods currently in common use (e.g. scanning densitometry) using real samples and well-documented analytical methods would be desirable.

References

Ahrens B., Blankenhorn D., Spangenberg B. (2002) *J. Chromtogr B.* **772** 11.

Allwohn J., Ebel S. (1989) *J. Planar Chromatogr.* **2** 71.

Amelio G. F., Tompsett M. F., Smith G. E. (1970) *Bell Syst. Tech. Jour.* **49** 593.

AstroCam Ltd, Operations guide, 4200 series cameras, 1995

Belchamber R. M., Read H., Roberts J. D. M., (1987) *J. Chromtogr.* **395** 47.

Benyon J. D. E. (1980) in *Charge-coupled devices and their applications*, (Editors Benyon and Lamb), McGraw-Hill, Maidenhead.

Bereznitski Y., Thompson R. R., O'Neill E., Grinberg N. (2001) *J. AOAC Int.* **84** 1242.

Bergström E. T., Goodall D. M., Pokrić, B., Allinson N. M. (1999) *Anal. Chem.* **71** 4376.

Betheke H., Santi W., Frei R. W. (1974) *J. Chromtogr. Sci.* **12** 392.

Betheke H., Frei R. W. (1974) *J. Chromtogr.* **91** 433.

Blouke M. M., Cowens M. W., Hall J. E., Westphal J. A., Christensen A. B. (1980) *Appl. Optics* **19** 3318.

Borman (1982) *Anal.Chem.* **54** 790A Botz L., Nyiredy S., Sticher O. (1990) *J. Planar Chromatogr.* **4** 115.

Boyle W. S., Smith G. E. (1970) *Bell Syst. Tech. Journ.* **49** 587.

Brain K. R., Turner T. D. (1971) *J. Chromatogr.* **61** 157.

Burns D. H., Callis J. B., Christian G. D. (1986) *Anal. Chem.* **58** 1415.

Burt D. J. (1980) in *Charge-coupled devices and their applications*, (Editors Benyon and Lamb), McGraw-Hill, Maidenhead.

Busch K. L. (1992) *J. Planar Chromatogr.* **5** 72.

Bush I. E., Greeley H. P. (1984) *Anal. Chem.* **56** 91.

Buss D. D., Tasch A. F., Barton J. B. (1980) in *Charge-coupled devices and systems*, (Editors Howes and Morgan), Wiley-Interscience, New York.

Butler H. T. Schuette S. A., Pacholec F. Poole C. F., (1983) *J. Chromatogr.* **261** 55.

Butler H.T., Poole C. F. (1983) *J High Resolut. Chromatogr.* **6** 77.

Butler H. T., Coddens M. E., Poole C. F. (1984) *J. Chromtogr.* **290** 113.

Campbell A. N., Sherma J. (2003) *J. Liq. Chromtogr. & Rel. Technol.* **26** 2719.

Chen H., Horvath C. (1995) *Analytical Methods and Instrumentation*, **2** 122.

Cheng M. L., Poole C. F. (1983) *J Chromatogr.* **257** 140.

Coddens M. E., Poole C. F (1983) *Anal. Chem.* **55** 2429.

Coddens M.E., Khatib S., Butler H. T., Poole C. F. (1983) *J. Chromatogr.* **280** 15.

Consden R., Gordon A. H., Martin A. J. P., (1944) *Biochem. J.* **38** 224.

Cosgrove J. A., Bilhorn R. B. (1989) *J. Planar Chromatogr.* **2** 362.

Cowens M. W., Blouke M. M., Fairchild T., Westphal J. A. (1980) *Appl. Optics* **22** 3727.

De Spiegeleer B. (1985) *Chromatographia* **20** 249.

Degtiar W. G., Tyaglov B. V., Degterev E. V., Krylov V. M., Malakhove I. I., Krasikov V. D. (1994) *J. Planar Chromatogr.* **7** 54.

Degtiar W.G., Tyaglov B.V., Degterev E.V., Krylov V.M., Malakhova I.I., Krasikov V.D. (2000) *J. Planar Chromatogr.* **13** 217.

Degterev E.V., Degtiar W.G., Polanuer B.M., Tyaglov B.V., Krylov V.M., Malakhova I.I., Krasikov V.D., (1996) *J. Planar Chromatogr.* **9** 35.

Degterev E.V., Degtiar W.G., Tyaglov B.V., Tarasov A.P., Krylov V.M., Malakhova I.I., Krasikov V.D. J. (2000) *J. Planar Chromatogr.* **13** 191.

Ebel S., Hocke J. (1976) *J. Chromatogr.* **126** 449.

Ebel S. (1984) *Topics Curr. Chem.* **126** 71

Ebel S., Glaser E. J (1979) *J. High Resolut. Chromtogr.* **2** 36.

Ebel S. (1990) *J. Planar Chromatogr.* **3** 42.

Ebel S. (1996) *J. Planar Chromatogr.* **9** 4.

Ebel S., Henkel T. (2000) *J. Planar Chromatogr.* **13** 248.

Epperson P. M., Sweedler J. V., Bilhorn R. B., Sims G. R., Denton M. B. (1988) *Anal. Chem.* **60** 327A.

Epperson P. M., Jalkian R. D., Bonner Denton M. (1989) *Anal. Chem.* **61** 282.

Essig S. Kovar K. A. (1999) *J. Planar Chromatogr.* **12** 63.

Felton H. R. (1979) *Moisture and Silica Gel* Technical Report 7905, Analtech, Newark.

Fenimore D., Davis D. (1981) *Anal. Chem.* **53** 252A.

Fenimore D., (1980) in *Instrumental HPTLC*, (Editors Bertsch, Hara, Kaiser and Zlatkis), Huethig, Heidelberg.

Garcia Sanchez F., Navas Diaz, A., Fernandez Correa M. R. (1993) *J. Chromatogr.A* **655** 31.

Freid B., Sherma J. (1994) *Thin-Layer Chromatography: Techniques and Applications*, Marcel Dekker Inc, New York.

Geiss F. (1987) *Fundamentals of Thin Layer Chromatography*, Huethig, Heidelberg.

Geiss F. (1988) *J. Planar Chromatogr.* **1** 102.

Gianelli M. L., Callis J. B., Anderson N. H., Christian G. D. (1981) *Anal. Chem.* **53** 1357.

Gianelli M. L., Burns D. H., Callis J. B., Christian G. D., Anderson N. H. (1983) *Anal. Chem.* **55** 1858.

Giddings J. C. (1965) *Dynamics of Chromatography*, Marcel Dekker, New York.

Goldman J., Goodall R. R. (1968) *J. Chromatogr.* **32** 24.

Goodall R. R. (1972) *J. Chromatogr.* **73** 161.

Gries W., Jork H. (1989) *J. Planar Chromatogr.* **2** 290.

Grushka E., Snyder L. R., Knox J. H. (1975) *J. Chromatogr. Sci.* **13** 25.

Guiochon G., Siouffi A. M. Engelhardt H., Halasz I. (1978) *J. Chromatogr. Sci.* **16** 152.

Guiochon G. Siouffi A. M. (1978) *J. Chromatogr. Sci.* **16** 470.

Guiochon G., Siouffi A. M. (1978) *J. Chromatogr. Sci.* **16** 598.

Guiochon G. (1979) *J. Chromatogr.* **185** 3.

Guiochon G., Bressolle F., Siouffi A. M. (1979) *J. Chromatogr. Sci.* **17** 368.

Guiochon G., Siouffi A. M. (1982) *J. Chromatogr.* **245** 1.

Gumieniczek ., Hopkala H., Berecka A. (2002) *J. Liq. Chromtogr. & Rel. Technol.* **25** 1401.

Habdas J., Matysik G. (2003) *J. Planar Chromatogr.* **16** 289.

Hahn-Deinstrop E., Koch A., Müller M. (1998) *J. Planar Chromatogr.* **11** 404.

Hauck H. E., W. Jost. (1983) *J. Chromatogr.*, **262** 113.

Hauck H. E., Bund O., Fischer W., Schulz M. (2001) *J. Planar Chromatogr.* **14** 234.

Hayakawa T., Hirai M. (2003) *Anal. Chem.* **75** 6728.

Hjerten S., Liao J. L., Zhang R. (1989) *J. Chromatogr.*, **473** 273.

Hopkala H., Poykalski A. (2003) *J. Planar Chromatogr.* **16** 107.

Hopkala H., Poykalski A., Mroczeck T., Ostep M. (2003) *J. Planar Chromatogr.* **16** 280.

Hopkala H., Poykalski A. (2004) *J. Planar Chromatogr.* **17** 383.

Howard A.G., Shafik T., Moffatt F., Wilson I.D. (1999) *J. Chromatogr. A* **844** 333.

Huf F. (1988) *J. Planar Chromatogr.* **1** 46.

Hyunh T. K. X., Leipzig-Pagani E. (1996) *J. Chromatogr. A* **746** 261.

Izmailov N. A., Schraiber M. S. (1938) *Farmatsiya* **3** 1.

Jain, R., Sherma J. (2000) *Encyclopedia of Analytical Chemistry*, (Editor Meyers R. A.) Wiley & Sons Ltd, Chichester.

Jansen E. H. J. M, Van Den Bosch D., Stephany R. W., Van Look L. J., Van Peteghem C. (1989) *J. Chromatogr.*, **489** 205.

Jork H. (1962) *Dtsch. Apotheker Z.* **40** 1263.

Jupille (1977) *Critical Reviews in Anal. Chem.* **6** 325.

Kaiser R. (1985) *International Symposium on Instrumental HPTLC*, Interlaken, Institut fur Chromatographie 475.

Kaiser R. (1988) *J. Planar Chromatogr.* **1** 265.

Kaiser R. (1989) *J. Planar Chromatogr.* **2** 323.

Kalasz H. (1984) *Chromatographia* **18** 628.

Karger B. L., Snyder L. R., Horvath C. (1973) *An Introduction to Separation Science*, Wiley, New York.

Katz E., Ogan K. L., Scott R. P. W. (1983) *J. Chromatogr.* **270** 51.

Kim C. K. (1980) in *Charge-coupled devices and systems*, (Editors Howes and Morgan), Wiley-Interscience, New York.

Kirchner J. G., Miller J. M., Keller G. E. (1951) *Anal. Chem.* **23** 420.

Kirchner J. G. *J. Chromatogr. Sci.* (1973) **11** 180.

Kirchner J. G. (1978) *Thin Layer Chromatography*, Wiley-Interscience, New York.

Knox J. H. *J. Chromatogr. Sci.* 18 (1980) 453.

Koglin E. (1994) *GIT* **6** 627.

Kowalczuk D., Hopkala H., (2001) *J. Planar Chromatogr.* **14** 126.

Kowalczuk D., Hopkala H., (2002) *J. Planar Chromatogr.* **15** 345.

Kozma I. Z, Krok P., Riedle E. (2005) *J. Opt. Soc. Am. B* **22** 1479

Kubelka P., Munk F. (1931) *Z. Tech. Phys.* **12** 593.

Kuhn R., Lederer E. (1931)*Ber. Dtsch. Chem.* Ges. **64** 1349.

Lancaster M., Goodall D. M., Bergström E. T., McCrossen S., Myers P. (2005) *J. Chromatogr.* **1090** 165.

Lancaster M., Goodall D. M., Bergström E. T., McCrossen S., Myers P. (2005) *Anal. Chem.* **78** 905.

Lee K. Y., Poole C. F., Zlatkis A. (1980) *Anal. Chem.* **52** 837.

Liang Y. L., Baker M. E., Yeager B. T., Denton M. B., (1996) *Anal. Chem.* **68** 3885

Liang Y. L., Baker M. E., Gilmore M. D., Denton M. B., (1996) *J. Planar Chromatogr.* **9** 247.

Lochmuller (1987) . *J. Chromatogr. Sci.* **25** 583.

Martin A. J. P., Synge R. L. M. (1941) *Biochem. J.* **35** 1358.

Meinhard J. E., Hall N. F. (1949) *Anal. Chem.* **21** 185.

Miller J. M. (1975) *Separation Methods in Chemical Analysis*, Wiley, New York.

Misztal G., Paw B., Skibiński R., Komsta L., Kolodziejczyk J. (2003) *J. Planar Chromatogr.* **16** 433.

Mustoe S., McCrossen S. (2001) *J. Planar Chromatogr.* **14** 252.

Mustoe S., McCrossen S. (2001) Chromatographia **53** S474.

Neher R. (1956) *J. Chromatogr.* **1** 122.

Novaković J. (1999) *J. Chromatogr. A* **846** 193.

Nurok D., Frost M.C., Chenoweth D.M. (2000) *J. Chromatogr. A* **903** 211.

Nyiredy S., Botz L., Sticher O. (1989) *J. Planar Chromatogr.* **2** 53.

Nyiredy S., Dallenbach-Tolke K., Zogg G. C., Sticher O. (1990) *J. Chromatogr.* **499** 453.

Nyiredy S., Dallenbach-Tolke K., Sticher O. (1990) *J. Planar Chromatogr.* **1** 336.

Nyiredy, S. (2002) *J. Planar Chromatogr.* **15** 454.

Oldham P. B. (1990) *Anal. Instrum.* **19** 49

Petrović M., Kaštelan-Macan M. (1999) *J. AOAC Int.* **82** 25.

Petrović M., Kaštelan-Macan M., Ivanković D., Matečić S. (2000) *J. AOAC Int.* **83** 1457.

Petrović M., Babić S., Kašteln-Macan M. (2000) *Croatica Chemica Acta* **73** 197.

Pollack V. A., Schulze-Clewing J. (1988) *J. Chromatogr.* **437** 97.

Pollack V. A. (1989) *J. Adv. Chromatogr.* **30** 221.

Pollack V. A., Schulze-Clewing J. (1990) *J. Planar Chromatogr.* **3** 104.

Pollack V. A., Doelemeyer A., Winkler W., Schulze-Clewing J. (1992) *J. Chromatogr.* **596** 241.

Ponder E. L., Fried B., Sherma J. (2004) *Acta Chromatographia* **14** 70.

Poole C. F. et al (1985) *J. Liq Chromatogr.* **8** 2875.

Poole C. F. (1988) *J. Planar Chromatogr.* **1** 373.

Poole C. F. (1989) *J. Planar Chromatogr.* **2** 95.

Poole C. F., Poole S. K. (1989) *J. Chromatogr.* **492** 539.

Poole C. F., Poole S. K. (1989) *J. Planar Chromatogr.* **2** 165.

Poole C. F., Poole S. K. (1989) *Anal. Chem.* **61** 1257A.

Poole C. F. (1989) *J. Chromatogr.* **492** 539.

Poole C. F., Poole S. K. (1991) *Chromatography Today*, Elsevier, Amsterdam.

Poole C. F. (1999) *J. Chromatogr. A* **856** 399.

Poole C. F., Butler H. T., Coddens M. E., Schuette S. A. (1986) *Analytical Techniques in Radiopharmaceutical Chemistry,* Springer Verlag, New York.

Poole C. F. (2003) *J. Chromatogr. A* **1000** 963.

Poole S. K., Ahmed H. D., Belay M. T., Fernando W. P. F., Poole C. F. (1990) *J. Planar Chromatogr.* **3** 133.

Prošek M., Pukl M. (1996) in *Handbook of thin-layer chromatography* (Editors Prošek M., Golc-Wondera A., Vovk I. (2001) *J. Planar Chromatogr.* **14** 100.

Sherma J., Fried B.), Marcel Dekker, Inc., 2nd ed., New York, p. 273.

Randerath K. (1968) *Thin-Layer Chromatography,* Verlg Chemie Academic Press, New York.

Ratzlaff k. l., Paul S. L. (1979) *Appl. Spectrosc.* **33** 240.

Reitsema R. H. (1954) *Anal. Chem.* **26** 960.

Renger B. (1998) *J. AOAC Int.* **81** 333.

Samoc A. (2003) *J. App. Physics* **94** 6167.

Samson J. A. R., (1967) *Techniques of vacuum ultraviolet spectroscopy*, Wiley, New York.

Sequin C. H. (1974) *IEEE J. Solid State Circuits* **9** 134.

Sequin C. H., Sealer D. A., Bertram W. J., Tompsett M. F., Buckley R. R., Shankoff T. A., McNamara W. J. (1973) *IEEE Trans. Electron Devices* **20** 244.

Sherma J.(1991) *J. AOAC Int.* **74** 435.

Sherma J. (2000) *Anal. Chem.* **72** 9R.

Simon R. E., Walton L. K., Liang Y., Bonner Denton M. (2001) *Analyst* **126** 446.

Siouffi A. M., Bressolle F., Guiochon G. (1981)

Skibiński R., Misztal G. (2004) *J. Planar Chromatogr.* **17** 224.

Smolarz H. D., Matysik G. (2001) *J. Planar Chromatogr.* **14** 199.

Snyder L. R. (1967) *Advances in Chromatography,* Dekker, New York.

Snyder L. R. (1968) *Principles of Adsorption Chromatography,* Dekker, New York.

Snyder L. R, Saunders D. L. (1969) *J. Chromatogr.* **44** 1.

Snyder L. R. (1971) *J. Chromatogr.* **63** 15.

Snyder L. R. (1974) *J. Chromatogr.* **92** 223.

Snyder L. R. (1975) *Adsorption in Chromatography,* Reinhold, New York.

Snyder L. R. Kirkland J. J. (1979) *Introduction to Modern Liquid Chromatography,* Wiley, New York.

Snyder L. R, Poppe H. (1980) *J. Chromatogr.* **184** 363.

Spangenberg B., Post P., Ebel S. (2002) *J. Planar Chromatogr.* **15** 88.

Stahl E. (1956) *Pharmazie* **11** 633.

Stahl E. (1958) *Chemiker-Ztg.* **82** 323.

Stahl E. (1958) *Parfümerie u. Kosmetik* **39** 564.

Stahl E. (1959) *Pharmaz. Rdsch.* **2** 1.

Stahl E. (1961) Angew. Chem. **73** 646.

Stahl E. (1969) *Thin Layer Chromatography: A Laboratory Handbook,* Springer Verlag, New York.

Stahl E., Mangold H. K. (1966) in *Chromatography (2nd ed.)*, (Editor, Heftmann E.), Reinhold Publishing Corporation, New York.

Stewart G. H., Wendel C. T. (1975) *J. Chromatogr. Sci.* **13** 105.

Stober J.C. (1995) *Optical scattering: measurement and analysis*, SPIE Optical Engineering Press, 2nd ed., Washington.

Summanen J., Yrjönen T., Hiltunen R., Vuorela H. (1998) *J. Planar Chromatogr.* **11** 421.

Spangenberg B., Klein K. F. (2000) *J. Chromatogr.* **898** 265.

Spangenberg B., Post P., Ebel S. (2002) *J. Planar Chromatogr.* **15** 88.

Sweedler J. V., Bilhorn R. B., Epperson P. M., Sims G. R., Denton M. B. (1988) *Anal. Chem.* **60** 252A.

Sweedler J. V., Shear J. B., Fishman H. A., Zare R. N., Scheller R. H. (1991) *Anal. Chem.* **63** 496.

Tompsett M. F., Amelio G. F., Smith G. E. (1970) *Appl. Phys. Lett.* **17** 111.

Tompsett M. F. (1972) *J. Vac. Sci. Technol.* **9** 1166.

Touchstone J. C., Levin S. S., Murawec T. (1971) *Anal Chem.* **43** 858.

Touchstone J.C., Bobbins M.F. (1983) *Practice of thin-layer chromatography*, Wiley & Sons Inc. New York.

Touchstone J. C. (1993) *American Laboratory* **25** 24I.

Treiber L. R. (1974) *J. Chromatogr.* **100** 123.

Tswett M. (1903) *Proc. Warsaw Soc. Nat. Sci., Biol.* **14** minute No. 6.

Tyaglov B. V., Zvenigorodskii V. I., Sizova I. A. (1997) *J. Planar Chromatogr.* **10** 200.

Tyihak E., Mincsovics (1988) E. *J. Planar Chromatogr.* **1** 6.

Tyihak E., Mincsovics (1989) E. *J. Chromatogr.* **471** 375.

Unger I. (1979) *J. Chromatogr.* **16** 76.

Vovk I., Prošek M. (1997) *J. Chromatogr.A* **768** 329.

Vovk I., Prošek M. (1997) *J. Chromatogr.A* **779** 329.

Vovk I., Franko M., Gibkes J., Prošek M., Bicanic D. (1997) *J. Planar Chromatogr.* **10** 258.

Vovk I., Franko M., Gibkes J., Prošek M., Bicanic D. (1998) *J. Planar Chromatogr.* **11** 379.

Vovk I., Franko M., Gibkes J., Prošek M., Bicanic D. (1997) *Anal. Sci.* **13** (Suppl.) 191.

Vovk I., Simonovska B. (2001) *J. AOAC Int.* **84** 1258.

Vujic Z., Radulovic D., Lucic B., Eric S., Kuntic V. (2003) *Chromatographia* **57** 687.

Weins C. Jork H. (1996) *J. Chromatogr.A* **750** 403.

Witkiewicz Z., Bladek J. (1986) *J. Chromatogr.* **373** 111.

Wu X. Z., Wu J. Q., Pawliszyn J. (1995) *Electrophoresis* **16** 1474.

Wulardari L., Indrayanto G. (2003) *J. Planar Chromatogr.* **16** 438.

Yamamoto H., Kurita T., Sukuzi J., Hira R., Nakano. K., Makabe H., Shibata K. (1976) *J. Chromatogr.* **116** 29.

Zlatanov L., Gonnet C., Marichy M. (1986) *Chromatographia*, **21** 331.

Zlatkis A., R. E. Kaiser (1977) *HPTLC: High Performance Thin-Layer Chromatography*, Elsevier, Amsterdam.

Bibliography

Publications

Lancaster M., Goodall D. M., Bergström E. T., McCrossen S and Myers P. (2005) Quantitative measurements on wetted thin-layer chromatography plates using a charge coupled device camera. *J. Chromatogr.* **1090** 165.

Lancaster M., Goodall D. M., Bergström E. T., McCrossen S and Myers P. (2005) Real-time image acquisition for absorbance detection and quantification in thin-layer chromatography. *Anal. Chem.* **78** 905.

Presentations

Lancaster M., Goodall D. M., Bergström E. T., McCrossen S and Myers P. (2003) Quantitative thin-layer chromatography with charge coupled device detection. Proceedings of the international symposium for HPTLC, Lyon, France (oral).

Lancaster M., Goodall D. M., Bergström E. T., McCrossen S and Myers P. (2004) Quantitative thin-layer chromatography with charge coupled device detection in real-time. Royal Society of Chemistry EYP 2004:The role of analytical techniques, Glasgow, UK (oral).

Poster

Lancaster M., Goodall D. M., Bergström E. T., McCrossen S and Myers P. (2005) TLC separations followed by imaging technology in real-time, Shell poster exhibition, York, UK.